Measurement Protocols for Exchange Biased Systems

By

Luis Eugenio Fernández Outón

Submitted for the Degree of

Doctor of Philosophy

University of York

Department of Physics

March 2006

Abstract

A study of exchange biased systems has been made focused on the development of measurement protocols that yield measurement reproducibility. The materials studied were IrMn(t_{AF})/CoFe(10nm) thin films, with t_{AF} being 3nm and 5nm. These materials were selected due to their industrial applications. The thicknesses were chosen as they were the most appropriate for the purpose of this study.

Vibrating sample magnetometry has been used to investigate thermal activation properties in the set of samples. The measurement protocols developed allowed measurement reproducibility. They lead to a better understanding of the exchange biased phenomenon. It was found that the changes occurring in the exchange biased systems during measurement are due to thermal activation in the antiferromagnetic layer which reduced the degree of order within the antiferromagnet. It was observed that the peak in the coercivity with the temperature of thermal activation does not correlate with the median blocking temperature.

A study of training effects and their behaviour with temperature has led to the identification of three different contributions to exchange bias which are spin freezing, spin reorientation, and thermal activation. Each of these effects contribute to the shift of the hysteresis loop and the coercivity of exchange biased systems through different mechanisms.

The results obtained are consistent with a grain size dependence of the exchange bias phenomenon, and are in accordance with grain models of exchange bias. Also, the measurement protocols obtained have been used by other researchers in FeMn/NiFe exchange coupled bilayers. The results obtained were in accordance with the conclusions of this thesis.

Contents

List of Figures

List of Tables

Acknowledgements

It is a difficult task to list all the people to whom I should express my gratitude. This thesis completely changed my life; I left my country; I met my wife while I was trying to work out what exchange bias is about; I met people that became friends during this time. All of them are an important part of this thesis.

I feel in debt to my supervisor Prof. Kevin O'Grady for his guidance, his support, and everything I have learnt working with him. I am also grateful to the members of the technical staff, especially to R.M. Armitage, D.R. Coulthard and R.J. Hide.

I also wish to thank all the members of the NEXBIAS research training network, especially to Dr. J. Nogués for the fruitful discussions. Also, to Dr. B. Dieny, for his support, to S. Auffrett, and G. Cassali for their help and for being so kind and to Dr. J. Sort for his help and for being such a nice host during my secondment at the CEA-Spintec, Grenoble. I also wish to thank Prof. B. Hillebrands and M.O. Liedke for their help and collaboration during my secondment at TUKL, Kaiserslautern. These collaborations and training would have not been possible without the sponsorship of the Marie Curie Fellowship Programme.

I wish to thank as well all the colleagues with whom I shared the office during all this time for their comradeship, especially to G. Vallejo for making exchange bias a matter of friendship and also to Mrs. J. Barry for her help and friendly affection.

Finalmente quisiera agradecer a toda mi familia el cariño que siempre me han brindado, especialmente a mis padres, por su apoyo incondicional y comprensión. No me olvido de mis amigos, los de siempre. Tampouco esqueço a minha família no outro lado do Atlântico. Eu desejo agradecer a Xenia por todo seu amor, carinho, amizade, compreensão, paciência, e por fazer minha vida ainda mais bonita. Meu coração é seu.

Declaration

I declare that the work presented in this thesis is based purely on my own research, unless otherwise stated, and has not been submitted for a degree in either this or any other university.

Signed

Luis Eugenio Fernández Outón

Chapter 1

Introduction

The phenomenon called exchange anisotropy or exchange bias was discovered almost fifty years ago, by William H. Meiklejohn and Charles P. Bean. They studied partially oxidised Co particles. This system exhibited a shifted, hysteresis loop when measured after cooling to a low temperature in a field. Also the loops were broader than those measured for pure Co particles. Their first paper was called "A New Magnetic Anisotropy" and was published in Conference on Magnetism and Magnetic Materials, Boston, MA, October 16-18, 1956: "We now have an additional mechanism involving an interaction between an antiferromagnetic material and a ferromagnetic material. Since the origin of this effect is postulated as being an interaction between the spins of the cobalt atoms in the metal and the cobalt ions in the antiferromagnetic cobaltous oxide, it might properly be termed an exchange anisotropy". Exchange anisotropy is responsible for an enhancement of the width and a shift of the hysteresis loop in the field axis by an amount known as exchange field (H_{ex}). Figure 1 shows a schematic of the hysteresis loop of an exchange biased system, showing the shift, defined as an exchange field, H_{ex}, and the half width known, as the coercivity (H_C). Full descriptions of the phenomenon and its effects have been extensively covered in review articles by Nogués and Schuller (1999), Berkowitz and Takano (1999), and Nogués *et al.*, (2005).

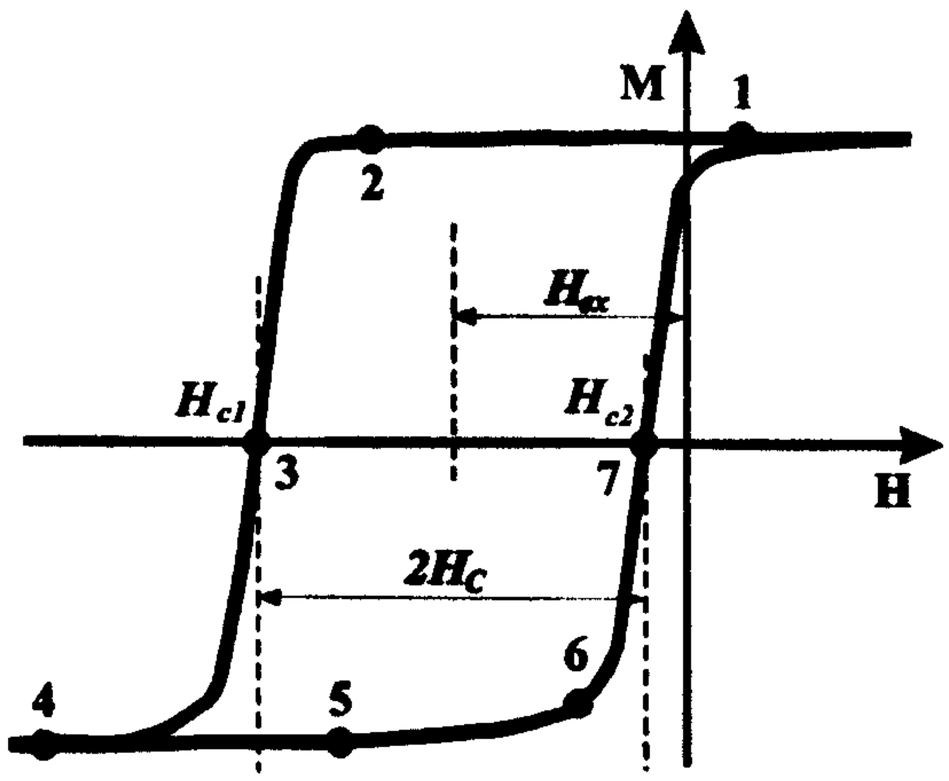

Figure 1 Schematic of the hysteresis loop of an exchange biased system. The exchange field, H_{ex}, is given by the shift of the loop from zero field. The half-width of the loop is called coercivity, *Hc*.

Proposed applications of the exchange biased phenomenon include permanent magnets, magnetic recording media or magnetic domain stabilisers in recording heads. Since its discovery, several thousand of papers have been published on the topics of exchange bias or exchange anisotropy phenomena. This is mainly due to the fact that exchange bias is the principle of operation of read heads in magnetic hard drives used not only in computers but also other media and entertainment devices. Therefore the information storage industry is the epicentre of the investigation and development of exchange biased systems and applications.

Technological applications of exchange bias involve the use of thin film exchange coupled ferromagnets, antiferromagnets and in some cases ferrimagnets. The nature of the interfacial exchange interaction between the ferromagnet and antiferromagnet is of quantum origin. Hence, detailed atomic-level information about the structure and the magnetic state is needed to obtain reliable models. The development of measurement techniques facilitates the provision of data so that more accurate models of exchange biased can be designed. However, all state of the art models still contains fitting parameters to cope with this many body problem. In addition to this, to compare the predictions of exchange biased models with experimental data it is necessary to specify the experimental conditions prior to and during the measurement of the exchange biased system. However this is not often done in the literature, leading to measurement irreproducibility, and misleading modelling. Furthermore, it is not often appreciated that the state of the antiferromagnetic layer can change during measurements due to the exchange field from the ferromagnetic layer changing sign as the loop is measured. Also the state of the antiferromagnet can change due to thermal processes during measurement. Due to the application of exchange biased systems as read heads, it is of interest to know which are the best materials to be used, which offer the best performance at reduced thicknesses and stability at the elevated working temperatures. These factors are the motivation to obtain a deeper understanding of the exchange bias phenomenon.

It is the purpose of this thesis to develop and test measurement procedures that provide reproducible data. The resulting procedures need to be simple to use and should allow traceability of all stages of measurement to be able to check any detail of the process easily. That is why this thesis is not a survey of materials for exchange biased systems,

nor a study of the structural properties that give rise to the exchange coupling across the interface of a ferromagnet/antiferromagnet bilayer. This thesis is focused on the experimental conditions that give rise to measurement reproducibility so that measurement protocols can be established. Also, it is of interest that such protocols are developed to study exchange bias phenomena such as thermal activation and training effects, where the loop shift reduces with repeated measurement.

Most of the models published on exchange bias are based on the domain state of the interfacial layers between the ferromagnet and antiferromagnet [e.g. Mauri (1987), Malozemoff (1987,1988 (a,b), Stamps (2000), Stamps *et al.* (2000), Nowak *et al.* (2002)]. These models cannot be applied to systems of particles, such as the Co particles studied by Meiklejohn and Bean, and can only be applied directly to single crystal thin film systems. Systems such as those studied in this thesis, which are composed of IrMn/CoFe bilayers are granular in nature. Hence, models have been proposed which are based in the interpretation of both the ferromagnet and the antiferromagnet as ensembles of grains [e.g. Fulcomer and Charap, 1972(a,b), Nishioka *et al.*, 1996, Takano *et al.* 1997, Stiles and McMichael, 1999(b), Tsunoda and Takahashi, 2002]. The grain models usually treat the ferromagnetic layer as a single grain. However changes in the ferromagnet due to its granular nature can lead to changes in the interactions between ferromagnet and antiferromagnet and consequently in the antiferromagnet itself with field cycling.

All the models proposed for exchange bias agree to some extent with experimental results. However there is no model that can predict all the features of exchange bias. The success of the various models is described in the reviews of exchange bias [e.g. Berkowitz and Takano (1999), Nogués and Schuller (1999), Stamps (2000), Nogués *et al.*, (2005)]. In general granular models include the effect of thermal activation, whilst generally the domain models do not include temperature dependent effects.

The Gaussian c.g.s system of units has been used in this work. The equations that appear in the following chapters are in the c.g.s. system. These units have been used since it is the system most widely used by the magnetic recording industry and the applied magnetism community. More information about the principal units used in magnetism can be found in e.g. Cullity (1972).

Chapter 2

Magnetism of Thin Films

2.1 Introduction to Exchange Coupled Films

An exchange bias system consists of an antiferromagnetic material, *AF*, in intimate contact with a ferromagnetic material, *F*. These systems exhibit some characteristic features when field cooled, from a temperature higher than the Néel temperature, T_N, of the antiferromagnet, to below T_N, under the influence of an applied magnetic field, high enough to saturate the ferromagnet. The effect was first discovered by W. H. Meiklejohn and C. P. Bean (1956) in a seminal paper "New Magnetic Anisotropy".

During such a process the ferromagnet, *F*, acquires uni-directional anisotropy. Its magnetisation M_F is biased in the direction of the applied field in which the *F* was cooled. The applied field necessary to reverse M_F is then higher than that needed to reverse the magnetisation of the same isolated *F*. Hence, the hysteresis loop associated with the *F-AF* structure is centred about a non-zero magnetic field. This phenomenon is called exchange bias (*EB*). The shift in the loop from zero-field is known as the exchange bias field or bias field (H_{ex}). See figure 1.

The memory of this preferred direction for the magnetisation of the ferromagnet persists as long as the bias field is not modified by heating over T_N or over a blocking temperature T_B, under the influence of a saturating magnetic field. The temperature T_B, at which H_{ex} equals zero, is known as blocking temperature. There are other features characteristic of exchange bias such as an increase in the loop width, defined as $2H_C$, of the *F* material even when the *AF* is cooled in zero-field [Gökemeijer *et al.* (1999), Stiles and McMichael (2001), Kume *et al.* (2005)]. There is also a peak in the value of the coercivity, H_C, in the region of T_B (Carey *et al.*, 2001), and an asymmetric loop for the *F*. An anomalous reduction in the value of H_{ex} is observed when the magnetisation is repeatedly cycled, known as training, and their uncharacteristic form of the magnetic viscosity in the ferromagnet [Fulcomer and Charap (1972 a,b), Goodman *et al.* (2000)].

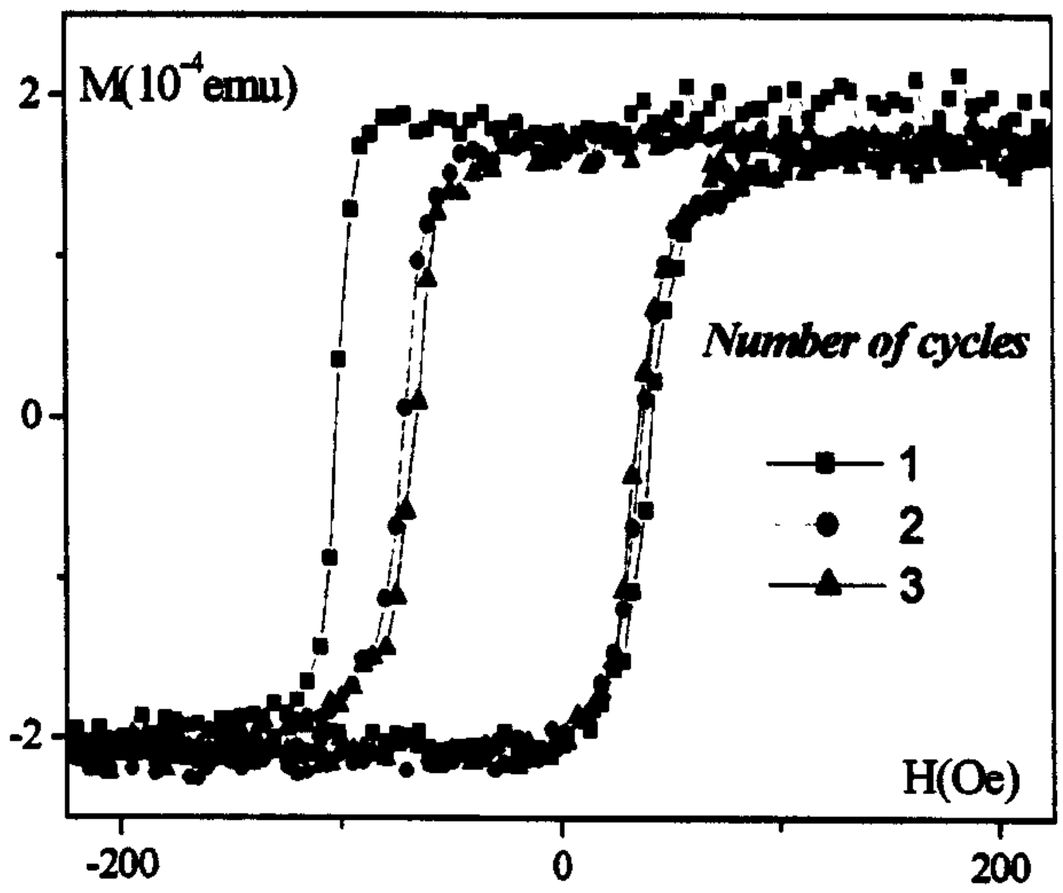

Figure 2 Training effect in IrMn(3nm)/CoFe(10nm) at 300K.

This thesis describes a study of these features of the exchange bias phenomenon in thin film systems composed of a single ferromagnet-antiferromagnet bilayer and the development of protocols for their reproducible measurement.

2.2 Preparation of Thin Films

There are basically two types of nanogranular magnetic thin films. There are magnetic films that are composed of grains that are exchange coupled together which reverse by domain wall motion generally having low coercivity. On the other hand, there are magnetic thin films formed by grains that are segregated by nonmagnetic elements that have limited solubility in the magnetic host and as result of this segregation to grain boundaries causing exchange decoupling. The hysteresis is then dominated by the anisotropy and volume of the grains.

The importance of exchange-coupled films lies in the fact that they exhibit Giant Magneto-Resistance, GMR, (see section 3.4). To maximise the magneto-resistance effect it is necessary to induce an easy direction in the film, i.e. uniaxial anisotropy, and so preparation routes are important. Among the methods for thin film fabrication, electrodeposition, evaporation and sputtering are the most widely used.

Electrodeposition is used for the fabrication of sensors, especially recording heads, having the advantage that all components can be deposited in a single cell including the leads via a series of lithographic steps. Deposition is performed in a field to induce an easy axis. Often the films are annealed at 350°C in a field to improve their crystallography. The problem with electrodeposition is the production of anions, such as Cl^- or SO_4^{2-}, inside the chamber, which lead to contamination and corrosion, leading to pinning. Thin films produced by electrodeposition have thicknesses larger than 100nm to obtain uniformity.

Thinner, less contaminated films can be made by evaporation in vacuum. In this process the use of a heated substrate removes the need for annealing and there is less contamination. Uniaxial anisotropy is generally obtained by applying an external field in the plane of the substrate. The quality of the substrate can have important effects on the magnetic properties of the thin film. Unfortunately the films are highly granular leading to pinning at grain boundaries. Lithography is more difficult as the process is on a batch basis and is not always reproducible.

Sputtering is capable of producing layers of extremely low thickness and high uniformity. Generally a magnetic field is applied to the substrate to promote the uniaxial anisotropy in the sputtered thin film. Of course in very thin films the effect of the demagnetising field forces the moment to lie in plane distorting the form of the domain walls. Figure 3 shows a schematic of a DC magnetron-sputtering system. DC sputtering applies a DC voltage between substrate and a target of the source material that is to be deposited. The chamber is filled with an inert gas of positively charged ions, generally Argon. These ions are accelerated towards the target, and knock off atoms from the source material, which on average are directed towards the substrate. The energy of the atoms that are deposited on the substrate will depend on the pressure of the gas.

To sputter insulating materials, such as MgO, a radio-frequency (RF) voltage is applied. By using an asymmetric geometry on the target, substrate holder and chamber shielding the deposition on the substrate is achieved (e.g. Mee and Daniel, 1996). This technique is used to produce thin films for the magnetic recording industry, such as magnetoresistive, GMR, and TMR materials (see section 3.4).

The crystallographic structure of the substrate plays an important role in the growth of the thin film, as it has a determining influence on its crystalline structure. The samples used in this work have been produced by DC-sputtering (Carey *et al.*, 2001). The crystal structure is γ-fcc as shown in section 2.8. Growth in the (111) crystallographic direction is achieved by using Si (111) as seed layer. All samples produced by sputtering are polycrystalline.

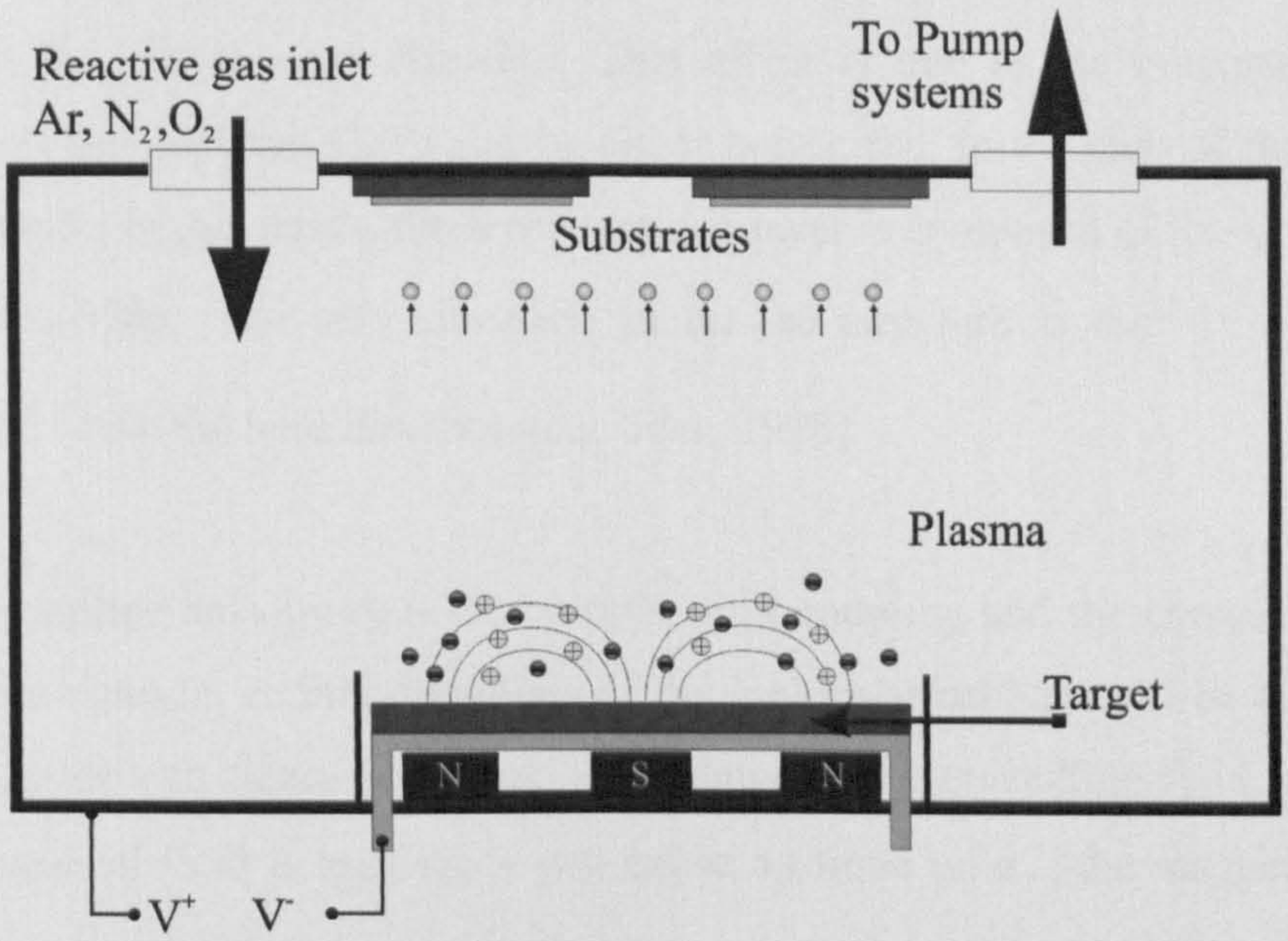

Figure 3 Schematic of a DC-magnetron-sputtering system.

2.3 Anisotropy in Ferromagnetic Thin Films

The definition of anisotropy is any physical quantity that exhibits different values depending on the direction of measurement. Magnetic anisotropy refers to the preference for the magnetisation to lie in a particular direction or directions. There are several factors that determine or give rise to magnetic anisotropy, which can be intrinsic to the material, magnetocrystalline, or dependent on the preparation of the sample. The main types of extrinsic anisotropy are: shape, stress, and exchange anisotropy.

2.3.1 Magnetocrystalline Anisotropy

Direct observations of the magnetisation of materials with different crystalline structures, such as bcc Fe, fcc Ni or hcp Co, showed that the material would magnetise more easily when the field is applied in certain directions. In the case of bcc Fe, $\langle 100 \rangle$ are *easy* directions, and $\langle 111 \rangle$ are *hard* directions. Removal of the applied field, after saturation is reached, will leave the sample with a higher remanence if the direction of the applied field is an easy direction. This effect is due to the magnetocrystalline anisotropy of the material. CoFe can be either bcc or fcc. In the case of the exchange coupled samples in this thesis, the ferromagnetic layer is composed of fcc-CoFe and the *AF* layer fcc-IrMn. The easy direction in an fcc structure is the $\langle 111 \rangle$, $\langle 110 \rangle$ the medium, and $\langle 100 \rangle$ the hard direction [e.g. Jiles, 1998].

Magnetocrystalline anisotropy is due to spin-orbit coupling and the crystalline electric field. In consequence, certain directions of the molecular orbitals will be energetically more favourable and hence preferred, depending on the crystalline field symmetries. When an external field is applied, it will cause a torque on $\boldsymbol{\mu}_S$, the magnetic moment due to spin angular momentum. The response of this moment will depend on the strength of the coupling between the spin, $\boldsymbol{S}$, and the orbital, $\boldsymbol{L}$, angular momenta. Tsunoda and Takahashi (2002) suggested magnetocrystalline anisotropy to be the origin of the magnetic anisotropy of the *AF* in their study on NiFe/IrMn and NiFe/NiMn on the basis of the single spin model proposed by Meiklejohn and Bean (1956, 1957).

Exchange bias depends on the intrinsic properties of the *AF*, such as the magnetocrystalline anisotropy and the exchange coupling between *AF* spins and between the *AF* and *F* spins. An increase in these quantities will lead to an increase in the exchange bias (Xi *et al.*, 2003). Magnetocrystalline anisotropy plays a key role in the modelling of exchange bias systems, as it is a driving parameter for the availability of possible energy states of the magnetic moments in the *AF*. The symmetry of the magnetocrystalline anisotropy in the *AF* depends on the crystalline structure of the material (Cai *et al.*, 2001). The magnetocrystalline anisotropy is sensitive to the

environment, also being influenced by the direction of the magnetic moments at the interface between the *F* and *AF* (Nakamura *et al.*, 2000).

2.3.2 Shape Anisotropy

L. Néel in 1947 explained the origin of this anisotropy due to the formation of uncompensated free poles at the surfaces of a magnetised material, giving rise to dipole interactions. It can be represented in terms of the external field applied to the sample as a demagnetising field. This field opposes to the state of magnetisation of the sample. It can be expressed as:

$$\boldsymbol{H_D} = -N_D \boldsymbol{M_S} \tag{2.1}$$

where $\boldsymbol{H_D}$ is the demagnetising field, $\boldsymbol{M_S}$ the saturation magnetisation, and N_D the demagnetising factor, which is a tensor function of the shape of the sample. The values of its components vary between 0 and 4π (cgs). For thin film geometries, the demagnetising factor N_D is 0 in the in-plane directions, and 4π in the direction perpendicular to the plane (Jiles, 1998). Hence the magnetisation of a magnetic thin film tends to lie in the plane. The use of exchange-biased systems in industry is based on thin film geometries [e.g. Childress *et al.*, 2001].

Giant Magneto-Resistive (GMR) spin valve sensors take advantage of exchange bias phenomenon to set the magnetisation direction of one of its layers. The use of these GMR-spin-valves (Gregg *et al.*, 2002) for read heads for the magnetic storage industry require an increasing miniaturisation of the elements used (See section 3.4). In a GMR-spin-valve the thickness of the AF is the dominant factor in the size of the spin valve. As described in section 3.4 the current used in a GMR device flows parallel to the interface plane (CIP) of the stack. For this configuration the magnetisation direction in the free and pinned layers in the spin valve lie in plane. Reduction of the size of the head is achieved if the configuration changes and the current flows perpendicular to the plane (CPP) of the spin valve. For this configuration the magnetisation also lies in plane.

The demagnetising field plays an important role when the magnetisation of the F is required to stay out of plain as N_D equals 4π in this direction. In some cases techniques such as adding Pt interlayers between F and AF are used to promote the orientation of the magnetisation to lie perpendicular to the plane [e.g. Sort *et al.*, 2004].

2.3.3 Other types of anisotropy

Stress anisotropy is a direct consequence of the magnetocrystalline anisotropy and its influence in the change of the sample's dimensions when a magnetic field is applied. This is due to orbital reorientation of the magnetic atoms in the direction of the applied field due to energy minimisation. In most of the cases, grain boundaries, or any type of defects, restrict this change to the direction of the orbitals. The energy stored in the system due to this effect is known as magnetoelastic energy.

Studies by Platt *et al.* (2000), on $Si/Co_{50}Fe_{50}$ suggested that the behaviour of coercivity with temperature for CoFe is influenced by small changes in strain due to the large magnetostriction of CoFe. Some anisotropic effects, which affect exchange bias, are those related to field annealing and the effect of deposition in a field. These two effects will be described in chapter 6.2.

Other mechanisms that introduce anisotropy in thin films are ion irradiation [e.g. Fassbender *et al.*, 2004] and impurity addition; both methods can also be applied to tailor exchange bias properties.

2.3.4 Anisotropy in soft thin films

The use of exchange bias systems for the fabrication of read heads for magnetic recording systems add some requirements for the materials that form the exchange coupled bilayer. A read head must have low coercivity, low noise and extremely high permeability, μ_r. Nickel-iron alloys and cobalt-iron alloys are the most widely used soft ferromagnets. $Ni_{78}Fe_{22}$ has almost zero magnetostriction and magnetocrystalline anisotropy and has one of the highest permabilities (O'Handley, 2000).

CoFe alloys can have bcc or fcc crystalline structure. See figure 5. These alloys are characterised by a relatively low magnetic anisotropy and substantial magnetostriction. In these materials the grain size is the primary factor that determines the permeability and coercivity (Chin and Wernick, 1980). The value of μ is proportional to M_S/K_{eff}, where K_{eff} may include various sources of anisotropy: magnetocrystalline, magnetoelastic, heat treatment with or without an applied field (thermomagnetic anisotropy), cold working or plastic deformation, slip-induced anisotropy (English and Chien, 1967).

For very small thicknesses, much less than a domain wall width, the magnetostatic energy dominates over all other terms and the magnetisation tends to lie predominantly in plane. Canted spin configurations or perpendicular to plane magnetisation can also be found in CoFe thin films. These orientations may appear when there is inhomogeneous magnetisation in the film. In this case, the effective uniaxial anisotropy, K_{eff}, can be described by a first order, uniaxial, positive term. In the case of K_{eff} being negative the magnetisation would lie in plane (O'Handley, 2000).

The nature of grain growth and inter-grain interactions plays an important role in the magnetisation reversal of thin films. Jung *et al.*, (2002) studied $Cu/Fe_{100-x}\,Co_x$, in the range $30 \le x \le 50$, they concluded that the reduction of H_C was a result of the reduction in grain size, in accordance with the ripple theory (Hoffmann, 1973). These results are similar to those of Platt *et al.*,(2000) for $Fe_{50}Co_{50}$ grown on CoO. Controlling the grain size by change in the sputtering rate, Vopsaroiu *et al.*, (2005) were able to tailor the coercivity in CoFe sputtered thin films. Figure 4 shows room temperature hysteresis loops of $Co_{60}Fe_{40}$ samples with different grains sizes after Vopsaroiu *et al.* (2005).

In the case of random local anisotropy in continuous films, exchange coupled grains reduce the anisotropy by averaging when the length scale, i.e. the grain size, is smaller than the exchange length. Another possible effect is that the magnetisation shows orientational coherence over a length that varies depending on the ratio of the exchange stiffness to the strength of local anisotropies. By comparison of the exchange length and the grain diameter the influence of the exchange and anisotropy energy on the

magnetisation reversal from grain to grain in polycrystalline films can be determined (Craik, 1995).

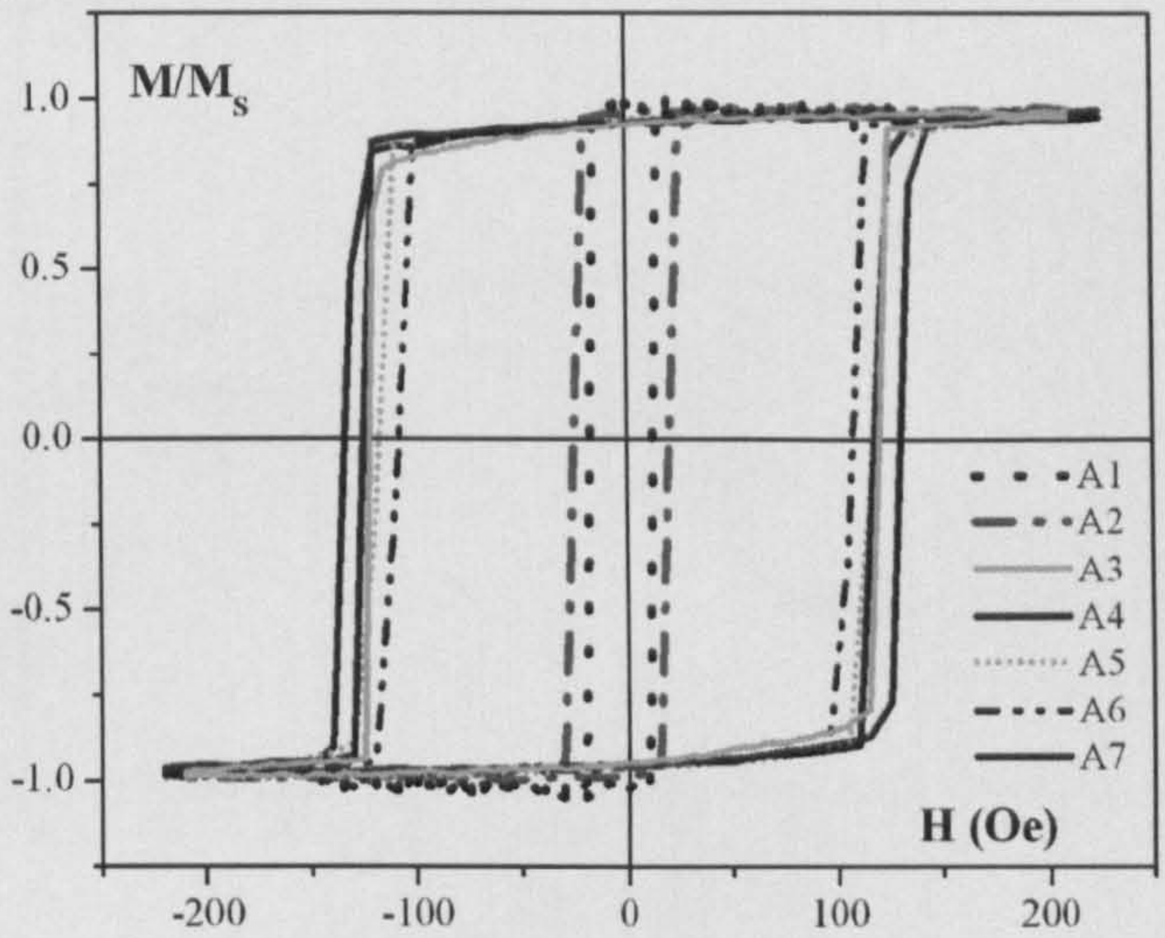

Figure 4 Room temperature hysteresis loops for $Co_{60}Fe_{40}$, (Vopsaroiu *et al.*, 2005)

The samples studied in this work contain a $Co_{90}Fe_{10}$ film 10 nm thick for the ferromagnetic layer. The crystalline structure of CoFe alloys is shown in figure 5. Hence $Co_{90}Fe_{10}$ has fcc (γ) structure up to 1000°C. CoFe alloys have a T_C of the order of 1253K (Kaye and Laby, 1986). The exact value of T_C for $Co_{90}Fe_{10}$ is not known and may vary when the material is in thin film form.

Sample	Mean grain size D (nm)	Coercivity H_C (Oe)
A1	7.20	12
A2	14.1	20
A3	17.1	120
A4	20.0	126
A5	21.2	117
A6	24.1	108
A7	26.3	121

Table 1 Data relative to the hysteresis loops for $Co_{60}Fe_{40}$ from figure 4 (Vopsaroiu *et al.*, 2005)

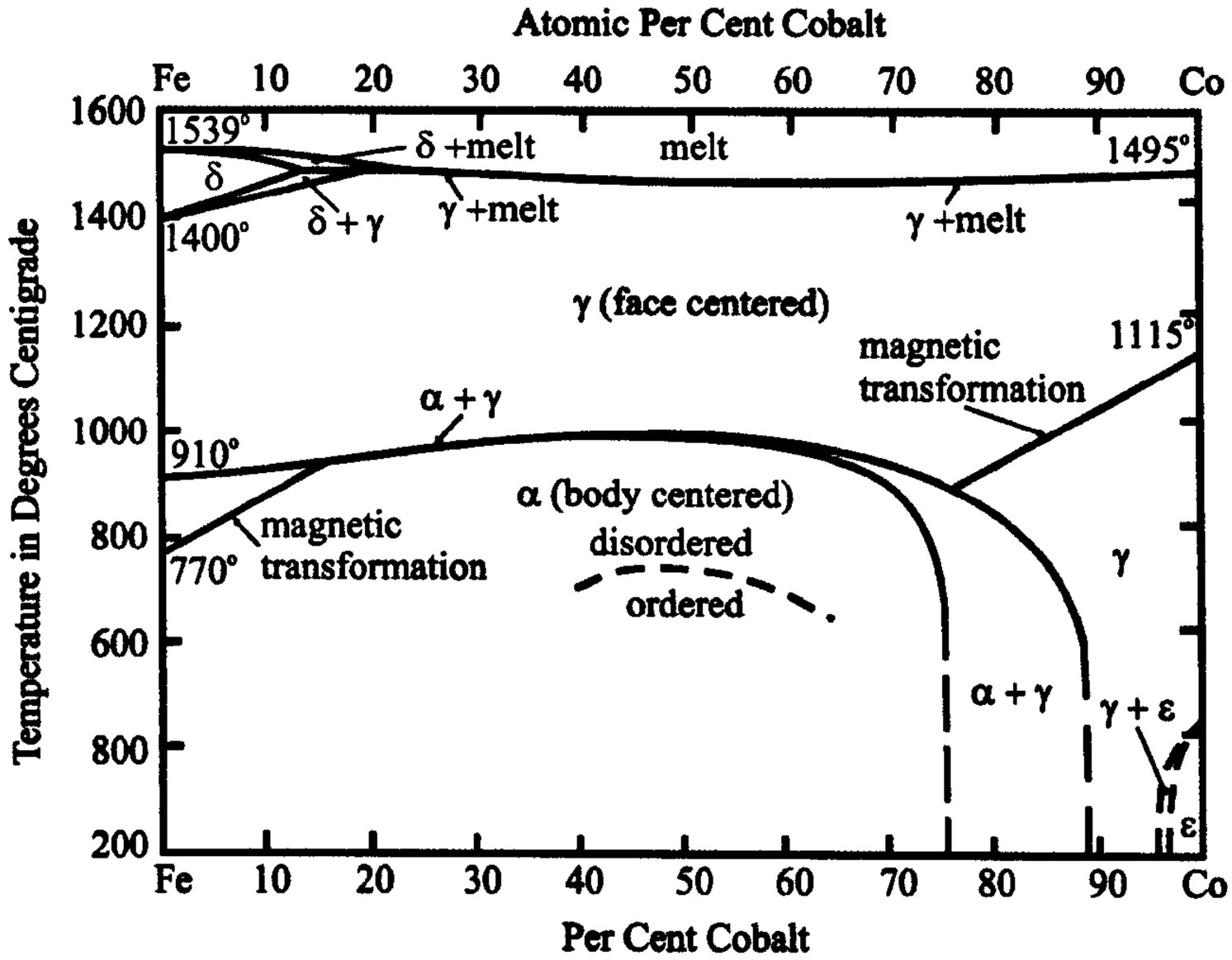

Figure 5. Phase diagram of CoFe alloys (Bozorth, 1951)

2.4 Interactions in Ferromagnetic Thin Films

Nanoscale dimensions play an important role in composites of particles as well as thin films. At this scale, phenomena such as magnetostatic effects, exchange anisotropy, single domain behaviour, superparamagnetism, random anisotropy and exchange coupling play an important role in the understanding of the magnetic behaviour of these systems (Koch, 2002). In this section the different forms of interaction between the magnetic moments of atoms from different sites of ferromagnetic thin films and the influence these have on bulk magnetic behaviour in thin films are discussed.

2.4.1 Exchange Interaction. Direct Exchange

The tendency of electron spins to align parallel or antiparallel can be understood via the exchange interaction. This interaction can be quantified through the exchange strength, J, or exchange integral, which depends on the orbital overlap and is a result of the requirement for the electrons to be indistinguishable (Heisenberg, 1924). The values taken by J depend on the interatomic distance related to the radii of the orbitals of the

interacting electrons. For $J > 0$ the spins of these electrons will align parallel while for $J < 0$ they will align antiparallel, resulting in ferromagnetism and antiferromagnetism respectively (e.g. Cullity, 1972). The exchange interaction is responsible for the magnetic state of the materials. For localised electrons on fixed ions, the Hamiltonian is

$$H = -2\sum_{i<j} J_{ij}\vec{S}_i \cdot \vec{S}_j \qquad (2.2)$$

Depending on the value of the exchange integral, J, the spins will lie parallel, leading to ferromagnetism when $J > 0$, or will lie antiparallel when $J < 0$, leading to antiferromagnetism. The magnitude of the sign of J_{ij} depends on the separation of the spins.

This form of exchange applies for systems with localised wave functions such as Mn and Cr, which are antiferromagnetic, or MnAs, MnSb, which are both ferromagnetic (Bozorth, 1951). However, Heisenberg exchange does not explain how a magnetic moment of an atom from one site couples to another from another site in the case of rare-earth metals. The magnetic moment of atoms of this type is due to electrons in the partially filled 4f orbitals, which are very localised and too small, typically 10% of the interatomic spacing, for electron hopping from one site to another. For theses cases indirect coupling applies[e.g. O'Handley, 2000].

2.4.2 Indirect Exchange

This indirect exchange or RKKY interaction [e.g. Kittel, 1968] describes the coupling in rear-earth metals and alloys. For these materials the magnetic moments are given by partial filling of the highly localised 4f states. The radius of a 4f state is about 10% of an interatomic spacing. Hence, there is no 4f-orbital overlap between neighbouring atoms. The interaction between the magnetic moments at different sites is provided by mediation of conduction electrons. The $4f^n$ magnetic moment at one site polarises the conduction electrons in the 6s orbital, whose wavelength is quite extended and therefore these electrons communicate their spin polarisation state to other sites.

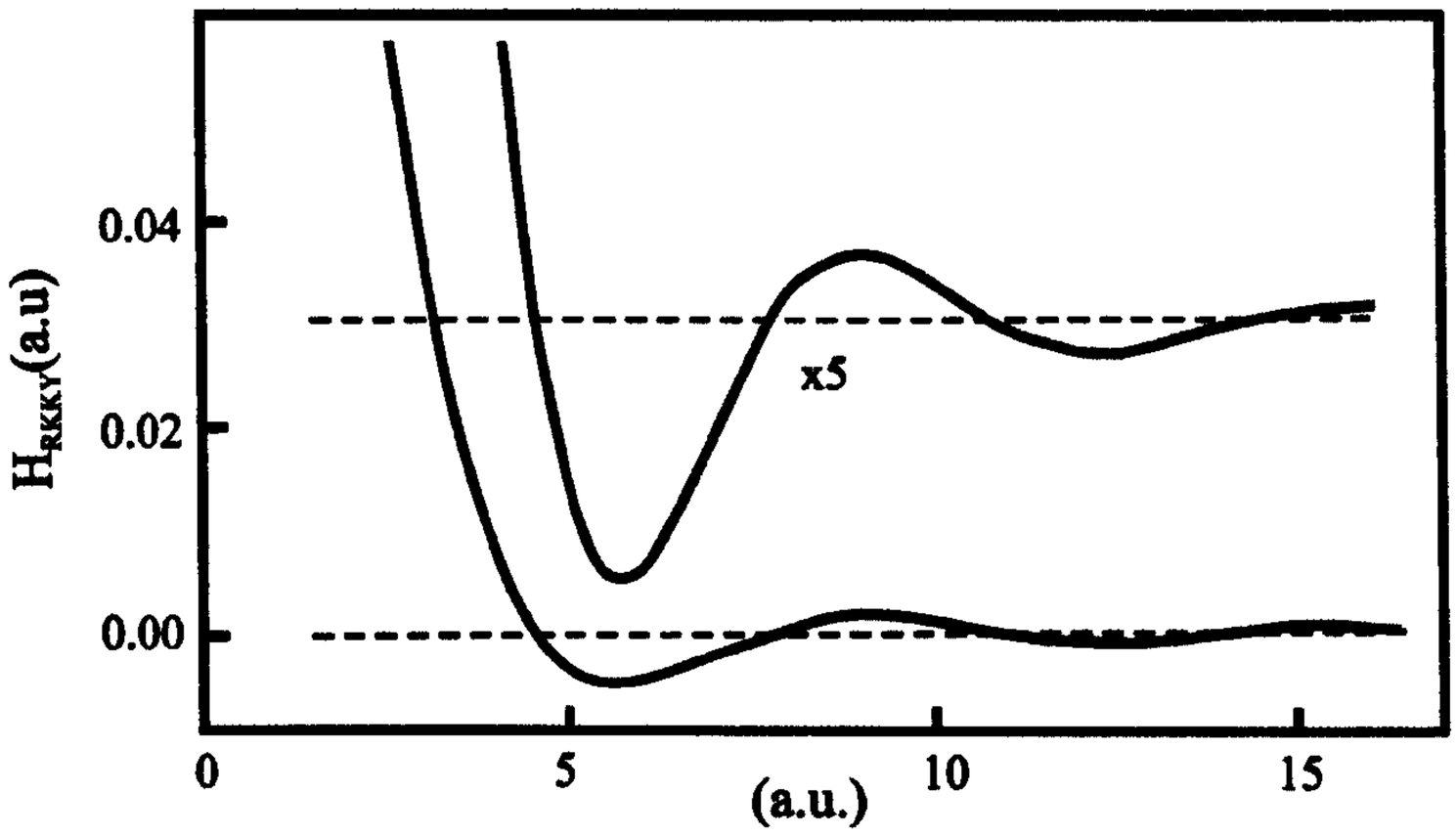

Figure 6 Variation of the RKKY interaction, showing the change in sign of the indirect interaction with atoms at different distances from a given site in the material. (O'Handley, 2000)

The conduction electron spin density is damped and oscillates with the distance from the local moment. Added to the spin polarisation of the conduction electrons is the fact that the amplitudes of the oscillations have different periods depending on the crystallographic directions. Hence, neighbours at different distances may experience different signs of exchange coupling. Hence, the RKKY interaction can give rise to ferromagnetism, antiferromagnetism, or helimagnetism but is weaker than interatomic exchange coupling in 3d metals and weaker than super-exchange in 3d magnetic oxides.

2.4.3 Super-exchange

Super-exchange is a variation of indirect exchange which applies mainly to 3d magnetic oxides with the rocksalt structures, spinel, garnet and perovskite oxides. The mechanism of super-exchange can be described as shown in figure 7. It shows two transition metal ions, e.g. Mn^{2+}, which are separated by an oxygen ion O^{2-}. The p orbital on the oxygen, filled in the ground state, can exchange an electron with each of the 3d orbitals of the Mn^{2+}. This gives divalent ionic bonding but some hopping is allowed. The positive and negative phase parts of the orbitals are shown in the figure.

To be in the ground state, the 3d and p orbitals must exchange electrons, so some excited states must be partially occupied. When one of the electrons is excited into one of the empty 3d states, the other electron, which is of opposite spin can exchange with a

3d orbital of the other neighbouring transition metal ion coupling to the p orbital. In the case of the two 3d orbitals having the same ground-state electronic configuration, this will result in antiferromagnetic spin coupling between the two M^{2+} ions. Therefore, the basis of this antiferromagnetism is in the symmetry of the 3d and the p orbitals and the conservation of the spin polarisation for electron hopping [e.g. O'Handley, 2000].

The most important consequence of this type of exchange is that it is highly anisotropic. The bonding gives a direction for the coupling, which is very strong. Also because the moments are very small (atomic), and cancel, an applied field cannot couple to them so they are hard to reverse. In many materials the spin alignment is not perfectly co-linear. This gives rise to spin canting and therefore to a measurable susceptibility. In complex oxides, e.g. Fe_3O_4, FeO, Fe_2O_3, the cancellation is imperfect, resulting in ferrimagnetism. In the case of Fe_2O_3 the structural effect is dominant so different phases of Fe_2O_3 are antiferromagnetic or ferromagnetic. Due to direct exchange, the behaviour of alloys can give similar properties, e.g. Néel ferrigmagnets.

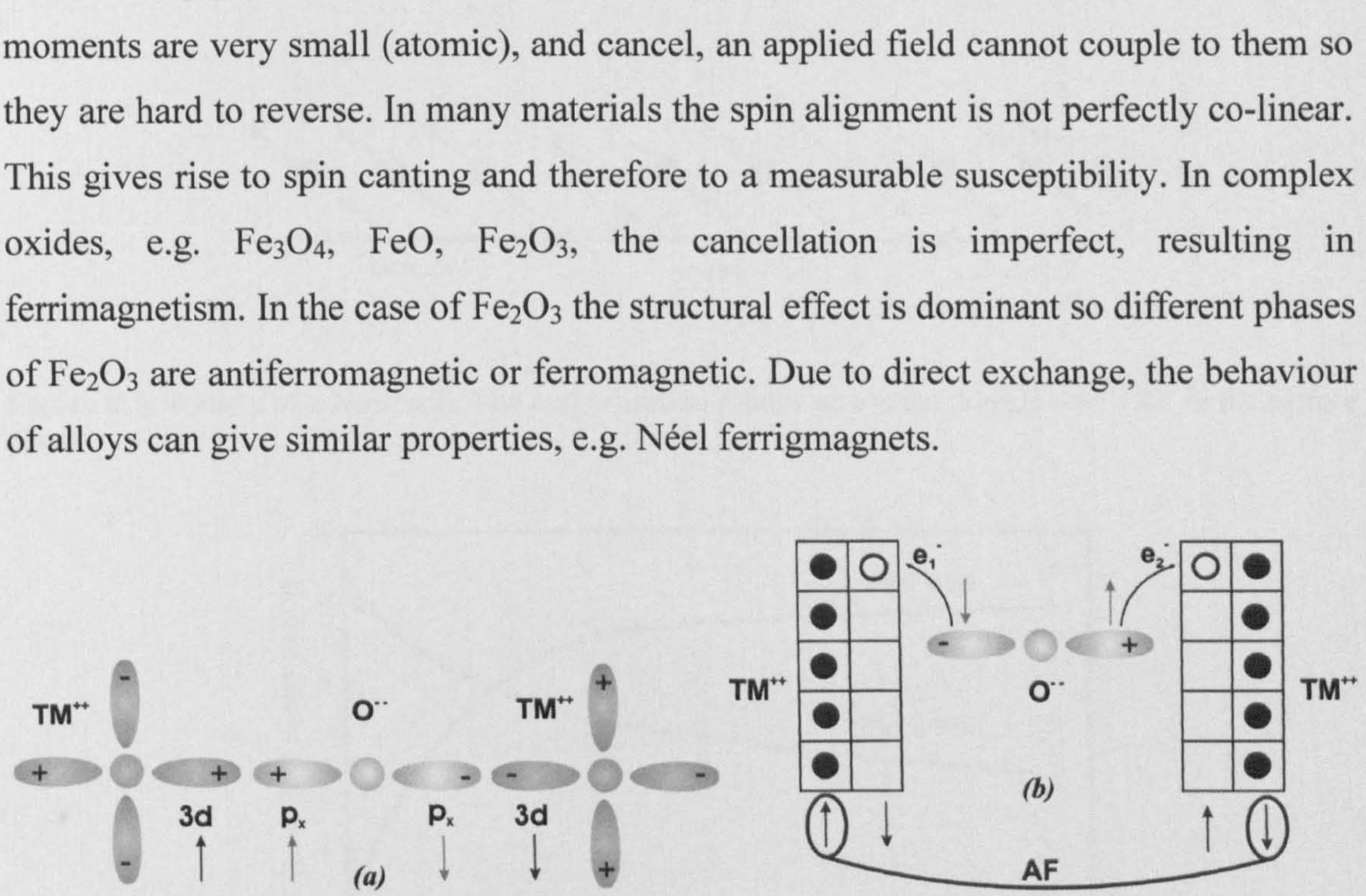

Figure 7 (a) Schematic of p and d orbitals. **(b)** Schematic of the electronic state of the p and 3d orbitals.

2.5 Magnetic Domains and Domain Walls

2.5.1 Néel walls.

In bulk materials a domain wall consists of a region of spin rotation. The width of the wall is determined by the balance between exchange and anisotropy energies. However in thin films magnetostatic energy is also important, as high anisotropy is required to orient spins perpendicular to the plane. Thus the rotation of the spins must lie in the plane forming a special form of domain wall known as Néel wall (see figure 8). This

type of wall is characterised by the rotation of spins inside the walls in the plane of the surface. The magnetostatic energy would be smaller at the internal interface of the wall.

Figure 9 show the thickness dependence of the wall energy density for Bloch and Néel walls (a), and the domain wall width as a function of the film thickness for Bloch and Néel walls. Bloch walls can transform into the Néel walls near a surface in materials with film thickness larger than the thickness of a Néel domain wall (O'Handley, 2000). In general, domain wall widths change with film thickness.

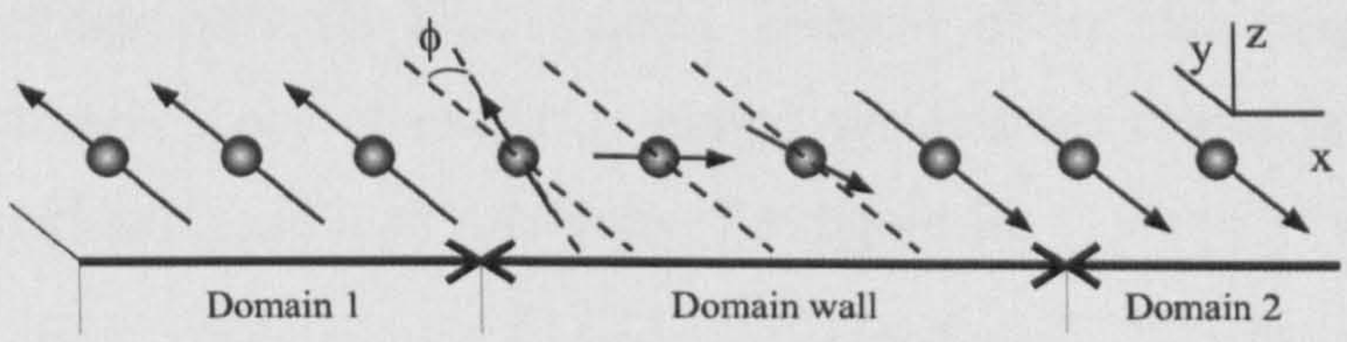

Figure 8 Schematic of a Néel wall. The magnetisation rotates across the domain wall 180° in the surface plane.

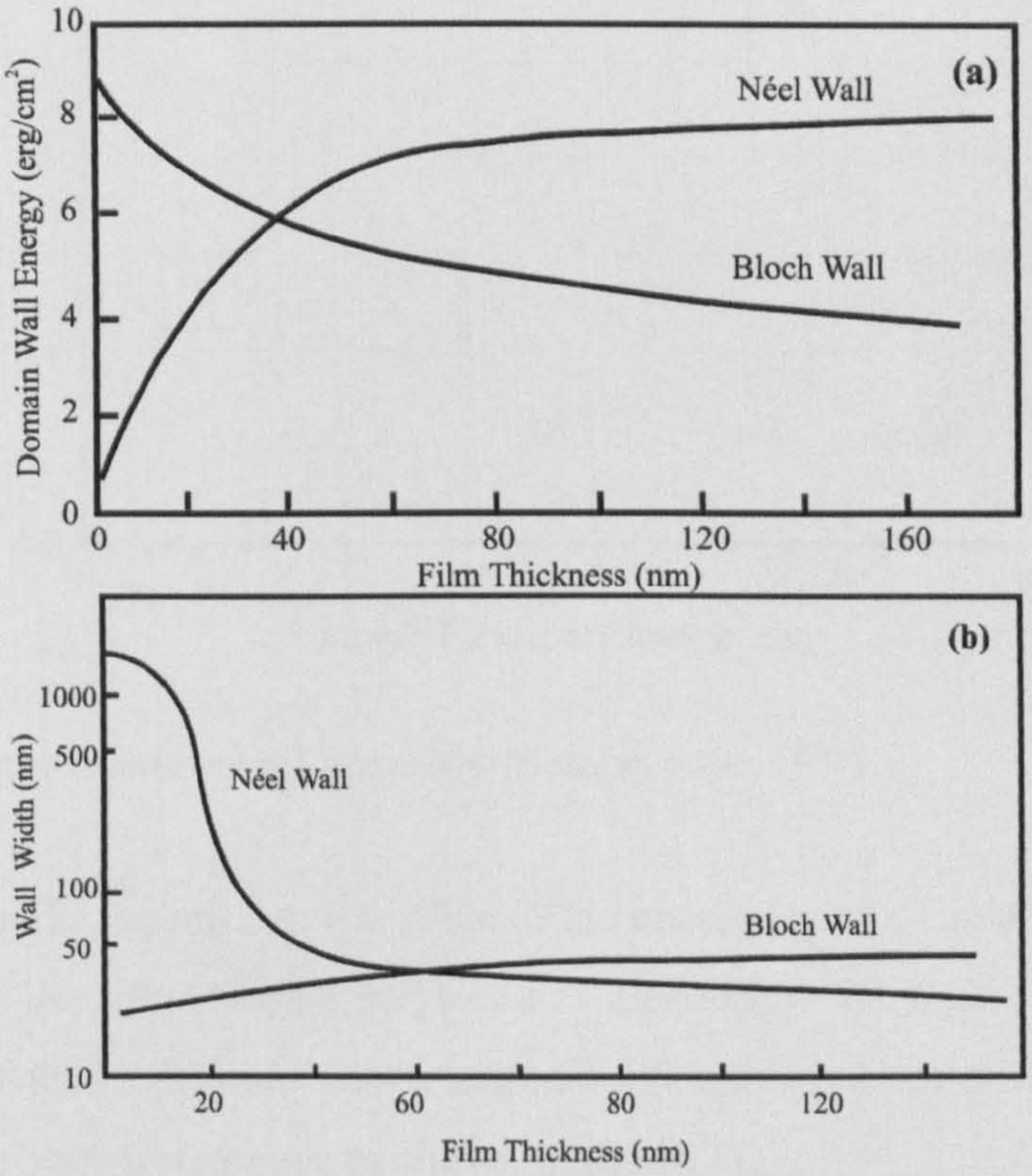

Figure 9 (a) Thickness dependence of the wall energy density for Bloch and Néel wall, **(b)** domain wall width as a function of the film thickness for Bloch and Néel walls. (O'Handley, 2000)

For 30nm thick $Co_{50}Fe_{50}$, typical domain wall widths vary between 8 and 40 nm for 180° domain walls (Platt *et al.*, 2000). As shown in the figure 9, the energy of Néel walls increase and the domain wall widths decrease with increasing film thickness.

2.5.2 Domain Formation

Cobalt-Iron, the ferromagnet used in the samples studied, is characterised for having a much higher magnetocrystalline anisotropy than NiFe, the other ferromagnet that is extensively used for exchange bias systems. Because of its high magnetocrystalline anisotropy, hysteresis loops of exchange-biased systems are characterised by a high saturation magnetisation and high coercivity. See figure 10.

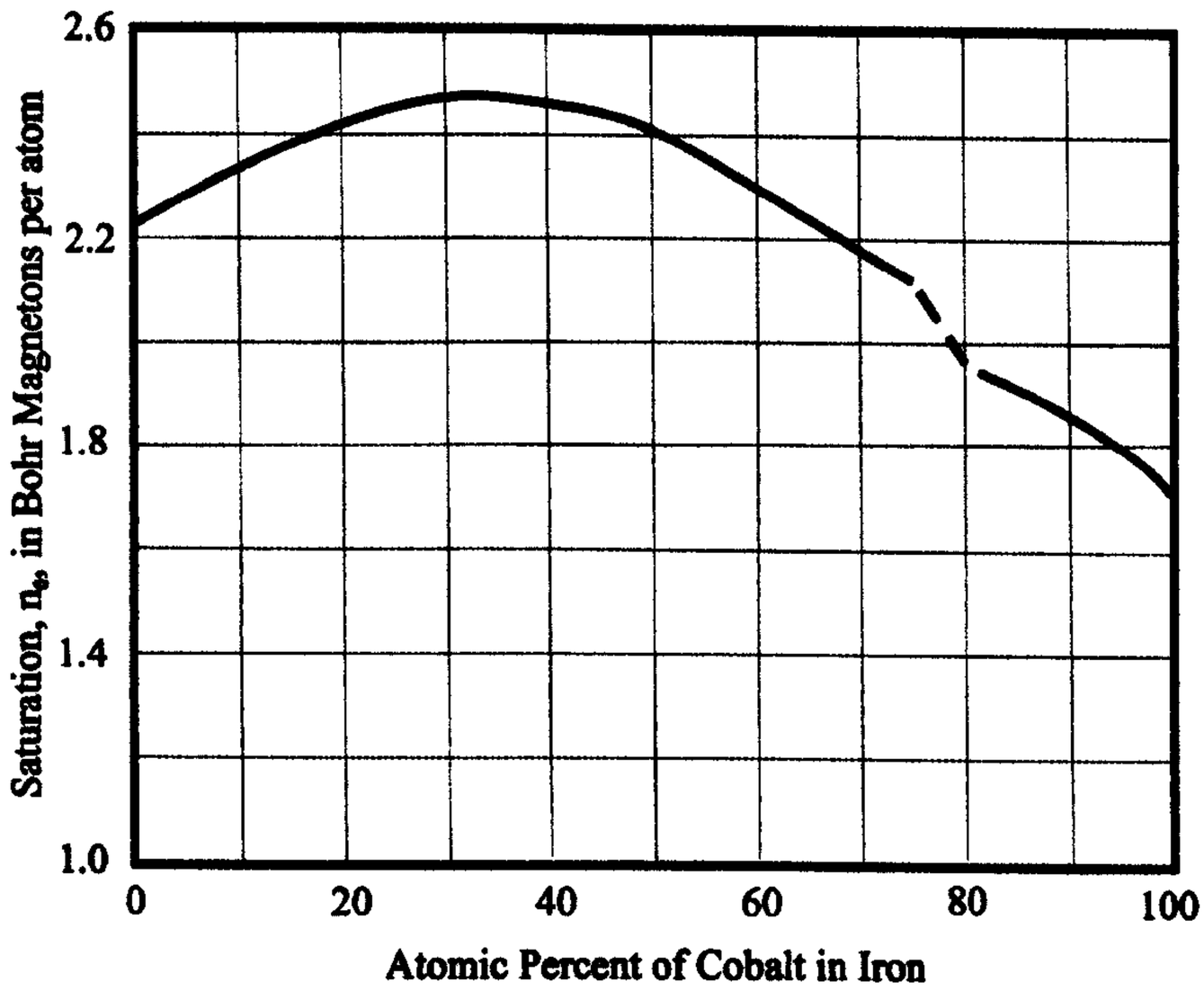

Figure 10 Bohr magneton numbers in CoFe alloys. (Bozorth, p.195, 1951)

As seen in chapter 2, section 3.4, the value of the coercivity of a CoFe layer depends on the grain size. As the magnetocrystalline anisotropy is high, the reversal of magnetisation of these alloys is characterised by domain nucleation leading to a high squareness in the hysteresis loops, as shown in figure 11.

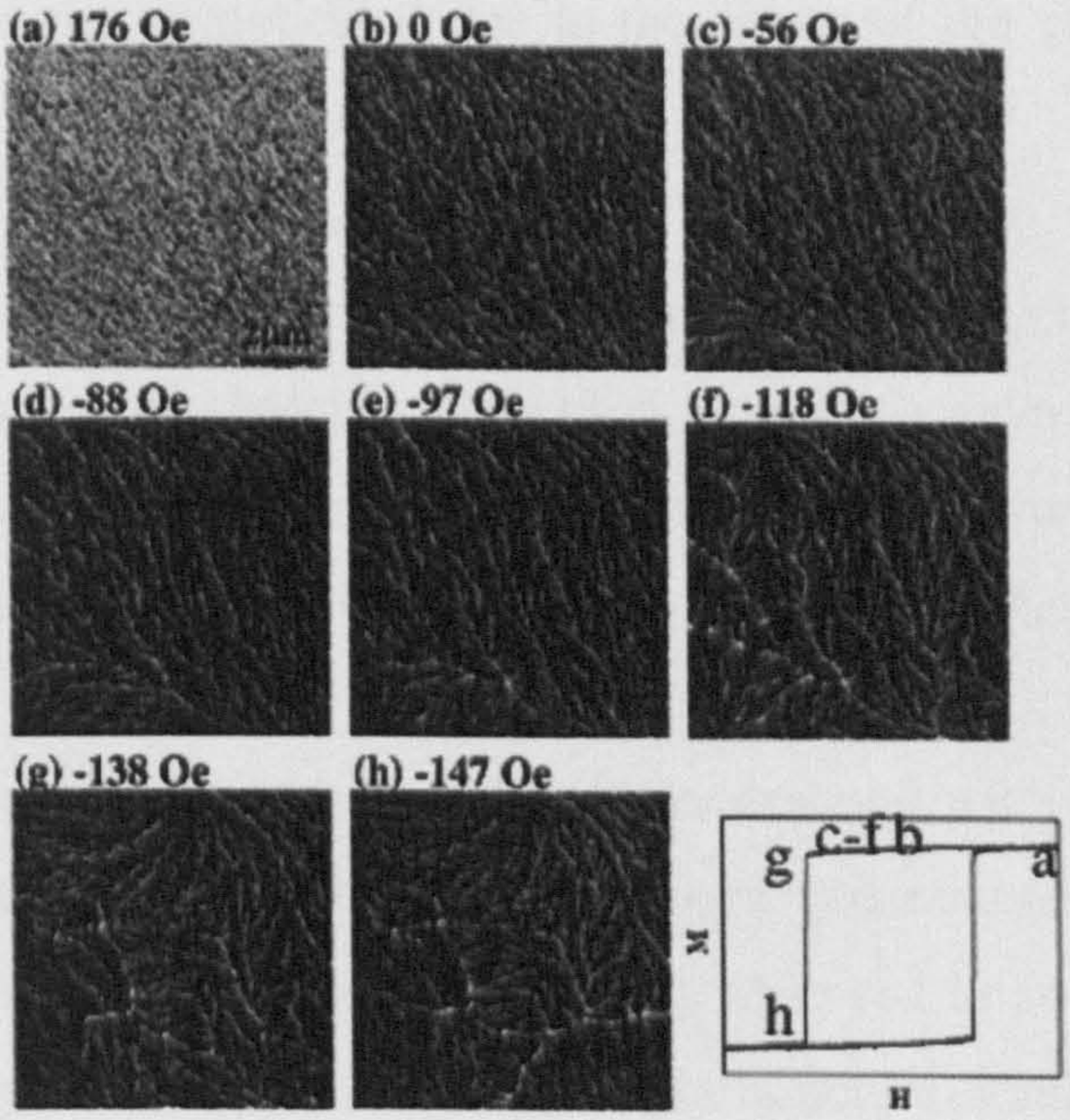

Figure 11 Lorentz image of $Co_{50}Fe_{50}$(30nm)/SiO_2(10nm). The hysteresis loop was measured by AGM (Alternating Gradient Magnetometer) (Platt *et al.*, 2000).

The formation of multidomain structures is governed by energy minimisation, which involves different energy densities: the Zeeman energy, the exchange energy, and the magnetostatic energy. To describe coercivity and irreversibility it is necessary to take into account the spatial variation of $\boldsymbol{M}$ and domain walls, each having different energy densities.

A single domain state has high magnetostatic energy due to the formation of poles at its ends. In the case of cubic anisotropy systems such as, Fe, the formation of 90° closure domains allows the flux to be contained within the sample reducing the magnetostatic energy. In the case of uniaxial anisotropy materials, the formation of closure domains will increase the anisotropy energy and cause elastic energy due to strain incompatibilities.

The materials studied in this work include $Co_{90}Fe_{10}$ as *F* layer and $Ir_{30}Mn_{70}$ for the *AF* layer. The formation of domains and domain walls in polycrystalline thin films such as CoFe has great importance in the study of magnetisation reversal processes on CoFe/IrMn systems. The fact that these films are composed of grains makes the study

of the reversal properties complicated due to the nature of the grain growth and the interactions between grains (Platt *et al.*, 2000).

Domain observation by Lorentz transmission electron microscopy (TEM) of magnetisation reversal on single-layer 30nm thick $Co_{50}Fe_{50}$, grown on 10nm thick SiO_2, shows the formation of ripple domain structures, which are almost stationary up to applied fields close to the coercive point as shown in figure 11 (Platt *et al.*, 2000).

There is an increase in the contrast of the ripple structure with the reduction of the applied field towards negative values showing more pronounced spatial variation of magnetisation. At H_C, an 180° domain wall was observed to sweep across the film. Hence, low mobility domain walls and the ripple structure dominate the reversal of CoFe, and therefore higher coercivity values would be expected than for the case of higher mobility. When the CoFe is exchange coupled to IrMn the magnetisation reversal mechanisms change depending on several factors such as the thickness of the IrMn layer, the direction of the applied field, as shown in figure 12 (Gogol *et al.*, 2002), and the crystallographic orientation of the bilayers (Sato *et al.*, 2005). Magnetisation ripple can be induced in the CoFe layer by the IrMn as reported by Pokhil *et al.* (2002).

Sato *et al.* (2005) studied epitaxial (110) and (001) $Ir_{25}Mn_{75}/Co_{70}Fe_{30}$ bilayers. For (110) the reversal process is by movement of 180° domain walls separating large domains. In the case of (001), the magnetisation reversal proceeded by nucleation of small domains formed homogeneously across the whole film. Gogol et al. (2002) using Fresnel mode Lorentz microscopy, observed different domain features in the $Co_{90}Fe_{10}$ layer depending on the thickness (t_{AF}) of the $Ir_{20}Mn_{80}$ layer. For t_{AF} = 2nm, ripple structures were observed to intensify as the applied field was swept to lower values. Domain wall nucleation during reversal of the applied field and formation of 360° wall loops were also observed. For $t_{AF} \geq 6$nm, the reversal of magnetisation was by nucleation events and a high density of walls separating submicron-sized domains. Magnetisation ripple was observed to behave similarly for lower t_{AF} increasing, in contrast with decreasing applied field, with a high dispersion or a high density of low angle walls. The domain structure evolved to domain walls lying almost parallel to the applied field. During the return of the field cycle the magnetic structures were similar.

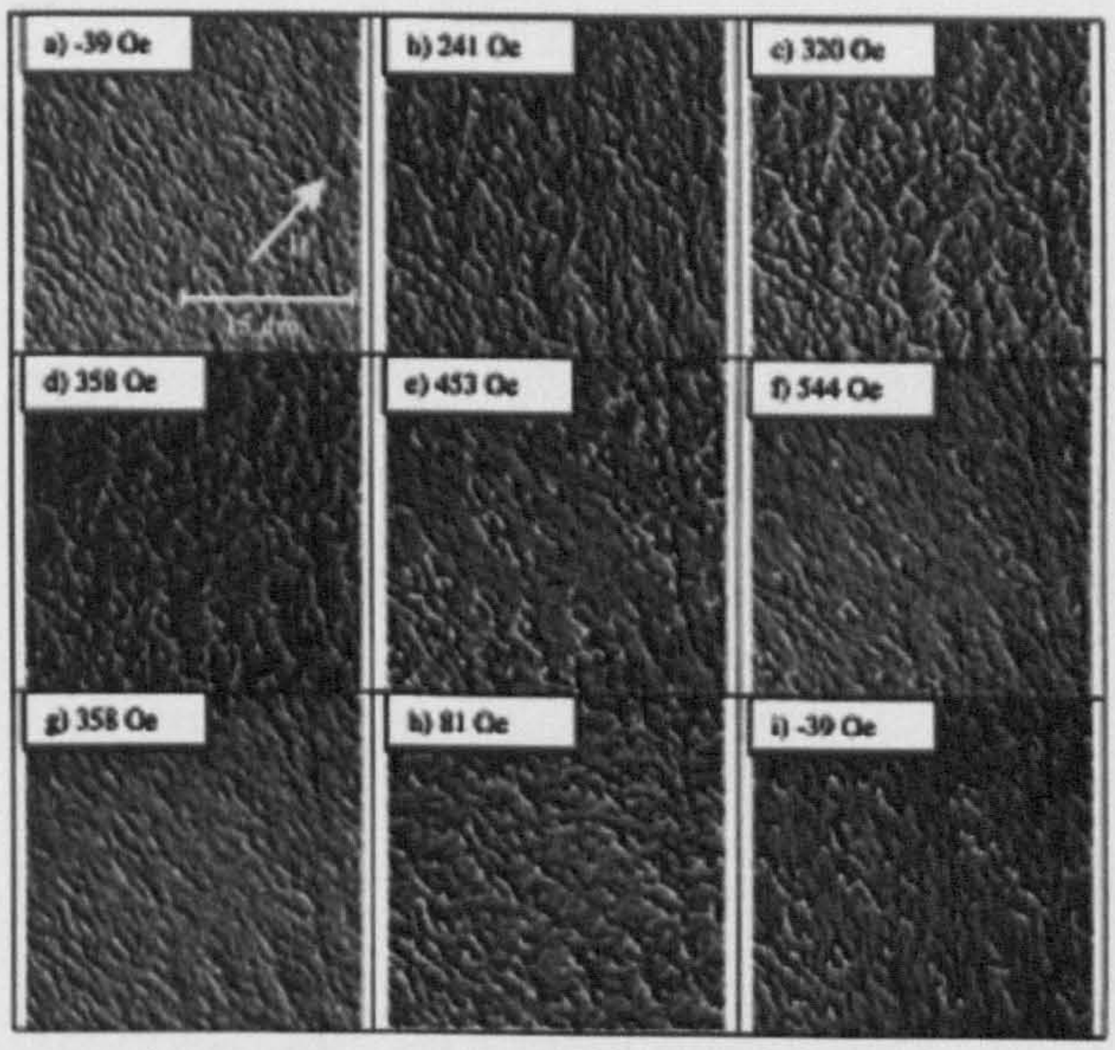

Figure 12 Fresnel images of as deposited $Ir_{20}Mn_{80}$(6nm)/ $Co_{90}Fe_{10}$(4nm) subjected to various magnetic fields. The applied field was parallel to the field applied during deposition. (After Gogol *et al.*, 2002).

2.6 Magnetisation Ripple

This type of magnetisation state is found in polycrystalline films that are exchange coupled, e.g. Permalloy. In such materials domain walls can be wider than the grains (50nm). The reason for this to happen lies in the anisotropy being weak, so the rotation per spin is low. The walls can be as wide as 2 to 50μm, being almost visible to the naked eye.

The anisotropy is never uniform. The direction of the anisotropy easy axes varies from one place to another in the film, or the magnitude of the anisotropy varies due to crystal effects and defects. This is called anisotropy dispersion. As a consequence of this, the direction of the local magnetisation varies from one site to another even within a domain (figure 13). The non-parallel magnetisation vectors add extra energy to the system. In addition, the demagnetising field at the ends of the sample, especially in small elements, leads to the divergence of the magnetisation just inside the sample. This has an effect in the creation of free poles even within a domain, creating stray fields and magnetostatic energy. As an example, a Permalloy thin film can be demagnetised by saturation in the hard direction. However, the anisotropy dispersion and the divergence of magnetisation lead to this ripple effect so the magnetisation is never uniform.

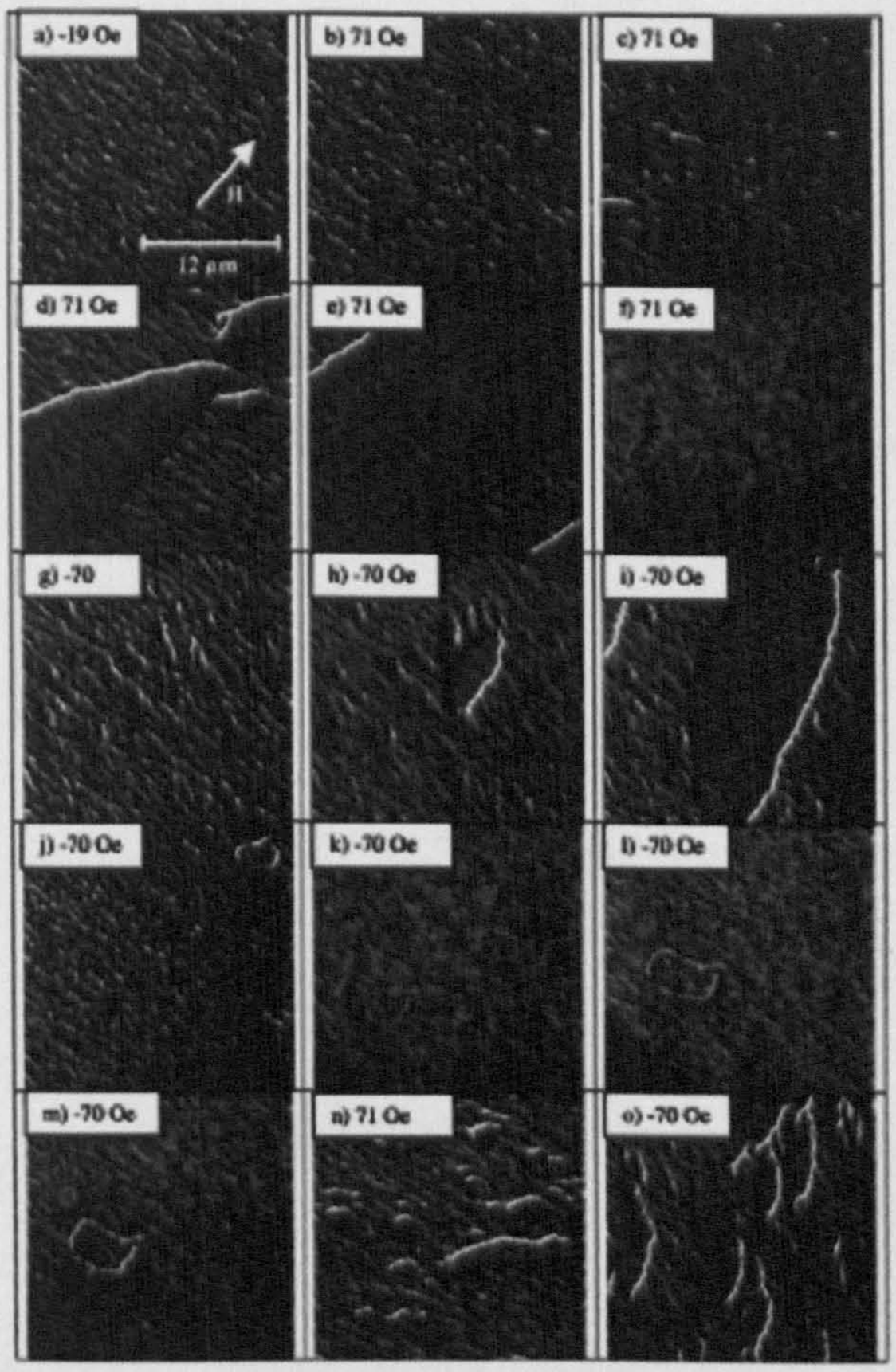

Figure 13 Fresnel images of as deposited $Ir_{20}Mn_{80}$(2nm)/ $Co_{90}Fe_{10}$(4nm) subjected to various magnetic fields. The applied field was parallel to the field applied during deposition. (After Gogol *et al.*, 2002).

Magnetisation ripple reduces the magnetostatic energy for a marginal increase in exchange energy. This type of magnetisation is characterised by a wavelike variation of the magnetisation. This ripple effect is depicted in figure 14(a), where the film is in a single-domain remanent state after saturation in an easy direction. If a field is applied transverse to the easy direction, as shown in 14(b), the magnetisation ripple persists. Its relation to the local easy axis direction is indicated. When the hard-axis field is removed half of the magnetic moments rotate clockwise while the other half rotate counter clockwise giving rise to the domain structure shown in 14(c). The vectors indicated in (b) and (c) apply only to a narrow horizontal strip. The ripple persists in the vertical direction in each domain (e.g. Cullity, 1972).

Hoffmann (1968) provided a review of the theory of magnetisation ripple in thin films. The theory included measurable parameters such as grain size, stresses and magnetostriction. The linear magnetisation ripple described the cases where the stray fields are transverse to the direction of the magnetisation. This makes the coupling of the spins to be perpendicular to the mean magnetisation direction. When the stray field is along the direction of the mean magnetisation a non-linear theory is necessary. Longitudinal stray field leads to the blocking of the magnetisation ripple (Hoffmann, 1966), which defines a state of small angle ripple domain walls (5°-10°) which is the beginning of a metastable state. This blocking state can be removed with small ac fields.

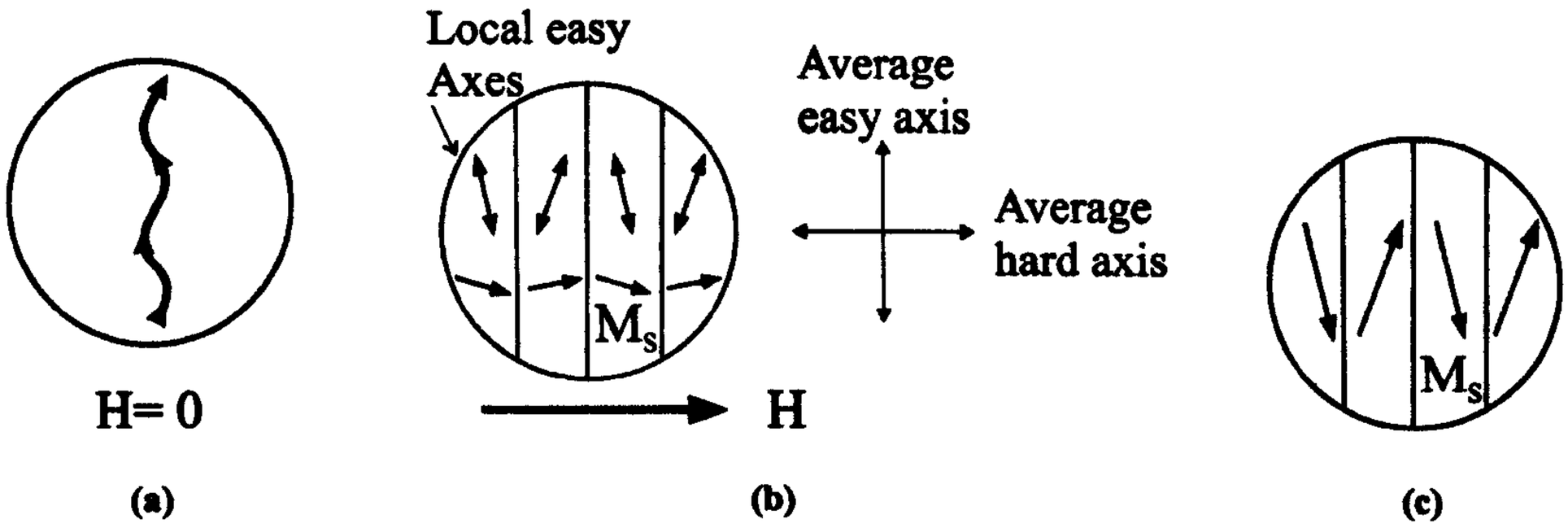

Figure 14 Schematic of domain formation in a thin film after magnetisation in the hard direction. (Prutton, M., 1964)

However the Hoffmann's ripple theory predicts a coercivity dependence on the median diameter of the grains proportional to $D^{0.5}$, where D is the median grain diameter. This prediction does not agree with the results obtained by Vopsaroiu *et al.* (2005), which are shown in figure 15. Their results show a coercivity dependence on D that has three different regimes. They explain their data on the basis of the random anisotropy model (Alben *et al.*, 1978). For very small grains, smaller than the exchange length, L_{ex}, H_C varies with D^6. For $D \cong L_{ex}$, H_C is constant. And for D larger than the domain wall width, H_C varies with D^{-1}.

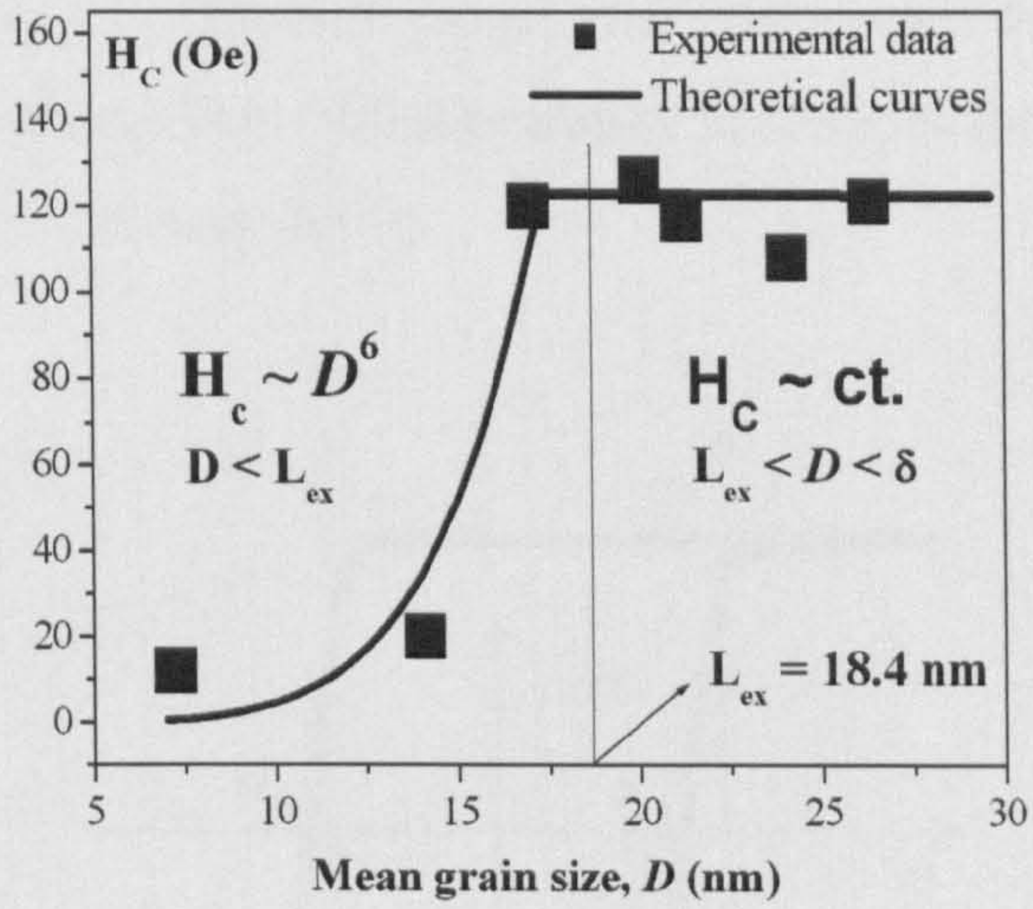

Figure 15 Coercivity dependence of grain size for CoFe (20nm). (Vopsaroiu *et al.*, 2005)

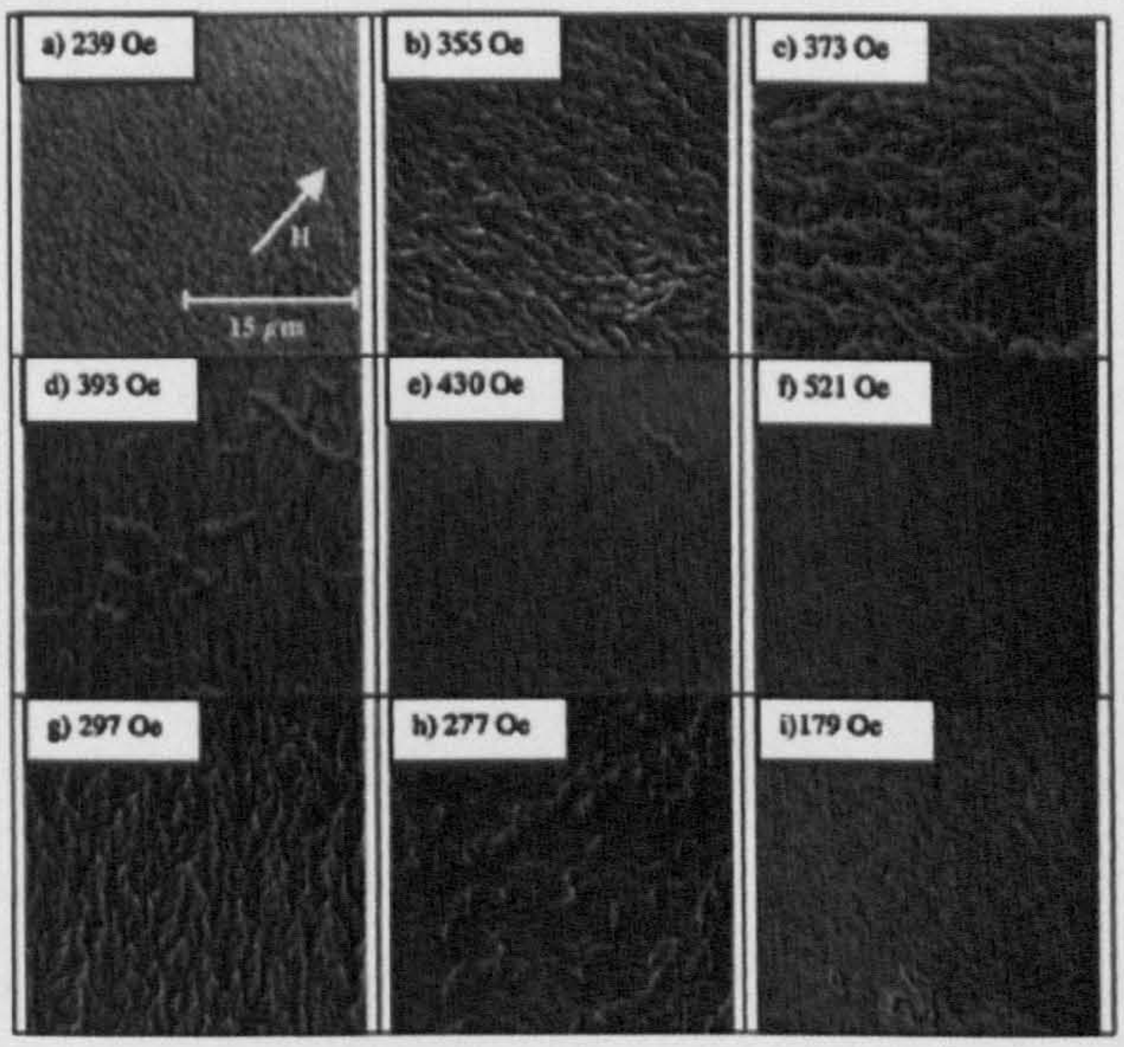

Figure 16 $Co_{90}Fe_{10}$(4nm)/$Ir_{20}Mn_{80}$(14nm) Fresnel mode Lorentz microscopy image. The applied field is parallel to the direction of the field applied during deposition (Gogol *et al.*, 2002)

For exchange coupled $Co_{90}Fe_{10}$(4nm)/$Ir_{20}Mn_{80}$(14nm) Fresnel mode Lorentz microscopy images are shown in figure 16. The sample was previously annealed for 20 s at 300 °C on a field of 500 Oe (Gogol *et al.*, 2002). Inset images (a) to (e) are from the magnetising branch of the hysteresis loop. Images (f) to (g) correspond to the demagnetising branch. When the field is reduced there is an increase in the intensity of magnetisation ripple. In 16(e) the domain structure is more irregular with domains larger than those observed in (a). In fact the mean orientation of domain walls at 16(e), which corresponds to point 3 in the hysteresis loop in figure 17, and at 16(g) (point 7 in

the hysteresis loop) are very different. Gogol *et al.* interpreted this difference in terms of the "natural angle" arising from different energy landscapes for the F to pass through in a magnetisation cycle (Stamps, 2000).

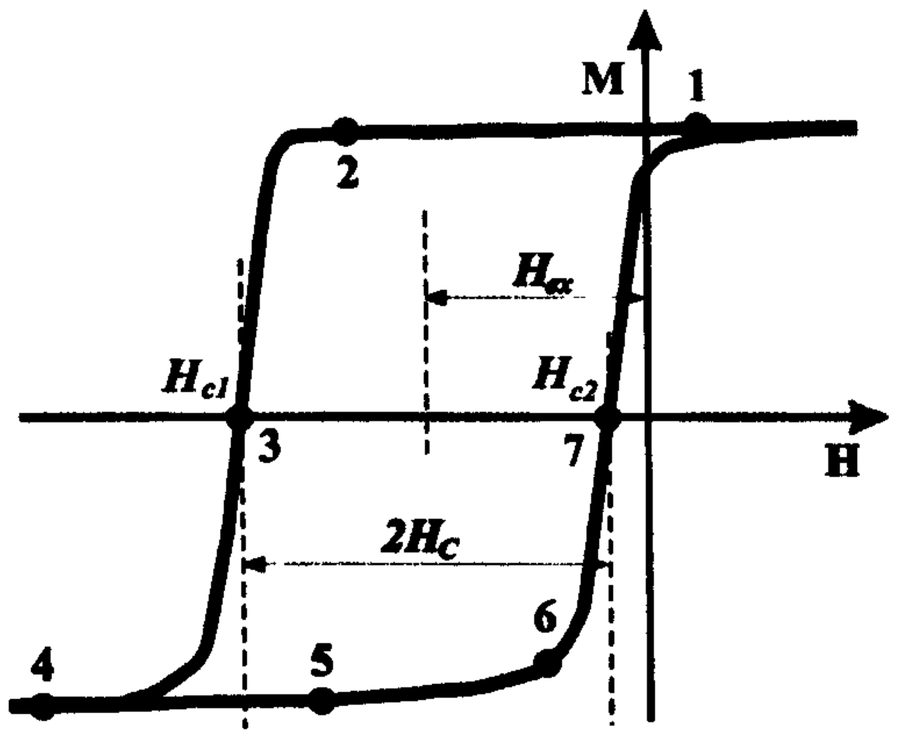

Figure 17 Seven point model hysteresis loop.

2.7 Antiferromagnetism

The role played by the *AF* is of critical importance in the understanding of the exchange bias phenomenon. Up until the 1980's *AF* materials were thought of as being of academic interest only in the study of the exchange interaction. Furthermore, there were no technical applications of *AF*s due to its zero net magnetisation. Even though the exchange bias phenomenon was discovered in 1956, in the quest for high coercivity particle magnets, it was not until the discovery of Giant Magneto-Resistance (GMR) in multilayers when *AF* materials and exchange bias became of great technological importance.

The exchange interaction was briefly described in section 2.4.1. Depending on whether the exchange integral between atoms, J, is positive or negative, their magnetic moment would lay parallel or antiparallel, giving rise to ferromagnetism or antiferromagnetism.

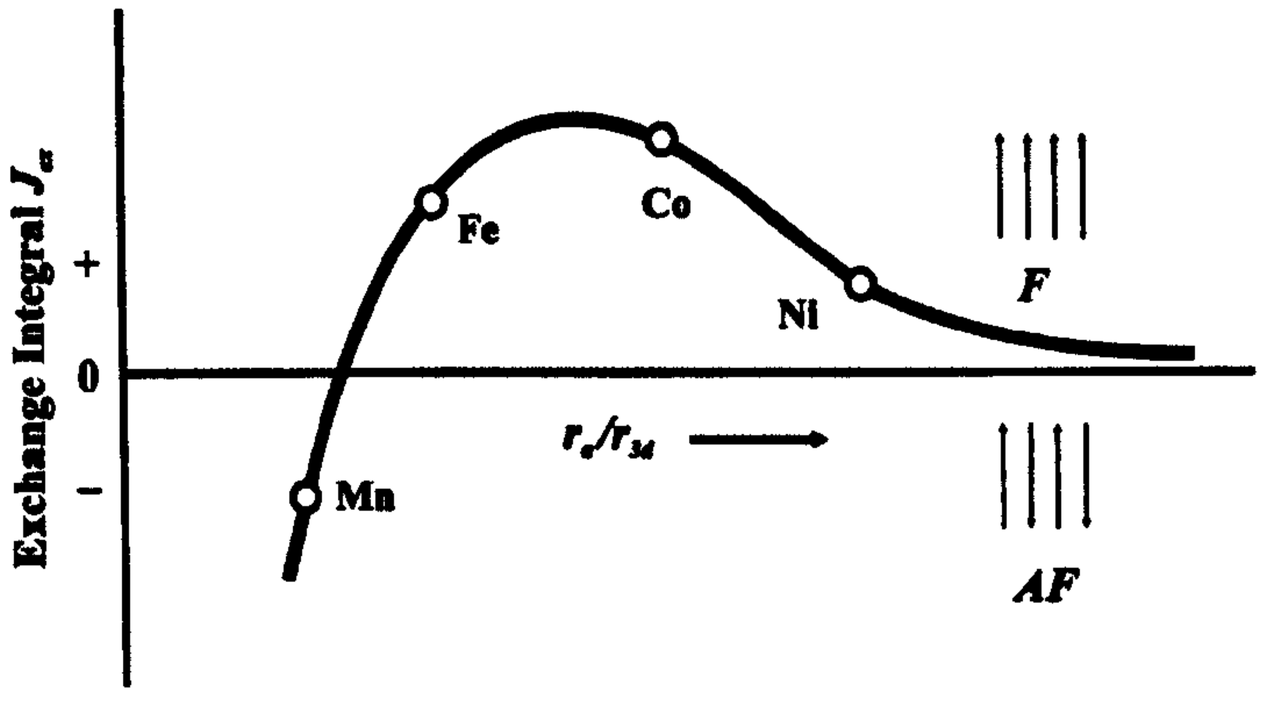

Figure 18 Schematic of the Bethe-Slater curve (e.g. Cullity, 1972).

Figure 18 shows the variation of the exchange integral with the ratio r_a/r_{3d}, where r_a is the atomic radius, and r_{3d} is the radius of its 3d shell of electrons. When this ratio is large the exchange integral is small and positive. When this ratio decreases, and the 3d electrons get closer, J is positive and gets stronger, leading to ferromagnetism, and then decreases to zero. If the spins are taken even closer, the exchange integral becomes negative and the spins have to lie antiparallel, giving rise to antiferromagnetism. Known the ratio r_a/r_{3d} this curve can be applied to different elements. A few pure metals are antiferromagnetic. Figure 18 shows that Mn is *AF*. Mn is antiferromagnetic below 100K, above this temperatures it is paramagnetic. The exchange integral also controls the Néel temperature. There are many oxides that are *AF*, having r_a/r_{3d} values much greater than these metals. The mechanism by which these oxides are *AF* is the super-exchange interaction. (See section 2.4.3).

Most of the studies of exchange bias in thin films with *AF* oxides involve CoO or NiO. All these oxides are fcc above T_N, with a slight distortion below T_N (Battle *et al,*.1979). The rocksalt structure shown in figure 19 is just two interweaved fcc structures with moments shown on the magnetic ions. Many oxides have this structure, e.g. NiO, CoO. The Néel temperature for these oxides decreases with decreasing film thickness (Wijn, 1991). Spins in any (111) plane are all parallel. All spins on adjacent planes are antiparallel to the spins in the reference plane, and parallel within the plane. These planes are too far apart for direct Heisenberg exchange. This arrangement is due to super-exchange interaction between nearest neighbouring ions along <100> via the intervening oxygen atom. The layer thickness dependence of T_N for CoO and NiO were obtained from heat capacity measurements (Abarra, *et al.* 1996). Both reach bulk T_N for

10nm thickness. Because of the variation of J_{ij} with ionic spacing it is possible to produce many alloys that are antiferromagnetic. Changing the interatomic distance r_{ij}, especially in alloys of Mn, leads to *AF* behaviour. Examples of *AF* alloys are MnSe, FeRh, NiMn. Technologically important in Exchange Bias are FeMn, IrMn, and PtMn.

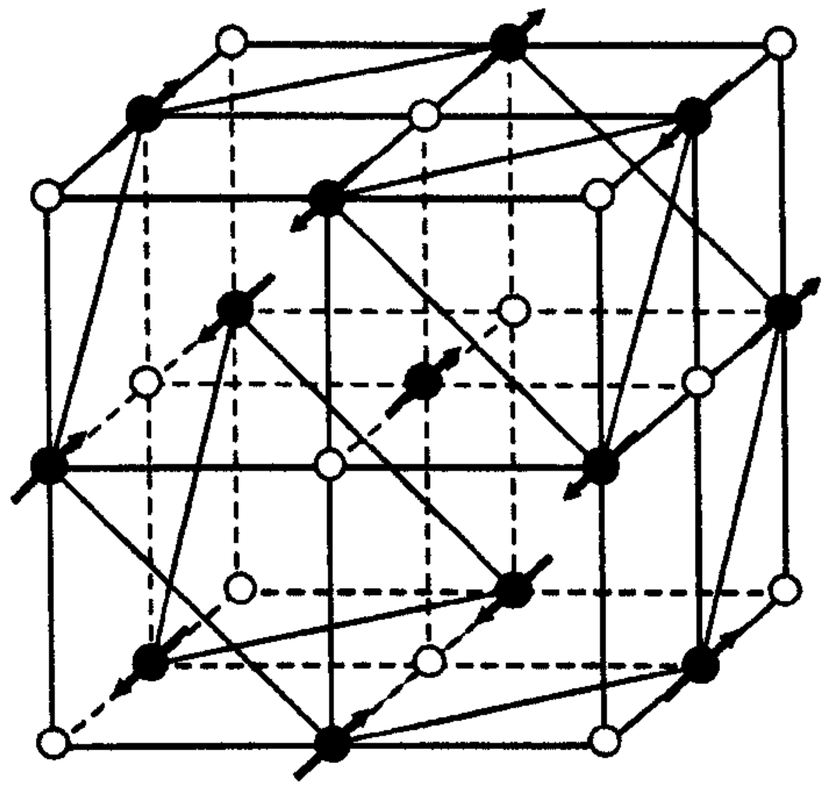

Figure 19 "Chemical and magnetic structure of NixCo(1~x)O antiferromagnetic materials. The shaded spheres represent the magnetic metal atoms, and the unfilled spheres represent the oxygen atoms". (After Berkowitz and Takano, 1999)

Metallic *AF*s are preferred to *AF* oxides for most applications due to their higher Néel temperatures and anisotropies. Despite this and that studies of exchange couples with metallic *AF*s are more numerous, it seems that there is less understanding of the exchange bias phenomenon involving metallic *AF*s. This is due to several factors, such as deviations of the crystal structures from the cubic symmetry, more complex spin structures than in the case of oxide *AF*s and higher T_N. This means that in some cases the field cooling procedure might damage the interface quality of the exchange coupled structure due to interdiffusion of the layers or grain growth (Berkowitz and Takano, 1999).

Oxides and Metals				Alloys			
Substance	Structure	T_N (K)	ΘT_0 (K)	Substance	Structure	T_N (K)	ΘT_0 (K)
MnO	fcc	122	610	FeF_2	bct	79	117
FeO	fcc	198	570	MnAn			
*CoO	fcc	293	280	MnSe			
*NiO	fcc	523	3000	FeRh			
				NiMn	fct	1070	-
Cr	bcc	310	Cr	FeMn	fcc	490	-
α-Mn	cc	100	α-Mn	IrMn	fcc	690	-
				PtMn	fct	480-980	-

Table 2 Common antiferromagnets.(Nogués *et al.*, 1999)

2.8 Crystalline and Magnetic Structure of $Ir_{30}Mn_{70}$

The most common metallic *AF* used in industry for the fabrication of spin-valve sensors is IrMn. This is due to fabrication requirements such as high resistance, high GMR signal, low total thickness and high exchange bias (Childress *et al.*, 2001). The samples studied in this work contain $Ir_{30}Mn_{70}$. The phase diagrams of IrMn alloys is shown in figure 20.

From figure 20, according to composition considerations, $Ir_{30}Mn_{70}$ should have a structure of the ordered $AuCu_3$-type $IrMn_3$ ($L1_2$-Pm3m) (Raub and Mahler, 1955). According to Yamaoka (1974) IrMn alloys in the composition range of 14 to 31 at% Ir, quenched from 1250-1350K are nominally disordered fcc. In the composition range of 8 to 13 at% Ir a disordered fct *AF*s with axial ratio $c/a>1$. The $AuCu_3$-type $IrMn_3$ structure is only found in alloys with approximately 25% Ir annealed below 1000K.

Yamaoka *et al.* (1971, 1974) extended the study of γ-phase Mn to IrMn alloys in both ordered and disordered states. Figure 21 shows the magnetic phase diagram of γ-phase Ir_xMn_{1-x} alloy obtained by magnetic susceptibility measurements. As shown by Umebayashi *et al.* (1966) there are three stable spin configurations which minimise the exchange interaction energy and the anisotropy energy of the fcc structures with identical spins. The three configurations are shown in figure 22.

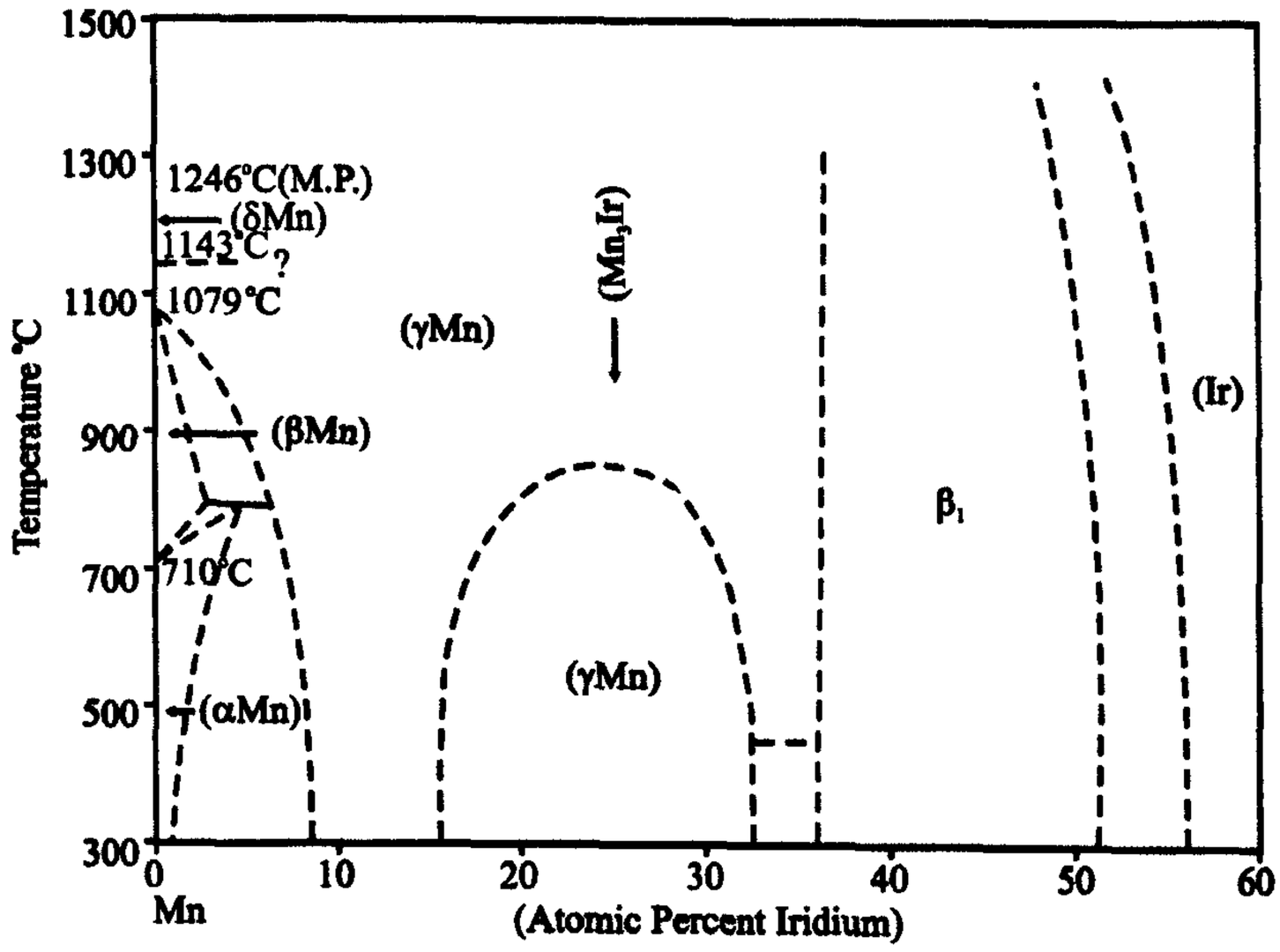

Figure 20 Phase diagram of IrMn alloys (Binary Alloy Phase Diagram, American Society for Metals, p1421 (1986)).

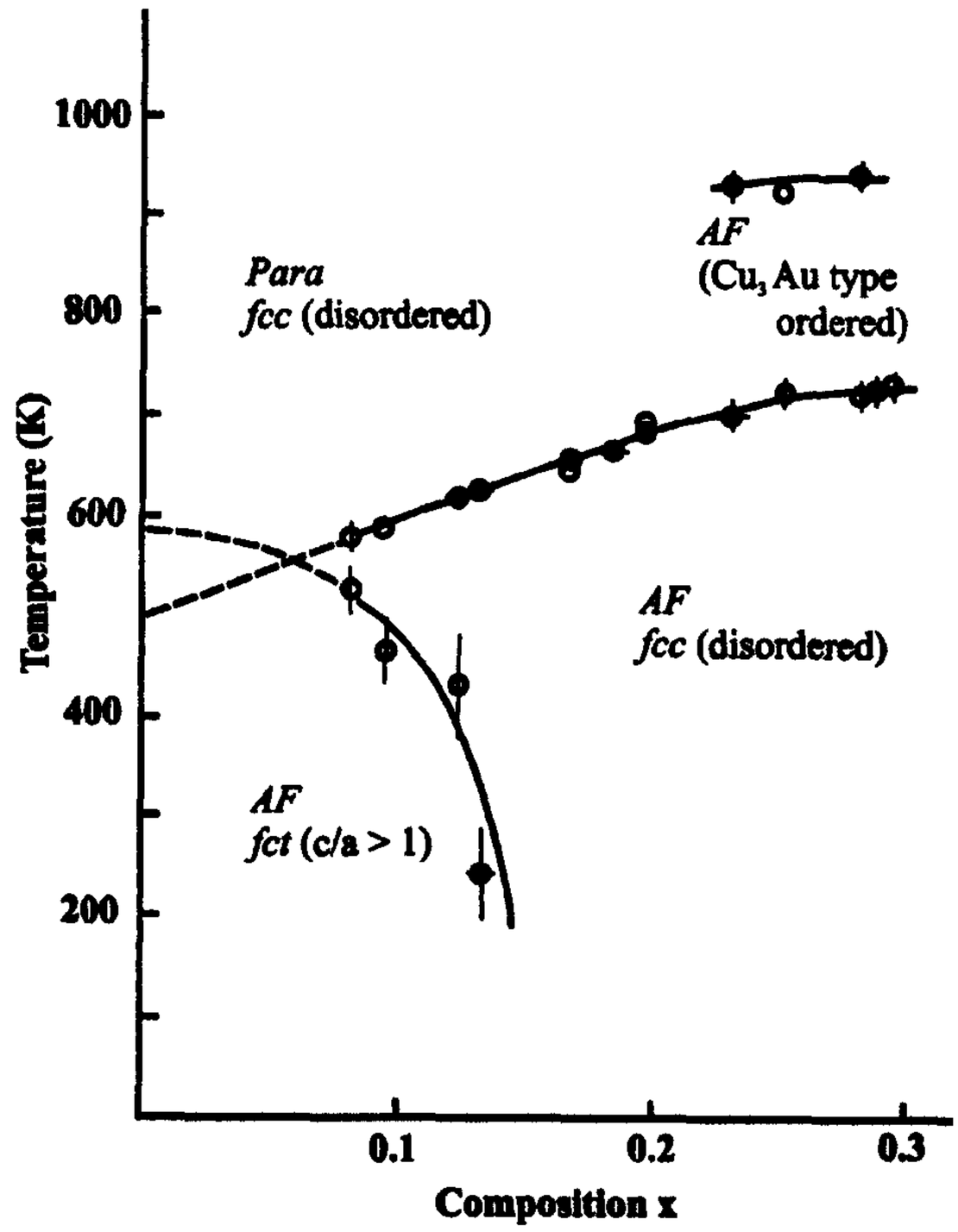

Figure 21 Magnetic phase diagram of γ-phase Ir_xMn_{1-x} alloy system. After Yamaoka (1974)

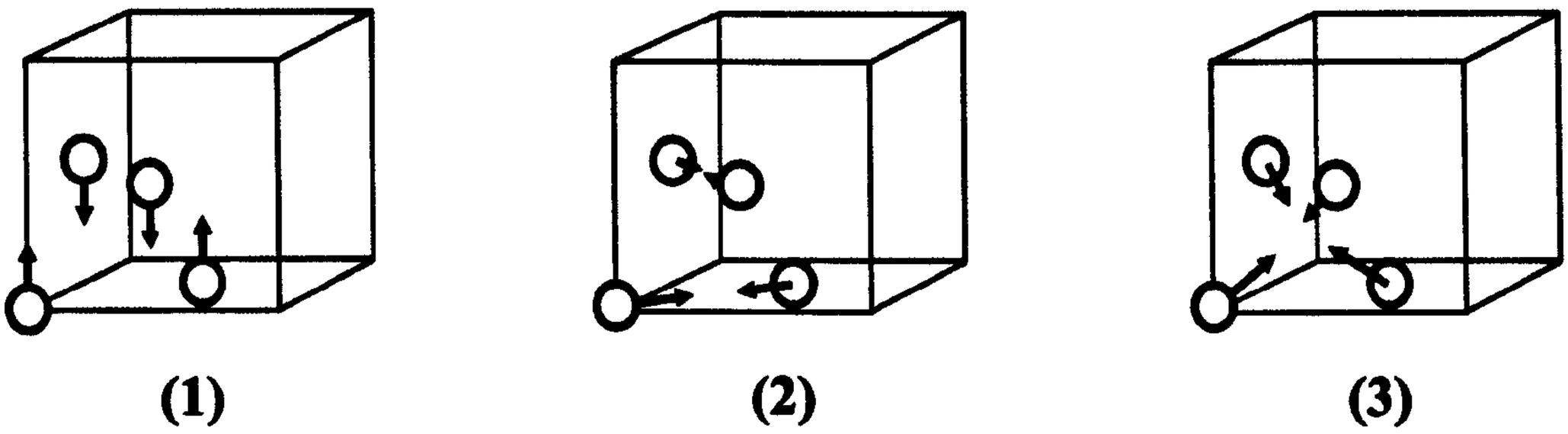

Figure 22 Stable spin structures of the fcc structure with identical spins (After Umebayashi *et al*, 1966).

FeMn alloys have spin configuration (3), (Umebayashi *et al*. 1966). Neutron diffraction studies (Yamaoka *et al*., 1971 and 1974) on single crystals showed that the most probable spin structure for the γ-phase IrMn alloys is configuration (1) which is depicted in figure 22, showing the two sublattice spin structure.

According to these data our $Ir_{30}Mn_{70}$ layer is nominally disordered fcc (γ) phase. For alloys with this structure, with the percentage of Ir varying from 14 to 31, the T_N varies from ~ 600 to 750K with increasing Ir (Yamaoka *et al*., 1974). The average spin on each (002) plane is aligned parallel along the c-axis, with alternating opposite sign in adjacent (002) planes. The average moment per atom is ~2.5μ_B up to ~20 at% Mn, and falls to ~0.8 μ_B at ~25.6 at% Mn (van der Heijden *et al*., 1998).

Deposition temperature conditions may cause the presence of ordered $IrMn_3$ within the disordered fcc phase, as reported by Imakita et al. (2004). They studied $Ir_{27}Mn_{73}$-$Co_{70}Fe_{30}$ bilayers. The $Ir_{27}Mn_{73}$ was deposited at substrate temperatures up to 200°C, the $Co_{70}Fe_{30}$ was deposited after cooling to room temperature and then the bilayer was annealed at 400°C for 1 hour in 1kOe. Their results showed superlattice lines in <111> textured $Ir_{27}Mn_{73}$ deposited at temperatures higher than 100°C, indicating the presence of ordered $IrMn_3$. Changes in the temperature of deposition and annealing resulted in variations of the interfacial coupling energy being a maximum ($\Delta\sigma$ = 1.3erg/cm^2) when the deposition of $Ir_{27}Mn_{73}$ was at 170°C the annealing at 320°C. They suggested that these superior properties were due to the increased presence of ordered $IrMn_3$. The effects of annealing in exchange biased couples will be described in more in detail in section 6.2.4.

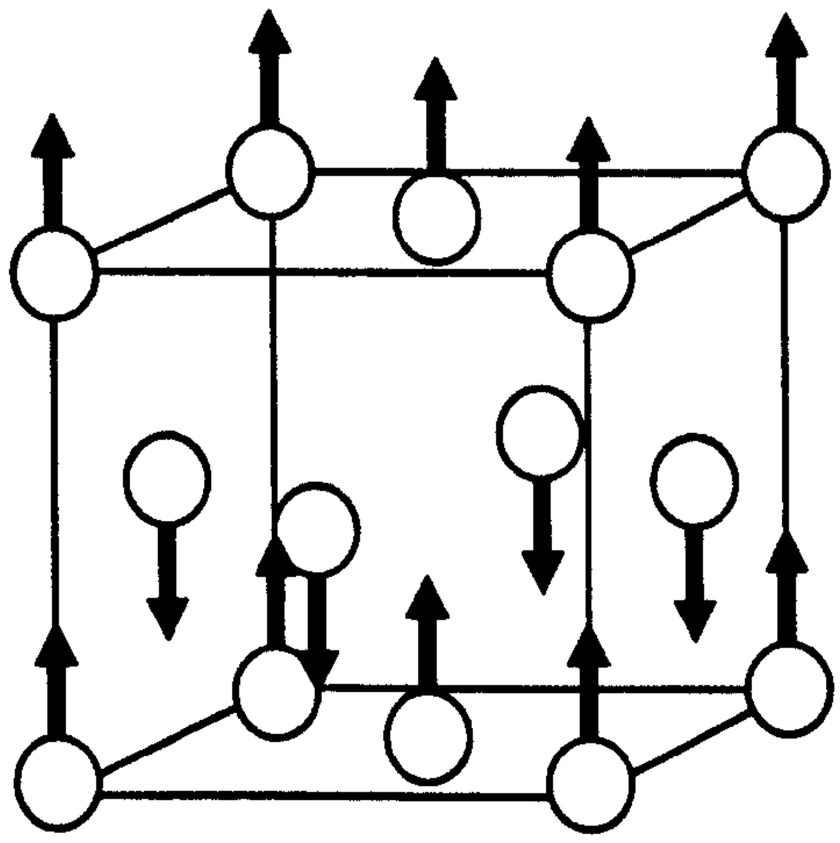

Figure 23 Antiferromagnetic two-sublattice structure of the disordered γ-phase of IrMn alloys. (After Yamaoka *et al.*, 1974).

2.9 Superparamagnetism

One of the basic features of the way that exchange bias is conceived in this work is the description of the *AF* as an assembly of grains. This conception of exchange bias is based on a model proposed by Fulcomer and Charap (1972). This model is described in chapter 4. The *AF* grains are thought to be in a single domain state, each of which interacts with the *F* through exchange interaction. The grains are distributed in size, also the anisotropy easy axis directions of each grain are distributed. The grains are susceptible to thermal activation in the orientation of its moment at the interface of the *AF*-*F* bilayer above their blocking temperature, giving rise to superparamagnetic behaviour.

2.9.1 Superparamagnetism in single domain particles

When atoms assemble to form nanoparticles these can be in a single domain or multidomain state. The former state will prevail if its energy is less than that required to form a domain wall. The size of particle that forms a single domain state depends on the anisotropy (Frenkel and Dorfman, 1930). Equation 2.3 relates the anisotropy to the critical radius, r_c, of a ferromagnetic particle to be in a single domain state, where A is

the exchange stiffness, K the unidirectional anisotropy, and M_S the saturation magnetisation (O'Handley, 2000).

$$r_c \approx 9\frac{(AK)^{1/2}}{\mu_0 M_S^{\,2}} \tag{2.3}$$

Single domain magnetic particles are of great importance for magnetic recording media. Magnetic nanoparticles with uniaxial anisotropy behave as a two state system. They are susceptible to magnetisation reversal under the influence of temperature in a given time of observation at zero applied field. This occurs when the ambient thermal energy is large enough to overcome the energy barrier to magnetisation reversal in the time of measurement, ΔE, which in zero applied field is given by the anisotropy energy, KV (Néel, 1949). In this case the particles are said to be in a superparamagnetic state (Bean and Livingston, 1959). The critical volume below which this behaviour is observed depends on the time of measurement relative to the relaxation time, τ, which is the time it takes for the magnetisation to decay to $1/e$ or 37% of its initial value (Néel, 1949),

$$\tau^{-1} = f_0 \exp\left(\frac{-\Delta E}{k_B T}\right) \tag{2.4}$$

where

$$\Delta E = KV\left(1 - H/H_K\right)^2 \tag{2.5}$$

f_0 is the attempt frequency which is taken to be 10^9Hz (Kneller *et al*, 1966), V the particle volume, k_B Boltzman's constant, K the anisotropy energy density and T the temperature. H_K is the anisotropy field which for aligned easy axes is given by

$$H_K = 2K/M_S \tag{2.6}$$

The size at which a particle becomes superparamagnetic is found when KV is less than a multiple of $k_B T$, for a given attempt frequency f_0. For $f_0 = 10^9$ Hz (e.g. Kneller, 1969), and an observation time of 100s, the superparamagnetic criterion

$$KV = 25 k_B T . \tag{2.7}$$

This means that when an applied field reduces the energy barrier KV to less than or equivalent than $25 k_B T$ the magnetisation of the nanoparticle will reverse in 100 seconds. This condition is applicable for the determination of the superparamagnetic limit on the particle size of recording media systems. For these systems the observation time is considered to be τ = 10 years leading to a proportionality constant of 40. Particles with volume bigger than the critical volume V_p, exhibit stable magnetic behaviour and are termed "blocked" particles,

$$V_p = \frac{25 k_b T}{K} . \tag{2.8}$$

Accordingly, given a particle volume, it will become "blocked", when its temperature is less than the blocking temperature, T_B, given by

$$T_B = \frac{K V_p}{25 k_B} . \tag{2.9}$$

Superparamagnetic systems exhibit no hysteresis and saturate in modest applied fields and their magnetisation can be described by the Langevin function $L(\alpha)$

$$L(\alpha) = \coth \alpha - \frac{1}{\alpha} \quad , \text{where} \quad \alpha = \frac{\mu H}{k_B T} . \tag{2.10}$$

Hence such systems exhibit superimposition of loops measured at different temperatures when they are plotted as a function of H/T. These phenomena have been observed by Bean and Jacobs (1956). Ferromagnetic systems of nanoparticles of these characteristics will behave according to the Langevin function when their volume is less

than V_p. In the case of "blocked" particles, those with volume greater than V_p, will behave as ferromagnetic systems. Particles with a volume equal to V_p will experience time dependence according to (Néel, 1949)

$$\frac{M(t)}{M(0)} = \exp\left(-t/\tau\right). \tag{2.11}$$

Accordingly, systems of nanoparticles with distributed sizes, or volumes, or distributed anisotropies will show a distribution of blocking temperatures. Substitution of equation 2.4 in equation 2.11 gives

$$M(t) = M(0)\exp-\left(tf_0 \exp\left(KV/k_BT\right)\right). \tag{2.12}$$

Street and Woolley (1949) obtained analytical solutions for equation 2.12 for the special case of $tf_0 >> 1$, and f_0 independent of the energy barrier, which to a first approximation is the case of the systems of nanoparticles: $\Delta E = KV$, and f_0 is independent of K and V. Hence, at first approximation the change of magnetisation, M, in time t is given by

$$\Delta M = S\ln t + const\,. \tag{2.13}$$

The variation of S with applied field for ferromagnets was considered by Gaunt (1976). Using a phenomenological theory, Gaunt predicted the maximum value of S to be at $H = H_C$ as observed by Street and Woolley (1949). O'Grady *et al.*, (1981) showed that eq.2.13 is generally true and gave a general analytic solution for eq.2.12 for systems containing a distribution of particle sizes. Uren *et al.*, (1988) showed that the maximum value of S occurs at H_r, the remanent coercivity, obtained from DC demagnetisation remanence measurements. According to eq. 2.13, the magnetisation decay is given by

$$M(H,t) = M(H,0) \pm S(H)\ln t\,. \tag{2.14}$$

Hence,

$$S(H) = dM(H)/d\ln t\,, \tag{2.15}$$

the magnetic viscosity coefficient, which is maximum when the applied field is close to the coercivity. This law has been shown to be a first order approximation of a series expansion (el-Hilo *et al.*1993). Only if the distribution of energy barriers $f(\Delta E)$ remains constant over the time of measurement the ln*t* law is followed. Otherwise, non-linear variations of magnetisation with ln*t* are observed. The variation will be convex when $f(\Delta E(t))$ is increasing with time and concave when $f(\Delta E(t))$ is decreasing with time.

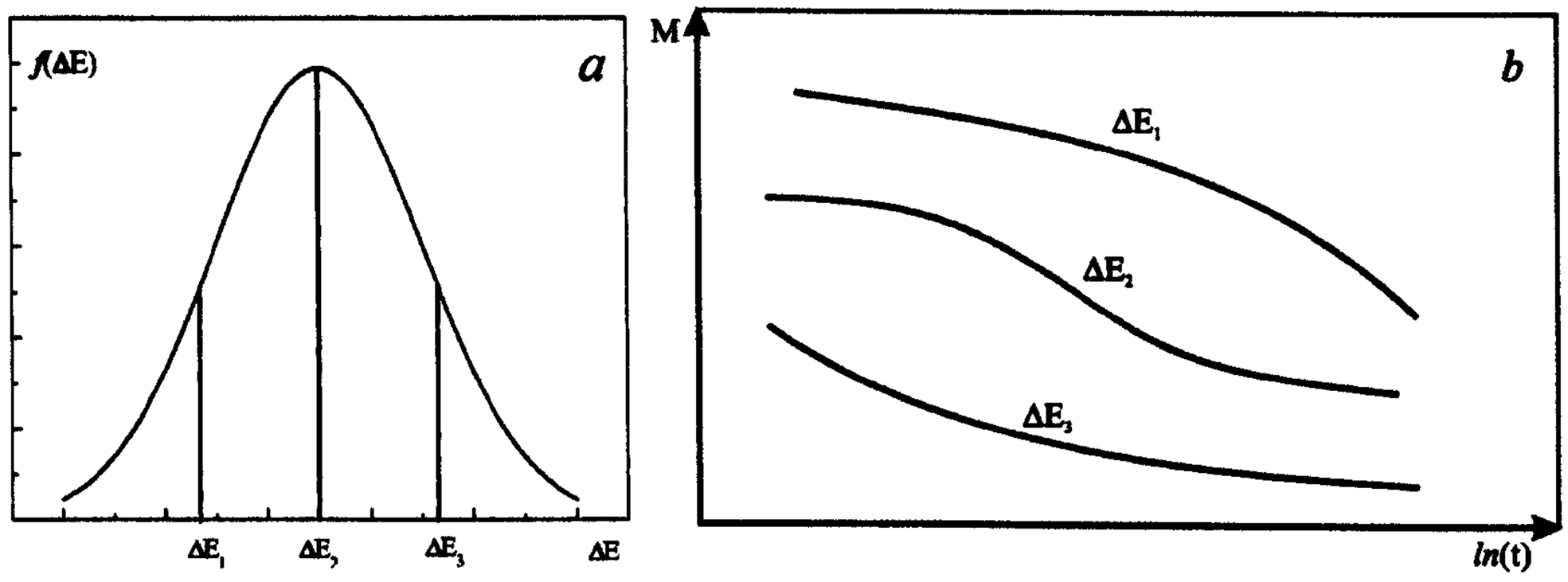

Figure 24 (a) Schematic of a symmetric energy barrier distribution showing three different values of energy barriers to reversal. **(b)** Non-linear time dependence of the magnetic viscosity coefficient shown at three different stages in the energy barrier distribution.

The magnitude of the non-linearity was found to increase when the energy barrier distribution becomes narrow. This is a result of $S(H)$ being a function of $f(\Delta E)$ (Gaunt, 1986). At a critical energy barrier ΔE_C activated by a field H,

$$S(H) = 2M_S k_B T f[\Delta E_C(H)] \qquad (2.16)$$

This explains the relation between the magnetisation time dependence and the energy barrier distribution.

2.9.2 Superparamagnetism and antiferromagnetism in exchange biased systems.

As shown in section 2.9.1, Néel's study (1949) of the reversal of ferromagnetic particles by thermal activation showed that the relaxation time of a system of particles with their easy axis aligned parallel to the direction of the applied field which reverse coherently under thermal activation is given by the Arrhenius-Néel law, obtained by substitution of eq. 2.5 in eq. 2.4,

$$\tau^{-1} = f_0 \exp\left(-\Delta E / k_B T\right) = f_0 \exp\left(-KV\left(1 - H/H_K\right)^2 / k_B T\right). \qquad (2.17)$$

where ΔE is the height of the energy barrier to reversal, and f_0 is taken to be 10^9 Hz, (Kneller *et al*, 1966). For a relaxation time of 100s, the superparamagnetic criterion is given by

$$\Delta E = KV(1 - H/H_K)^2 = 25 k_B T \qquad (2.18)$$

Hence, a distribution of particle sizes, anisotropy orientation , or coupling orientation give rise to a distribution of energy barriers. Accordingly, a distribution of blocking temperatures would appear given by,

$$f(T_B) = k_B{}^{-1} f(\Delta E/25) \qquad (2.19)$$

For the case of sputtered, polycrystalline exchange biased systems such as the ones studied in this work, magnetisation switching similar to that described by equation 2.19 would be expected. The origins of the distribution of energy barriers to reversal will be discussed in section 6.2 and 6.3 in which the possible origins of the training effect will be investigated. To give an idea of the complexity of this task, it should be acknowledged the number of different models proposed for exchange bias, some of which are briefly described in chapter 4.

A typical hysteresis loop for an exchange-biased system has been shown in figure 17. Different stages on the hysteresis loop are marked with numbers according to the 7-point description (Goodman *et al.*, 2001), which is described in section 2.11.

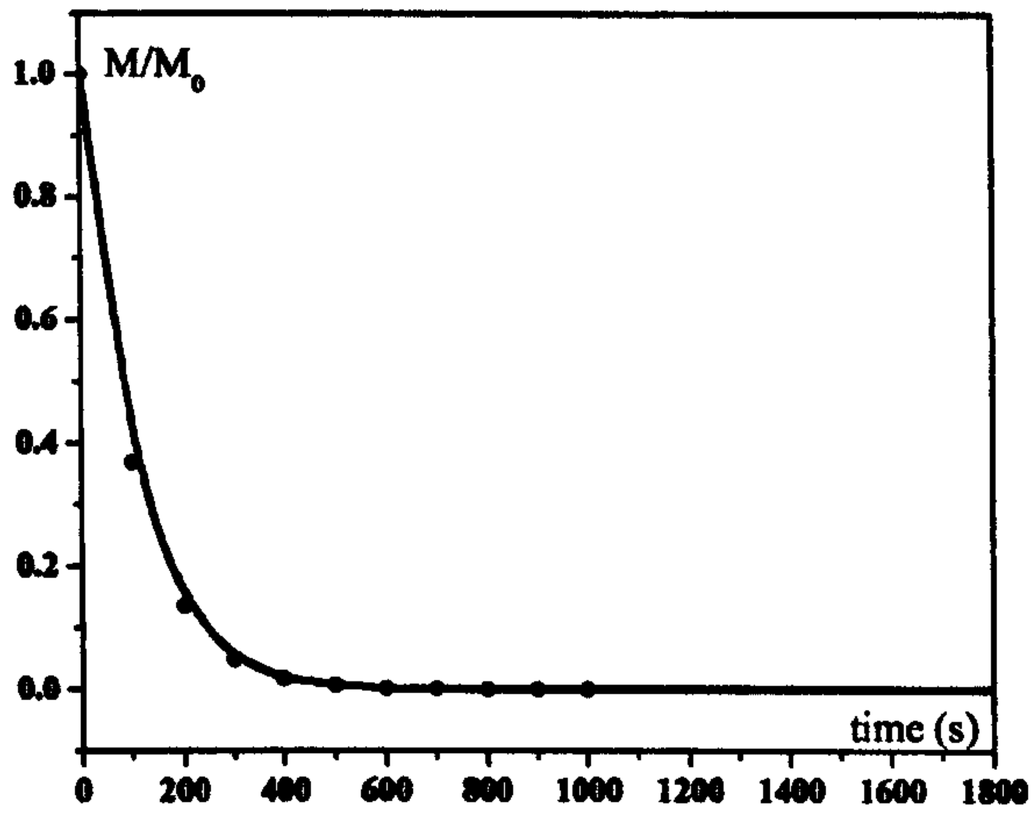

Figure 25 Decay of the initial magnetisation.

According to equation 2.7, after 100s at a temperature T, the initial magnetisation will decay to 37% of its initial value, after 10^3s the rate of reversal will decrease rapidly with increasing time.

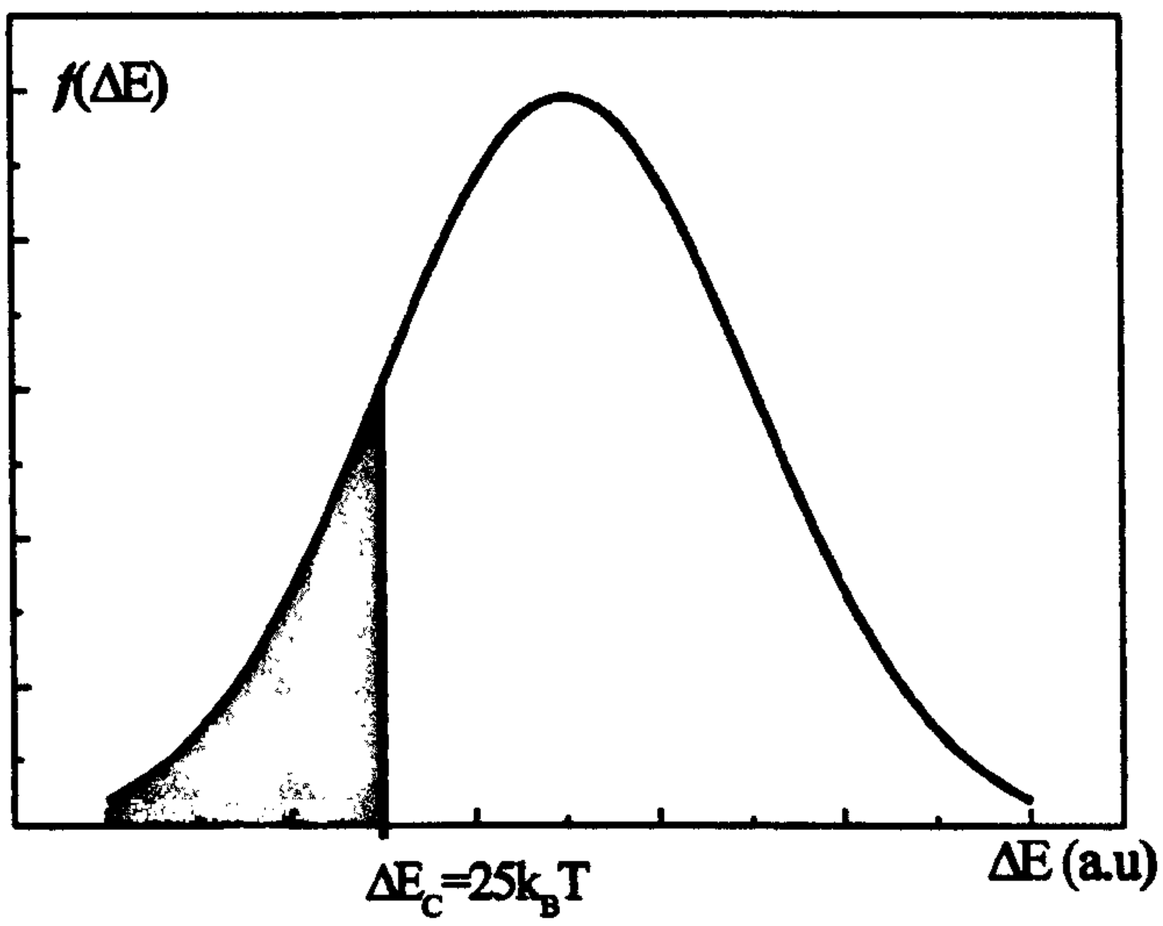

Figure 26. Schematic of a distribution of energy barriers to reversal. showing an energy barrier to reversal $25k_BT$. Grains with $\Delta E_C = 25k_BT$ will undergo time dependent reversal. Those with lower ΔE_C will reverse, and those with higher ΔE_C will remain "blocked".

In the samples studied the granular *AF* layer, fcc IrMn (a = 3.76Å), is grown epitaxially on the *F*, fcc CoFe (a = 3.6 Å), with a magnetic structure as shown in figure 23. Hence there are two easy axes available for the magnetisation of the *AF* spins. If they were not grown epitaxial there would be three easy axes. When the field applied to the exchange biased system reverses the direction of the *F* layer (points 2-4 in figure 17), the effect of the reversal of the exchange field on the *AF* grains and thermal activation promote the reversal of the *AF* ordered state.

As time progresses, the *AF* spins will become more decoupled from the anisotropy axes. When the thermal energy equals $\Delta E = KV$, the spins decouple from their easy axes although they are still antiferromagnetically coupled to each other. This occurs when the temperature of the system reaches T_B for the grain, given by equation 2.6. If the temperature is increased to T_N, the spins become decoupled from each other and lose their antiferromagnetic order.

The fact that the *AF* grains become "unblocked" and have superparamagnetic behaviour over T_B, is used in the work developed in this thesis to modify the amount of *AF* material that remains in its original state and to "reset" the state of the *AF* after measurement. See chapter 6, section 2.

2.10 Domains in AF thin films

Systems exhibit superparamagnetism when the thermal energy $25k_BT$ overcomes the energy barrier *KV*. Néel derived his equation for superparamagnetism independently of the nature of the energy barrier involved. For example, in the case of systems subject to domain wall pinning, given that the energy barrier, ΔE, to unpin the domain walls is equal or less than $25k_BT$ a similar relaxation would take place in 100s. Hence, superparamagnetism and time dependence would occur in CoFe or in IrMn if there are pinned domain walls.

Several authors have observed *AF* domains in thin films (see Stöhr *et al.*,1999, Scholl *et al.*, 2000, and Hillebrecht *et al.*, 2001). Observation of domains in exchange biased systems in both the *F* and *AF* layers has been claimed by Nolting *et al.*, (2000) on

$LaFeO_3$/Co grown epitaxially by molecular beam epitaxy (MBE). X-ray magnetic dichroism spectro-microscopy measurements showed that the alignment of the *F* spins is determined, domain by domain, by the spin directions in the *AF* as shown in figure 28.

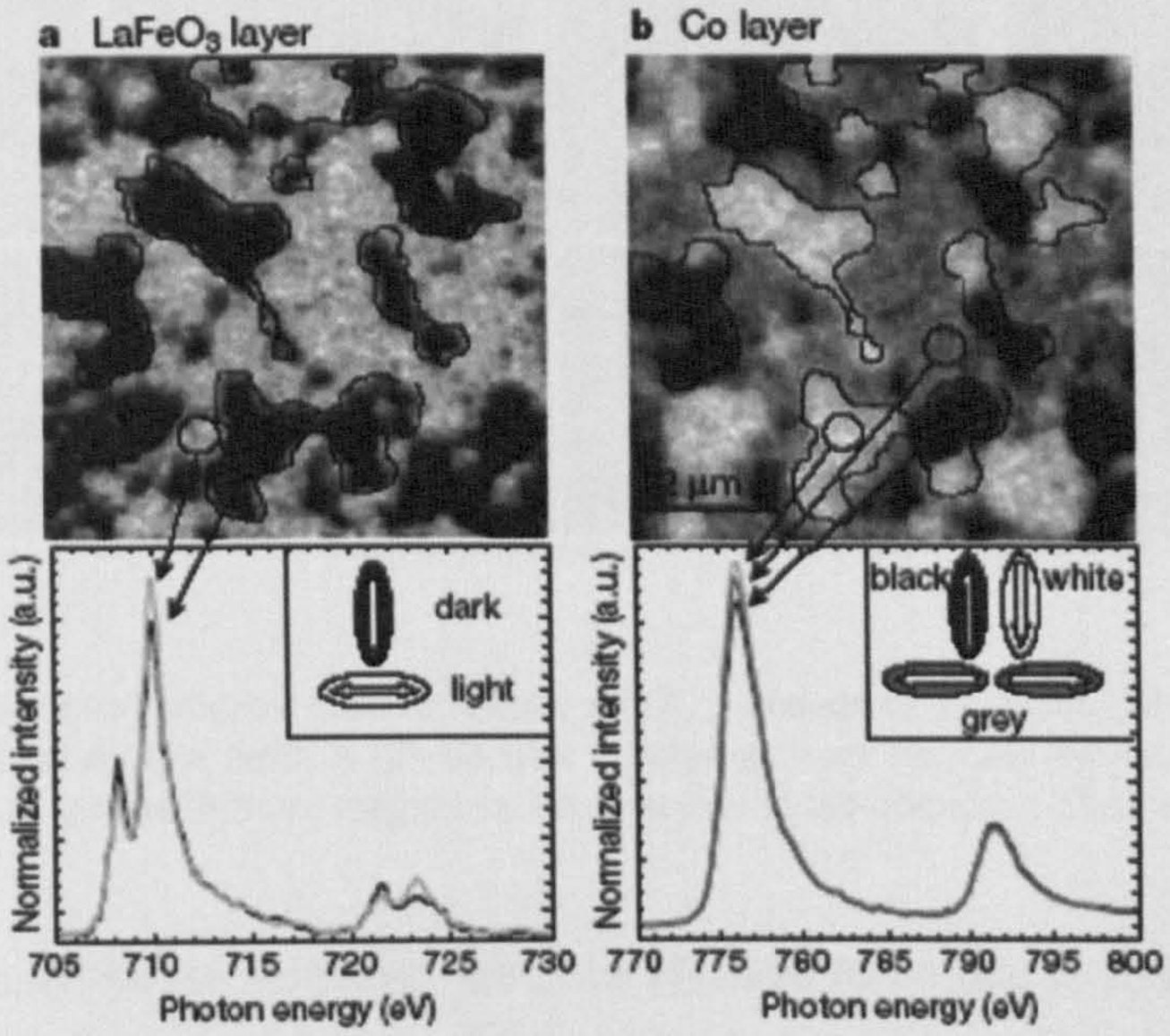

Figure 28 Images of the domain structure in the *AF* layer (a) and in the 12Å thick *F* layer (b) grown on top of the same substrate region. Spectra shown recorded by PEEM. (Nolting *et al.*, (2000))

Sputtered exchange coupled bilayers are granular. The grains that form each layer can be in a single domain state or contain domain walls. Domains can be also be formed by exchange coupled grains, i.e. magnetic domains can traverse the grain boundary apparently undisturbed as observed by Hubert and Schäfer (1998) on Fe polycrystalline thin films. As far as the author is aware, there has not been observed magnetic domains in polycrystalline *AF* thin films.

Shull *et al.*, (2003), using a magneto-optic indicator film technique (MOIF), observed that the domains in the *AF* are stationary during magnetisation reversal of the *F*. In FeMnC/FeMn exchange coupled systems that showed zero exchange bias as deposited, they concluded that domain wall movement in the *F* does not imply domain wall movement in the *AF*. The resulting domain structure is an exchange spring parallel to the *AF*/*F* interface created during the reversal of the *F* magnetisation.

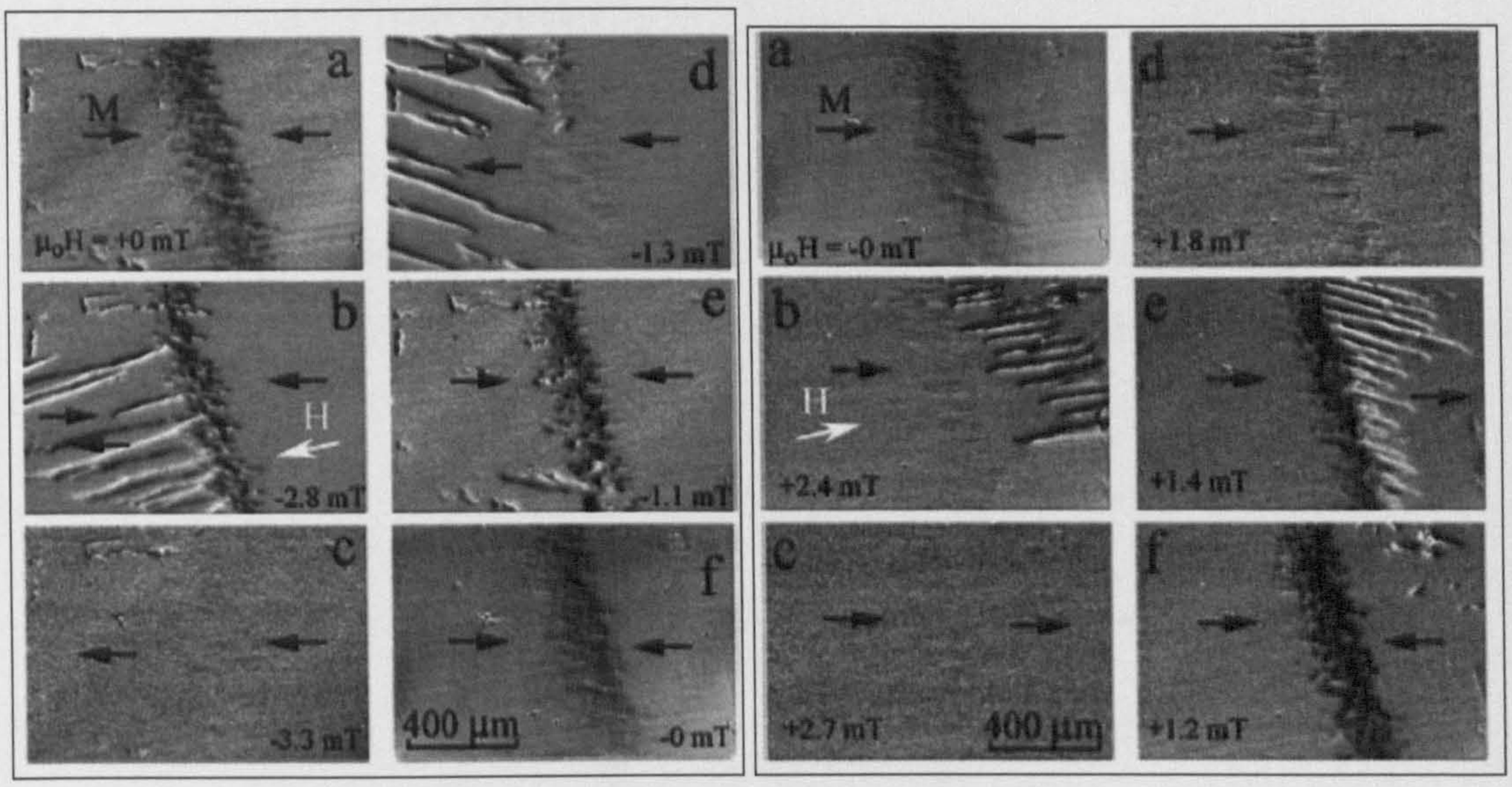

Figure 29. Magneto-optic indicator film technique (MOIF) images of FeMn/$Fe_{76}Mn_6C_{18}$ bilayer during application and reduction of a field $\approx 12°$ counter clockwise from the easy magnetisation direction in both directions. Black arrows indicate magnetisation direction in the domains (Shull *et al.*, 2003).

The stabilisation of the *AF* domains has been claimed to be due to interface roughness (Malozemoff, 1987, 1988a, 1988b), or due to volume defects (Keller *et al.*, 2002) such as grains, twin boundaries, or crystal defects. All of these are sources for domain wall pinning, which give rise to energy barriers. Changes in the magnetic state in the *AF* can arise within 100s by processes such as domain nucleation or wall motion when the energy barrier to unpin a domain wall is $\leq 25k_BT$, or by a change of the magnetisation state within a grain when the energy barrier to reverse its state is $\leq 25k_BT$, assuming that all spins within a grain behave coherently [Fulcomer and Charap (1972a,b) , Nishioka *et al.*(1996)]. Any of these processes result in the change of the original state related to a local energy minimum, to another energy magnetisation state in another local minimum, which are separated by an energy barrier, ΔE.

2.11 The Seven-Point Model

This so-called model is a description of the distinct features of a hysteresis loop of an exchange biased system. The model, developed by Goodman *et al.*(2001), describes the different stages of the magnetisation processes that occur while the *F* magnetisation is cycled in seven points depicted in figure 30.

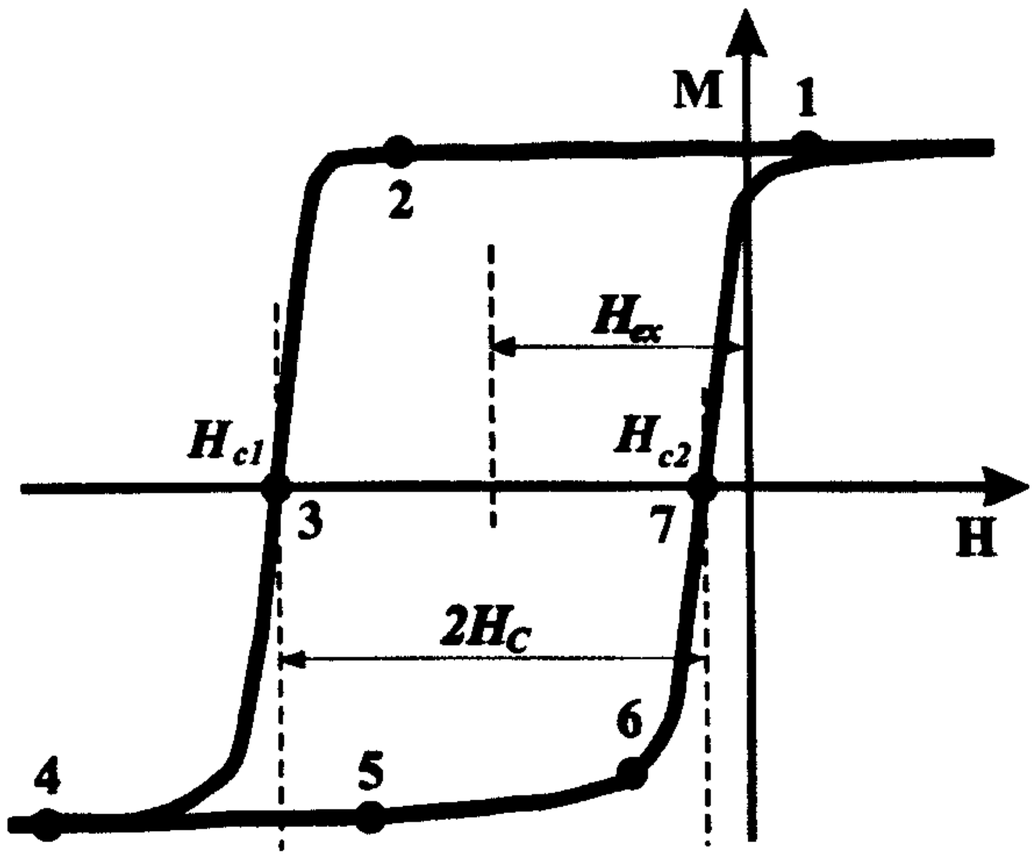

Figure 30 Schematic diagram of the magnetisation reversal of an exchange biased system.

The features described are as follows:

1. At point 1 in the hysteresis loop the *F* is saturated in the positive field direction.
2. At point 2 the reversal of the *F* is initiated. Nucleation of reverse domains in the *F* appears due to the degree of saturation at point 1.
3. At point 3 the domains nucleated at point 2 grow. Their growth is promoted by the applied field, the exchange coupling inside the layer and the thermal activation. At this point the coercivity exhibits normal magnetic viscosity. A fast sweep rate from point 1 to point 3 leads to an increase in the value of the coercive point H_{c1}.
4. At point 4 the *F* is saturated in the negative field direction. However, thermal activation of *AF* reversal continues. Goodman *et al.*, (2001) proposed that a this stage there is growth of domains within the *AF* dominated by the exchange field exerted by the *F* on the *AF*.

5. At point 5 it would be expected that the F would reverse back to positive magnetisation, as would be the case of a single layer F material. This does not occur due to additional energy barriers arising from the pinning of domain walls by the AF. Hence an additional anisotropy appears in the F via the exchange interaction between the F and AF.
6. At point 6 the nature of reversal is different to the nucleation of domains that occurs in point 2. Domains develop via domain wall movement over pinning sites or via domain rotation. At this point, pinning must be significant to account for the viscosity effects at point 4. The AF domain processes can only be observed via their effect on the F.
7. At point 7, Goodman *et al.* (2001) observed what they called anomalous behaviour of the second coercivity, H_{c2}. They believed that H_{c2} is indeterminate and depends critically on the amount of time spent with the F layer saturated, and therefore on the exchange field between F and AF layer on the growth of domains in the AF layer.

Although the AF layer is not affected by the applied field, the exchange field from the F acting on the AF influences the AF domains (Goodman *et al.*, 2001), which added to thermal activation processes gives rise to time dependence of the values of H_{c2} and hence H_{ex}. This model provides a point description of the hysteresis loop that will be used along this thesis to refer at the different stages during the hysteresis loop.

Chapter 3

Exchange Biased Systems

3.1 The Nature of Exchange bias

An exchange bias system consists of an *AF* material, in intimate contact with a *F* material. These systems, when cooled down from $T_N<T<T_C$ to a temperature less than the T_N of the *AF* in the presence of a strong magnetic field, show some characteristic features.

In such structures, the ferromagnet acquires uni-directional anisotropy. This phenomenon is called exchange bias, because the hysteresis loop associated with the *F*-*AF* structure can be centred about a non-zero magnetic field. It was discovered by Meiklejohn and Bean (1956), while they were studying small Co particles, which are ferromagnetic. These particles were covered with an outer layer of CoO, which is *AF*. The hysteresis loop of this system was not symmetrical about the origin but shifted to negative field when cooled in a positive applied field. The phenomenon of exchange bias has been studied for the last forty years due to its complexity, which arises from the competing interactions for magnetic order between the ferromagnetic and *AF* layers.

The mechanism of exchange bias can be explained as follows:

1. At temperatures above T_N and below T_C, the Curie temperature of the *F* layer has all its spins magnetically ordered, meanwhile, the *AF* is in a paramagnetic state. When a magnetic field is applied, all the *F* spins are aligned parallel to the field (Fig. 31).

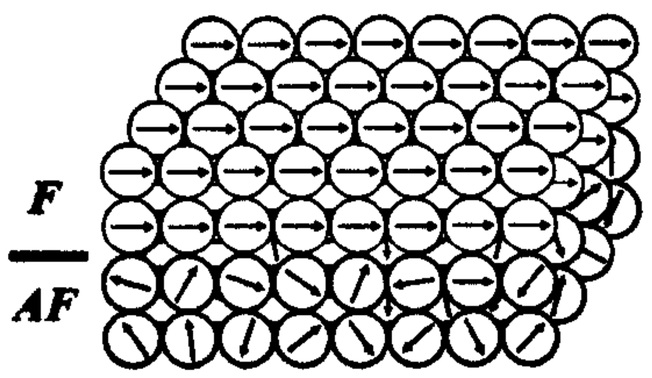

Figure 31 Schematic of the spin structure of an exchange coupled bilayer. At zero applied field, and above the Néel temperature, the ferromagnetic spins stay ordered, while the *AF* stays in its paramagnetic state.

2. When the sample is cooled to below T_N, in a field, the spins of the *AF* order. The spins in the closer layers to the interface align parallel to the ferromagnet's magnetisation, M_F, due to the exchange interaction. This corresponds to point 1 in the seven-point hysteresis loop. See figures 32 and 33(a).

3. When the field applied begins to reverse, M_F tends to reverse. The spins of the *AF* layer do not change their orientation, as they are insensitive to the applied field. The *AF* spins exert an exchange field, on the *F* spins, which is in opposition to their reversal. This implies an increase in the field necessary to reverse the *F* spins. At this stage, the system is at point 2 as shown in figure 32 and 33(b). Eventually reversal is initiated by the nucleation of reversed domains.

4. Point 4 of the hysteresis loop in figure 32: At this stage the ferromagnetic layer is saturated in the reverse direction. The *F* spins and the *F-AF* exchange field are now antiparallel to the interfacial *AF* spins. See figure 33(c).

5. Point 5 of the hysteresis loop in figure 32: At this point the field applied starts to reverse towards positive values.

6. Point 6 of the hysteresis loop in figure 32: The exchange field exerted by the *AF* layer on the ferromagnet promotes the rotation on the ferromagnetic spins; hence, a weaker magnetic field is required to reverse their orientation. See figure 33(d).

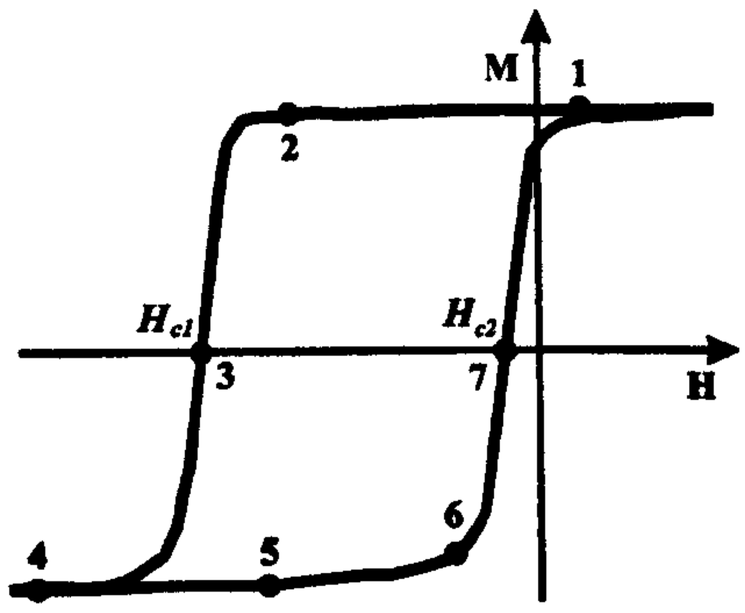

Figure 32 Seven-point hysteresis loop model. The exchange field is given by the shift of the loop. The values H_{c1} and H_{c2} are used to obtain the coercivity, which is defined as the half width of the loop.

The unidirectional anisotropy acquired by the ferromagnet results in a hysteresis loop shifted by an amount H_{ex}. This is known as the exchange field, which is applied by the *AF* layer on the ferromagnet. It also exhibits a coercivity enhancement. This means that the values of the coercive fields change, resulting in a wider hysteresis loop as a consequence of the exchange anisotropy. Other effects associated with exchange bias is the uncharacteristic form of the *F* magnetisation dependence on time, known as magnetic viscosity (Fulcomer and Charap, 1972a, 1972b), (see section 2.9), and the memory effect, which is related to the fact that the exchange biased system keeps a memory of the undergone field cooling process (Ambrose *et al.*, 1997).

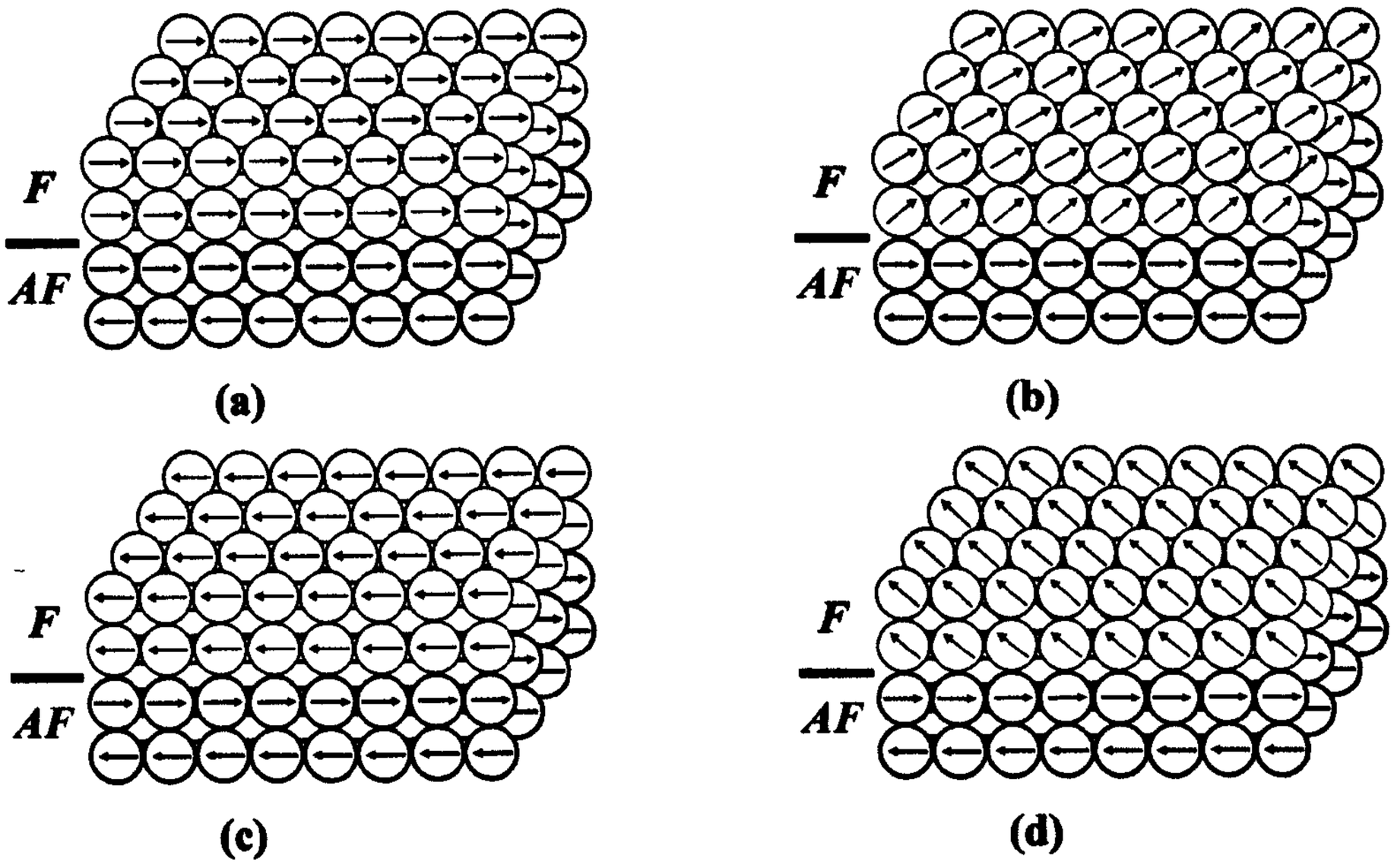

Figure 33 Mechanism of a shifted loop. Schemes of the spin structure in an exchange coupled bilayer at different stages of the hysteresis loop. (a) Point 1 in the seven-point model, (b), (c) and (d) correspond, respectively, to points 2, 3, and 6 in the seven-point model.

3.2 Historical Perspective

In an exchange biased system the competing interactions at the interface between the *F* and the *AF* spins lead to complex phenomena, which are the reason several models are proposed. Interest in the exchange bias phenomenon was merely academic until the late-eighties, when the Giant Magneto-Resistive effect (GMR) was discovered (Baibich, *et al.*, 1988). The technological potentiality of this effect renewed the interests in the

exchange bias effect and new models appeared. The development of the techniques available to study the magnetic structure, magnetic properties, and the improvement of computing capabilities have lead to the development of the theories of exchange bias.

Meiklejohn & Bean (1957) and Jacobs & Bean (1963) showed a simple description of the mechanisms that would produce a shifted hysteresis loop. Néel's (1967) studies highlighted the different processes that are involved in exchange bias. The models can be grouped into three categories. The first is that the reorientation of the ferromagnet through an applied magnetic field can involve the formation of magnetic domain wall structures in the *AF*. See Mauri *et al.* (1987), Koon (1997), Schulthess and Butler (1998), Stiles and McMichael (1999 a, 1999b, 2001).

The second category was defined with considerations of domain formation and domain wall motion, pinning and depinning during reversal of the ferromagnet (Meiklejohn (1962), Schlenker and Paccard (1967), Schlenker (1968) and Néel (1967). Since this time, theories have been put forward to describe domain wall dynamics and wall dynamics in the ferromagnet (Malozemoff (1987), Nemoto *et al.*, (1999), Kiwi *et al.*, (1999a, 1999b), Nikitenko *et al.*, (2000)), and also domain dynamics in the *F* (Li *et al.*, (2000), Leighton *et al.*, (2000)).

Considerations of time dependence and irreversible processes are also relevant, since exchange bias is intimately connected to the magnetisation process during reversal, (Schlenker (1968), Fulcomer and Charap (1972a,b), Schlenker *et al.*, (1986), Nishioka *et al.*,(1996)). This has lead to more recent examinations of thermal effects (van der Heijden *et al.*, (1998a, 1998b), Gökemeijer *et al.*, (1999a, 1999b). Magnetic viscosity experiments and field rate studies have also been reported (Goodman *et al.*, 1999, 2000). The importance of thermal processes on exchange bias and coercivity show that the magnetisation history of the sample is important (Miltényi *et al.*, (1999), Stiles and McMichael (1999a, 1999b), Nogués *et al.*,(2000a)), and can result in a variety of behaviours including positive exchange bias (Nogués *et al.*, 1996, 2000b) and domain wall processes in the *AF* (Nowak and Usadel (2002), Kim and Stamps (2005)).

The third category comprises the granular models. These models treat both *F* and *AF* as an assembly of grains, each of them is considered to be in a single domain state. The

first of them was published by Fulcomer and Charap (1972) who considered the effect of temperature fluctuation on non-interacting single domain *AF* grains exchange coupled to the ferromagnetic moment of the underlying film. They proposed an explanation of the temperature dependence of the coupling between *F* and *AF* given by the thermal instability of the grains. Nishioka *et al.*(1996) extended Fulcomer and Charap's model to explain the coupling dependence on the *AF* grain size. Stiles and McMichael (1999a, 1999b), developed a grain model that differs from Fulcomer and Charap in the fact that the *AF* grains have random orientations and contain domain walls. The *AF* grains are also independent, however they are coupled to the *F* not only by direct coupling but also by spin-flop coupling.

Even though there are several models proposed. None of them have managed to give a complete explanation for exchange bias. In fact some of the models predict correct values for certain materials, but not all, or do not contain temperature dependence. All models proposed until now are designed for uniaxial materials and do not contain considerations for biaxial materials such as IrMn studied in this work.

The work done in this thesis is focused on measurement reproducibility. Hence, control of the sample history is taken into consideration. The protocols developed are based on this idea and the interpretation of exchange bias broadly follows Fulcomer and Charap's (1972b) work. Temperature and time dependencies are studied under a grain model description. The *AF* magnetic behaviour is considered in terms of energy barrier distributions to reversal as discussed in section 2.9.

3.3 Exchange Biased Systems

The first systems where exchange bias was found were systems of fine particles. The materials studied were mainly ferromagnetic particles covered with their native *AF* oxide. Other materials have been used, such as nitrides or sulphides (Berkowitz and Takano, 1999). The size of these particles is normally in the nanometre range. They are produced by different methods, such as vapour deposition, electrodeposition, and reduction of the oxalate or mechanical alloying. These systems are non-ideal for studies of fundamental aspects of exchange bias, since there is always a distribution of particle

sizes and shapes, which makes it difficult to identify the nature of the interface, stoichiometry, crystallinity, etc. of the *AF* layers.

There are some systems that don't have a clearly defined *AF-F* interface or that have multiple *AF-F* interfaces, where due to the arrangements of the magnetic ions, different areas or domains with *AF* or *F* interactions are created. In this category are spin glasses and some ferrimagnets. Other systems studied are coated *AF* single crystals (*AF* single crystal polished along a specific crystallographic direction, coated with a *F* material) (Nogués and Schuller, 1999).

The most widely studied materials have been in the form of thin films. In these systems the interface can be effectively controlled and characterised. These types of materials have been used to study different phenomena related to exchange bias, such as *AF* thickness, interface disorder, or orientation dependence of H_{ex} (Nogués and Schuller, 1999).

The ferro-*AF* group can be divided in three main categories depending on the AF used: oxide, metallic, others.

- Oxide antiferromagnets

After works on oxidized *F* particles, most of the early work on exchange bias was on oxidized transition metal films, Co-CoO, Ni-NiO, Fe-FeO, or oxidized $Fe_{20}Ni_{80}$. To avoid some of the problems that these systems may present, antiferromagnet oxides have been sputtered directly from oxides from the metal or in a reactive oxygen atmosphere.

- Metallic antiferromagnets

The first fully metallic thin film was reported in 1964. $Fe_{20}Ni_{80}$/Mn bilayers were annealed to enhance diffusion, creating *AF* $Fe_xNi_yMn_{1-x-y}$ compounds at the interface. One of the most studied *AF* systems was $Fe_{50}Mn_{50}$, which was the basis for most exchanged biased GMR spin valves (Baibich *et al.*, (1988), Dieny *et al.*, (1991)) until recently. Materials currently being used are PtMn and IrMn due to their higher thermal stability and higher anisotropy. The development of spin valves lead to research for new *AF*, with high T_N and resistance to corrosion.

- Other antiferromagnets

Non-metallic or non-oxide systems exhibiting exchange bias include sulphides, fluorides and nitrides. The details of these structures are not very clear. Recently, FeF_2 has been extensively studied (Nogués *et al.*, 1996). Since its structure is simple, it is suitable for the study of basic properties of exchange bias.

- Ferrimagnets

These systems are similar to *AF*s. They also have two sublattices with opposite magnetisation, but ferrimagnets have the peculiarity that the net magnetic moment is non-zero, as one of the sublattice magnetisations is larger that the other. Their magnetic structures can play the role of the *AF* or the ferromagnet in bilayer systems. These systems are difficult to analyse theoretically, due to the complexity of the two layers in the ferrimagnet (Nogués and Schuller, 1999).

3.4 Technological Importance of Exchange Bias

The application of exchange bias is generally related to the magnetic recording industry (Berkowitz and Kodama, 2005). Since the discovery of Giant Magnetoresistance in 1988 (Baibich *et al.*, 1988) and its early implementation in spin-valves (Dieny *et al.*, 1991), exchange bias is being used in all modern computers. The read-write head uses the exchange bias in the magnetic thin film sensors that read the bits of information from the hard drive. Figure 3.4.1 shows a schematic of a typical read-write head used in a computer disk drive. The recording medium is a magnetic thin film typically about 10nm thick, with high coercivity and remanence, which is on a flat disk that rotates at about 7200 to 15000 rpm. On top of the magnetic layer there is a 5 to 10nm thick carbon coating and a 1nm thick lubricant layer. The read-write head is suspended on a lever arm 10nm above the lubricant layer. The lever arm controls its radial position over the disk. The write element uses pulsed currents to write the bits by magnetising small regions in the recording layer. There are stray fields arising from consecutive bits magnetised in opposite regions, which added to the random grain size that form the magnetic layer create a noise region between bits.

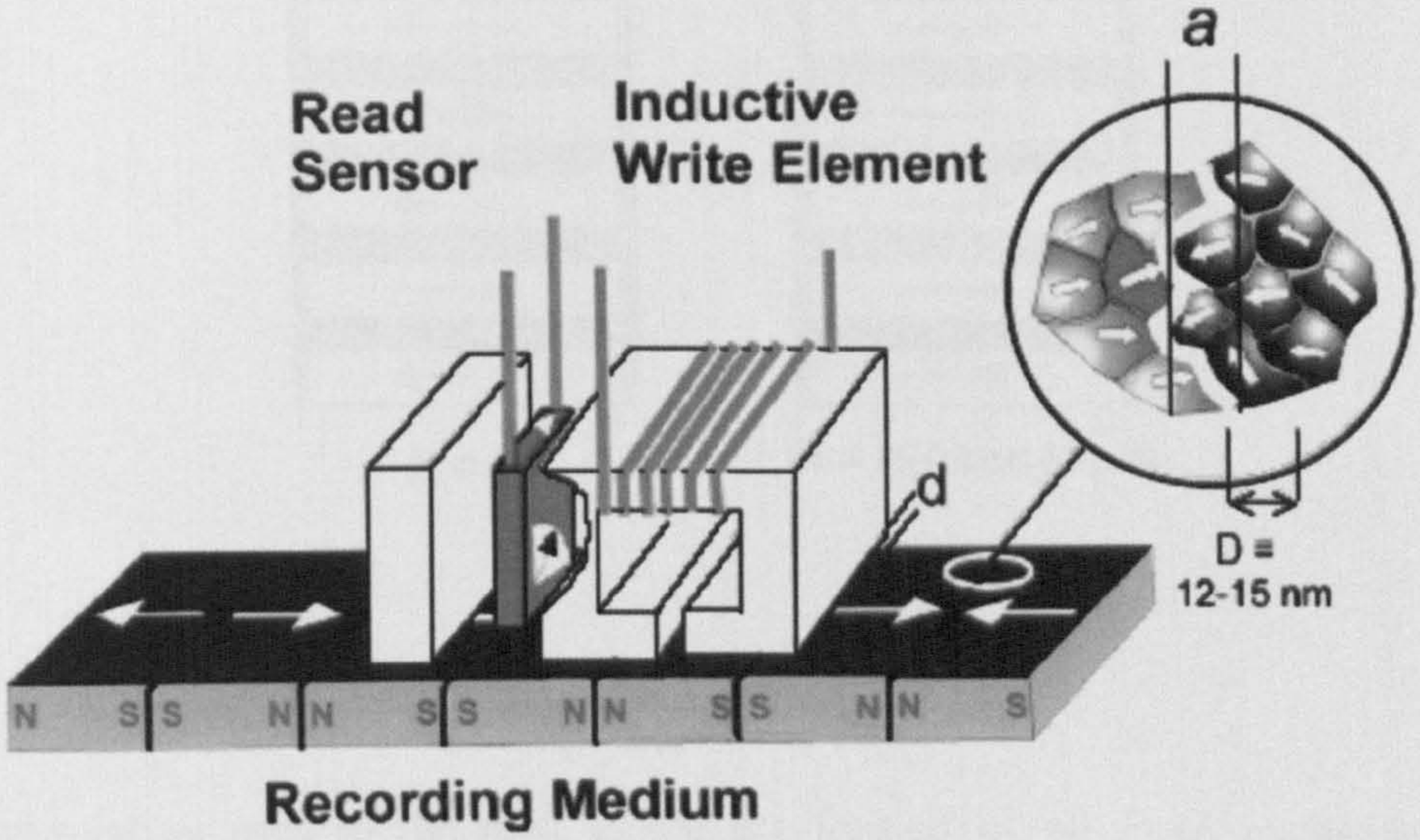

Figure 34 Schematic of a read-write head. (Berkowitz and Kodama, 2005)

As seen in figure 34 the read sensor is shielded from exposure to surrounding bits. The arrow depicted in the read sensor indicates the magnetisation direction of the sensing film. Its direction rotates depending on the magnitude and direction of the stray flux from the read bit. The thin film sensor consists of a multilayer structure called a spin valve. A schematic of the cross section of spin valve is shown in figure 36. The spin valve uses the GMR phenomenon, i.e., the change in the magnetisation direction of the sensor layer in the spin valve due to the stray field from the read bit produces a change in the resistance of the spin valve, which is monitored by a bias current that passes through it. The output signal is this change in the resistance. The GMR phenomenon was discovered in thin film multilayers of alternating ferromagnetic layers separated by non-magnetic spacers. The *F* layers are exchanged coupled through the non-magnetic layer. The sign of the exchange coupling oscillates with increasing thickness of the non-magnetic layer (Parkin, *et al.*, 1990). Figure 35 shows the case of a multilayer with antiferromagnetic coupling between the *F* layers, given the right thickness for the non-magnetic layers. The resistance for this structure is a maximum. If a saturating field is applied, the ferromagnetic alignment of the *F* layers leads to a minimum in the resistance across the multilayer.

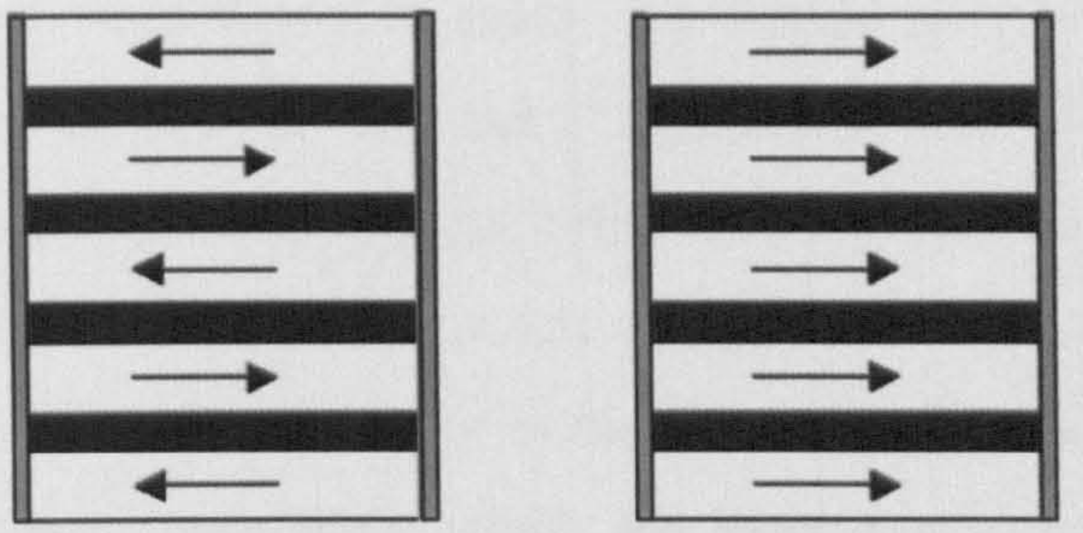

Figure 35 Schematic of a spin valve.(Berkowitz and Kodama, 2005)

The spin-valves used in the read sensor are formed by an *F-AF* exchange coupled bilayer, a non-magnetic conducting spacer and a *F* layer as shown in figure 36. The non-magnetic layer thickness is chosen to minimise the exchange coupling between the free and the pinned *F* layers. The easy axis in the free *F* layer is determined by its intrinsic anisotropy field direction and the residual exchange coupling to the pinned *F* layer. The magnetisation of the free layer rotates under the influence of the stray field from the bits in the recording film. This produces a change in the resistance in the multilayer, sensed by a bias current in the plane of the field. The pinned *F* layer and the easy axis direction of the *F* layer are crossed to produce a linear response in the resistance output.

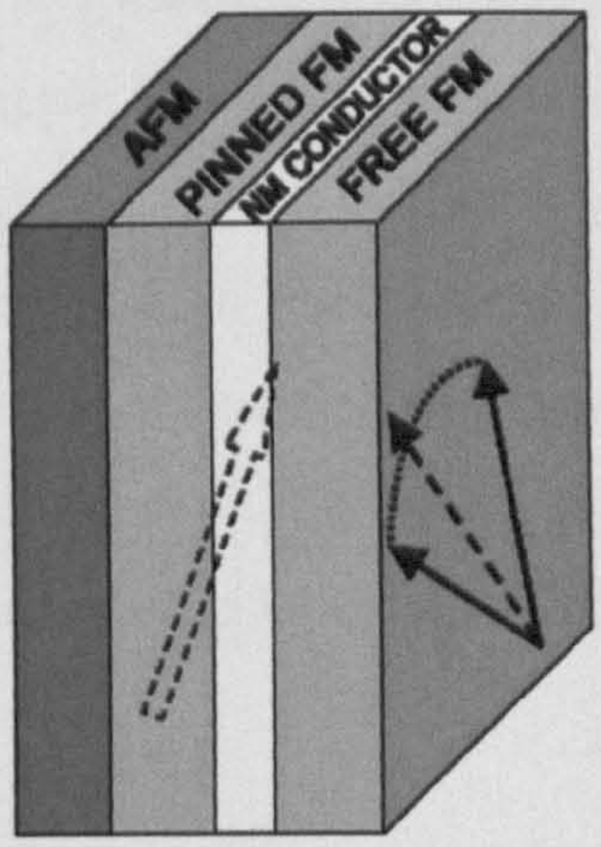

Figure 36 Schematic of a GMR spin valve. The open arrow represents the magnetisation direction of the pinned ferromagnetic layer, which is crossed with the easy axis (dashed arrow) of the free ferromagnetic layer. (Berkowitz and Kodama, 2005)

It is of technological importance to make the sensor as thin as possible. Typical thicknesses are <8nm for the *AF* and the *F* layers and 2nm for the spacer, which is normally Cu. The exchange field must be larger than the stray flux from the bits, which is normally about 100 Oe. The bias current is minimised to reduce the possibility of heating the sensor to temperatures close to the blocking temperature of the pinned *AF*. Materials frequently used were NiO, which has been substituted for Mn-based alloys such as IrMn and PtMn due to their higher T_B.

Structures like the one shown in figure 36 are improved by replacing the free *F* single layer for a trilayer of two antiferromagnetically exchange coupled *F*s with a Ru or Cu interlayer. The purpose of this is to eliminate the curling of magnetisation on the edges of the free *F* layer close to the recording medium.

Spin polarised magnetic tunnel junctions have a basic structure similar to figure 35. The simplest structure is formed by two *F* layers separated by an insulator of thickness in the order of 1nm. The principle of operation is based on the production of electron transport across the trilayer by the application of a bias voltage to the *F* layers. The conductance between the *F* layers depends on the relative orientation of the magnetisation of both layers. The development of magnetic-random-access-memory (MRAM) based in magnetic-tunnel-junction structures has been of industrial interest since high tunnel magnetoresistance can be achieved with these structures, e.g. Moodera *et al.*, (1995 and 1999). Figure 37 shows a schematic of a magnetic tunnel junction cell used for MRAM. It contains a *F* layer exchange biased to *AF* layer and separated by an insulating interlayer from the free *F* layer. A high resistance is achieved when the free *F* layer magnetisation is antiparallel to that of the pinned *F* layer. Resistance ratios larger than 100% have been reported by Parkin *et al.*, (2004) and Yuasa *et al.*, (2004) and recently 350% TMR by Parkin, 2005, as reported by S. Mao (York, 2005).

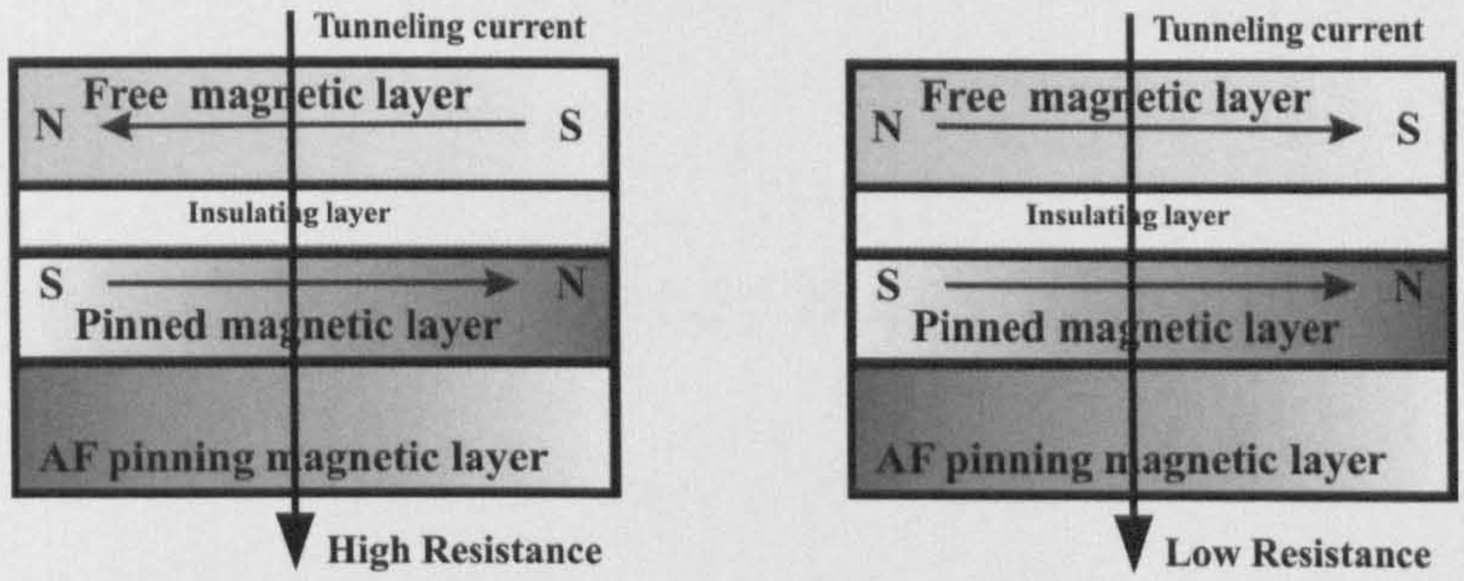

Figure 37 Schematic of an spin tunnel junction.

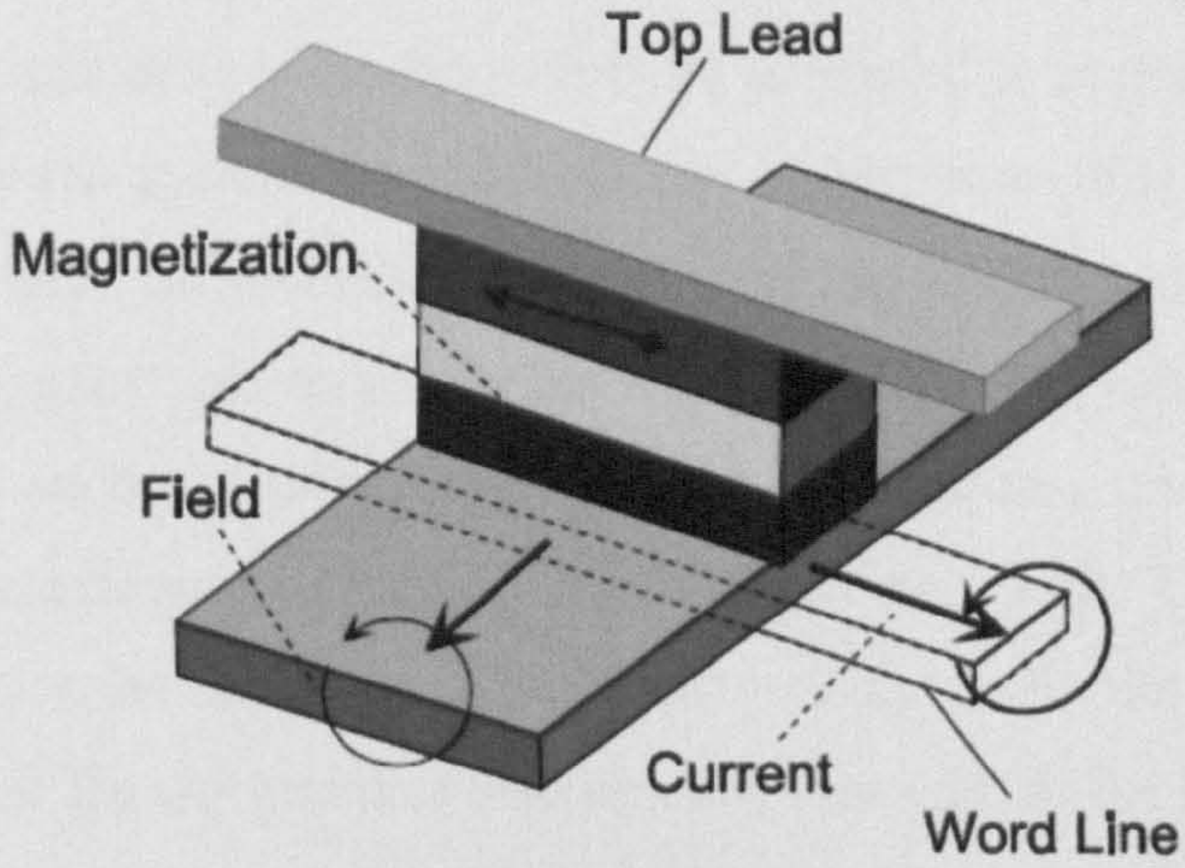

Figure 38 Schematic of cross-point architecture matrix of magnetic tunnel for MRAM junctions. Courtesy of Paulo Freitas

Other applications of the exchange-bias phenomenon are based as well in the use of *AF*s and antiparallel-pinned *F*s. The use of a magnetic tunnel junction transistor using IrMn to bias the emitter has been reported by Parkin *et al.*(2003). Field sensors sensitive to picotesla fields are based on magnetic tunnel junctions (Tondra *et al.*, 1998).

Chapter 4

Theoretical Models of Exchange Bias

4.1 Introduction

After fifty years of study there is no universal theoretical basis that explains the exchange bias phenomenon because the effects of exchange coupling are of short range. Hence a detailed model of the interface structure is needed to explain the behaviour of each exchange coupled system. In the majority of the cases this information is not available. Furthermore, differences in samples of the same materials produced in different growth systems lead to properties that have different values due to different growth conditions, such as different grain size distributions, crystallinity, interface quality and other defects such as impurities or oxygen inclusions. The spin structure of the *AF*, which governs the anisotropy of the system, is generally not known because the easy axis direction of the *AF* grains is also unknown, as well as the spin structure at the interface, and if it is compensated, i.e., the same number of spins of both sublattices are present, or whether it is uncompensated or partially uncompensated.

This thesis relates to the effects of thermal activation on exchange biased systems. Whether the thermal activation effects on the reversal of the *AF* material is due to the reversal of the magnetic state of the *AF* grains or due to domain processes is not known. Due to all these matters, there is no unified theory that is able to explain the exchange bias phenomena for all different materials.

This chapter contains a selection of theoretical models which have made a significant contribution to the understanding of exchange bias phenomenon and which at the same time are of relevance to the work done in this thesis.

4.2 *Early models*

4.2.1 Meiklejohn and Bean's model

The model of exchange bias proposed by Meiklejohn and Bean suggests that the shift in the hysteresis loop appears due to a large anisotropy in the *AF* and a weaker exchange energy coupling the *AF* to the *F*. A shifted loop for an exchange couple is shown in figure 39.

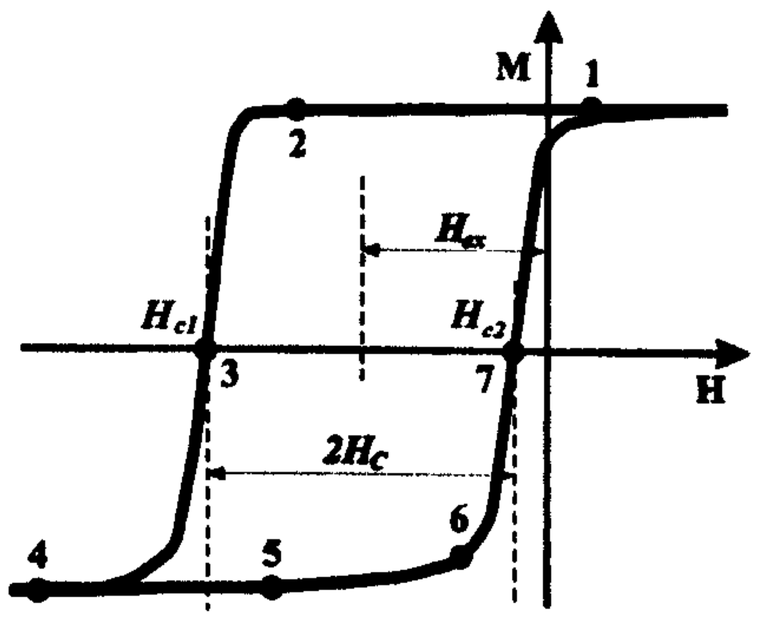

Figure 39 Schematic hysteresis loop for an exchange biased system.

The mechanisms of exchange bias suggested by Meiklejohn and Bean (1956) were described in chapter 3.1 where a perfectly uncompensated *AF* interface spin structure is assumed. A saturating magnetic field is applied at a temperature above T_N, figure 40(a). After cooling the system in a field, the magnetisation of the ferromagnet remains pinned along the original direction for small negative fields. See figure 40(b). The magnetisation of the *F* is reversed when the field applied is large enough to overcome the interlayer exchange, as shown in figure 40(c). The effective field associated with the interlayer exchange gives the magnitude of the shift.

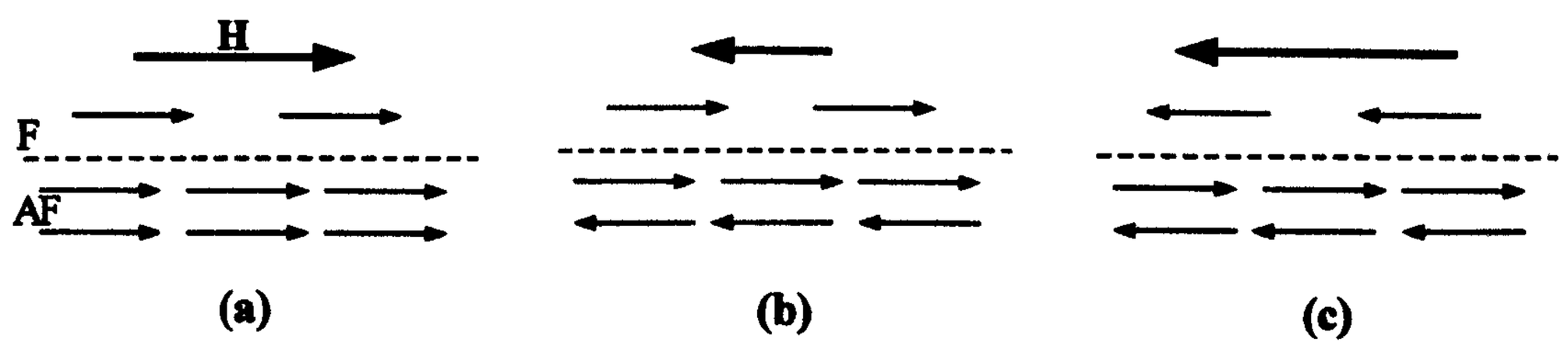

Figure 40 Spin structures at different stages of the reversal of the ferromagnet, (a) before field-cooling, (b) and (c) after field-cooling. The *F* spins reverse when the applied field is large enough (c).

Since they were working on oxidised cobalt nanoparticles, Meiklejohn and Bean considered single domain spherical particles with uniaxial anisotropy with their easy axis aligned parallel to the field, $\boldsymbol{H}$, applied in the opposite direction to their saturation magnetisation, $\boldsymbol{M_S}$. Examining the stability of the energy per unit area for this model (Stamps, 2000), we can find the values of the coercive fields, H_{c1} and H_{c2} (see fig. 39).

$$E = -HM_S t_F \cos\theta - J\cos\theta + K_F t_F \sin^2\theta \qquad (4.1)$$

In this model, t_F is the thickness of the ferromagnet, J is the interlayer exchange between the ferromagnet and the AF, K_F is the uniaxial anisotropy constant of the ferromagnet, and θ is the angle between M_S and the uniaxial anisotropy easy axis. The field is aligned along the easy axis, and the magnetization is assumed uniform. Another important assumption is that the AF remains rigidly aligned along the direction of its easy axis, which is assumed to lie parallel to the ferromagnet easy axis. This restriction is the reason why this model is known as *the rigid antiferromagnet model.* The energy has extrema corresponding to saturation for values $\theta = 0$ and $\theta = \pi$. Stability arguments for these configurations give the values of the coercive fields, H_{c1}, H_{c2}, and the coercivity H_C,

$$H_{c1} = -\frac{2K_F t_F + J}{M_S t_F} \qquad (4.2) \qquad H_{c2} = \frac{2K_F t_F - J}{M_S t_F} \qquad (4.3) \qquad H_C = \frac{2K_F}{M_S} \qquad (4.4)$$

Since the coercive fields are different in magnitude, the hysteresis loop is biased. The bias field in this model is defined as the midpoint of the hysteresis loop, and is directly proportional to the exchange coupling:

$$H_{ex} = \frac{J}{Mt_F} \qquad (4.5)$$

The bias can also be interpreted as an exchange coupled anisotropy field acting on the ferromagnet. The magnitude of the exchange field depends directly in the value of the exchange constant between the F and the AF. This result leads to values of H_{ex} which

are two orders of magnitude larger than the experimental values observed (Meiklejohn, 1962) and predicts a thickness dependence of H_{ex} proportional to $1/t_F$.

4.2.2 Néel's model. The continuum approximation.

Néel's exchange bias model (Néel, 1967) assumed an uncompensated *AF* spin interface coupled to the *F* layer, uniform magnetisation of each sublayer, being parallel to the interface and uniaxial anisotropy. Néel wrote a discrete hamiltonian for the magnetisation state of each of the sublattices. The main result of this continuum approximation is the formation of domains both in the *F* and the *AF* although a minimum thickness of both layers is required to allow for domain formation.

This model again failed to predict reasonable values for H_{ex}, which were several orders of magnitude larger than those observed experimentally (Meiklejohn, 1962). It was also expected that compensated interfaces would not give rise to H_{ex} and that the increased roughness at the interface would increase H_{ex}.

4.3 Domain walls in the AF

Domains in exchange biased bilayers has been observed by several authors. The study of domains on wedged-NiFe and uniform FeMn samples by Nikitenko *et al.*(2000), using a magneto-optical technique, showed domain wall motion that was asymmetric in the forward and reverse branch of the hysteresis loop. This asymmetry, incompatible with a static *AF* spin structure, probed the existence of a moving domain wall within the *AF*, forming an exchange spring in the *F*.

4.3.1 Domain walls parallel to the interface

Mauri et al. (1987) proposed a model which resulted in a lower interfacial energy than that of Meiklejohn and Bean, and gave more reasonable values for H_{ex} compared to the experimental results. They assumed that the magnetisation of the *F* and the order in the

AF sublattices are parallel to the interface and coupled to each other across a perfectly plane interface. They also assumed a *F* thickness smaller than the domain wall width and the formation of a domain wall inside the *AF* parallel to the interface. The energy required to form such a (90°) domain wall is $2\sqrt{A_{AF}K_{AF}}$, where A_{AF} is the exchange stiffness and K_{AF} the crystalline anisotropy in the *AF*. The magnetic energy per unit area of an interface like this is given by

$$E = 2\sqrt{A_{AF}K_{AF}}(1-\cos\alpha) + A_{F-AF}/\xi[1-\cos(\alpha-\beta)] + K_F t_F \cos^2\beta + HM_S t_F(1-\cos\beta) \tag{4.6}$$

where α is the polar angle formed by the spins in the closest *AF* sublattice layer to the *F* with the *AF* uniaxial anisotropy axis (z axis) , and β is the angle formed by the F spins with the z axis. $A_{F\text{-}AF}$ is the exchange stiffness at the interface, K_F is the ferromagnet anisotropy constant, M_S is the saturation magnetisation of the *F*, t_F is the thickness of the *F*, and ξ the interface thickness. Minimising eq. 4.6 with respect to α and β for a given value of the applied field *H* gives the value of the H_{ex}. In the case of the interface energy being much less than the domain wall energy (α small)

$$H_{ex} = -\frac{A_{F-AF}}{\xi M_S t_F}. \tag{4.7}$$

The substitution of $J = A_{F-AF}/\xi$, gives the same expression as eq. 4.5 obtained by Meiklejohn and Bean. In the case of the interface energy being much larger than the domain wall energy, the exchange field is

$$H_{ex} = -2\frac{\sqrt{A_{AF}K_{AF}}}{M_S t_F}. \tag{4.8}$$

Magnetisation curves are constructed assuming coherent rotation showing loop asymmetry for the case of the interface energy being of the order of the domain wall energy. In the case of the interface energy being larger, 180° domain walls appear in the *AF*. This model does not explain the enhanced coercivity of the *F* when it is exchange

coupled to the *AF*, or the decrease of H_{ex} and H_C when the field is cycled repeatedly. The pinning of the domain walls due to imperfections appears as an explanation of the effects of the *AF* on the coercivity in the same way as in the Néel (1967) model.

4.3.2 Random field model. Domain walls perpendicular to the interface.

Malozemoff (1987) introduced a random interface roughness between the *AF* and the *F*. This gives rise to compensated and uncompensated areas at the interface. In consequence, there is a random field that acts on the interfacial spins. Due to anisotropy energy minimisation the *AF* breaks up into domains, with domain walls perpendicular to the interface. Assuming that the *F* is in a single domain state, uniaxial anisotropy in the *AF*, and a fixed size of the *AF* domains given by

$$L \approx \pi \sqrt{A_{AF} / K_{AF}} \tag{4.9}$$

the exchange field predicted is

$$H_{ex} = \frac{2z\sqrt{A_{AF} K_{AF}}}{\pi^2 M_S t_F} \tag{4.10}$$

The number z is of the order of unity (Imry and Ma, 1975). This parameter arises from interface irregularities, whose local energy magnitude is taken to be on average $2zJ$, where J is the exchange constant, assumed to be constant on both sides of the interface. This model assumes that A_{AF} and K_{AF} are temperature independent to a first approximation. Equation 4.10 is similar to eq. 4.8 resulting in values of H_{ex} of the same order of magnitude. Malozemoff suggests an explanation for the reduction in H_C when the *F* magnetisation is repeatedly cycled. Movement of the *AF* walls would generate the reduction of H_C. The results of this model depend crucially on the concentration of defects.

Malozemoff (1988a, 1988b) also considered the case of *AF* materials with cubic anisotropy, such as FeMn, and IrMn. The latter is studied in this thesis. The result of

random interfacial fields in these materials would be to stabilise the domains which would have a different topology to those formed in uniaxial materials. In the case of the uniaxial materials an *AF* domain width independent of temperature would be expected for uniaxial materials while in the case of cubic materials it would be expected to vary as $(1- T / T_N)^{-1/2}$. Hence, domains formed at high temperatures would be larger than those formed at low temperatures.

The predicted variation of H_{ex} with temperature is $(1 - T / T_N)^{1/2}$ for uniaxial systems and $(1 - T / T_N)$ for cubic systems. This is discussed in chapter 6.3, where measurements on IrMn/CoFe bilayers show that it is only true for certain temperature regions. Furthermore, the model of Malozemoff (1987,1988) is proposed for a single crystal *AF*, whereas in this work polycrystalline *AF*/*F* bilayers have been studied. Malozemoff (1988b) also predicted a critical thickness for the *AF* (t_{AF}) below which there is no H_{ex}. Above this critical thickness H_{ex} decreases with increasing t_{AF} up to a second critical thickness at which H_{ex} achieves a minimum value.

All the models described above and many others consider the exchange stiffness, A_{AF}, $A_{F\text{-}AF}$, and the anisotropies, K_F, K_{AF} to be first approximations to the models. In fact, these parameters are considered to be uniform in the *F* and *AF* layers, and temperature independent. Ultimately they are used as fitting parameters to predict the values of H_{ex}. In section 6.2, it is shown that the degree of order in the *AF* is temperature dependent and controls the H_{ex}.

4.3.3 Random interface and orthogonal magnetic arrangements.

The experimental observation of perpendicular spin arrangement at the *AF*-*F* interface was made by Jungblut *et al.*(1994, 1995) and Nogués *et al.*(1996a) showing that compensated and uncompensated interfaces lead to similar results for H_{ex}. Koon (1997) gave a microscopic explanation for exchange bias in which the spins in the *AF* close to the interface align perpendicular to the direction of the *F* spins close to the interface due to magnetic frustration of those spins when the interface is compensated. This type of configuration is known as spin-flop coupling. When the *F* is reversed exchange bias would appear as result of the formation of a domain wall parallel to the interface.

Schulthess and Butler (1998) showed that spin-flop coupling does not lead to the formation of a parallel domain wall in the *AF* and therefore would not lead to exchange bias, although it does lead to an increase in the value of H_C by two possible mechanisms (Schulthess and Butler, 1999). One is the reversal of some small *AF* domains during the reversal of the *F* magnetisation, leading to irreversible effects in the *AF*. This mechanism leads to a coercivity that is dependent on the magnetic history of the sample. The other mechanism is the reduction of domain wall widths when the *F* is coupled to the *AF* increasing H_C due to pinning of domain walls. In this case H_C would depend on the morphology and the spin-flop coupling rather than the magnetic history.

The mechanisms proposed for the loop shift are random fields at the interface originating at defects and interface roughness on the same basis as the Malozemoff theory. These would give rise to the formation of domains in the *AF* with walls perpendicular to the interface. The increase of H_{ex} with increasing interface roughness (Morán *et al.*, 1995) is explained when the random field is due solely to interface roughness. Interface roughness can also decrease H_{ex} (Nogués *et al.*, 1996b). This would happen when the random field is induced by uncompensated regions through lattice strain. These results are also explained in terms of the domain state model, which is described in section 4.5. Assuming that the interface is of a fractal nature and that the density of defects that can pin a domain wall increases with d_w^{-1}, where d_w is the domain wall width, the coercivity is then expected to vary as (Schulthess and Butler, 1999)

$$H_C \propto 1/t_F^{3/2} \tag{4.11}$$

where the parameter t_F is the thickness of the *F* layer, in contrast with the H_{ex} variation with $1/t_F$, as generally observed. A similar expression was derived by Zhang *et al.*, (1999) who assumed random interactions at the interface and the formation of a domain wall in the *F*. Keller *et al.*, (2002) based on the domain state model (Nowak *et al.*, 2002), briefly described in section 4.5, performed measurements that showed how roughness is not the main parameter that influences H_{ex}. Contrary, measurements on Co/CoO showed that H_{ex} was controlled by the concentration of defects within the *AF* layer by keeping the interfacial roughness constant and varying the defect concentration.

4.3.4 Domain wall processes in the antiferromagnet

Several authors showed that a perfectly rigid *AF* can not predict the observed values of exchange bias. The existence of a twisted magnetic structure within the *AF* by distributing the twist across a number of spins leads to more reasonable values for H_{ex} (Néel, 1967, Mauri *et al.*, 1987, Koon 1997, Kiwi *et al.*, 1999b).

Stamps (2000) addressed two different types of exchange bias depending on whether the processes involved are reversible formation of partial domain walls or whether irreversible processes give rise to asymmetric hysteresis loops. However, asymmetric hysteresis can be caused without complete loss of partial wall bias when mixed interfaces are present resulting in shifted asymmetric loops. The energy barriers to partial domain wall formation are considered to be of two types, those involved with in-plane rotation of the magnetisation of the *F* and those related to out-of-plane rotation. Consideration of these energy barriers showed that H_C can appear in exchange biased systems without the need of anisotropy in the *F* (Stamps, 2000) in contrast with the rigid *AF* models.

Thermally averaged behaviour of exchange bias was studied in terms of mean field theory (Kim *et al*, 1999, McGrath and Camley, 2000, and Stamps and Wee, 2000). This was applied to both compensated and uncompensated interfaces. As a result a decrease of the H_C with increasing temperature is predicted. This result is at odds with data presented in this thesis of thermal activation in IrMn/CoFe systems (See chapter 6.2). Thermal behaviour studies (Stamps, 2000) described by a fluctuation mechanism (Fulcomer and Charap, 1972b, van der Heijden *et al.*, 1998a) showed a initial H_C increase with increasing temperature, which is more in accordance with the results presented in chapter 6.2. Also, H_C increased with decreasing sweep-rate as result of the increase of the time for thermal activation effects in the *AF*, leading to irreversible changes in the *AF* state (Goodman et al., 2000). Stamps and Wee (2000) considered the temperature dependence of H_{ex} and H_C to have similar origins, namely wall pinning and de-pinning mechanisms, although the resulting temperature dependencies were different.

The theoretical study of the effects of inclusion of magnetic impurities within the *AF* can account for some of the features observed in exchange biased systems (Kim and Stamps, 2005a). Such impurities modify the domain walls in the *AF* giving rise under certain conditions to H_C enhancement and asymmetric hysteresis loops. These are a reduction of the *AF* wall energy due to the presence of defects which induces no irreversible behaviour and which is dominant at low defect densities. The other is related to the pinning of the *AF* wall formed during reversal in a metastable state. This effect is more important at moderate and high defect densities and results in irreversible behaviour, leading to H_C enhancement. At finite temperatures similar domain wall processes are predicted using a local mean-field theory (Kim and Stamps, 2005b) . In this case, pinning is due to displacement of the domain wall from the interface due to thermal fluctuations and similarly depinning of metastable states is predicted to occur from thermal effects at temperatures close to the ordering temperature of the *AF* giving rise to a reduction of the blocking temperature.

4.4 Granular Models

Fulcomer and Charap (1972a) studied the exchange bias phenomenon on NiFe films. They partially oxidised the NiFe samples (*F*), getting part of the surface covered with NiFe oxide (*AF*).They investigated the H_C and H_{ex} of these oxidised NiFe layers over a range of sweep-rates, varying the frequency at which they measured the hysteresis loops. Films that were free of any surface oxide did not show a displacement of the easy-axis loop along the field axis. H_C and H_{ex} were found to be a very weak functions of temperature. Oxidised films showed striking exchange anisotropy effects. Displaced loops appeared below a transition temperature ranging from 30 to 90K as the film was progressively oxidised.

They observed that H_{ex} decreases with increasing temperature and goes to zero at a temperature that is dependent upon the amount of oxidation. H_C was observed to increase at higher frequencies. H_C shows a peak around the temperature at which the H_{ex} goes to zero. This result is of great controversy nowadays. Some authors state that this peak occurs in the proximity of this temperature, called the blocking temperature (T_B). Another remarkable result was that while the loop shift increases with increasing

frequency, the coercivity decreases with increasing frequency (Fulcomer and Charap, 1972, a) in contrast to normal *F*, whose coercivity increases with increasing frequency (de Witte *et al.*, 1993).

These phenomena were attributed to exchange anisotropy arising from small nickel oxide particles forming on the surface that increase in quantity and size as oxidation proceeds. They suggested that there is only one possible mechanism responsible for the temperature and frequency dependence of coercivity and the anisotropy field, as well as for the appearance of a displaced loop well below the Néel point of the oxides. Fulcomer and Charap (1972b) proposed a thermal fluctuation after effect model that was based in the theory of magnetic aftereffect for very small particles (Néel, 1949) to explain the features described previously. The *AF* layer is regarded as an assembly of uniaxial particles with a distribution of particle sizes with no net moment. These *AF* particles or grains remain fixed during the reversal of the *F* layer. They considered the effect of thermal activation of those particles on the energy of such system (Fulcomer and Charap, 1972b)

According to their theoretical model, the magnetisation of the film biases, and is biased by the particles through an interfacial exchange coupling. Above a blocking temperature (T_B), dependent on the size of the oxide particles, these are able to reverse rapidly due to thermal fluctuations, exhibiting as a consequence of this, quasi-paramagnetic behaviour. As described in §2, the exchange field vanishes at the blocking temperature T_B. This temperature is the blocking temperature for the largest of the *AF* particles. Studies carried out in this work following a careful and methodologically detailed procedure revealed that this peak does not correlate with the median T_B. This is described in chapter 6.2.

Assuming a physically reasonable distribution of particle sizes, the model by Fulcomer and Charap was in good agreement with their results. Even though it is probably incomplete in certain aspects. For example, they suggested a non-interacting coherent rotation mechanism. However, it is very likely that the *AF* grains interact and it is possible that the reversal involves the formation of domain walls (Mauri, 1987, Malozemoff, 1988, van der Heijden, 1998a, 1998b). Stiles and McMichael (1999a,

1999b, 2001) proposed a similar and more general granular model which contains fewer restrictions in their assumptions.

Stiles and McMichael (1999a) considered polycrystalline *F-AF* bilayers where the *F* is supposed to be in a uniform saturated magnetic state with no or very few domain walls. The *AF* is assumed to have uniaxial anisotropy, and to be formed by independent *AF* grains; each with randomly distributed easy axes. The coupling between *F* and *AF* is via direct and spin-flop coupling. The interface is considered to be rough. Hence, the coupling is frustrated to a large extent due to compensation of the *AF* sublattices present at the interface. Therefore, each *AF* grain will have a small net moment. The formation of domain walls parallel to the interface in the *AF* is allowed. Stiles and McMichael introduced the concept of a critical angle, α_{crit}, to account for irreversible transitions in the *AF*. Partial domain walls which lie at an angle larger than α_{crit} would switch to another state with reverse *AF* order to that at the interface. Defects in the *AF*, which provide stabilisation and nucleation sites for reversal at small α_{crit}, and grain boundaries, which provide nucleation sites are considered in the model by allowing larger values than this critical angle. For *AF* thicknesses less than a partial domain wall width, domain walls would unwind.

Schlenker *et al.* (1986) showed that "distributions of coercivities in the *AF* grains" can give both reversible and irreversible effects. Stiles and McMichael (1999,a) showed that distributions of other properties, such as crystallographic orientation in the *AF*, of direct coupling strengths or distributions of critical angles, α_{crit}, can also produce this behaviour. At the interface of the *F-AF* system there is direct collinear coupling and indirect spin-flop coupling. The direct coupling will depend on the degree of compensation and the interfacial area of the spins. On average, the direct coupling per spin, J_{net}, is shown to be $J_{int}/\sqrt{N}$, where J_{int} is the interfacial exchange constant between the *F*, which is supposed to have uniform magnetisation in the *AF* grain and *N* is the number of interfacial spins per *AF* grain. For spin-flop coupling, it is assumed that the *F* spins are orthogonal to the *AF* spins, the effective spin-flop exchange per spin, J_{sf}, is given by J_{int}^2/J_{eff}, where J_{eff} is the effective exchange coupling between *AF* spins, which is proportional to J_{AF}. Hence the interfacial exchange J_{int} is reduced by $1/\sqrt{N}$ for direct coupling, while for spin-flop coupling it is reduced by J_{int}/J_{eff}.

Therefore, exchange biased systems where $J_{int} \cong J_{AF}$, spin-flop coupling will be stronger than direct coupling, making the *AF* interfacial spins coupled orthogonally to the *F* spins. Hence the coupling at the interface will be dominated by the strongest of these interactions. However, it has been shown that spin-flop coupling does not contribute to the unidirectional anisotropy (Schulthess and Butler, 1999). This would imply that the loop shift is caused by direct coupling at the interface between the *F* and the predominant *AF* sublattice in each grain. According to Stiles and McMichael, exchange bias exists because the *AF* order is set in the presence of the *F* magnetisation. The strength of the bias would be set by the lesser of the strength of the average direct coupling and domain wall energy in the *AF*. Irreversible processes are produced in the *AF*, as domain walls are wound past α_{crit}, leading to irreversible transitions to another state with reverse *AF* order to that in the interface. For this to occur the coupling needs to be strong enough to reverse *AF* spins far from the interface. These irreversible transitions put the system in a lower energy state. This implies that on average, the easy direction of the *AF* points towards the magnetisation of the ferromagnet.

Stiles and McMichael (2001) proposed a model for the temperature dependence of exchange bias based on the same concepts as those described above. Temperature dependence arises from thermal instabilities in the state of the *AF* grains, as described for superparamagnetic grains in section 2.9, and from the domain wall energy in the *AF* grains. They assumed that the domain wall energy varies as

$$\sigma = \sigma_0 (1 - T/T_N)^{5/6} \tag{4.12}$$

where T_N is the Néel temperature and σ_0 is the domain wall energy at 0 K. The 5/6 factor results from the assumption of $\sigma \propto (A_{AF}K_{AF})^{1/2}$ and the approximations of $K_{AF} \propto m_{AF}^3$ for the uniaxial anisotropy and $A_{AF} \propto m_{AF}^2$ for the exchange stiffness.

Thermal instabilities in the *AF* arise from thermal fluctuations, which cause small *AF* particles to switch their magnetic state. These *AF* grains are considered not to interact with external applied fields, are assumed to be of a columnar nature and longer than an *AF* domain wall. Grain size determines the type of switching. Small grains will switch by coherent rotation while big grains would switch by domain wall nucleation and

motion. The switching rate is determined in a similar way as for superparamagnetic grains. An energy barrier, ΔE, separates the set AF state and the reversed AF state. Hence the energy barrier, according to Stiles and McMichael (1999, b) is given by the final reversed energy state plus a domain wall far from the interface. These energy barriers will be higher for those grains which are more strongly coupled to the F. At a temperature T the probability of remaining in an initial state for a period t is given by

$$P(t) = \exp(f_0 t \cdot \exp(-\Delta E / k_B T) \tag{4.13}$$

Where, as described in section 2.9, f_0 equals 10^9 Hz, k_B is Boltzmann's constant. The value of ΔE is dependent on the coupling strength distribution, the distribution of the axes of the AF grain orientations and the domain wall energy at that temperature. The fast switching transition between states is approximated by a probability chosen to be either zero or one with the border between both states given by

$$\Delta E / k_B T = \ln(f_0 \tau) = 20 \tag{4.14}$$

where τ = 1s. In chapter 2.9, it has been shown that when τ = 100s, then $\Delta E / k_B T = 25$. The chosen value of τ depends on the measurement time. Hence, considering a measurement time of the order of one second, a particular grain will be stable if $\Delta E < 20 k_B T$ and unstable if $\Delta E > 20 k_B T$. The model allows instabilities in both states. Thus, after a time τ, these grains can occupy any of the states with equal probability. The critical angle description given before is closely related to the approximation of the state of each AF grain, as stable, partially stable, i.e. remains in one of the states as the energy barrier for that state is high, but the other has a low energy barrier, or unstable where both states have low energy barriers, so the grain will flip from one state to the other on a fast time scale compared to the measurement time. A particular grain will behave according to these processes depending on the temperature of the system. High temperatures make the grain more unstable in the given measurement time, while low temperatures increase the relaxation time, which makes the grains more stable as the relaxation time approaches the measurement time. The manner in which each grain behaves determines its contribution to the unidirectional anisotropy, and therefore to the shift of the loop. Consequently, the thermal activation of the switching causes a

blocking temperature, T_B. Above T_B, the AF order in the grains is not stable and therefore those grains do not contribute to the unidirectional anisotropy.

The unidirectional anisotropy saturates at low temperatures depending on ratio between the average interfacial coupling energy, J_{net}, to the zero temperature domain wall energy, $\sigma_0 a^2$, where a is the area of the interface per spin. The smallest of both determines the size of the unidirectional anisotropy. If J_{net} is the smallest, the unidirectional anisotropy saturates at low temperature due to the assumed temperature independence of the interfacial coupling at low temperatures.

A distribution of grain sizes and hence of blocking temperatures would explain the history dependence found in some systems. If there are such distributions, each grain would start to contribute to the unidirectional anisotropy at a different temperature. If the magnetisation direction in the F is changed as temperature is reduced, different grains will contribute to the unidirectional anisotropies in different directions.

Regarding the increase in the values of the coercivity in relation to those observed for a single F layer, the model of Stiles and McMichael (2001) exhibited two contributions to the enhancement of H_C. The first is due to inhomogeneous reversal in the F, which arises from the inhomogeneous environment to which the F is coupled in the exchange biased system, taking into account the random distributions of easy axes in the AF grains. The second is due to irreversible transitions occurring in the AF grains. The temperature dependence of H_C is then governed by the behaviour of these factors. At low temperatures the contribution of inhomogeneities is higher. This contribution depends on the ratio of the exchange coupling of the F to the AF grains to the intergranular exchange coupling in the F, given by the exchange stiffness. As a result H_C is predicted to decrease as $1/t_F^2$. At higher temperatures, irreversible transitions in the AF grain are predominant. This effect is independent of the ratio of the interlayer coupling to F exchange stiffness. In this range of temperatures H_C is estimated to decrease as $1/t_F$. This model also accounts for the observed peak in the value of H_C with temperature close to the blocking temperature. This is associated with instabilities in the AF grains. These simulations have been carried out with a finite sweep-rate. For

large values of t_F, the behaviour of both H_C and H_{ex} are obscure due to the dependence of both on the sweep-rate and the time-scale of the measurements.

4.5 Domain Models

Nowak *et al.*, (2002) proposed a different approach to explain the exchange bias phenomenon. Based on the fact that the models of Stiles and McMichael (1999a,1999b, 2001) does not explain the occurrence of instabilities in the uncompensated interface during a hysteresis loop, Nowak *et al.*, (2002) reported on a model of exchange bias in which the *F* is exchange coupled to a diluted *AF*. The *AF* is modelled as an Ising system, and Monte Carlo simulations used to study the behaviour of the *F-AF* bilayer. They include the effect of the whole *AF* layer on the basis of its influence on the formation of domains close to the interface. The basic concept of this model is that on field cooling, in which the *AF* spins are in contact with the *F* spins, it is also exposed to the applied field, there is a development of a domain state in the *AF* which carries magnetisation. The magnetisation of the domain is a metastable state which is formed and becomes frozen during the field cooling process. The model assumes that the domain wall widths are close to zero, and the domains have small size, so that it would be possible to fit a large number of domains in the system. The dilution of nonmagnetic defects in the *AF* promotes the formation of domains in the *AF*, increasing its magnetisation (M_{AF}) and in consequence, H_{ex} would increase. The existence of M_{AF} is shown to give rise to a vertical shift of the resulting hysteresis loops from the simulation. The whole *AF* would contribute to this M_{AF}.

The temperature dependence of H_{ex} obtained is a linear decrease with increasing temperature. The exchange field goes to zero at a temperature T_B, smaller than T_N. The reduction of H_{ex} with repeated field cycling is explained as being due to a loss of magnetisation in the *AF* during the hysteresis loop due to a rearrangement of the *AF* domain spins. In their simulations, this loss is estimated to be less than 10% of the M_{AF}. These two predictions of exchange bias are discussed in chapter 6.

Keller *et al.* (2002) studied the exchange bias dependence on dilution on Co/CoO with nonmagnetic inclusions of CoMgO. They studied various exchange bias phenomena

such as the vertical shift in the magnetisation, the dependence of H_{ex} on temperature the cooling field dependence, training effects, and the variation of H_{ex} with the thickness of the *AF*. Their results are consistently described by the domain state model (Nowak *et al.*, 2002).

The appearance of positive exchange bias due to a high applied field during field cooling (Nogués *et al.*, 2000) is explained as being due to the sign of the exchange coupling between the *F* and the *AF*. Negative *F-AF* coupling overcome by a strong field applied during field cooling would bias the M_{AF} resulting in positive H_{ex}.

The dependence of H_{ex} on the *AF* thickness, t_{AF}, has also been studied. For a low dilution, increasing t_{AF} increases the energy of the domain walls . The energy required to form domain walls can be reduced by increasing the domain sizes and reducing the number of domain walls. Hence a decrease of H_{ex} is expected. For higher dilutions an increase in t_{AF} would have a smaller effect on the domain wall energies, leading to a constant H_{ex}. For very small t_{AF}, H_{ex} is almost zero up to a critical thickness where H_{ex} is set, as explained by Stiles and McMichael (1999a). The main achievement of this model is that it explains features of exchange bias without the need to assume compensated or uncompensated interfaces. Without domain formation, it predicts that there is no H_{ex} for compensated interfaces, and a very high H_{ex} for uncompensated interfaces. The inclusion of defects favours the formation of domains, independently of the nature of the interface.

Using a different approach in the numerical treatment, Scholten *et al.*, (2005) performed mean-field calculations in a diluted system similar to the one described by Nowak *et al.*, 2002, with the difference that this time the interface is assumed to be compensated. The results obtained are similar to those of Nowak *et al*. According to this model the H_C enhancement shows a maximum around the Néel temperature, independent of the dilution of the *AF*. The enhancement of H_C persists at temperatures higher than T_N, although it decreases slowly for thick *AF*s. Nowak *et al*. investigated the origins of this coercivity enhancement as well as the origin of H_{ex}. They concluded that both H_C and H_{ex} have different origins. They observed larger coercivity enhancement for antiferromagnetic coupling at the interface between *F-AF* than for the case of ferromagnetic coupling. The enhancement of H_C is due to the coupling to the *AF* layer as well as the appearance of a shift in the hysteresis loop. They considered the

interfacial magnetisation of the *AF* as the sum of two components, an irreversible metastable *AF* magnetisation, M_{AF}^{irr}, which does not change when going through the hysteresis loop at low temperatures, and a reversible *AF* magnetisation, M_{AF}^{rev}, which follows the field. They concluded that H_{ex} exists only if the interfacial magnetisation contains a component that is frozen during field reversal. Hence, M_{AF}^{irr}, would contribute to H_{ex}. Regarding the enhancement of H_C, they predict the peak with temperature. The peak shifts to lower temperatures for increasing t_{AF}, while H_{ex} decreases with increasing temperature. Depending on the degree of dilution, the peak in H_C is found to appear at the same temperature at which H_{ex} vanishes, T_B. For higher dilutions the peak is found to shift to lower temperatures. Hence, an assignation of the origin of the coercivity enhancement to M_{AF}^{rev}, and the origin of H_{ex} to M_{AF}^{irr} is predicted by these simulations and observed experimentally (Keller *et al.*,2002). In fact the percentage of the *AF* spins that contribute to M_{AF}^{rev}, i.e. that part of the *AF* spins that are dragged with the *F*, increases with temperature (Nogués *et al.*, 1999). Therefore, a direct proportionality between each pair of parameters would be expected, leading to the simultaneous occurrence of a minimum in M_{AF}^{irr} and a maximum of M_{AF}^{rev} at the temperature at which H_{ex} vanishes, i.e. T_B. In chapter 6 it will be shown that H_{ex} vanishes at different temperatures depending on the measurement procedure, and that the peak in H_C does not correlate with the median blocking temperature. Thus, different locations for such particular state that maximises M_{AF}^{rev} can be found. Scholten *et al.* (2005) suggest that both the enhancement of H_C and H_{ex} are not directly related as one of them can be changed without changing the other.

4.6 *Experimental Studies*

Experimental studies by van der Heijden *et al.*, (1998a, 1998b) showed that when the M_F is antiparallel to the unidirectional anisotropy in the *AF* the decrease of H_{ex} increases with temperature and is independent of the field applied to the *F*. This dependence is interpreted as a thermally assisted relaxation process of the magnetic order in the *AF* grains in the same manner as explained by Fulcomer and Charap (1972b). This can lead not only to a decrease of H_{ex} but also to a reversal of H_{ex}. The

results obtained by van der Heijden (1998a) also showed that the time dependence of H_{ex} cannot be described as a single exponential function as proposed by Fulcomer and Charap (1972b), but needs to be described by a distribution of relaxation times, τ. Due to the fact that the *AF* grains are non identical, neither are the domains that form in the *AF*. The relaxation of the magnetic order of the *AF* grains, is not only dependent on the magnetisation direction of the *F*, but also on the temperature and the cooling rate of the field cooling procedure in which the *AF* order is set (van der Heijden *et al.*, 1998b, Gökemeijer *et al.*, 1999a,1999b). Similar results obtained for different thicknesses in the *AF*, showed the limitations of the assumption made by Fulcomer and Charap (1972b) that the *AF* grains were monodomain. The study of magnetisation reversal in FeMn spin valves (van der Heijden *et al.* 1998a) showed that reversal over a distribution of energy barriers is similar to the thermal activation of reversal in a ferromagnet. van der Heijden *et al.* (1998b) observed the decrease of H_{ex} with increasing temperature while the field applied is kept in reverse bias. This was interpreted as a thermally assisted reversal of the grains in the *AF*.

Goodman *et al.*, (1999) studied the effect of the sweep-rate and time at negative saturation on exchange biased systems. They found that each of these two effects is dominant over the other depending on the time spent at negative saturation. When the time spent in negative saturation is less than a certain time the sweep-rate is the dominant and due to viscosity effects a decay of the values of H_{ex} was observed. Otherwise, the effect of time spent in negative saturation dominates. This effect was observed to be manifest as a decay of the H_{ex} due to thermal reversal of the *AF* grains over a distribution of energy barriers to reversal $f(\Delta E)$, which occured while the *F* was kept in negative saturation (Goodman *et al.*, 2001). This study did not address the origin of $f(\Delta E)$, although they suggested interfacial effects as a possible mechanism in the same context as Stiles and McMichael (1999a).

The study of the temperature dependence of thermal activation at negative saturation on the hysteresis loop leads to a progressive shift of H_{ex} towards zero. As the amount of *AF* grains that reverse increases H_{ex} achieves positive values. Differentiation of the variation of H_{ex} with respect to the temperature of thermal activation gives a measure of the distribution of the energy barriers to reversal $f(\Delta E)$, (O'Grady *et al.*, 2002).

The model of Stiles and McMichael (1999b) describes exchange bias in a similar way to the interpretation that it is given in this thesis. This will be described in chapter 6 where results of the experiments are shown and interpreted. The main difference between the granular models described and the interpretation of exchange bias is the fact the systems studied in this thesis are cubic systems, hence, the uniaxial anisotropy used in the model is an approximation for biaxial systems. Furthermore, the fact that most of the parameters related to exchange bias are distributed or unknown, it is possible to find experiments that would fit any model, or vice versa. This is why, measurement reproducibility is the basic pillar of the experiments performed in this work.

It seems unlikely that there is a single explanation for all exchange bias effects. In this thesis it is shown that the effects of interface and the effects of volume of the *AF* appear to be independent. From the data obtained, it is very clear that any model that ignores thermal effects cannot predict exchange bias. This explains the use of fitting parameters in the models. Also, the majority of experimental measurements reported in the literature are not made on samples for which the magnetic and thermal history is known. It is the objective of this work to develop methods of measurement where this issue is rectified.

Chapter 5

Measurement Techniques and Protocols

5.1 Introduction

As explained in chapter 4, the critical aspect of this work is the development of measurement protocols. The objective is not to do a survey of samples. The samples selected for use were IrMn/CoFe in a range of thickness of IrMn. They were selected because IrMn is the favourite material for application in recording heads (Carey, 2003). The development and use of the measurement protocol is a lengthy process. It can take up to two weeks to fully characterise one sample. Therefore, only two samples were selected for measurement. As the focus of the work is on thermal activation, samples with the thinnest *AF* layers, which are most thermally active, were selected. This is important because for the need of CPP read heads and ultimately perpendicular recording, the overall thickness of the head stuck is a critical parameter and thinner *AF* layers must be used. It should be noted that in a head stuck the thickest layer is the one formed by the *AF*.

The samples used in this work are described in the next section. The equipment used to develop the measurement protocols subject of this thesis is described in sections 5.3 and 5.4. After development of the protocols measurement and thermal characterisation of an exchange bias sample should be straight forward. Each of the protocols developed is a further step in the characterisation of the subject exchange biased system. Each protocol is formed by different stages, some of them common to all the protocols. These stages are such as saddle pointing, *AF* reset, and cool to the free thermal activation temperature. The measurement protocols are described in section 5.5. Each of the experiments is described briefly and the measurement protocol followed is given in section 5.6.

The physical reasons to develop the protocols like they are is given in chapter 6 where the experiments are described. In chapter 6, it is presented the experimental procedure

with its motivation, as well as the results of the experiment and the corresponding discussion.

5.2 Sample Preparation

Exchange biased thin films are produced mainly by dc, or rf sputtering (see section 2.2). Sputtered magnetic thin films are polycrystalline, while single-crystal samples are grown by Molecular Beam Epitaxy (MBE).

The samples used in this work were grown by magnetron sputtering on silicon wafers with $\langle 111 \rangle$ texture. The multilayer structure is the following: //Seed(5nm)/Cu(1nm)/ $Ir_{30}Mn_{70}(t_{AF})/Co_{90}Fe_{10}$(10nm)/Ta(5nm), where t_{AF} is the AF thickness, equal to 3 and 5 nm. Both samples were deposited in a field and post annealed at 250°C for two hours. Samples were provided by M. J. Carey, from Hitachi Global Storage Technologies, San Jose, CA.

5.2.1 Polycrystalline Samples

Sputtered samples are polycrystalline and formed of grains each of which is single crystal. Magnetic properties of the polycrystalline materials depend crucially on the distribution of grain sizes (Vopsaroiu *et al.*, 2005). The grain size distribution has been probed by use of the cumulative percentage method, and is best fitted by a lognormal distribution (Park *et al.*, 2000). The lognormal distribution of the grain size, by which the logarithm of the particle diameter has a Gaussian distribution, also applies to other types of films such as ultrafine metal particles (Granqvist and Buhrman, 1976)

Magnetic properties of exchange coupled systems are very sensitive to the grain size distribution. It has been ten years of work to reduce thermal activation due to small grains. In F material it has been shown that thermal activation arises from crystallinity. This arises from the dependence of the anisotropy on the crystallinity. Recent work by Tsunoda *et al.* (2005) showed that the increase in the degree of order in the IrMn layer, measured as the increase in $L1_2$ phase (figure 41) that could be formed in the IrMn,

resulted in giant exchange anisotropy (1erg/cm^2). The increase in the degree of order was obtained by substrate heating and thermal annealing (Tsunoda *et al.*, 2004). This indicates that the crystallinity of the *AF* grain in polycrystalline grains may be critical. Hence, the use of seed layers and thermal annealing to improve crystallinity and reduce thermal effects. These are discussed in section 6.2. Depending on the degree of crystallinity, the interface quality and how susceptible to thermal activation, only a certain portion of the *AF* grains will contribute to exchange bias. The percentage of grains in the *AF* needed to produce exchange bias was probed to be much less than the expected in measurements of thermal activation shown in section 6.2. At 300 K the percentage of active *AF* grains for IrMn(5nm)CoFe(10nm) resulted to be 11%, while for IrMn(3nm)CoFe(10nm) is 80%.

Manzoor *et al.*, (2005), have shown that FeMn/NiFe exchange biased bilayers are more thermally active for smaller grain size in the *AF* layer. Their results showed that H_{ex} increased with increasing *AF* grain size, which was measured as the median of the distribution. This effect shows that for FeMn the energy barriers to reversal are grain size dependent although it is not clear if this is a volume or area dependence. The influence of the *AF* grain size on the H_C was small, suggesting different origins for H_{ex} and H_C. All these results were obtained for samples with the same parameters in the multilayer structures (composition thicknesses, and the *F* grain size) while keeping the *AF* grain size as the only variable and measured at room temperature.

Exchange bias features have been observed in both single crystal and polycrystalline samples and spin glasses (Kiwi, 2001). This shows that exchange bias is an intrinsic property of the materials. Most of the studies of exchange bias to investigate the magnetic structure of the *F-AF* interface have focused in single crystal *AF* films due to the fact that single crystals are easier to simulate in theoretical models (Matsuyama *et al.*, 2000). Nogués *et al.*, (1996b), found that H_{ex} increases with decreasing interface roughness FeF_2/F single crystal samples grown on MgO seed layers, Notling *et al.*, 2000, observed the alignment of spins of polycrystalline Co grown over single crystal $LaFeO_3$.

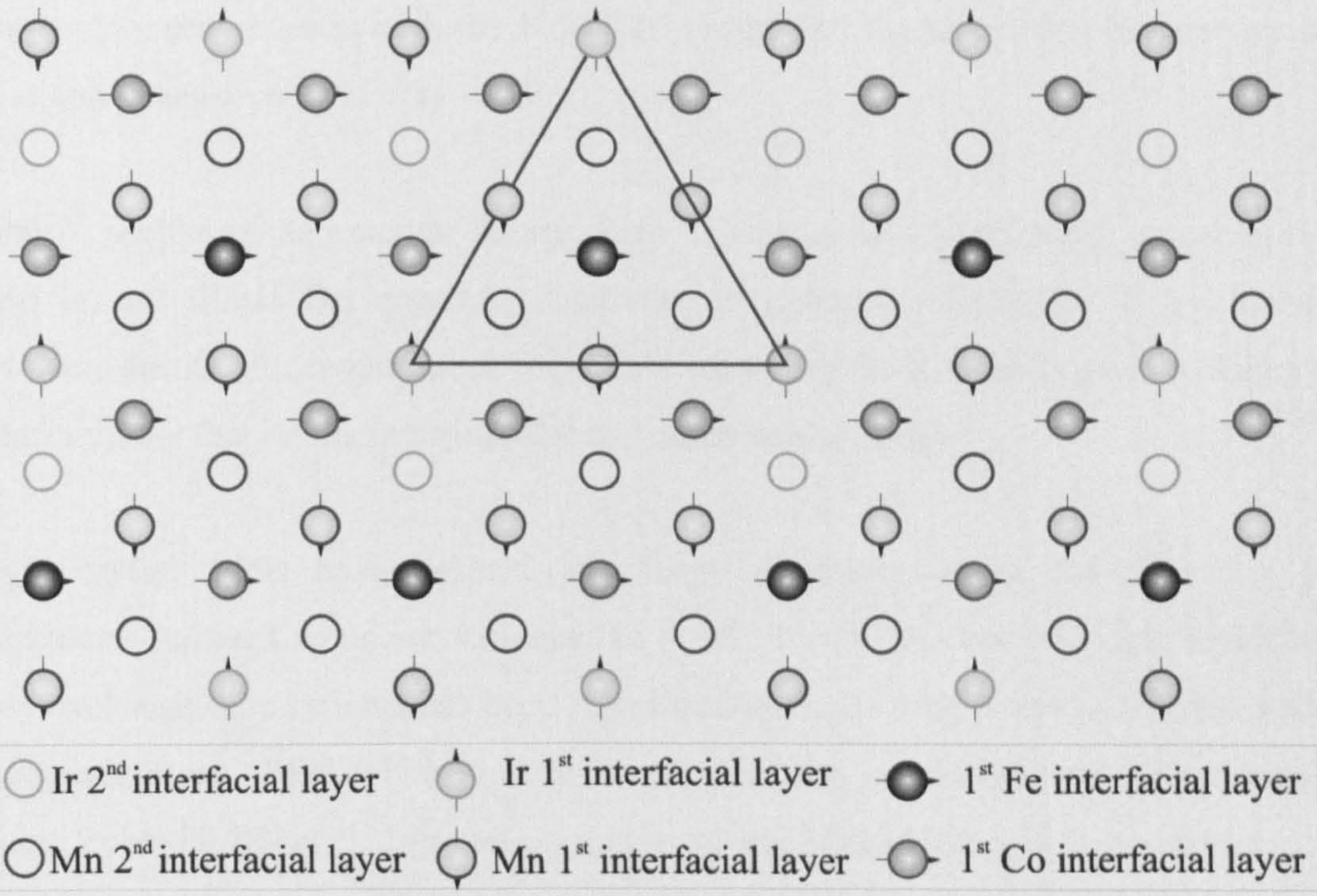

Figure 41 Worked out spin structure of IrMn- $L1_2$ structure as viewed in the (111) direction. The IrMn was grown onto Si (111). Three (111) planes are shown in the figure belonging to the *F-AF* interface. Top plane corresponds to the *F* atoms. Below are the first and second (111) *AF* planes.

5.2.2 Single Crystal Samples

Single crystal samples are mostly grown by MBE. This deposition technique is based in the evaporation of the materials to be deposited by heating them to temperature close to their melting point. Other techniques used, such as chemical vapour deposition (Yang *et al.*, 2000), have in common with MBE that the deposition rates are very slow to achieve epitaxial single crystal growth, even when single crystals are used as substrate (Riedling *et al.*, 1999, Fitzsimmons *et al.*, 2000). The miniaturisation of GMR spin-valves for read heads used in the magnetic recording industry will reach a stage where the dimensions of the spin valves will be similar to the thin film grain diameter. This implies that spin valves could be formed by single crystal elements whose magnetic and transport properties might differ significantly from polycrystalline spin-valves (Sato *et al.*, 2005). It is known that the change from single crystal to polycrystalline structure modifies the formation of domain walls in the *AF* (Gökemeijer *et al.*, 1999a). There are two main differences between single crystal and polycrystalline thin films. Polycrystalline films

have random easy axes in both the *F* and *AF* grains and the interaction between grains varies and in some cases is very weak.

In the *F*, despite of its granular nature there is strong RKKY coupling, as commonly found in soft films. The nature of exchange in granular alloyed *AF* is not known. However, due to the requirement for atomic ordering on a crystallographic lattice it seems unlikely that strong intergranular exchange would occur.

Single crystal films have defined anisotropy directions along the film and the interactions between spins are stronger (Li *et al.*, 2001). The use of single crystals to study exchange bias systems has been based mainly in *AF* single crystals coated with a *F* (Nogués *et al.*, 1999). The growth direction of the *AF* determines the anisotropy values. Epitaxial IrMn(110) grown on single crystal MgO(110), which has a very well defined crystal structure and very smooth interface, showed higher anisotropy than in the other (001), (111) orientations (Sato *et al.*, 2005). Single crystals have the advantage that they can exhibit a more perfectly compensated or uncompensated spin structure, depending on the growth direction, leading to different properties such us interface roughness, *F/AF* relative spin orientations, different magnitude of H_{ex} (Berkowitz and Takano, 1999, Nogués and Schuller, 1999).

5.2.3 Effects of Deposition in a Field

In the deposition of a *F/AF* bilayer, the order in which the *F* and the *AF* are deposited plays a significant role. If the *AF* is grown first, it will grow with a certain texture depending on the seed layer that it is used (Tsang *et al.*, 1981, Kerr *et al.*, 2005). After this the *F* layer is deposited and to induce uniaxial anisotropy in the *F* and orient its magnetisation, a dc field is applied in the plane of the film during deposition (Ambrose *et al.*, 1998). The magnitude of the field that is normally used for deposition of CoFe varies in the range of 50-300Oe (Jung *et al.*, 2003). The application of a field during deposition, reduces the anisotropy dispersion in the *F* as an effect of the applied field on the magnetocrystalline anisotropy of the *F* grains during growth.

The effect of the deposition of the *F* prior to the deposition of the *AF* in a dc field provides uniaxial magnetic anisotropy in the *AF* due to the exchange interaction of the *F* spins acting on the *AF* spins. If the *F* is deposited in zero field, the *AF* will have no unidirectional anisotropy as the *F* spins will be deposited with no preferential direction. To obtain higher unidirectional anisotropy it will be necessary to field anneal the bilayer. These effects have been observed on CoFe/IrMn spin valves (Anderson *et al.*, 2000). When the *AF* is grown first the exchange bias obtained is less than for the opposite case. When these samples are field annealed H_{ex} increases for the samples with the *AF* layer deposited first while for the ones with the *AF* grown on top both magnitudes decrease. These effects are suggested to be due to the H_{ex} dependence on the crystalline texture and the impact of thermal annealing on texture and interdiffusion (Anderson *et al.*, 2000). In comparison, field annealed samples with the AF on top show larger H_{ex} than those with the *AF* layer at the bottom (Kerr *et al.*, 2005). Growth order also influences the temperature dependence of H_{ex} , which resulted to be quasi –linear for samples with the *F* grown first, while H_{ex} showed a plateau and a sudden drop for temperature close to T_B when the *F* was grown on top (Ambrose *et al.*, 1994). No explanation has been suggested for this by the authors. A possible explanation for this could be based on different anisotropy temperature dependence due to different degrees of crystallographic ordering (Tsunoda *et al.*, 2005), or due to different grain growth results as a consequence of different growth order.

5.2.4 Effects of Annealing

The effects of annealing have been subject of many studies of exchange biased systems as a means to improve the performance of GMR and MR heads (Gregg *et al.*, 2002). They were mainly aimed at improving the thermal stability of the exchange bias field. The effects of annealing on an exchange bias system depends on the temperature of the anneal, the time of the anneal, the stage of sample growth at which it has been applied and whether a field is applied during the anneal. The system most studied in the literature has been FeMn/NiFe, although PtMn/CoFe and IrMn/CoFe are the most promising for industrial applications.

Typical temperatures of thermal annealing are 250-350ºC. Studies by Imakita *et al.*, (2005) on an $Ir_{27}Mn_{73}/Co_{70}Fe_{30}$ exchange coupled bilayer containing CrNiFe/Cu as a under layer showed the increase of the lateral size of the Cu grains before growth of the *AF*/*F* bilayer with increasing temperature of annealing. The increase of the grain size has a narrowing effect on the distribution of blocking temperatures of the *AF* grains through the change in grain size distribution of the IrMn layer. Hence thermal stability of H_{ex} is achieved when the sample is annealed under a field of 1 kOe for 1 hour. Figure 42 shows a TEM image of the Cu underlayer.

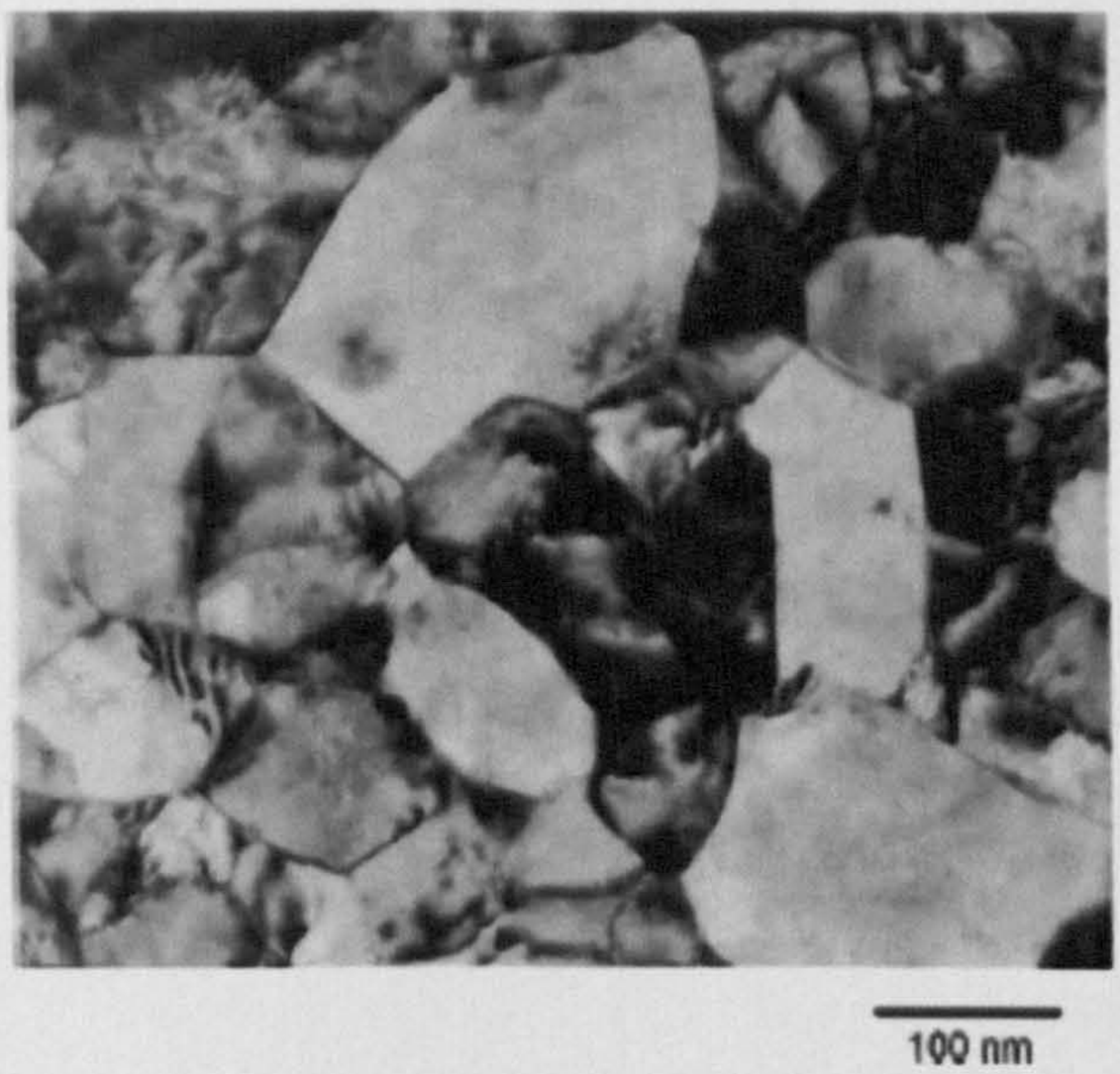

Figure 42 TEM plane view of a Cu 50nm underlayer, deposited on Cr-Ni-Fe 5nm buffer layer at 250ºC in ultra-high-vacuum, annealed at 250ºC, 30Oe for 10min (Imakita *et al.*, 2005).

An increase in the exchange field and coercivity through annealing has been reported by several authors. Studies on NiFe/CrMn by Xi *et al.*,(2000), reported an increase of H_{ex} and H_C after annealing at 310ºC in a 600Oe applied field as consequence of the diffusion of Mn into the NiFe layer. This produces an *AF* NiMnFe interlayer increasing the exchange field. As a matter of fact, the T_N of alloyed NiMnFe exceeds the T_C of NiFe. Figure 43 shows VSM hysteresis loops for this system after annealing. It shows the results of field anneal on coercivity, exchange bias and saturation magnetisation.

The diffusion of Mn in the F layer reduces the magnetic moment of the *F* as observed by Rickart *et al.*, (2005), on PtMn/CoFe exchange biased bilayers after rapid thermal

anneal ($5.5°Cs^{-1}$) up to 320°C in a field of 3kOe. Another feature of annealing is the promotion of structural changes in the sample. A one minute anneal induces a structural phase transition in the PtMn from fcc to *AF* fct without cooling in a magnetic field. Toney *et al.*, (1991), observed two kinds of change on the exchange field depending on the time of annealing on NiFe/FeMn. Moderate annealing produced a change in the dependence of H_{ex} with temperature from linear to Brillouin shape dependence, reflecting the magnetisation of the *AF* with temperature. Auger spectroscopy showed significant interdiffusion. At extended annealing times; interdiffusion of Mn on NiFe produced a NiFeMn alloy which increased the H_{ex}.

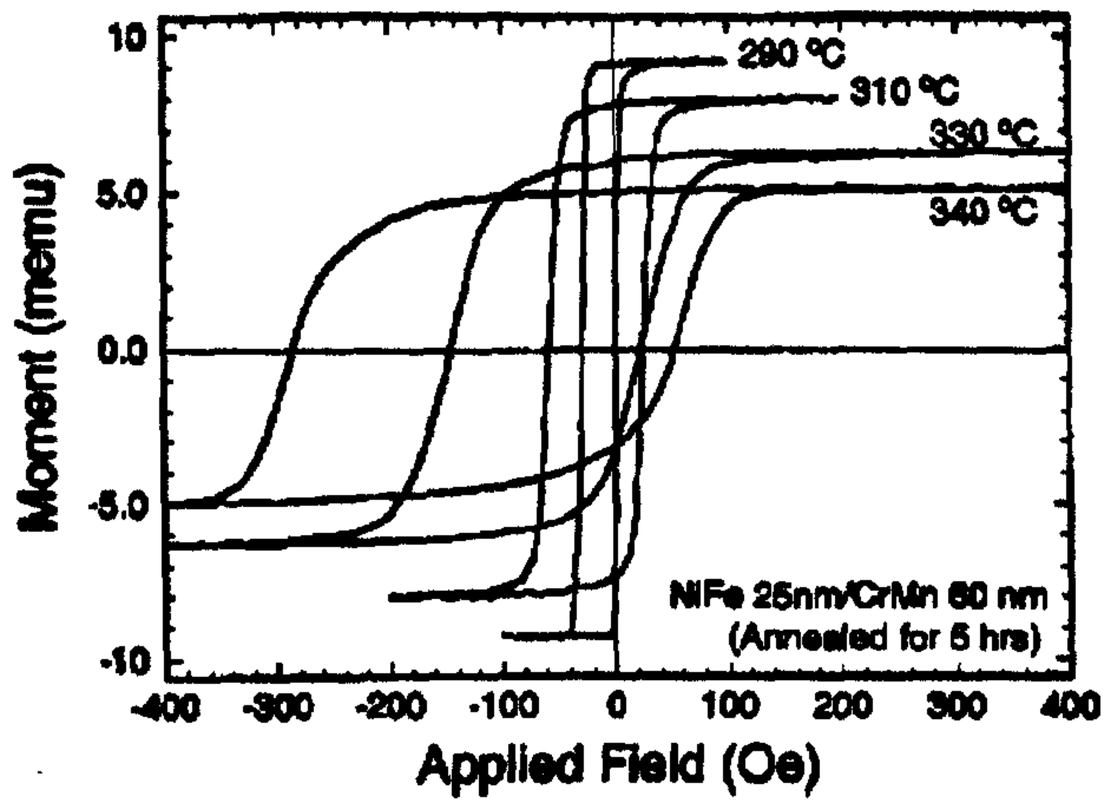

Figure 43 VSM hysteresis loops of annealed $Ni_{81}Fe_{19}/Cr_{50}Mn_{50}$ samples (Xi *et al.*, 2000).

The effects of annealing described up to this point can be summarised as a narrowing of the local blocking temperatures, increase of lateral grain size in the *AF*, phase transitions, diffusion, interface degradation through interdiffusion, alloying, and a decrease of the saturation magnetisation.

Kerr *et al.*, (2005), studied the effects of field annealing on top and bottom spin valves with IrMn/CoFe as the exchange biased layer. It was observed that for bottom spin valves the H_{ex} increased drastically with the magnitude of the field applied during annealing, showing that the interfacial spin structure of the IrMn improves with the anneal field strength. The explanation provided for this was based on the uncompensated interfacial spin structure. The annealing temperature promotes diffusion of Mn increasing the number of defects and therefore the number of pinning sites,

increasing the number of uncompensated interfacial spins. The effect of the annealing field is to improve the alignment of the uncompensated interfacial spins in the direction of the applied field. For the sake of clarity, table 3 quotes some of the results obtained in this study.

Anneal Field ($x10^4$Oe)	H_{ex} (Oe)	ΔR/R
0	230	7.8%
0.5	360	8.2%
5.5	390	8.2%

Table 3 Exchange field dependence on the anneal field strength (Kerr *et al.*, 2005).

It was also observed that in the case of bottom spin valves although the H_{ex} dependence on temperature of anneal has a peak around 180°C the magnetoresistance stayed approximately independent of temperature up to 300°C. For top spin valves H_{ex} as well as the magnetoresistance decreased with increasing annealing temperature. It was observed that interdiffusion of Mn from IrMn to the CoFe/Cu interfaces was more pronounced than in the case of bottom spin valves. Therefore, although there is interdiffusion in both top and bottom spin valves, it is activated by different thermal processes in each case.

5.3 The Vibrating Sample Magnetometer

All the measurements contained in this thesis were made using a Vibrating Sample Magnetometer, VSM. The first VSM was developed by Foner in 1956 (Foner, 1956, 1959, 1996). This instrument has been shown to be very versatile and have high sensitivity, being simple and inexpensive and offering advantages over force methods for magnetic measurements (Wolf, 1957). These advantages include temperature variation, sample rotation and sample changing and reproducible sample positioning.

Since 1956 this instrument has been improved and modified for specific measurement needs (Mallison, 1966; Flanders *et al.* 1993), being used for most accurate measurements of the properties of recording media and magnetic materials. Commercial

*VSM*s are equipped with features such as computer control and automatic data acquisition, temperature control and sample positioning (Mee and Daniel, 1996).
The *VSM* used to perform the experiments described in this thesis is a modified *EG&G Princeton Applied Research Model 4500 VSM* .

5.3.1 Principle of Operation

The principle of operation of the *PAR 4500 VSM* is the induction of a magnetic moment on the sample studied by means of an applied DC magnetic field to the sample. This field is generated by a water-cooled electromagnet that can apply fields up to 1 Tesla. The sample is placed in the centre of the uniform magnetic field and vibrated at small amplitude with known frequency and phase. The vibration of the magnetic sample is perpendicular to the magnetic field lines. This produces a field distortion around the sample position and therefore a change in the magnetic flux of a set of 4 pick-up coils placed near the sample. The voltage out-put from the pick-up coils is processed to give a measurement of the magnetic moment induced as emu/volt. These pick-up coils are clamped to the poles of the electromagnet to avoid vibration of the coils with respect to the applied field. A schematic of this *VSM* is shown in figure 44.

The *PAR 4500 VSM* used is controlled with LabView software designed in the magnetism group. The original analogue lock-in amplifier and synchronous detector have been replaced with an *EG&G 7265 DSP* lock-in amplifier. This resulted in an increase of the sensitivity to less than $5x10^{-6}$ emu for a time constant of 100ms. The field resolution depends on the field range selected for the type of measurement, being less than 1% in the range of applied fields less than 1kOe, and better than 0.1% in the range of applied fields below 10 kOe. Set fields are stable to better than 1Oe/hour.

The vibration mechanism is a head transducer assembly with a power amplifier. It produces a sinusoidal oscillation of the sample perpendicular (z-direction) to the DC applied magnetic (x-direction) field via a carbon fibre rod. The frequency of oscillation is constant, 81.366Hz and its amplitude is 2mm. The 4 pick-up coils are arranged according to Mallison's design (Mallison, 1966) as shown in figure 45. Each pair of coils is located in each pole along the z-direction, with their centre of symmetry in the

middle of the homogeneous field space. Each pair of coils is wound in series opposition. The purposes of this are to add the induced voltages coming from the north and south poles of the sample and cancel any induced changes in the field. The ac voltage induced in the pick-up coils, V, is proportional to the sample moment and to the amplitude and frequency of the oscillation. The voltage V is given by Faraday's law,

$$V = -N\left(d\phi_f/dt\right) = NA\left(dm/dt\right) \tag{5.3}$$

N is the number of turns in the coil, ϕ_f, is the change in flux after a common field has been cancelled, t is the time, A is the cross sectional area, and m is the magnetic moment. The induced signal in the coils is compared to a reference signal produced by a three plate capacitor placed below the transducer that produces the oscillation. This reference signal is also proportional to the amplitude and frequency of the oscillation.

To obtain reproducible data it is necessary to relocate the sample exactly in the same position relative to the pick-up coils. To obtain good repositioning the sample has to be "saddle pointed" in the centre of symmetry of the pick-up coils. This is done using micrometer positioners, which change the position of the sample along x, y and z axes. At the centre of symmetry it is found that the output from the pick-up coils is a maximum in the z and y directions and a minimum in the x direction. This point is easier to find if the order z, x, and y positioning is followed.

To obtain absolute measurements of the magnetic properties of a material the *VSM* needs to be calibrated against a reference signal from a material with known properties. For accurate calibration the sample used for calibration must be of similar size and geometry as the sample of interest to obtain a similar geometric response from the coils. In the case of thin films, a Palladium or Nickel foil of known mass, and therefore magnetic moment is used. These are chosen depending on the value of the moment of samples to be measured. As Palladium is a Pauli paramagnet, it has a linear response to the applied field in a wide range of temperatures. Hence, a range of calibration moments can be obtained by applying different fields. In practice the process is aimed at obtaining the emu/volt constant of calibration. The field is calibrated with a hall probe.

This hall probe is calibrated using a NMR proton magnetometer with a frequency tuned according to the broadcast frequency standard.

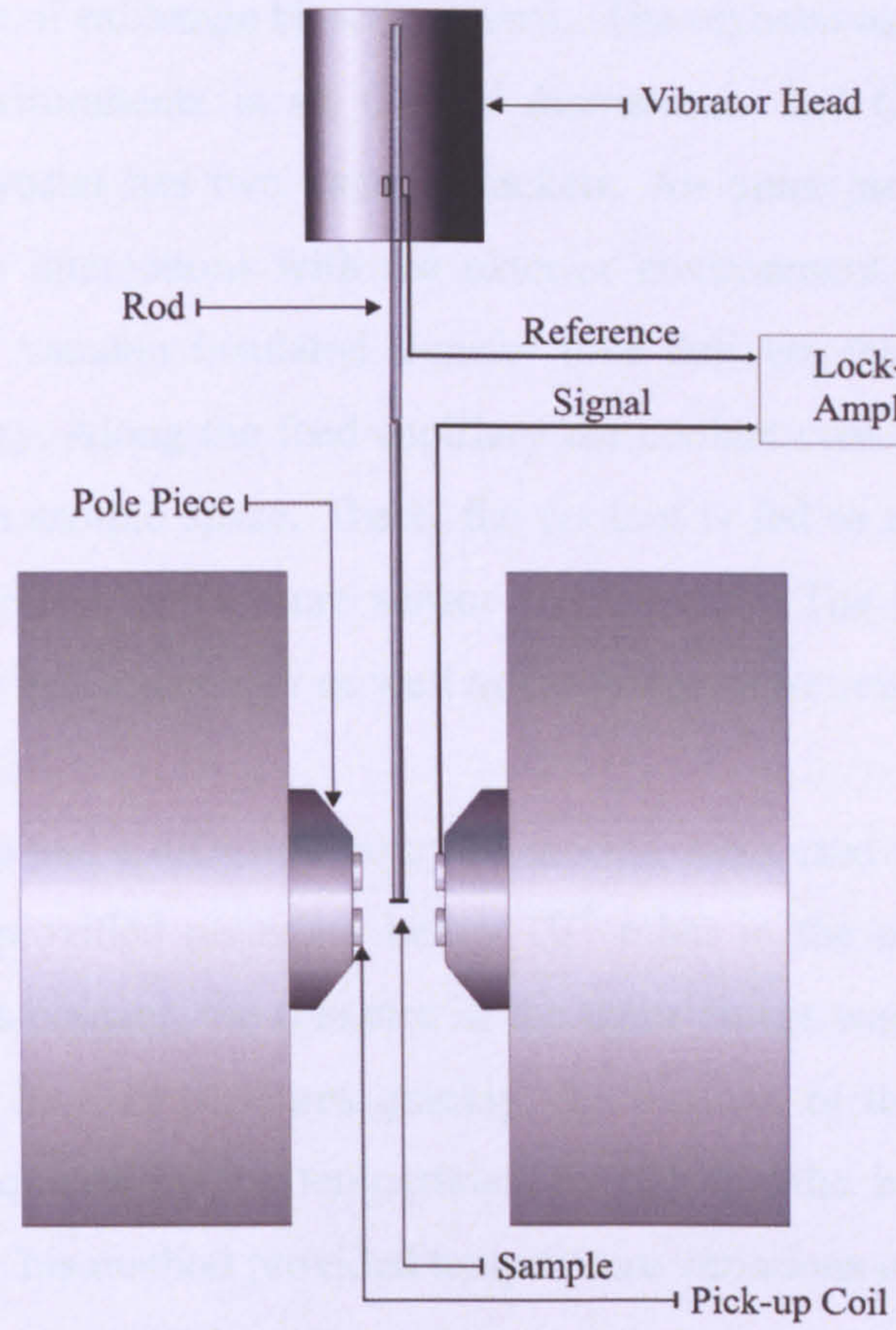

Figure 44 Schematic of a VSM.

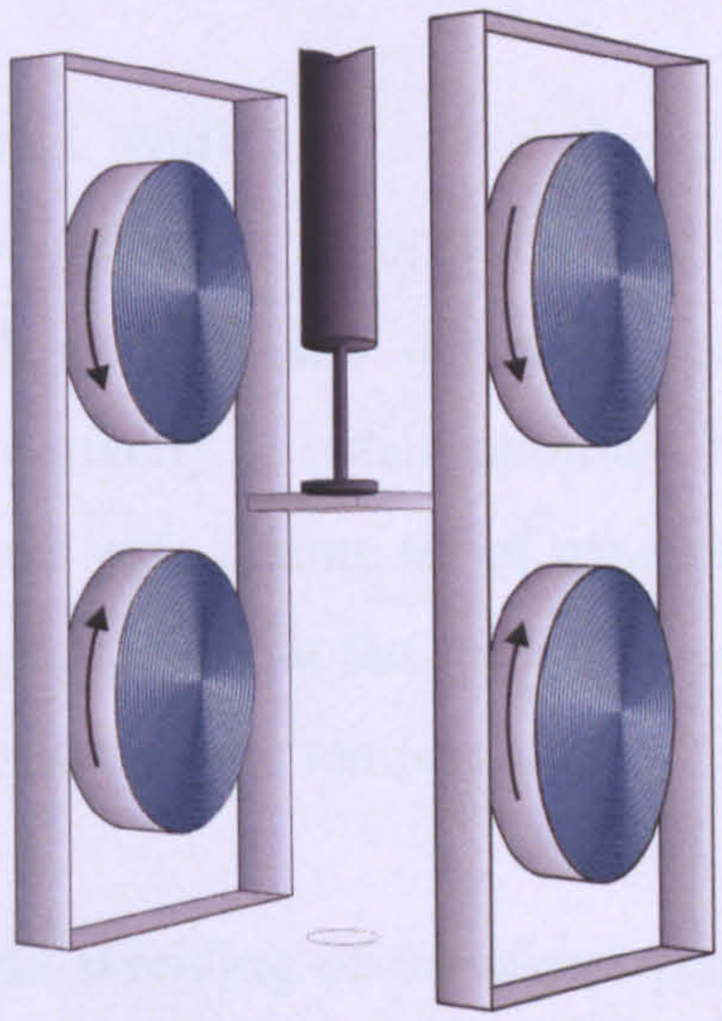

Figure 45 Schematic of a set of pick-up coils.

5.4 Temperature Control

The most of the work involved in this thesis is related to the temperature dependence of the magnetic state of exchange biased systems. The cryostat used to achieve the desired measurement environments is an *Oxford Instruments Ltd CF1200* continuous flow cryostat. This cryostat has two vacuum jackets. An outer jacket isolates the cryostat from temperature interactions with the exterior environment. The inner jacket is the sample space. A vacuum insulated transfer tube delivers the coolant to the cryostat through a capillary. Along the feed capillary the coolant runs down the outer jacket to the bottom of the sample space. There, the coolant is fed to a copper heat exchanger, which is fitted with a temperature sensor and a heater. The heater is a 70Ω resistor, located inside the heat exchanger as well as the temperature sensor.

A roughing pump and a diffusion pump connected were used to vent the cryostat. This vacuum system provided pressures below 10^{-5} mbar in the outer jacket. When using liquid nitrogen as coolant, the pressure in the inner jacket was as low as 10^{-3} mbar. In order to achieve low temperatures quickly, the vacuum in the outer jacket would be removed whilst quenching the temperature by dipping the bottom of the cryostat in liquid nitrogen. This method provided temperature variations of more than 40K/min. When the coolant was liquid helium this procedure is not possible, the sample space needs to be filled with an exchange gas such as He gas. Thus, a quenching process to reduce the temperature would be redundant.

The temperature is controlled with an *Oxford Instruments Ltd ITC4 Intelligent Temperature Controller*. The principle of operation of the temperature controller is governed by a proportional, integer, and derivative control. The values of these parameters must be selected correctly to obtain optimum control over temperature. The approach to the set temperature with a same set of parameters may vary with the range of temperatures involved. This means that the values chosen for a certain system had to be varied depending on the measurement temperature.

The cryostat produces a slight shielding of the signal produced by the sample. Also, careful control of the sample position relative to the cryostat walls must be taken. It is required that the sample, sample holder and the carbon-fibre rod do not touch the walls

of the cryostat at any point. The effect of this would be the addition of noise to the measurement. The cryostat must not touch the pick-up coils of the *VSM*. This fact would add noise, which would be proportional to the applied field. Another source of noise is the formation of eddy currents around the jacket of the sample space, which would have a stronger effect at lower temperatures. This manifests as a reduction in the signal that is picked-up by the search coils. To prevent the formation of eddy currents the inner jacket is fitted with a cooper belt with vertical slots.

Recently some changes have been made in the *Oxford Instruments Ltd CF1200* to increase the temperature range of utilisation of the cryostat. This implied the substitution of the platinum resistor Pt-100 sensor, which was originally fitted in the heat exchanger, for a 27Ω Rhodium-Iron resistance thermometer. Following this process, three point calibration was required. The cryostat could also be used as an oven for temperatures up to 400K. The materials used in the construction of the cryostat limited the highest temperature of measurement. In consequence, these changes allow temperature measurements in the range of 4.2K to 400K. The temperature resolution obtained is better than 0.5 K over experimental time scales. New sample holders had to be made to work in this range of temperatures.

5.5 Measurement Protocols

The protocols developed in this thesis are aimed at obtaining measurement reproducibility. The structure is the same for all measurements and is self contained, and complete. The format is similar to those used in industry according to ISO 9002 standards. A measurement protocol contains all the necessary steps to perform the experiment. Hence, the measurement process is simplified, clearer, and more efficient. The history of the sample for the experiment is registered, allowing simple and fast revision. In the case of any special occurrence during the experiment, there is a section for comments. The following sections describe these protocols for each experiment in a short paragraph followed by a copy of the measurement protocol itself.

5.5.1 Resetting of the *AF* state

The sample is aligned with the unidirectional anisotropy axis parallel to the applied field and saddle pointed in the VSM. The process of saddle pointing has been described previously in section 5.3.1. Following this step a positive field is applied which is strong enough to saturate the ferromagnet. The temperature is increased while the sample is kept under the influence of the applied field. This situation is maintained for a certain amount of time. The temperature is then lowered to the temperature of measurement. At this temperature a hysteresis loop is measured cycling the field from positive to negative values while the temperature is kept constant.

For IrMn(3nm)/CoFe(10nm) a temperature of 373K and 90min under a saturating field resulted to be good conditions to reset the *AF*. For IrMn(5nm)/CoFe(10nm) the use of the same conditions were sufficient to delete previous thermal activation and obtain reproducible data. See section 6.2.2. The procedure to determine the *AF* state resetting conditions is described in figure 46.

***AF* Reset**

1. Saddle point ☐
2. Align sample ☐
3. Temperature of measurement
4. T_m = ☐
5. (P, I, D) (T_{reset}) = ☐
6. **Positive Saturating Field**
7. H_{+sat} = ☐
8. ⇒ **Go to *point 1*** t_i = ☐
9. **Heat to** T_{reset} = ☐
10. Time needed to reach T_{reset}
11. t_i = ☐
12. t_f = ☐
13. t (T_{reset}) = ☐
14. (P, I, D) (T = T_m)= ☐
15. **Cool to** T = T_m ☐
16. **Time to reach** T_m
17. t = ☐
18. Time spent in ***point 1***:
19. t = ☐
20. ***Measure the loop*** ⇒

Figure 46(a) *AF* reset measurement protocol.

5.5.2 Thermal Activation Free Temperature

The alignment stage is the same as the previous experiment. Field and unidirectional anisotropy axis are set parallel. This is followed by the resetting of the magnetic state in the antiferromagnet. The conditions for this are characteristic of the sample under study. The outline of the process is the following: apply a positive saturating field to the ferromagnet, increase the temperature, and maintain these conditions for a fixed time. Then, the temperature is lowered to the temperature of measurement. This measurement is similar to the one described previously. In this case the variable is the temperature of measurement while previously the variables were the *AF* resetting conditions. The criteria that show when it is achieved the thermal activation free temperature, T_{NA}, is given in section 6.2.2. A copy of the measurement protocol for this experiment is shown in figure 47.

Thermal Activation Free Temperature

1. Saddle point and alignment section_☐
2. **Temperature of No thermal Activation?**
3. T_{NA} = _____☐
4. (*P, I, D*) (100°C) = _____☐
5. Positive Saturating Field
6. AF Resetting Section_____☐
7. Cool to T = T_{NA}_____☐
8. Time to reach T_{NA}- t = _____☐
9. **Time needed to stabilise T_{NA}**
10. t_S (T_{NA}) = _____☐
11. Time spent in ***point 1***:
12. t = _____☐
13. Negative Saturating Field
14. H_{-sat} = _____☐
15. ⇒ **Go to *point 4*** _t_I =_____☐
16. **Time at *Point 4*** = _____ ***min***☐
17. Total t at *Point 4* =_____☐
18. ***Measure the loop*** ⇒ _____☐

Figure 47(a) Measurement protocol for determination of T_{NA}.

5.5.3 Reversal of the Magnetic State in the *AF*

This procedure allows reordering the magnetic state of the *AF* and reversing its initial magnetic state. The first steps are to align and saddle point the sample. To obtain reproducible data the state in the *AF* is reset by sample dependent conditions found in

previous experiments. The temperature is then lowered to T_{NA}. At this point the field is reversed to saturate the ferromagnet in the opposite direction. The next step is to increase the temperature to T_{Act}, the temperature of thermal activation. Negative saturation at T_{Act} is maintained for a fixed amount of time. Then the temperature is reduced to T_{NA}. Immediately after this, the field is cycled from negative saturation, $-H_{sat}$ to positive saturation, measuring the hysteresis loop. The procedure can be repeated for differing values of T_{Act} but measurements are always made at T_{NA} to avoid changes in the *AF* state during the field sweep. A copy of the measurement protocol for this experiment is shown in figure 48.

Reversal *AF* Magnetic State

1. Saddle point and alignment section_☐
2. T_{NA} = _____☐
3. (*P, I, D*) (100°C) =_____☐
4. Positive Saturating Field
5. **AF Resetting Section**_____☐
6. **Cool to T_{NA}** _____☐
7. **Negative Saturating Field**
8. H_{-sat} = _____☐
9. ⇒ **Go to *point 4*** _t_1 =_____☐
10. (*P, I, D*) (T_{Act}) =_____☐
11. Time $_{Activ}$ at *Point 4* = _____*min*☐
12. **Heat to T = T_{Act}** =_____☐
13. t_1 = _____☐
14. t_f= _____☐
15. Total time at T_{Act} ⇒ t =_____☐
16. **Cool to T_{NA}** _____☐
17. Time to reach T_{NA} ⇒ t = _____☐
18. Time needed to stabilise T_{NA} _____t_S
19. (T_{NA}) = _____☐
20. Total t at *Point 4* =_____☐
21. ***Measure the loop*** ⇒

Figure 48(a) Measurement protocol for studying magnetic order reversal in the *AF*.

5.5.4 Angular Dependence of the Exchange Field and Coercivity

The first steps are alignment and saddle point the sample with the unidirectional anisotropy axis parallel to the direction of the applied field. After this, a positive field is applied and temperature is raised to a certain value for a fixed amount of time. The field was then set to zero after cooling and the angular position of the sample set to the angle at which H_{ex} and H_C are to be measured. A hysteresis loop is measured starting at positive fields. Comments about this process and how it could be improved are given in

sections 6.4 and 7.2. The measurement protocol for this experiment is shown in figure 49.

Angular Dependence of H_{ex} and H_C

1. Saddle point and alignment section_□
2. Align sample_⇒ Θ_0_____□
3. Angle Reading in Vibrating Head for this alignement_____Θ_0 =_____□
4. Temperature of measurement
5. T_m = _____□
6. Temperature of No thermal Activation
7. T_{NA} = _____□
8. **Positive Saturating Field**
22. **AF Resetting Section**_____□
10. **Select Field Values for Measurement**
11. **Cool to T_{NA}** _____□
12. ***Go to Zero Field*** t= _____□
13. ***Align Angle of Measurement*:**
14. Angle Increment from Θ_0⇒ $\Delta\Theta$ = _____□
15. Angle of Measurement Θ =_____□
16. Saddle point_____□
17. ***Measure the loop*** ⇒

Figure 49(a) Measurement protocol for studying the angular dependence of H_{ex} and H_C.

5.5.5 Study of Training Effects

The procedure starts with the alignment and saddle-point of the sample with the unidirectional anisotropy axis parallel to the direction of the applied field. The *AF* is reset as before. Immediately after this the temperature is set to the value at which the measurement is going to be made. At this temperature, the field is cycled over a number of loops, subsequently, the measurements of the hysteresis loops are done. The measurement protocol for this experiment is shown in figure 50.

Training Effects

1. Saddle point and alignment section_□
2. T_{NA} = _____□
3. **Positive Saturating Field**
4. AF Resetting Section_____□
5. ***Select Field Values for Measurement***
_____□
6. Cool to T_m_____□
7. ***Measure the loop*** ⇒

Figure 50(a) Measurement protocol for the study of training effects.

5.5.6 Measurement Protocol Files

Experiment /File: ***AF*** **Reset /**

Name: Luis E Fernández Outón

Date:

Sample:

Saddle point ☐

Align sample ☐

Temperature of measurement

T_m = ☐

(*P, I, D*) (T_{reset}) = ☐

Positive Saturating Field

H_{+sat} = ☐

⇒ **Go to *point 1*** t_i = ☐

Heat to T_{reset} = ☐

Time needed to reach T_{reset}

t_I = ☐

t_f = ☐

t (T_{reset}) = ☐

(*P, I, D*) (T = T_m) = ☐

Cool to T = T_m ☐

Time to reach T_m

t = ☐

Time spent in ***point 1***:

t = ☐

Measure the loop ⇒

H_{+sat} = ⇒ H_{-sat} = ☐

Step = - ☐

H_{-sat} = ⇒ H_{+sat} = ☐

Step = + ☐

SET SAMPLE DRIVE **ON** ☐

Start Measurement ☐

Go to **Zero Field** ☐

CHECK RESULTS ☐

MEMO

Figure 46 ***AF*** **reset measurement protocol.**

Experiment /File: Temperature of No thermal Activation /

Name: Luis E Fernández Outón

Date:

Sample:

Saddle point ☐
Align sample ☐

Temperature of No thermal Activation?
T_{NA} = ☐

(*P, I, D*) (100°C) = ☐

Positive Saturating Field
H_{+sat} = ☐
⇒ **Go to *point 1*** t_i = ☐

Heat to 100°C t_i = ☐
Time stabilise **100°C**
t_S(100°C) = ☐

Resetting Time at 100°C ***min*** ☐

Select Field Values for Measurement ☐

Total Time at (T=100°C)
t_S + Reset time = ☐

(*P, I, D*) (T_{NA}) = ☐
Cool to T = T_{NA} ☐
Time to reach T_{NA} t = ☐

Time needed to stabilise T_{NA}
t_S (T_{NA}) = ☐

Time spent in ***point 1***:
t = ☐

Negative Saturating Field
H_{-sat} = ☐
⇒ **Go to *point 4*** t_i = ☐

Time at *Point 4* = ***min*** ☐

Total t at *Point 4* = ☐

Measure the loop ⇒
H_{-sat} = ⇒ H_{+sat} = ☐
Step = + ☐
H_{+sat} = ⇒ H_{-sat} = ☐
Step = - ☐
SET SAMPLE DRIVE **ON** ☐
Start Measurement ☐
Go to **Zero Field** ☐
CHECK RESULTS ☐

MEMO

Figure 47 Measurement protocol for determination of T_{NA}.

Experiment /File: Reversal *AF* magnetic state /

Name: Luis E Fernández Outón

Date:

Sample:

Saddle point ☐

Align sample ☐

Temperature of No thermal Activation

T_{NA} = ☐

(*P, I, D*) (100°C) = ☐

Positive Saturating Field

H_{+sat} = ☐

⇒ Go to *point 1* ⇒ t_i = ☐

Heat to 100°C ⇒ t_i = ☐

Time stabilise **100°C**

t_S(100°C) = ☐

Resetting Time at 100°C ☐ *min*

Select Field Values for Measurement ☐

Total Time at (T=100°C)

t_S + Reset time = ☐

(*P, I, D*) (T_{NA}) = ☐

Cool to T_{NA} ☐

Time to reach T_{NA} ⇒ t = ☐

Time needed to stabilise T_{NA}

t_S (T_{NA}) = ☐

Time spent in *point 1*:

t = ☐

Negative Saturating Field

H_{-sat} = ☐

⇒ Go to *point 4* t_i = ☐

(*P, I, D*) (T_{Act}) = ☐

Time $_{Activ}$ **at *Point 4*** = ☐ *min*

Heat to T = T_{Act} = ☐

t_i = ☐

t_f = ☐

Total time at T_{Act} ⇒ t = ☐

Cool to T_{NA} ☐

Time to reach T_{NA} ⇒ t = ☐

Time needed to stabilise T_{NA}

t_S (T_{NA}) = ☐

Total t at *Point 4* = ☐

Measure the loop ⇒

H_{-sat} = ⇒ H_{+sat} = ☐

Step = + ☐

H_{+sat} = ⇒ H_{-sat} = ☐

Step = - ☐

SET SAMPLE DRIVE **ON** ☐

Start Measurement ☐

Go to **Zero Field** ☐

CHECK RESULTS ☐

MEMO

Figure 48 Measurement protocol for studying magnetic order reversal in the *AF*.

Experiment /File: Angular dependence of H_{ex} and H_C /

Name: Luis E Fernández Outón

Date:
Sample:

Saddle point ☐
Align sample ⇒ Θ_0 ☐
Angle Reading in Vibrating Head for this alignement Θ_0 = ☐

Temperature of measurement
T_m = ☐

Temperature of No thermal Activation
T_{NA} = ☐
(P, I, D) (T_{reset}) = ☐

Positive Saturating Field
H_{+sat} = ☐
⇒ Go to *point 1* ⇒ t_1 = ☐

Heat to T_{reset} ⇒ t_1 = ☐
Time stabilise T_{reset}
$t_S(T_{reset})$ = ☐
Resetting Time at T_{reset} *min* ☐

Select Field Values for Measurement ☐

Total Time at (T_{reset})
t_S + Reset time = ☐

(P, I, D) (T_{NA}) = ☐
Cool to T_{NA} ☐
Time to reach T_{NA} ⇒ t = ☐

Time needed to stabilise T_{NA}
t_S (T_{NA}) = ☐

Go to Zero Field t= ☐
Time spent in *point 1* ⇒ t = ☐

Align Angle of Measurement:
Angle Increment from Θ_0 ⇒ $\Delta\Theta$ = ☐
Angle of Measurement Θ = ☐

Saddle point ☐

Measure the loop ⇒
H_{+sat} = ⇒ H_{-sat} = ☐
Step = - ☐
H_{-sat} = ⇒ H_{+sat} = ☐
Step = + ☐
SET SAMPLE DRIVE **ON** ☐
Start Measurement ☐
Go to **Zero Field** ☐
CHECK RESULTS ☐

MEMO

Figure 49 Measurement protocol for studying the angular dependence of H_{ex} and H_C.

Experiment /File: Training Effects /

Name: Luis E Fernández Outón

Date:
Sample:

Saddle point ☐
Align sample ☐

Temperature of No thermal Activation
T_{NA} = ☐
(*P, I, D*) (100°C) = ☐

Positive Saturating Field
H_{+sat} = ☐
⇒ Go to *point 1*⇒ t_i = ☐

Heat to 100°C⇒ t_i = ☐
Time stabilise **100°C**
t_S(100°C) = ☐

Resetting Time at 100°C ***min*** ☐

Select Field Values for Measurement ☐

Total Time at (T=100°C)
t_S + Reset time = ☐

(*P, I, D*) (T_m) = ☐
Cool to T_m ☐
Time to reach T_m⇒ t = ☐

Time needed to stabilise T_m
t_S (T_m) = ☐

Time spent in ***point 1***:
t = ☐

Measure the loop ⇒
H_{+sat} = ⇒ H_{-sat} = ☐
Step = - ☐
H_{-sat} = ⇒ H_{+sat} = ☐
Step = + ☐
Number of Cycles ***n*** = ☐

SET SAMPLE DRIVE **ON** ☐
Start Measurement ☐
Go to **Zero Field** ☐
CHECK RESULTS ☐

MEMO

Figure 50 Measurement protocol for the study of training effects.

Chapter 6

Thermal effects on exchange biased bilayers

6.1 Introduction

Much of the published literature related to the phenomenon of exchange bias is not specific in terms of the exact experimental conditions used to obtain the measurements. In most of the cases the magnetic history prior to measurement of the exchange bias system is not described. Furthermore, it is often not appreciated that the state of the *AF* material can change either by maintaining the material with the *F* layer saturated in the opposite direction to that in which it was originally set, or due to unseen thermal processes occurring in the *AF*. Changes in the *AF* may occur during what appears to be a normal measurement of the properties of the *F*. These facts are the main motivation to develop the measurement protocols described in section 5.5.

Following these protocols measurements have been made on IrMn/CoFe exchange biased systems where we have ensured that the measurements are reproducible. This means that the history of the sample under study must be known prior to any measurement. Also any change in its magnetic state that might have occurred during a previous measurement needs to be erased in order to obtain a reproducible initial state.

6.2 Thermal activation in IrMn exchange biased systems

It has been shown previously by experiment that H_{ex} derives from the amount of *AF* material that exists in a state such that its orientation remains unaltered when the ferromagnet is reversed (O'Grady *et al.*, 2002). It has been shown experimentally that the bulk magnetisation of the ferromagnetic layer drives these changes in H_{ex} (Zhou *et al.*, 2001). Gökemeijer *et al.*, (1999a) studied H_{ex} in CoO/NiFe and FeMn/NiFe thin films by field cooling. By lowering the temperature from above T_N (292K for CoO, 690K for bulk IrMn) to a lower temperature so that order in the *AF* is established, it was found that the ordered state in the *AF* was dependent of the state in which the system

was cooled. In a similar way, Miltényi *et al.* (1999) showed that it is possible to set H_{ex} to different values depending on the remanent state of the *F* during field cooling.

Due to the lack of magnetic moment in the *AF* material, the observation of thermal activation effects in the *AF* layer is impossible due to the difficulty of detecting variations in the order of the *AF* material. The variation in the order in the *AF* has been studied through the effect its order has on the *F*.

Both *AF* and *F* layers in the exchange biased system are composed of grains, which are distributed in size according to a lognormal distribution as stated in section 5.2.1. Due to their polycrystalline nature there will be a distribution of anisotropy easy axes in the whole ensemble of grains that form each layer. The dispersion in the anisotropy easy axis of the *AF* is dependent of the deposition process used. See sections 5.2.3 and 5.2.4. Also, effects such as domain wall pinning, which may arise from crystalline imperfections or grain boundaries, may give rise to distributed energy barriers due to reversal of the magnetic state of each *AF* grain. Therefore, the character of the distribution of energy barriers to reversal in the *AF* will be a crucial influence on the behaviour of the state of the *F*.

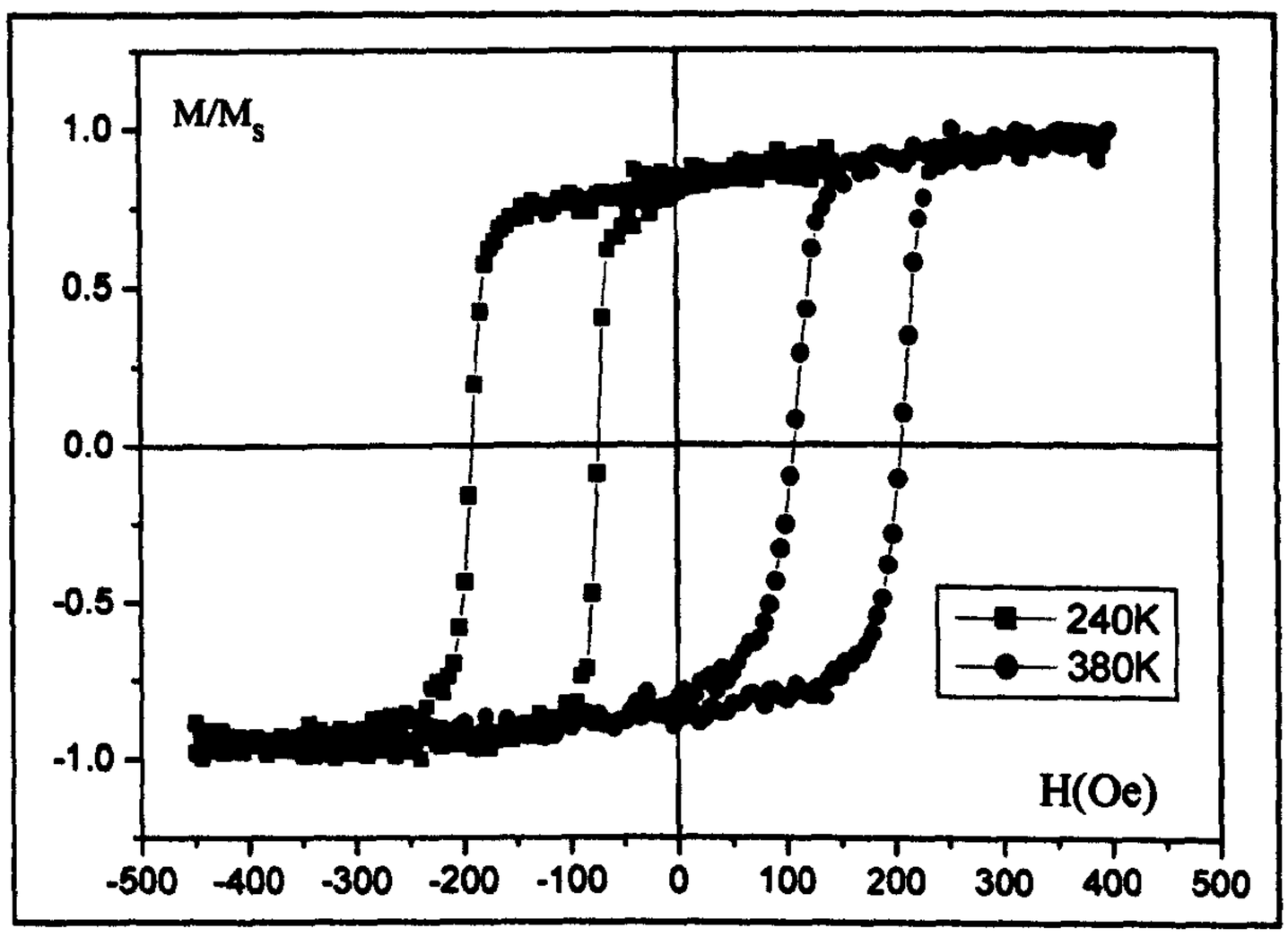

Figure 51 Effect of thermal activation on IrMn(5nm)/CoFe(10nm) measured at 100 K.

Figure 51 shows the effects of thermal activation on the *AF* grains under the influence of a reversed applied field for 30 minutes at two different temperatures. Increased thermal activation results in a shift of the hysteresis loop towards positive field values. The measurements shown were taken at the same temperature, 100K. At this temperature it has been determined that no further thermal activation occurred during measurement or at least if there is any, it is not significant, even if a reversed field is applied for longer times.(see section 6.2.2).

The reversal of *F* particles and grains by thermal activation has been widely studied as described in section 2.9. When a negative field is applied to an exchange biased system, the reversal of the *F* will be determined by the exchange interaction with the underlying *AF*, which is exerted through the interface of the materials. In a microscopic picture, the reversal of a *F* grain will depend on the strength of the exchange coupling to the neighbouring *AF* grains as much as on the properties of the *F* itself. The *AF* grains exert an exchange field on the neighbouring *F* grains that prevents them from reversing their state of magnetisation when a negative field is applied. Some of the *F* grains will change their spin orientation and reverse, therefore, the exchange interaction between *F* and *AF* will be modified. The *F* grains that are reversed exert an exchange field on the *AF* grains that promotes the reversal in the *AF* orientation of axis along which order is established. It should be noted that this effect occurs below T_N for the *AF*, and the *AF* order is maintained with spins paired in opposite directions. However the spins at the interface reverse orientation to maintain a "near" parallel alignment with a resulting reversal of the direction of all the spins in the *AF* grain to maintain the antiparallel state. As described in section 2.9, the energy barriers to reversal, ΔE, are distributed within the *AF*. When an energy barrier, ΔE, is overcome the state of the *AF* grain will flip to a reversed state. Figure 52(a) shows a schematic of the energy barriers to reversal for the original *AF* state after field cooling. Figure 52(b) shows the distribution of energy barriers to reversal after thermal activation of *AF* grains with low energy barriers to reversal. Those *AF* grains with higher energy barriers remain in the original state. The amount of *AF* grains that remain in their original spin state determines H_{ex}. See figure 51. In section 6.2.3 it is shown how H_{ex} varies as the amount of *AF* material that remains unaltered is tailored by thermal activation.

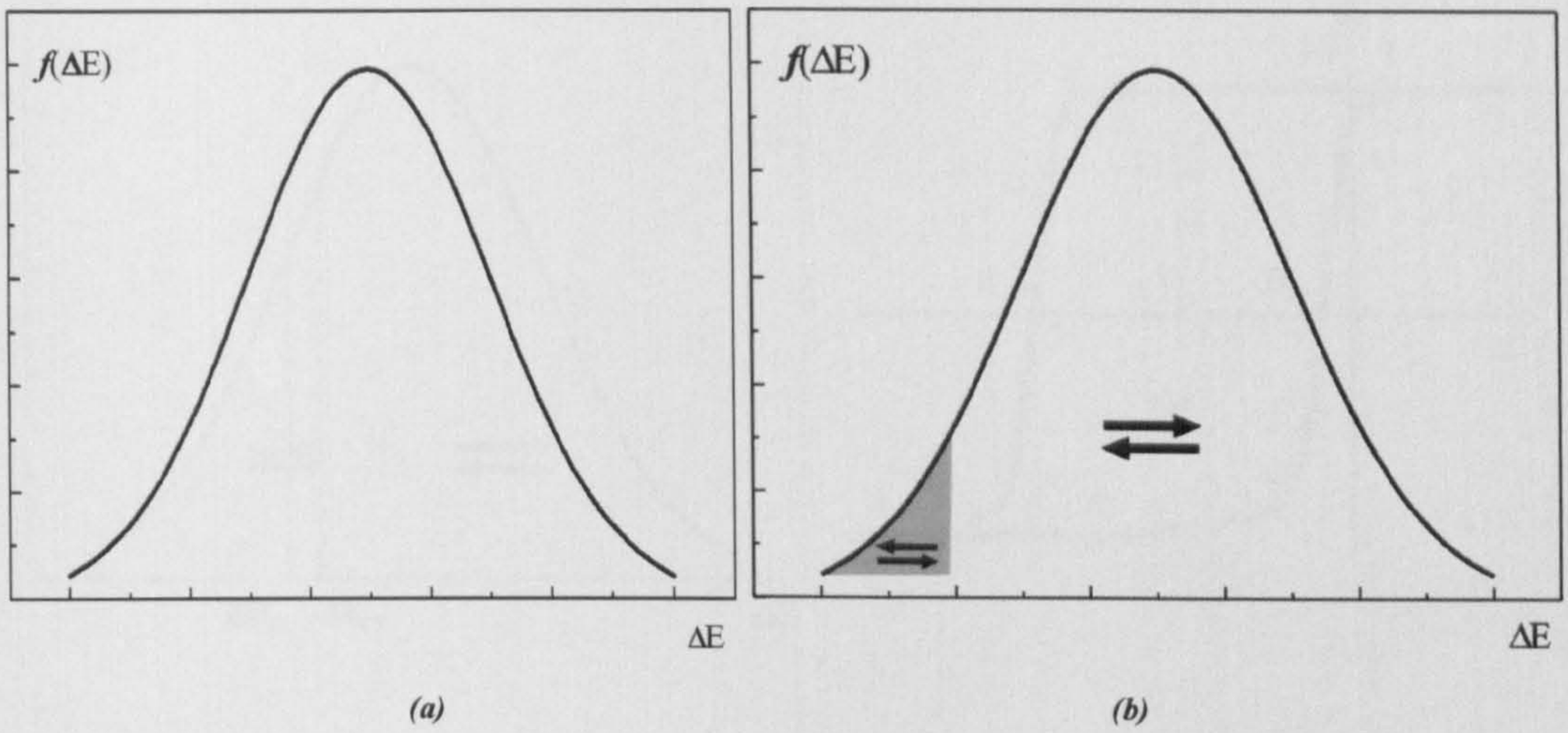

Figure 52 Schematic of distribution of energy barriers to reversal. (a) Original state after field cooling. (b) After thermal activation under a negative saturating applied field to the *F*.

6.2.1 Reset of the order in the antiferromagnetic layer

In order to obtain reproducible measurements, it is necessary to reset the magnetic state of the antiferromagnet. When the reset of the *AF* is achieved, hysteresis loops measured under the same circumstances would result in their superposition if the magnetic state of the sample measured were the same in both cases prior to measurement.

O'Grady *et al.* (2002) developed a procedure to reset the *AF* by which it is possible to reproducibly and reliably obtain the same magnetic state by taking advantage of thermal activation to "delete" any change which occurred in the *AF* from the original state due to thermal activation over the energy barriers to reversal. They investigated the reversal of the *AF* in two spin-valves formed by FeMn/NiFeCo/Cu/NiFeCo. To reset any previous thermal activation of the *AF* grains or *AF* domains, the sample was held at 373 K in a field of +300 Oe for 45 min. These conditions derive from the experimental fact that it is possible to completely reverse the state of the *AF* within a 15 minute period. Hence, maintaining the sample at positive saturating field for three times that period ensures that the state of the *AF* is fully reordered.

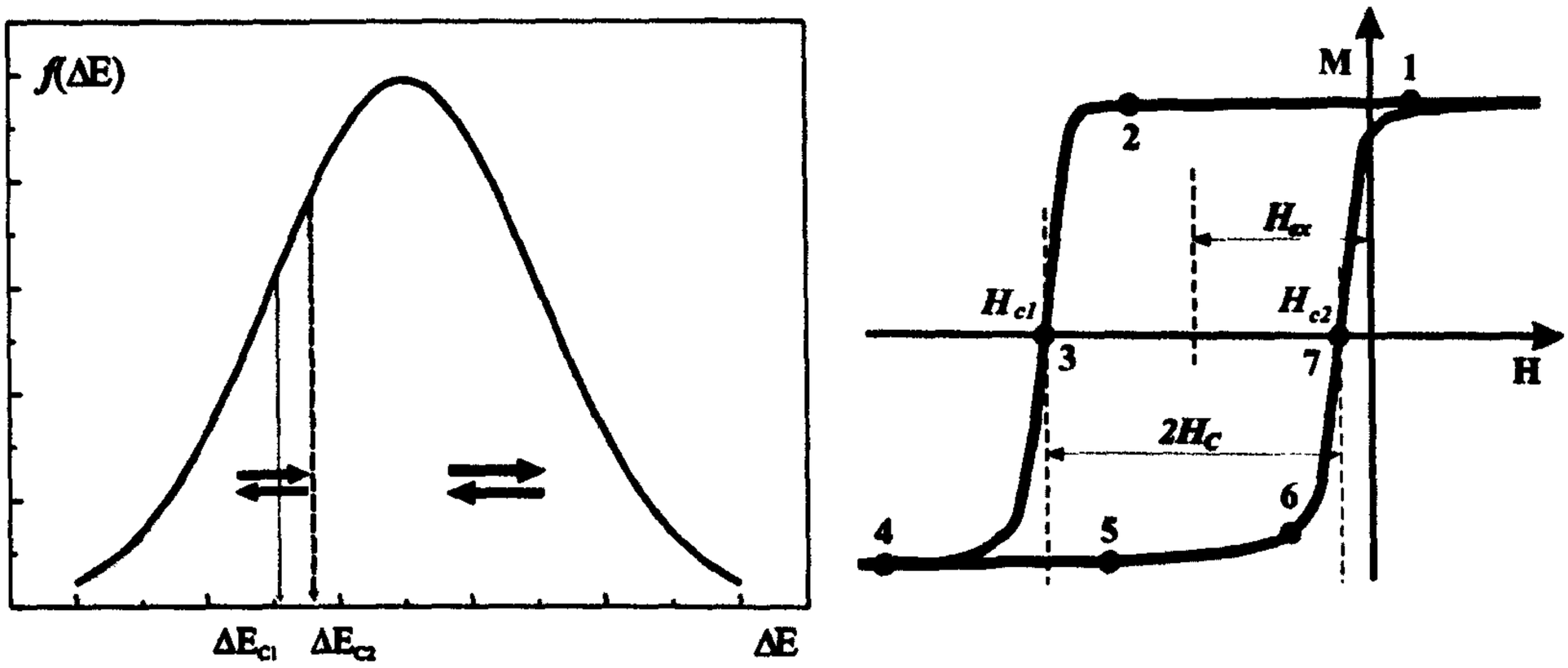

Figure 53 Schematic of distribution of energy barriers to reversal showing two energy barriers. Grains with $\Delta E<\Delta E_{C1}$ reversed their state due to thermal activation at point 4 of the hysteresis loop. Application of resetting conditions, at point 1, activates those energy barriers and reorders the state of those grains.

For the materials involved in our studies, i.e. IrMn(3nm)/CoFe(10nm) and IrMn(5nm)/CoFe(10nm), the influence of a positive applied field which is aligned parallel to the unidirectional anisotropy and heating to a temperature of 373K for a period of 90 min was established by experiment to result in maximum shift of the hysteresis loop once the sample was cooled to a thermal-activation-free temperature, T_{NA}. At this temperature thermal activation is minimised, if not "completely" eliminated. The experimental method by which this temperature is obtained is described in section 6.2.2.

Figure 54 shows the reproducibility of order for IrMn(3nm)CoFe(10nm) for different conditions. The hysteresis loops shown were measured at 77K. Heating at 373K for 90min at point 1, typically 2000Oe, (figure 53) ensures that the state of the *AF* is reproducible. The values of the coercive points H_{c1} and H_{c2} obtained for each set of resetting conditions are shown in table 4. The *AF* is fully reordered when heated at 383K for 22.5min when previously measured at 77K. For measurement times of 30 minutes at temperatures up to 373K, the resetting conditions obtained for both IrMn(3nm)/CoFe(10nm) and IrMn(5nm)/CoFe(10nm) are 373K for 90 min at point 1. Measurements shown in this figure were obtained by following the measurement protocol.

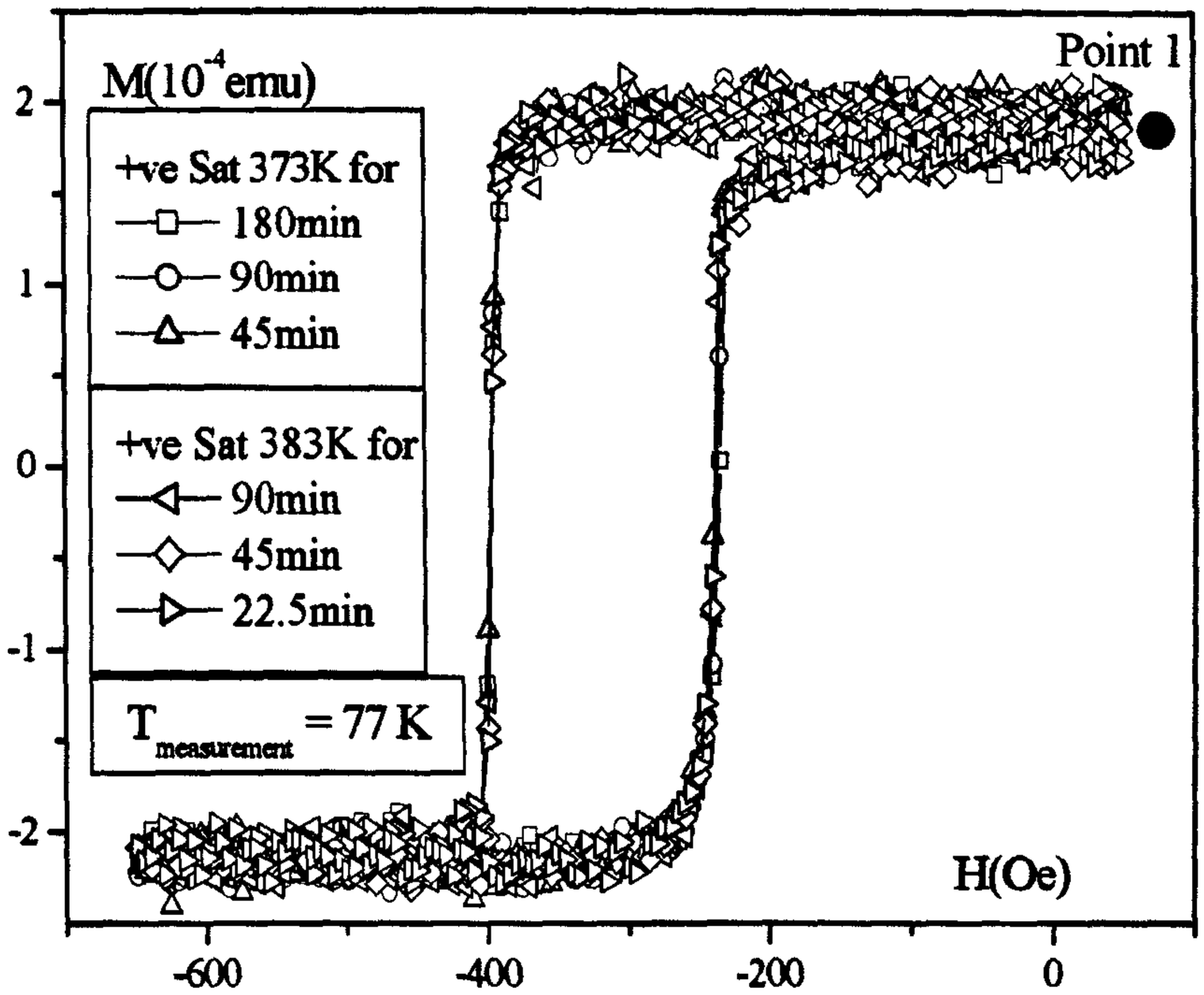

Figure 54 Reproducibility of order in the *AF* for IrMn(3nm)CoFe(10nm)

H_{Sat} = 900 Oe T (K)	t (min)	H_{c1}(Oe)	H_{c2}(Oe)	H_C(Oe)	H_{ex}(Oe)
373	180	-396	-235	80	-315
	90	-396	-237	80	-316
	45	-397	-239	79	-318
383	90	-396	-237	79	-317
	45	-395	-238	79	-317
	22.5	-396	-238	79	-317

Table 4 Values obtained after heating at 373K and 383K for different resetting times at point 1.

These same conditions allow erasure of any thermal activation in the *AF* during measurement. This is justified by the fact that the time spent to reset the *AF* at point 1 is more than 3 times larger that the typical measurement time, which can range from 10 to 30 minutes (See section 2.9).

6.2.2 Determination of thermal-free-activation temperature, T_{NA}.

In order to obtain the intrinsic behaviour of the exchange biased material it was necessary to establish a temperature at which the hysteresis loop could be measured without thermal activation taking place during the time of measurement. This was achieved by resetting the *AF* following the criteria indicated before, i.e. heating at 373K for 90 minutes, and subsequently cooling the sample to progressively lower temperatures, where holding the sample at reverse bias, i.e., at point 4 of the hysteresis loop in figure 53 for a fixed time did not result in any change in the subsequently measured hysteresis loop. The measurement procedure followed was described in section 5.5.2, figure 47. Figure 47(b) shows an schematic diagram of this measurement protocol. From these experiments we determined that a reasonable value for T_{NA} was 100 K for IrMn(5nm)/CoFe(10nm) and 77 K for IrMn(3nm)/CoFe(10nm).

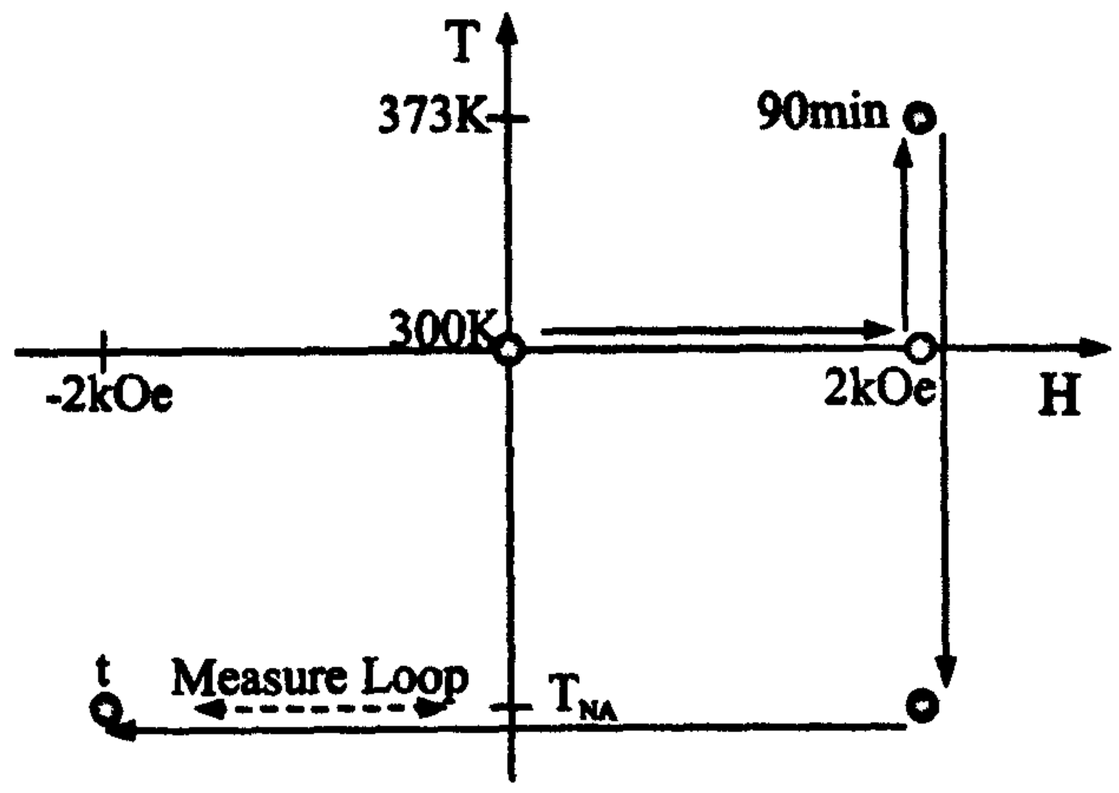

Figure 47(b) Schematic of describing the measurement protocol for the determination of T_{NA} shown in fig. 47, p.105.

Above T_{NA}, thermal activation produces changes in the *AF* that increase with time according to a series expansion of $ln(t)$ of an order that depends on the characteristics of $f(\Delta E)$ as described in section 2.9. Hence, the effect of thermal activation after 1 minute at point 4 and after 15 minutes at that point is a difference in the position of H_{c1} and H_{c2} and therefore H_{ex}. It is important to note that these loops are measured after 1 and 15 minutes spent at negative saturation (point 4), and measured starting at that point. The magnitude of the shift will be larger for those samples which are more thermally active, i.e. those that suffer more changes in the *AF* order. At T_{NA} and below, the superposition

of the hysteresis loops obtained after 1 and 15 minutes is expected with no shift in the position of H_{c1} and H_{c2} and therefore the same H_{ex}.

Figure 55 shows the effect of thermal activation at point 4 (see figure 53) for 15 minutes at different temperatures of activation for the sample with IrMn layer thickness of 5nm. Note that in the figure only the demagnetising branch of each loop corresponding to H_{c2} is shown. Note that due to thermal activation of the *AF* grains the shift is higher for higher temperatures.

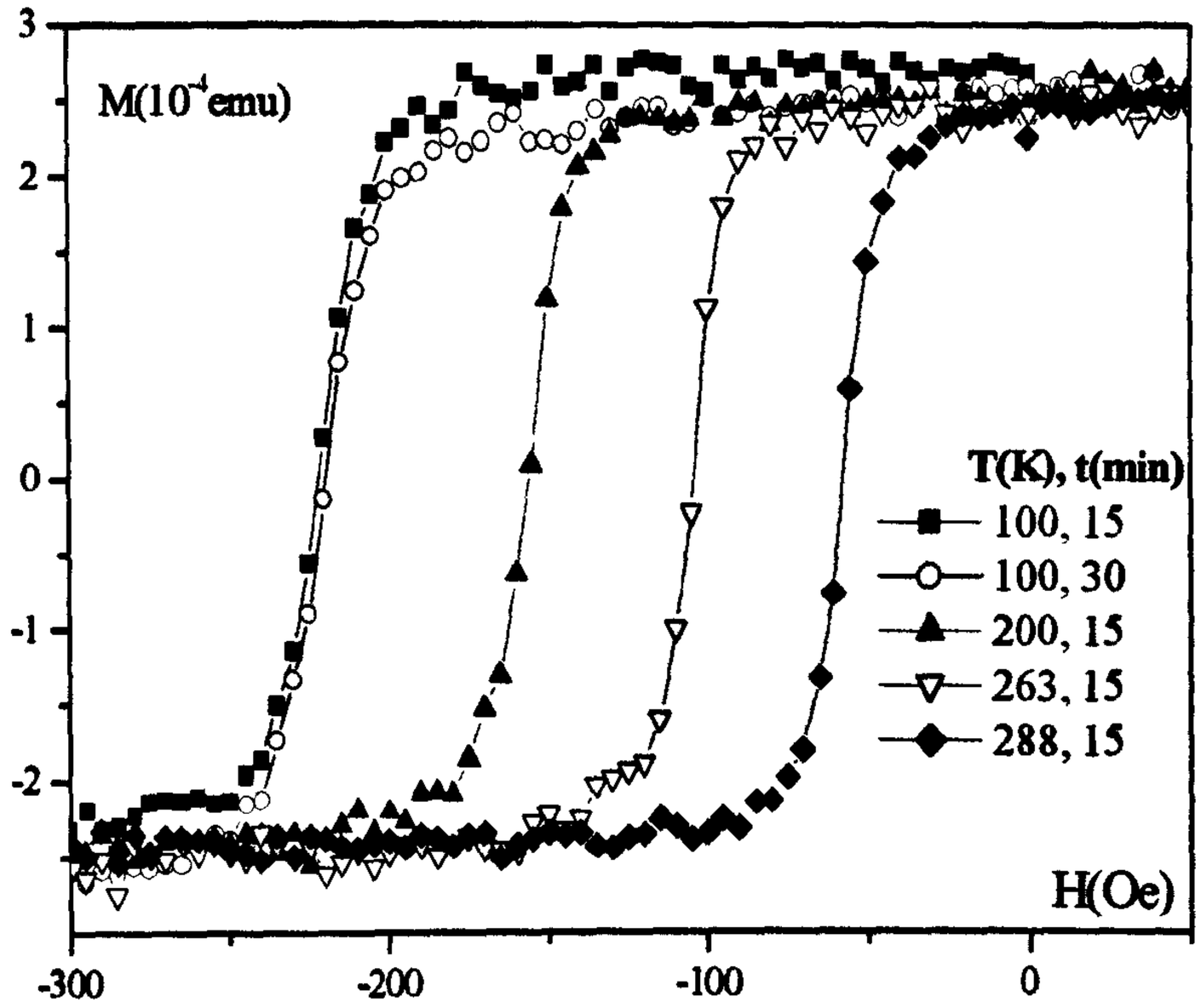

Figure 55 Recoil loops after exposure to reverse bias fields for various times at different temperatures for IrMn(5nm)/CoFe(10nm).

Figure 56 shows the shift that H_{c2} experiences when the IrMn(5nm)/CoFe(10nm) sample is held at reverse bias for 15 and 30 minutes at 100K after correction of the paramagnetic components.

The results obtained for IrMn(3nm)/CoFe(10nm) are shown in figure 57. Two measurements of hysteresis loops are shown. One hysteresis loop corresponds to the case of 1 minute at point 4, the other to 15 minutes. Previous to either measurement the state of the *AF* was reset, and then quenched to the temperature of measurement 77K.

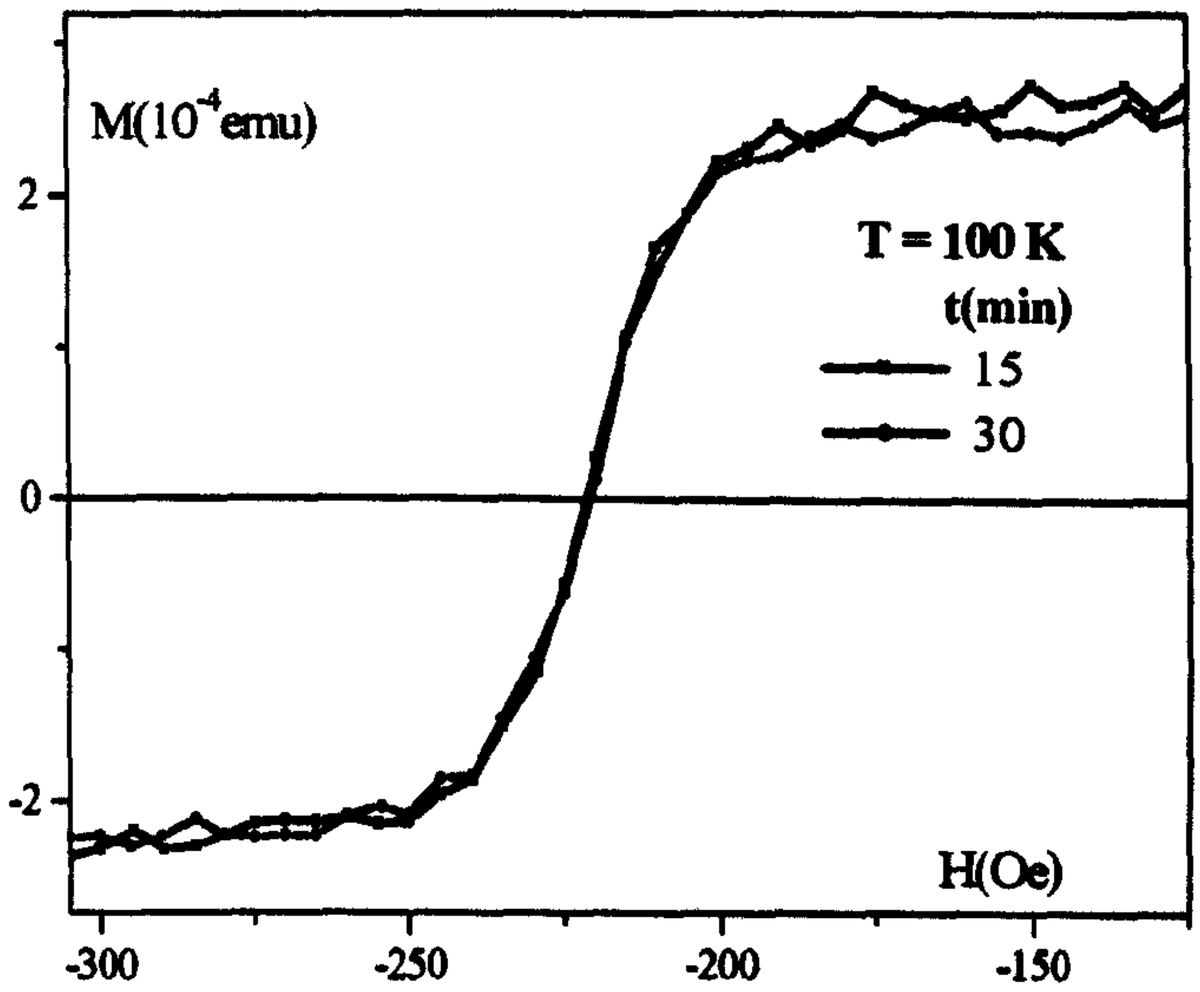

Figure 56 Expanded view of hysteresis loops from fig.55 after thermal activation in reverse bias for 15 and 30 minutes for IrMn(5nm)/CoFe(10nm).

The value of H_{c1} is the same in both cases as a consequence of the fact that at these temperatures the thermal activation of the *AF* grains is a minimum. There is a small difference in the value of H_{c2}, which is less than 5 Oe. It is not within error although this difference is small enough to be insignificant in terms of thermal activation of the *AF* grains. This shift in the value of H_{c2} for this particular measurement will be discussed in section 6.3.

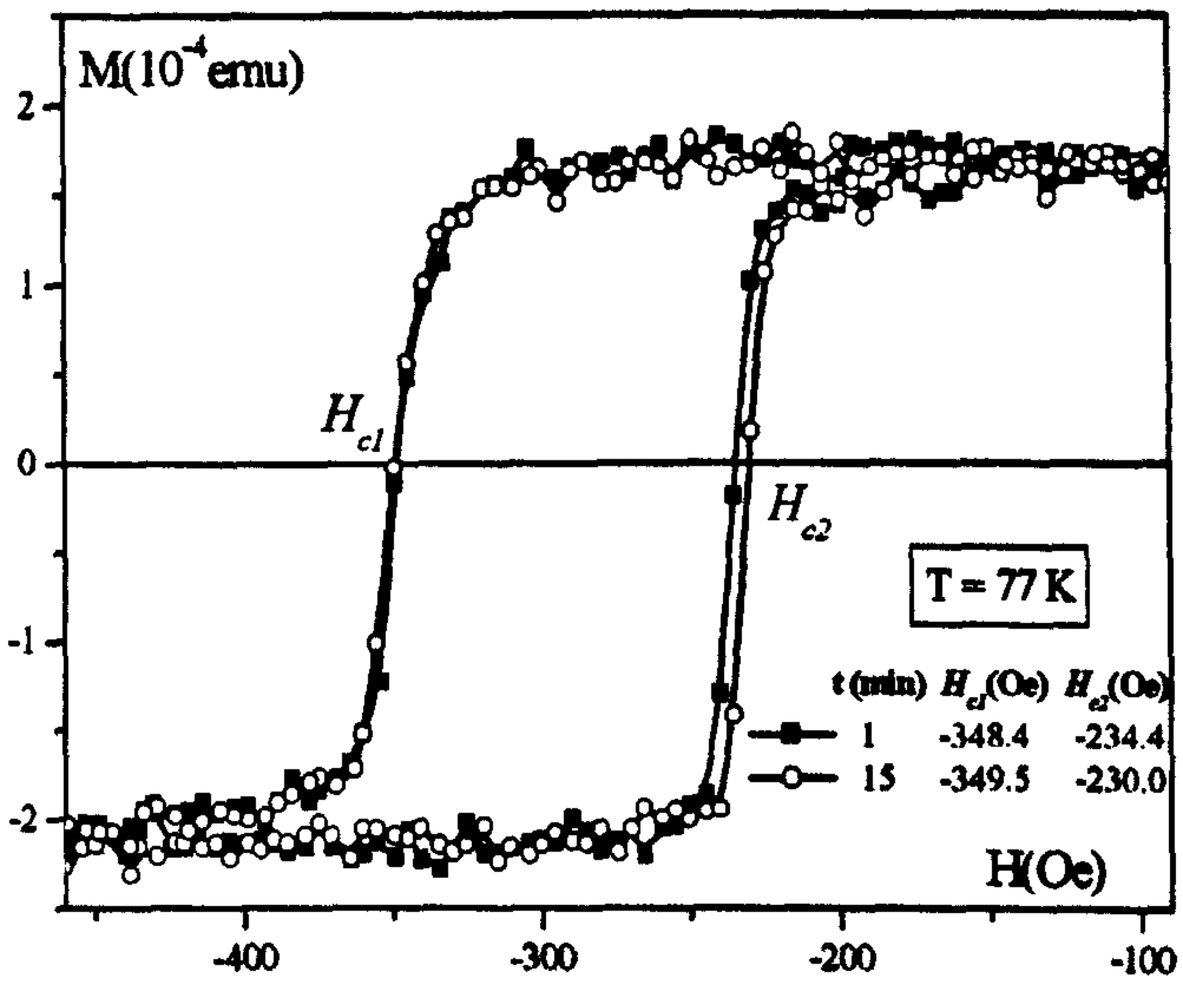

Figure 57 Hysteresis loops measured at the T_{NI} = 77 K for IrMn(3nm)/CoFe(10nm) after 1 and 15 minutes in reverse bias (point 4).

It is very important to stress that these hysteresis loops, related to the determination of T_{NA}, are measured starting from negative saturation, after resetting the AF in positive saturation, i.e. forward bias, as indicated in the measurement protocol of figure 47. Therefore, the first reversal of the F magnetisation is not included in the measurement of the hysteresis loops shown, e.g. measurements shown in figure 57. This allows interpretation of the cause of the shift of the value of H_{c1} as a result of thermal activation in the AF and removes the shift in H_{c1} due to spin reorientation. The origins of the shift of the value of H_{c1} and H_{c2} related to training effects and its dependence on temperature will be discussed in section 6.3.

6.2.3 Dependence on thermal activation of H_{ex} and H_C

Once that the thermal-activation-free temperatures have been determined for each of the samples the maximum shift in the loop, H_{ex} and H_C can be obtained with certainty that the results obtained are reproducible. Following the measurement protocol described in figure 48 (section 5.5.3) and sketched in figure 48(b) the dependence of both H_{ex} and H_C on the degree of order of the AF can be studied. The results obtained are shown in figures 58 and 59.

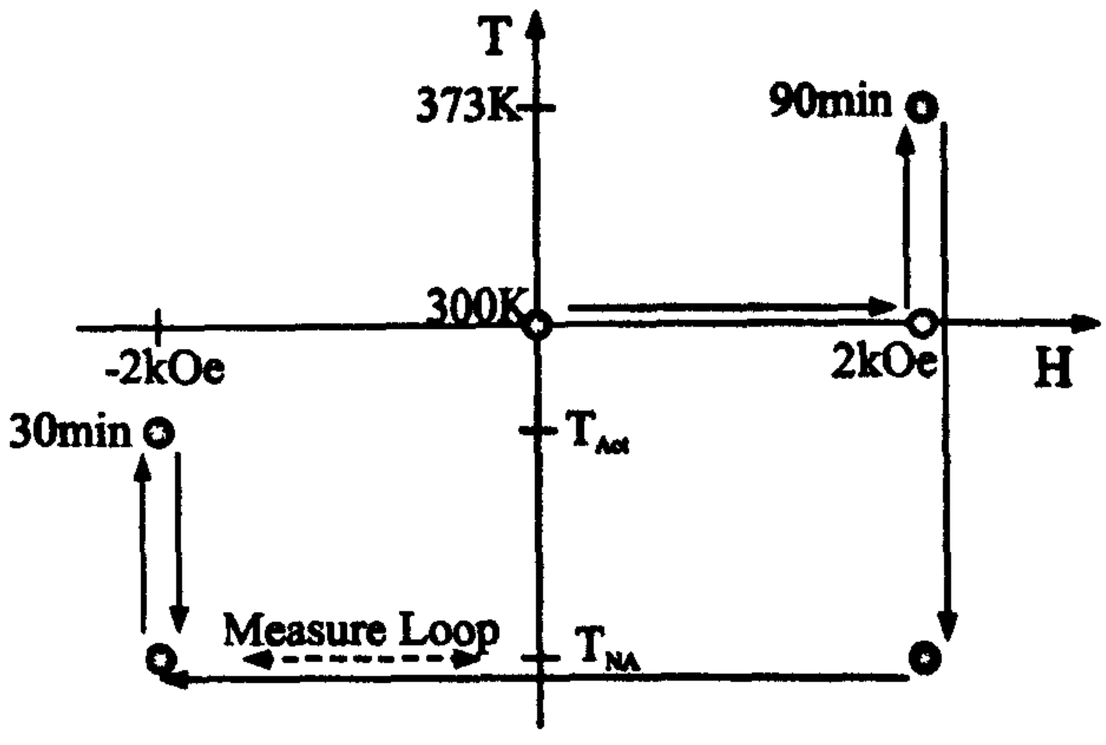

Figure 48(b) Schematic describing the measurement protocol for the determination of T_{NA} shown in fig. 48, p.106.

All measurements shown are made at the thermal activation free temperature T_{NA}, therefore no thermal activation occurs during the measurement. Hence, it is plausible to say that no change in the state of the AF occurs due to thermal activation during the time of measurement.

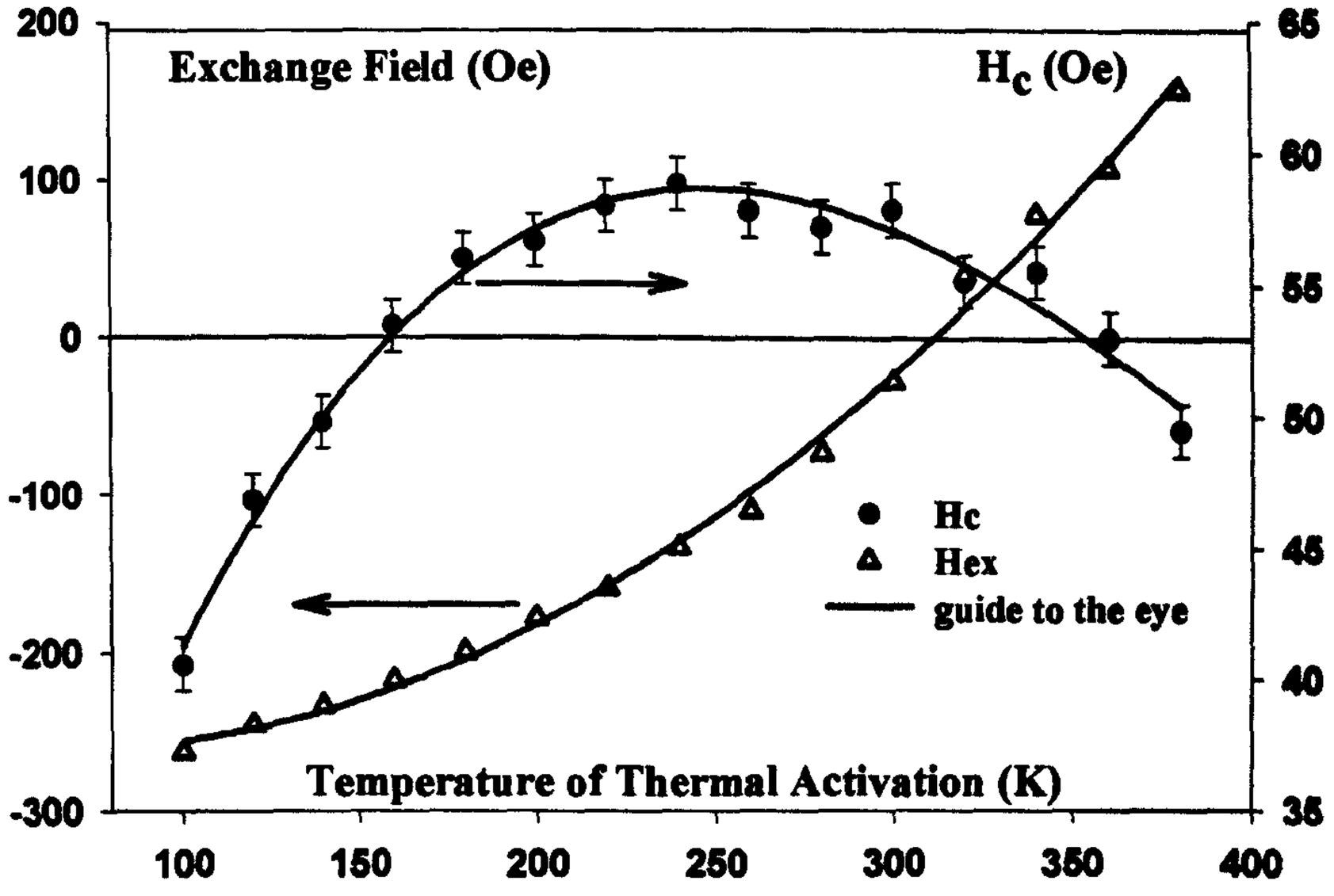

Figure 58 Variation of H_{ex} and H_C for IrMn(5nm)/CoFe(10nm). Errors in H_{ex} are within symbol.

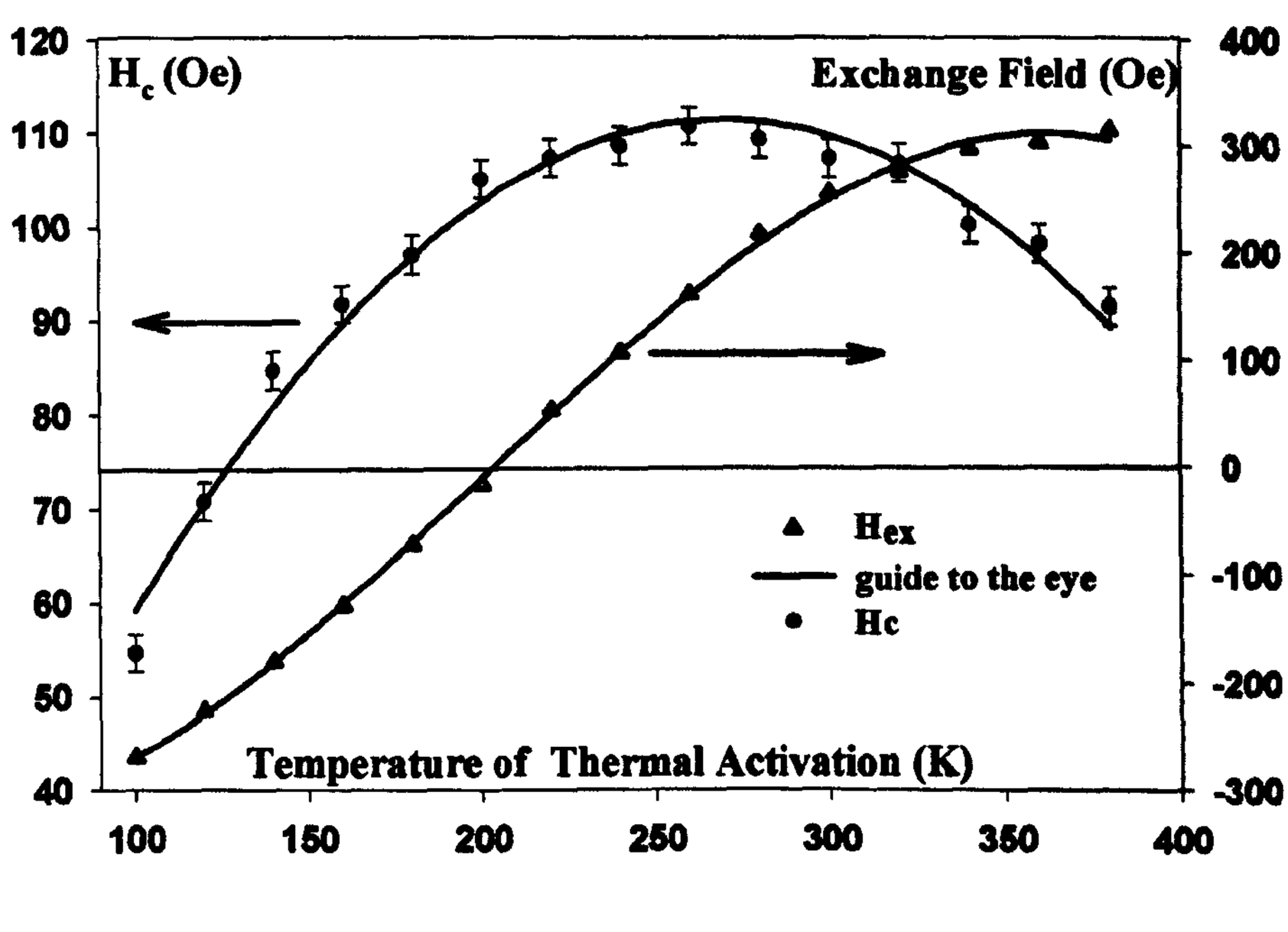

Figure 59 Variation of H_{ex} and H_C for IrMn(3nm)/CoFe(10nm). Errors in H_{ex} are within symbol.

The measurement of each hysteresis loop starts at point 4 (see hysteresis loop in figure 53). This way the variation of H_{ex} and H_C with the temperature of thermal activation,

T_{Act}, can be interpreted exclusively in terms of thermal activation during the time spent at point 4.

The heating stage in reverse bias is used to progressively change the order in the *AF* from the original state to the reverse orientation. The data displayed in figures 58 and 59 show the variation of H_C and H_{ex}, with the temperature of thermal activation, T_{Act}, at which the *AF* was heated at point 4 for IrMn(5nm)/CoFe(10nm) and IrMn(3nm)/CoFe(10nm). As T_{Act} is increased more *AF* material becomes thermally active. *AF* grains with higher energy barrier to reversal, ΔE, reverse their order under the influence of the exchange interaction that the negative saturated *F* exert on them. In consequence, the amount of *AF* that biases the *F* is reduced and the hysteresis loop shifts towards zero.

The exchange field, H_{ex}, equals zero when the amount of *AF* that remains with the original state is equivalent to the amount of *AF* material whose state was reversed by thermal activation. This would be the case of having reversed half the area under the curve of $f(\Delta E)$ due to thermal activation. The temperature of activation, T_{Act}, at which this situation is achieved is the median of the blocking temperatures, $\overline{T}_B$, of the distribution of blocking temperatures $f(T_B)$ within the *AF*.

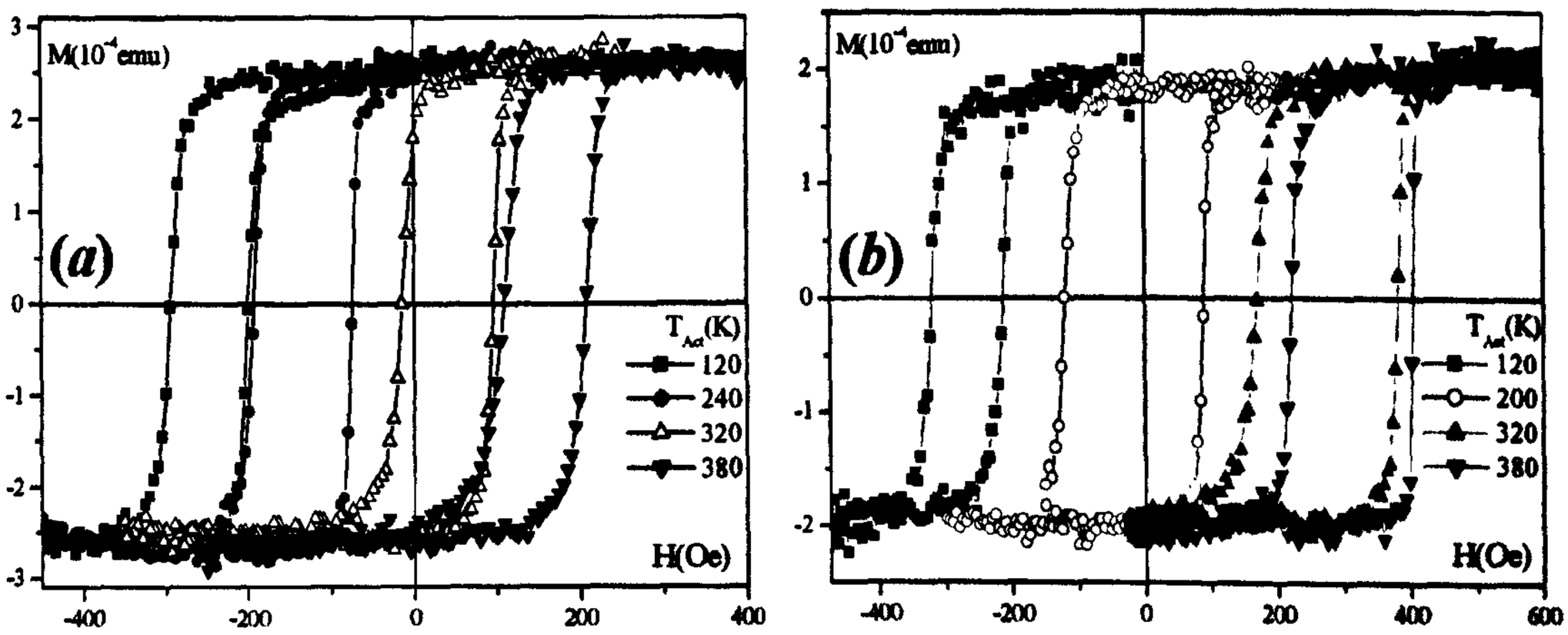

Figure 60 Part of the sample set of hysteresis loops obtained after thermal activation at different temperatures for IrMn(5nm)/CoFe(10nm) and IrMn(3nm)/CoFe(10nm).

In the case of a symmetrical distribution of energy barriers such as the one shown in figure 53, the position of $\overline{T}_B$ would be that at which $f(T_B)$ is maximum. This would not

be the case for asymmetrical distributions of energy barriers.The values obtained for the mean blocking temperature are the following:

IrMn(t_{AF})/CoFe(10nm), t_{AF}(nm)	Mean blocking temperature, $\overline{T}_B$ (K)
5	310
3	200

Table 5 Mean blocking temperatures obtained for the samples measured.

From the shift of the hysteresis loop of the *F*, information about the state of order of the *AF* is obtained. Conversely, the position of the hysteresis loop of the *F*, i.e., H_{ex}, can be considered as a measurement of degree of order of the *AF* layer, and ultimately of the magnetisation within the *AF*.

6.2.4 Measurement of the distribution of energy barriers to reversal in IrMn based exchange bias systems

For an experiment such as the one described in previous section, in which the *AF* is exposed to a reversed exchange field for a fixed and constant amount of time, the variation of H_{ex} with the temperature of activation, T_{Act}, allows the mapping of the energy barrier distribution to reversal, $f(\Delta E)$. This procedure ensures as well that the measurement is not affected by thermal activation during measurement. The resetting conditions of the *AF* previously established ensure that the *AF* state is that for which the H_{ex} is maximum. The variation of H_{ex} with T_{Act}, from the original state to that in which the magnetisation state of the *AF* is completely reversed is a sigmoidal-type curve.

Inspection of figure 58 shows that it was not possible to completely reverse the loop shift in the sample with a 5nm thick IrMn due to experimental temperature restrictions. The highest temperature that could be achieved in the equipment used was 400K. Furthermore, higher temperature would jeopardise the sample's condition, giving rise to possible damage of the interface between the *F* and *AF*. Hence a complete distribution of the energy barriers within the material could not be obtained. Figure 59 shows that

the order in the *AF* was completely reversed, as denoted by the saturation of H_{ex} at 400K. Temperatures lower than 100K would be required to show the saturation of H_{ex}. Equipment restrictions did not allow temperatures below 100K by the time these measurements were made. In the case of achieving saturation at low temperatures, the absolute value of the exchange field would be the same as that obtained at high temperatures. Both situations would correspond to the cases of having the *AF* state 100% with the original forward orientation or 100% with reversed orientation, respectively. These results demonstrate that the shift in the hysteresis loop derives exclusively from the degree of order in the *AF*, as it has been previously reported (O'Grady *et al.* 2002). As the temperature of thermal activation approaches to T_N a decay of H_{ex} to zero would be expected.

Differentiation of the shift in the hysteresis loop, H_{ex}, with respect to the temperature of thermal activation, T_{Act}, gives a measurement of the energy barrier distribution to reversal in the *AF*, $f(\Delta E)$. The exchange field measured in the experiment described in section 6.2.3 would be related to $f(\Delta E)$ by an expression of the type of eq.6.1, assuming that all the *AF* in the distribution contribute equally to the exchange bias and that this contribution can be represented by an average field H_0.

$$H_{ex} = H_0 \left\{ \int_0^{\Delta E_C} f(\Delta E) d(\Delta E) - \int_{\Delta E_C}^{\infty} f(\Delta E) d(\Delta E) \right\} \qquad (6.1)$$

Figures 61 and 62 show, respectively, the results obtained from these measurements for the distribution of energy barriers to reversal within the *AF* layer of the IrMn(5nm)/CoFe(10nm) and IrMn(3nm)/CoFe(10nm) samples studied. As it was not possible to reverse completely the order in the IrMn(5nm) sample, it was not possible to map completely $f(\Delta E)$ for this sample. The distribution of energy barriers for IrMn(5nm)/CoFe(10nm) was differentiated assuming the distribution to be symmetrical. Both distributions in figures 61 and 62 are normalised to unity.

From figures 61 and 62 it is clear that a distribution of energy barriers exists within the IrMn with significant barriers extending to low values. This is similar to the results obtained for FeMn based samples studied by O'Grady *et al.* (2002).

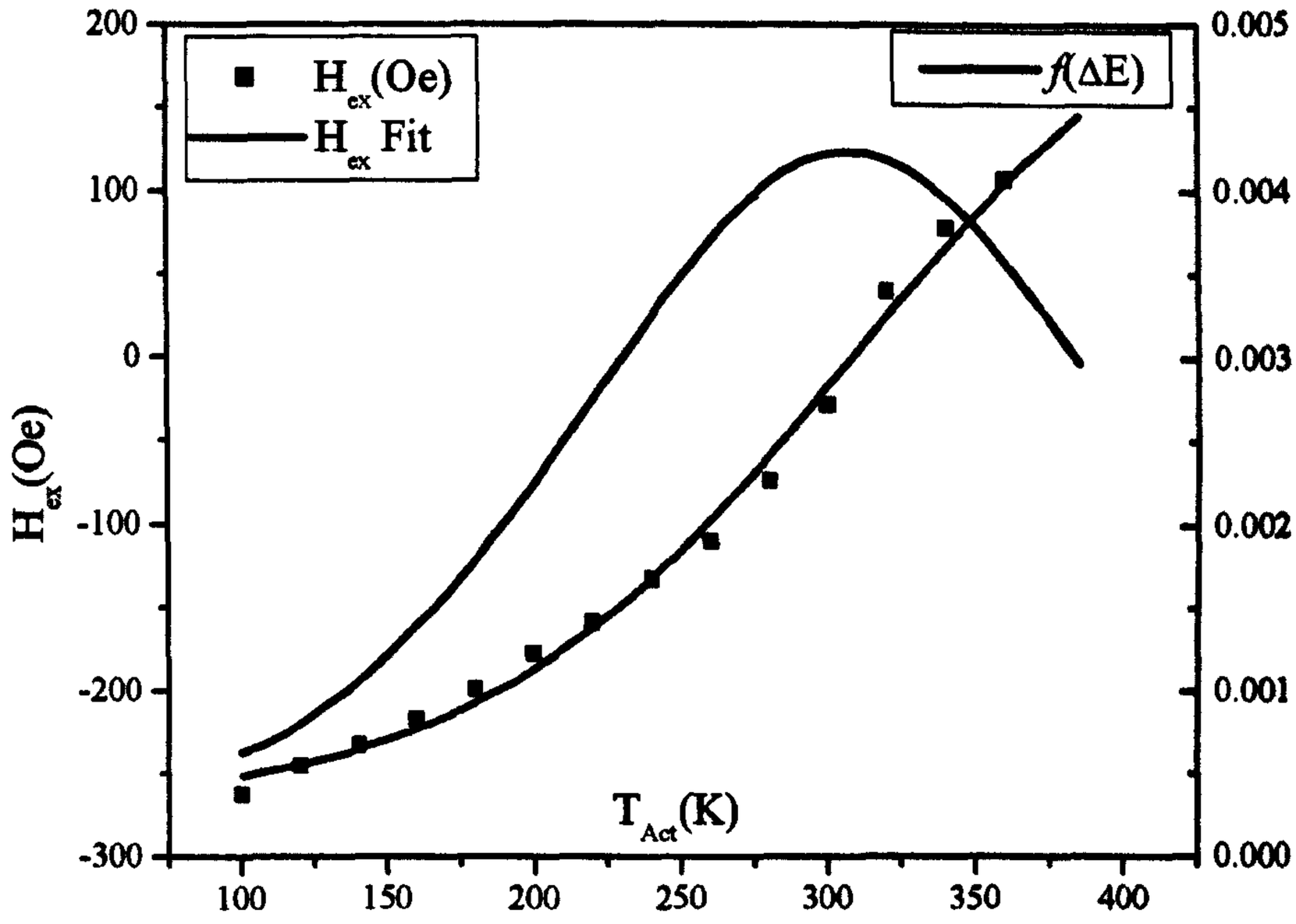

Figure 61 Distribution of energy barriers to reversal in IrMn(5nm).

For applications the amount of *AF* that remains thermally stable at room temperature and at those temperatures at which devices based on the exchange bias phenomenon work, which can range from 70°C to 100°C is critical. From figures 61 and 62, it is possible to estimate that percentage. For IrMn(5nm)/CoFe(10nm) at 300K the amount of *AF* that is pinning the *F* is 53% of the total whilst for IrMn(3nm)/CoFe(10nm) it is only 16%. These percentage values are estimated as the percentage of the area under the curve of the distribution of energy barriers, $f(\Delta E)$, between the temperature of interest, i.e., 300K, and infinity. The area under the curve between T_{NA} and the temperature of interest correspond to superparamagnetic spins with lower blocking temperature than those of interest. In other words, the percentage of the *AF* that remains stable at a given temperature T is represented by the second integral in eq.6.1, where the lower limit corresponds to the highest value of the energy barriers that can be activated at that temperature. The first integral in eq.6.1 corresponds to the amount of *AF* that is unstable at *T*. An ideal *AF* material would be that which is 100% thermally stable at the working temperature.

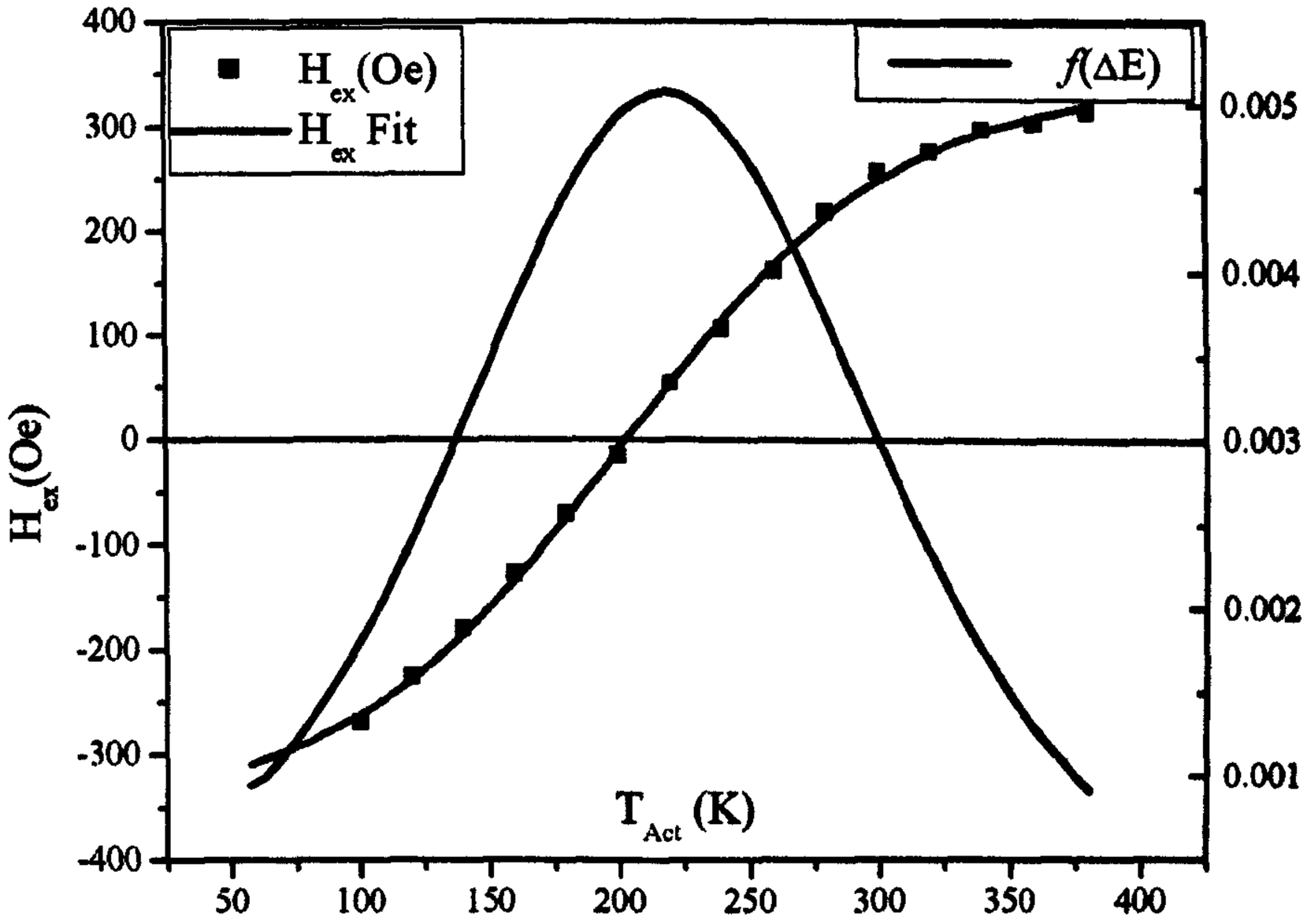

Figure 62 Distribution of energy barriers to reversal in IrMn(3nm).

6.2.5 Coercivity and temperature of thermal activation.

The behaviour of H_C with the temperature of activation, T_{Act}, is also shown in figures 58 and 59. A peak in H_C is observed in both graphs even though the temperature at which H_C was measured was the same for all measurements. Hence, it is expected that some relation would exist between H_C and the degree of order in the *AF*. The peak does not occur at the mean of the distribution of blocking temperatures in the *AF*, for any of the samples. For the sample with IrMn 5nm thick, the peak occurs about 60K below $\overline{T}_B$, whereas for the IrMn(3nm) it is 50K above. Consequently, there does not appear to be any correlation whatsoever between the mean of the distribution and the peak in the coercivity.

The enhancement of H_C for the exchange biased system has been qualitatively claimed to appear due to an increase in the energy required to reverse the M_F due to the exchange interaction between the *F* and the *AF* (e.g. Nogués and Schuller, 1999). The coercivity has been found to peak at temperatures close to the highest value of the blocking temperatures in the *AF* when the system is measured in a similar manner than that used for the measurement of training effects (see figure 50),(Nogués and Schuller,

1999). Pan *et al.*, (2004), showed that the position of the peak with the temperature of activation relative to T_B varied depending on the ratio of Fe to Mn contained in their specimen $Fe/Fe_xMn_{1-x}/Cu(001)$. This was explained in the same terms as the enhancement of H_C, due to an increasing amount of *AF* material that is being dragged by the *F* as the temperature of measurement increases towards the maximum blocking temperature within the $f(T_B)$. However, the protocol followed in the measurements described in section 6.2.3, ensures that the amount of *AF* that the *F* drags during measurement of a hysteresis loop is kept fixed to a minimum amount for all measurements. The amount of *AF* material, expected to be formed by superparamagnetic grains, can be considered negligible compared to the *AF* material that remains unaltered during measurement. Hence, the origin of the peak in H_C remains somewhat obscure and it is hard to imagine a mechanism whereby the amount *AF* material ordered in two different senses could lead to such a peak or to the position of such a peak relative to the mean of the blocking temperature distribution.

6.2.6 Grain size and *AF* thickness dependence of exchange bias features

Two samples that differ in the *AF* thickness have been measured, IrMn(3nm)/CoFe(10nm) and IrMn(5nm)/(10nm). Although it could not be measured, the grain size distribution within the IrMn layer is expected to increase with increasing thickness of IrMn (Fuke *et al.*, 1999). Therefore, the sample with IrMn(5nm) is expected to have larger grain size than the sample containing IrMn(3nm). This applies to DC magnetron sputtering; however, there are other sputtering techniques that allow control of the grain size independently of the layer thickness, such as controlled plasma sputtering (Vopsaroiu *et al.*, 2004, 2005).

Inspection of figures 58 and 59 shows that the maximum value of the exchange field is larger for the sample with thinner IrMn, as it predicted from the theoretical models described in chapter 4. All models agreed that H_{ex} varies inversely with the *AF* thickness [e.g. Meiklejohn and Bean (1956), Mauri et al.(1987), Malozemoff (1987), Stamps (2000)]. The variation of the exchange field with the temperature of thermal activation is more pronounced for the sample with smaller crystal grain size, i.e.

IrMn(3nm). Smaller grains are easier to activate as their volume contributes to smaller anisotropy energy. Hence, the effect of temperature on thermal activation is larger for IrMn(3nm) than for IrMn(5nm). As a result of this, figures 58 and 59 show that it was possible to reverse the order in the *AF* "almost completely" in the sample with thinner IrMn, therefore, smaller grain size. Also, the value of the mean blocking temperature is lower for IrMn(3nm) due to smaller grain size. The values of H_C are expected to vary $1/t_{AF}^{\lambda}$ where λ is a number related to the spin structure and the material and is generally close to 1. Typical values are 0.3, 1 (Sang *et al.*, 1999). The results obtained show that the larger values of H_C correspond to the sample with lower *AF* thickness. Figures 61 and 62 show that the distribution of energy barriers to reversal is considerably wider for IrMn(5nm) than for IrMn(3nm) which might be due to a wider distribution of the grain size or the anisotropy.

The results obtained support a grain size dependent model of energy barriers. The exchange field originated from domain wall formation at the interface would be independent of the *AF* thickness as long as the *AF* is thick enough to support a domain wall. The way that H_{ex} is reduced with thermal activation is consistent with a grain size model as shown in figures 61 and 62. Also results by Sadia Manzoor *et al.*,(2005), show that there is a direct correlation between the grain size or potentially the grain volume and exchange bias. Moreover, it is hard to imagine any mechanism leading to formation of domains in polycrystalline *AFs*, as the RKKY interaction is quite improbable due to the very small magnetic moment in the grains.

6.2.7 On the controversy of measurements of blocking temperatures.

If the blocking temperature, T_B, is defined as the temperature at which the exchange field, H_{ex} equals zero, the meaning of T_B intrinsically depends on the description of the process by which the exchange field is made zero. The standard measurement method to determine the blocking temperature of an exchange biased system involves the determination of the hysteresis loop of the material as the temperature is raised until a point is reached at which the shift of the hysteresis loop becomes zero, i.e., the hysteresis becomes symmetric about the magnetisation axis.

Theoretical studies of blocking temperature, T_B, and the dependence of H_{ex} on temperature are described in chapter 4 for the standard measurement method, similar to the measurement of training effects shown in figure 50 (pag. 109) for the measurement of one hysteresis loop. In this case the interpretation of T_B is generally conceived as the temperature beyond which the thermal energy is such that it is able to detach the *AF* spins from the anisotropy axes of the *AF* grains by overcoming the magnetic anisotropy energy. At such temperature H_{ex} is zero, as the spins of the *AF* grains are all dragged by the *F* when this is cycled. According to Fulcomer and Charap's interpretation (1972), T_B will correspond to the blocking temperature of the *AF* grain with the largest anisotropy energy. Above the blocking temperature the magnetisation of the uncompensated *AF* grain will follow the magnetisation of the *F*, i.e. will become superparamagnetic. Below T_B that grain will be "blocked", i.e. will not undergo magnetisation reversal with the reversal of the *F* magnetisation.

Figures 58 and 59 show that heating to temperatures higher than the mean blocking temperature leads to the hysteresis loop shifting in the opposite direction to that in which it was originally set. Hence, the standard measurement of the blocking temperature distribution is not a measurement of the energy barriers to reversal within the *AF*. Hysteresis loops measured at increasing temperatures, even after resetting of the *AF*, lead to a progressive increase of the amount of *AF* that is being dragged by the *F*. Such spins do not contribute to H_{ex}, whereas those that are not dragged are subject to thermal activation during measurement. Hence, H_{ex} shifts towards zero and does not become positive. This procedure is therefore similar to an AC field demagnetising process.

As explained (section 6.2.3 and 6.2.4), the exchange field is zero when half of the distribution of energy barriers is in its original state, and the other half is in the reversed state. This is achieved by thermal activation of the *AF* grains while kept in reverse bias (fig. 48, pag.107). This was shown to be exclusively dependent on the temperature of activation, T_{Act}, at which the thermal activation took place. Hence, the blocking temperature value obtained is the mean blocking temperature of the distribution of energy barriers in the *AF*. In the case of IrMn(5nm)/CoFe(10nm), T_B is 310K and for IrMn(3nm)/CoFe(10nm) it is 200K.

In the experiment described in section 6.2.3, and figure 48, the time spent in the thermal activation stage at reverse bias is 30 minutes. The thermal activation of the *AF* will be ongoing at a logarithmic rate during this stage. The time at negative saturation selected is much larger than the relaxation time of the *AF* grains in these samples. After this time, the number of reversals of the *AF* grains will be a small fraction of the number of reversals that have occurred in the first minutes. When the time of thermal activation in reverse bias or the time of measurement are of the order of the relaxation time of the *AF* grains, the shift of the hysteresis loop and therefore T_B, will depend on these temporal parameters.

Figure 63 shows the variation of H_{ex} obtained from measurements following the protocols in figures 48 and 50. Progressive reversal of the *AF* order following the protocol in figure 48 leads to $\overline{T}_B$, whereas a measurement procedure following the protocol in figure 50 leads presumably to the highest T_B within the blocking temperature distribution.

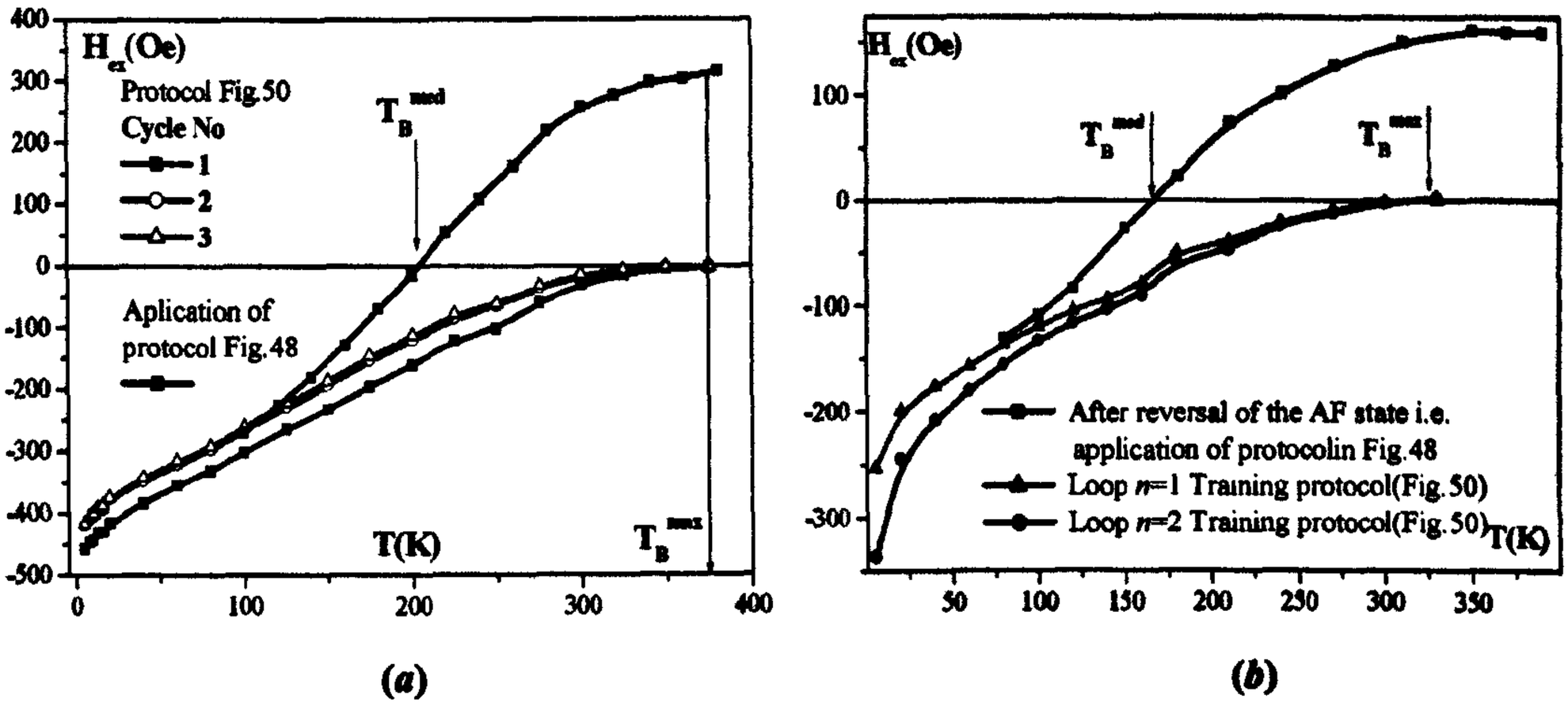

Figure 63 Variation of H_{ex} from application of protocol of figure 48 and 50 for two different materials, **(a)** IrMn(3nm)/CoFe(10nm) **(b)** FeMn(10nm)/NiFe(10nm). Figure 62 (b) is courtesy of Sadia Manzoor (to be published).

6.3 Contributions to exchange bias on IrMn/CoFe bilayers. Training effects.

It is known that training effects cause the reduction in the exchange field and coercivity with the number of the hysteresis loops measured repeatedly on an exchange biased system (Nogués *et al.*, 1999). The effects of training on IrMn/CoFe samples have been studied before by other authors (e.g. Wang *et al.*, 2002). In the scope of getting to a deeper knowledge of training this section describes the study of the effect of training on IrMn(3nm)/CoFe(10nm) and IrMn(5nm)/CoFe(10nm) and the dependence of this effects on temperature. Therefore, training effects were measured in a range of temperatures from 4.2K up to 400K.

The measurement protocol followed was described in section 5.5.5. Figure 50 shows the measurement procedure followed which is sketched below in figure 50(b). In order to obtain measurement reproducibility and to get the same state in the spin configuration of both *AF* and *F*, all measurements were done after resetting of the *AF* . Also the *F* was kept in saturation while the temperature was changed to the value of measurement. When the temperature was stabilised, hysteresis loops were measured consecutively. The number, *n*, of hysteresis loops measured was set to a maximum of 3. After this, changes in the values of H_{ex} and H_C due to repeated measurements were all within measurement error. Thus, no further information would be obtained from a larger number of measurements. The value of *n* at which both H_{ex} and H_C stabilise depends on the materials used and their susceptibility to suffer changes due to thermal activation.

In order to obtain a better description of the changes observed in the hysteresis loops due to field cycling and variation of the temperature of measurement, the behaviour of the coercive points H_{c1} and H_{c2}, have been studied. The following figures show a sample set of the hysteresis loops obtained.

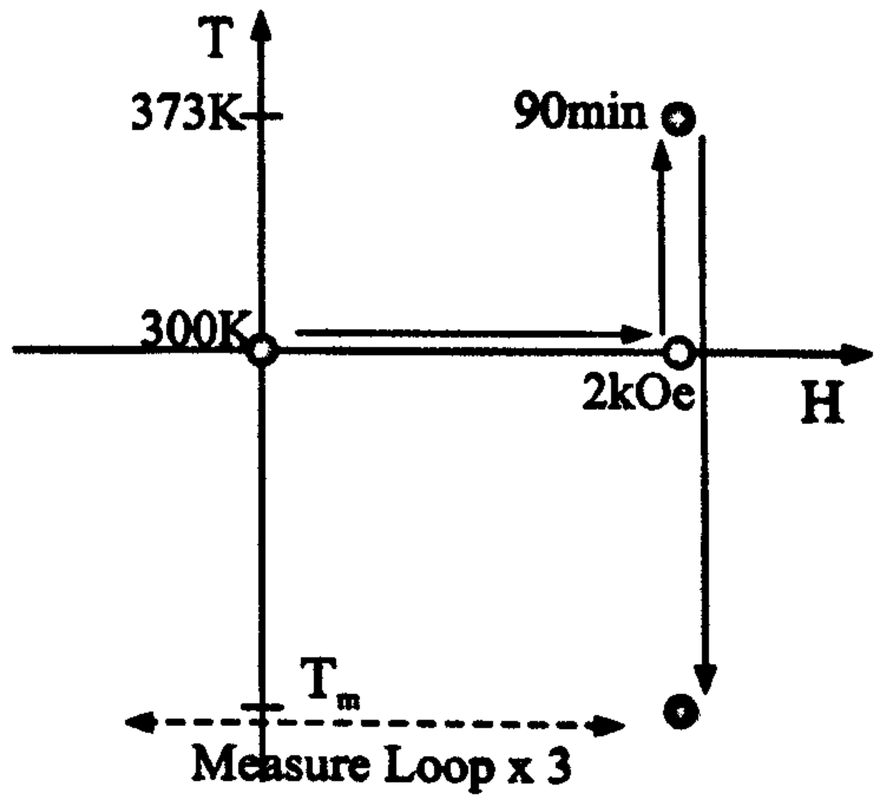

Figure 50(b) Description of the protocol for the measurement of training effects in fig. 50, p.109.

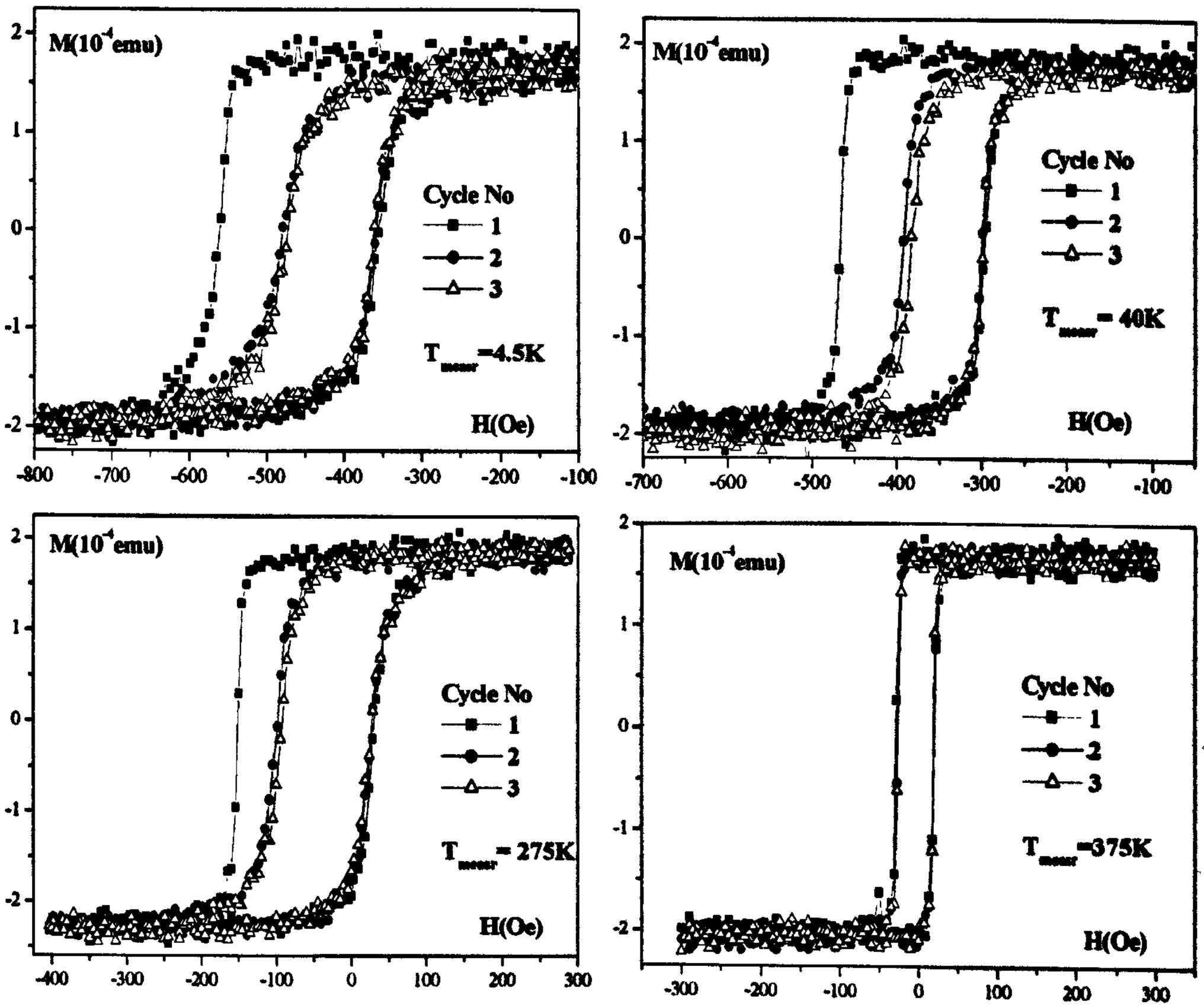

Figure 64 Sample set of hysteresis loops obtained at different temperatures of measurement for IrMn(3nm)/CoFe(10nm).

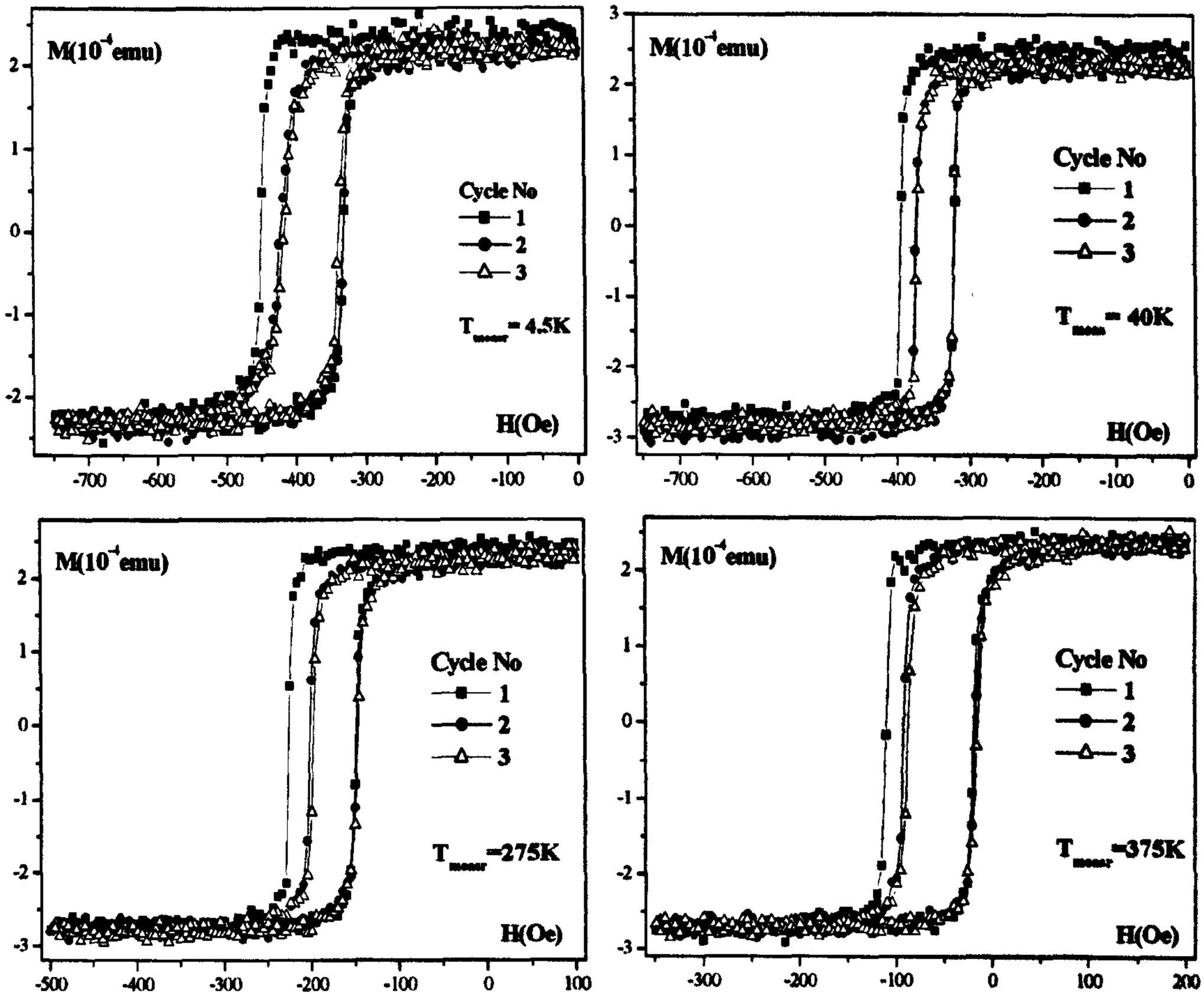

Figure 65 Sample set of hysteresis loops obtained at different temperatures of measurement on IrMn(5nm)/CoFe(10nm).

6.3.1 Measurements

It can be seen in figures 66 (a) and 67(b) that the hysteresis loops shift towards zero with cycling. Part of this shift must derive from thermal activation processes as described in section 6.2.3. However, inspection of figures 64 and 65 show high asymmetry in the shape of the loops for the first cycle of measurements, i.e., the hysteresis loops corresponding to $n = 1$. This asymmetry disappears with field cycling and increasing temperature. The asymmetry is more pronounced for the branch of the loop corresponding to point 3 in the hysteresis loop shown in figure 58 and consequently has a larger effect on H_{c1} than on H_{c2}. This asymmetry is discussed in section 6.3.3 where the loop shape is studied in depth. Also there is a reduction in the values of H_{ex} and H_C with field cycling and increased temperature of measurement (see figures 66 and 67). Given the fact that the coercive points H_{c1} and H_{c2} are affected

differently by training, figures 68 and 69 show the temperature dependence of H_{c1} and H_{c2} with field cycling at a range of temperatures.

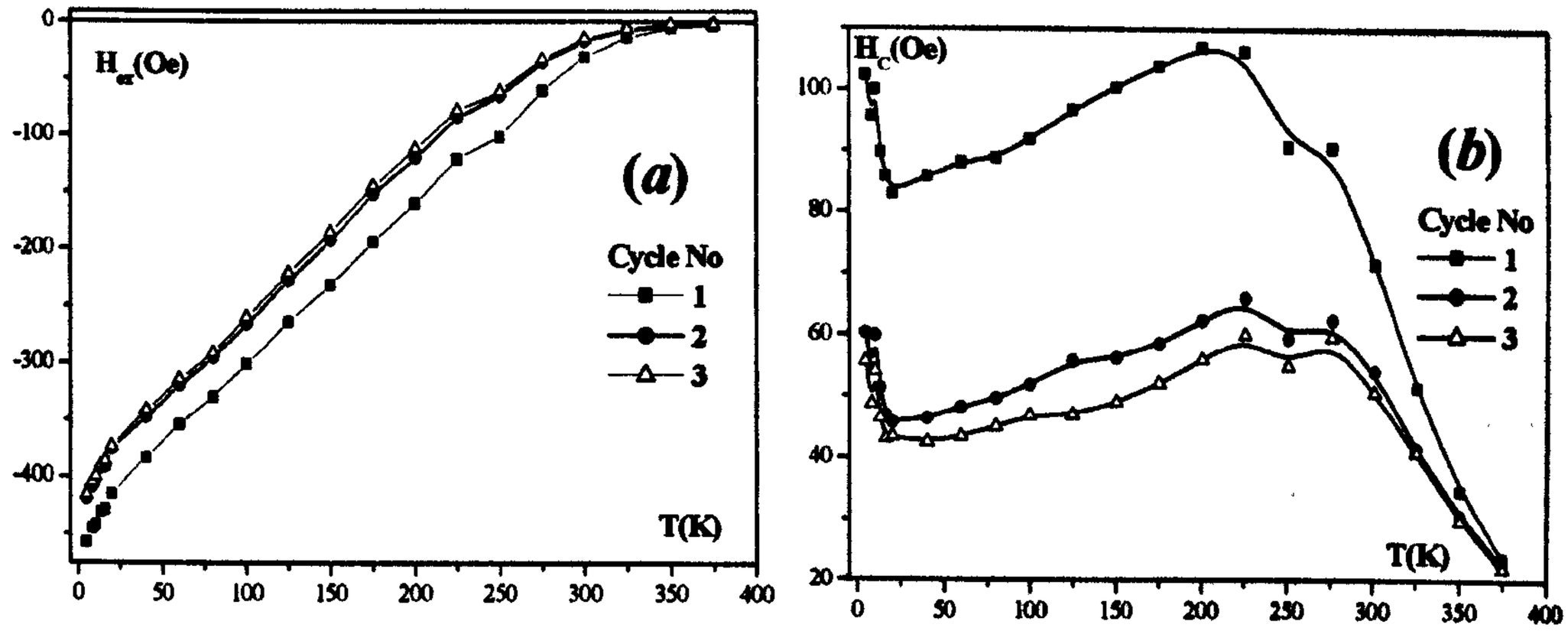

Figure 66 Variation of H_{ex} **(a) and** H_C **(b) with the temperature of measurement and field cycling for** IrMn(3nm)/CoFe(10nm).

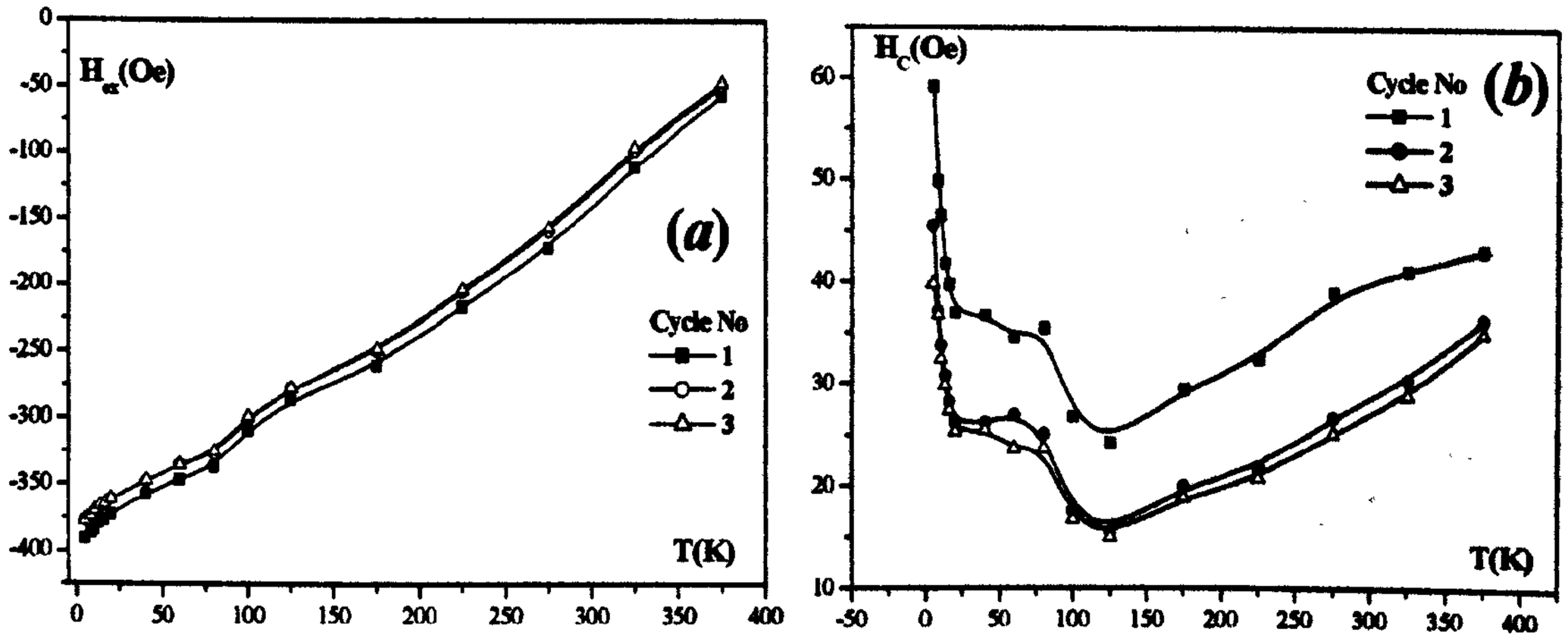

Figure 67 Variation of H_{ex} **(a) and** H_C **(b) with the temperature of measurement and field cycling for** IrMn(5nm)/CoFe(10nm).

The evolution of H_{ex} with field cycling shown in figures 66(a) and 66(b) can be more easily interpreted by inspection of figures 68 and 69. The different effect of field cycling on H_{c1} and H_{c2} is clear in these figures. While the value of H_{c2} is almost independent of field cycling, H_{c1} exhibits a pronounced shift between the first and second loops, and its value evolves with increasing number of cycles, n, towards a constant value. The number of loops required to saturate H_{c1} depends on the degree of activation of the AF to spin reorientation (see section 6.3.3).

Figures 66(b) and 67(b) show the behaviour of H_C with increasing temperature of measurement. Three different stages can be distinguished in H_C(T) for IrMn(3nm) in figure 66(b). At temperatures below 25K H_C increases abruptly due to a steeper variation on H_{c1} at that temperatures whilst H_{c2} increases monotonically. However, for IrMn(5nm) H_{c2} has a constant value in that range of temperatures. Similar effects were observed by Takano *et al.* (1997) at temperatures below 75K for CoO on MgO substrates, who argued to be due to spin freezing effects. Such effects, discussed in section 6.3.4, disappear above 25K in the samples measured. Above this temperature H_C increases up to a certain temperature. This is clearly observed in fig. 66(b). However in figure 67(b) there is a minimum around 100K which might be due to a sample repositioning that took place at that temperature. Any small angular error in the process of realignment of the sample may lead to significant variations in H_C as described in section 6.4. Higher temperature measurements would be required to observe the peak in H_C for the IrMn(5nm) sample.

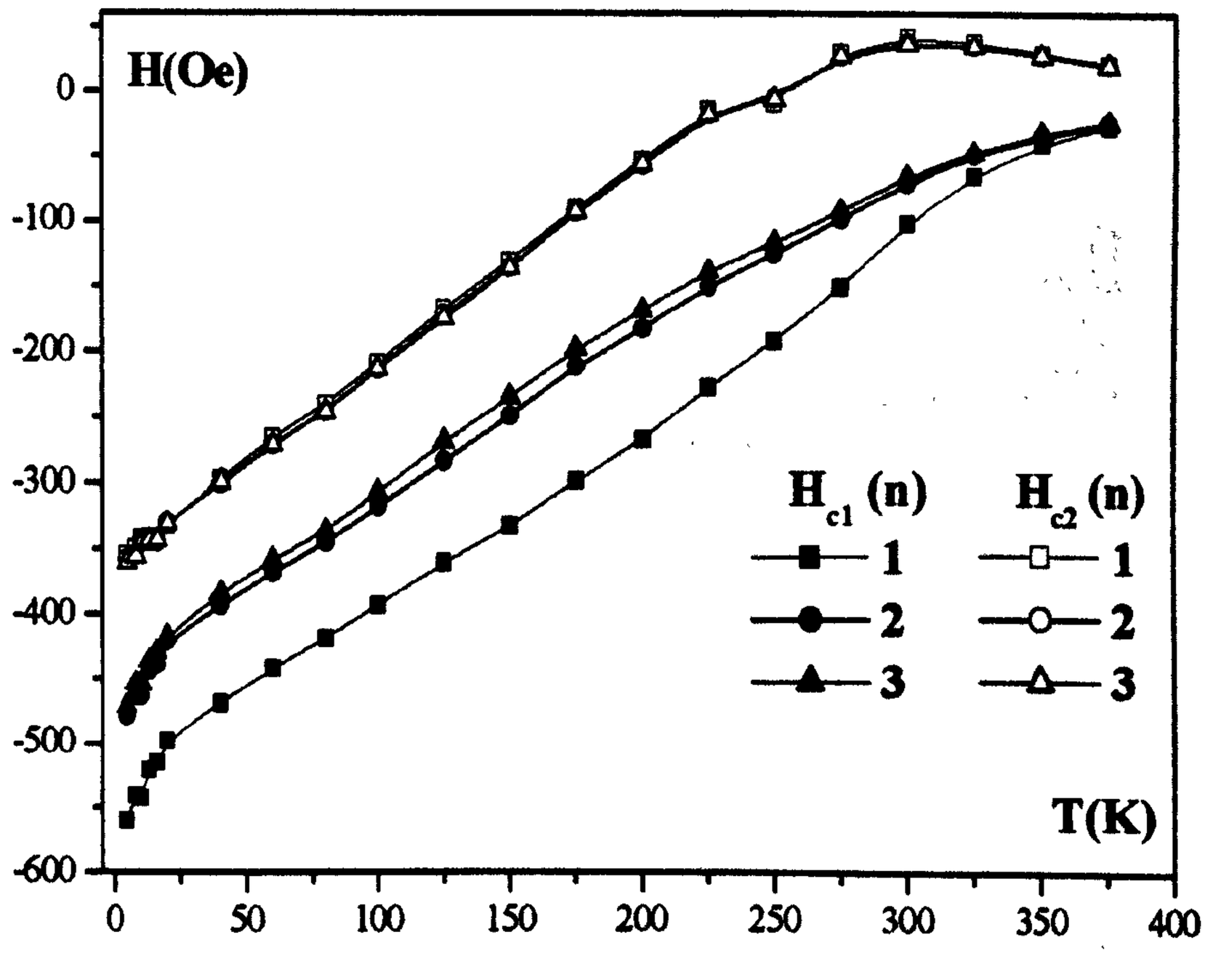

Figure 68 Variation of H_{c1} and H_{c2} with the temperature of measurement and field cycling for IrMn(3nm)/CoFe(10nm).

The maximum in H_C is not well understood, and its origin remains unclear (Nogués *et al.* (1999), Schulthess and Butler (1999), Leighton *et al.* (2000)). A possible explanation for the reduction of H_C at high temperatures could be that thermal activation

at high temperatures of the *AF* spins reduces the stiffness in the *AF* grains and therefore the energy required to reverse the *F* would decrease due to reduction of the energy required by the *AF* spins to be dragged with the *F*. In the intermediate range of temperatures spin frustration due to spin reorientation processes could be a competing interaction that would give rise to the peak in H_C, see figure 66(b), giving rise to a constant difference between $H_C(n=1)$ and $H_C(n=2)$.

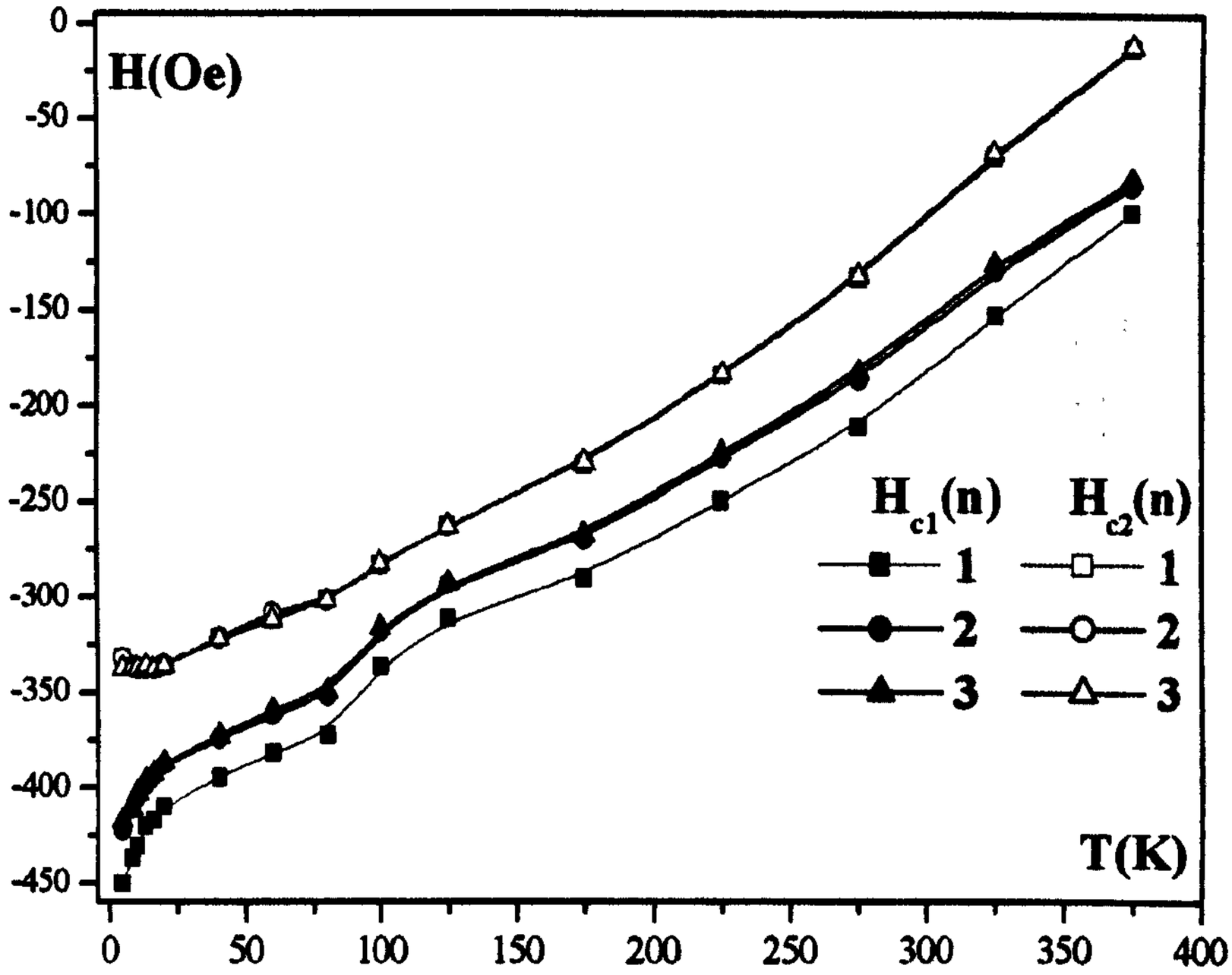

Figure 69 Variation of H_{c1} and H_{c2} with the temperature of measurement and field cycling for IrMn(5nm)/CoFe(10nm).

6.3.2 Thermal activation

In section 2.9 and 6.2 it has been shown that thermal activation processes depend on time according to a series expansion of $ln(t)$. In order to compare measurements done at different temperatures careful control has been taken to ensure, that equal periods of time are spent at positive and negative bias for all measurements. Therefore, the time spent with the F at positive and negative saturation is constant for all measurements within an error of 1min. This was achieved by selecting correctly the maximum values of the applied field before a measurement was done. This means that in some cases the measurement had to be repeated to balance the times spent at saturation. This is in

contrast with most measurements where fixed values of the saturating field are applied. Given that M_F generates the H_{ex} seen by the AF, this measurement protocol is more appropriate when thermal activation of the AF is known to be occurring during measurement. From the data shown in section 6.2.2 it is clear that there is a thermal activation regime responsible for part of the training effect above T_{NA}, i.e., 77K for IrMn(3nm) and 100K for IrMn(5nm).

The effect of thermal activation on training is shown in figures 70 and 71 where the variation of the exchange field with the number of cycles is shown for different temperatures for both samples. The data presented in these figures has been normalised to the $H_{ex}(n=1)$. The degree of thermal activation increases with increasing temperature, which is manifest in the variation of H_{ex} as a function of n. Both figures show that this variation increases with temperature and that it is significant at temperatures above T_{NA}.

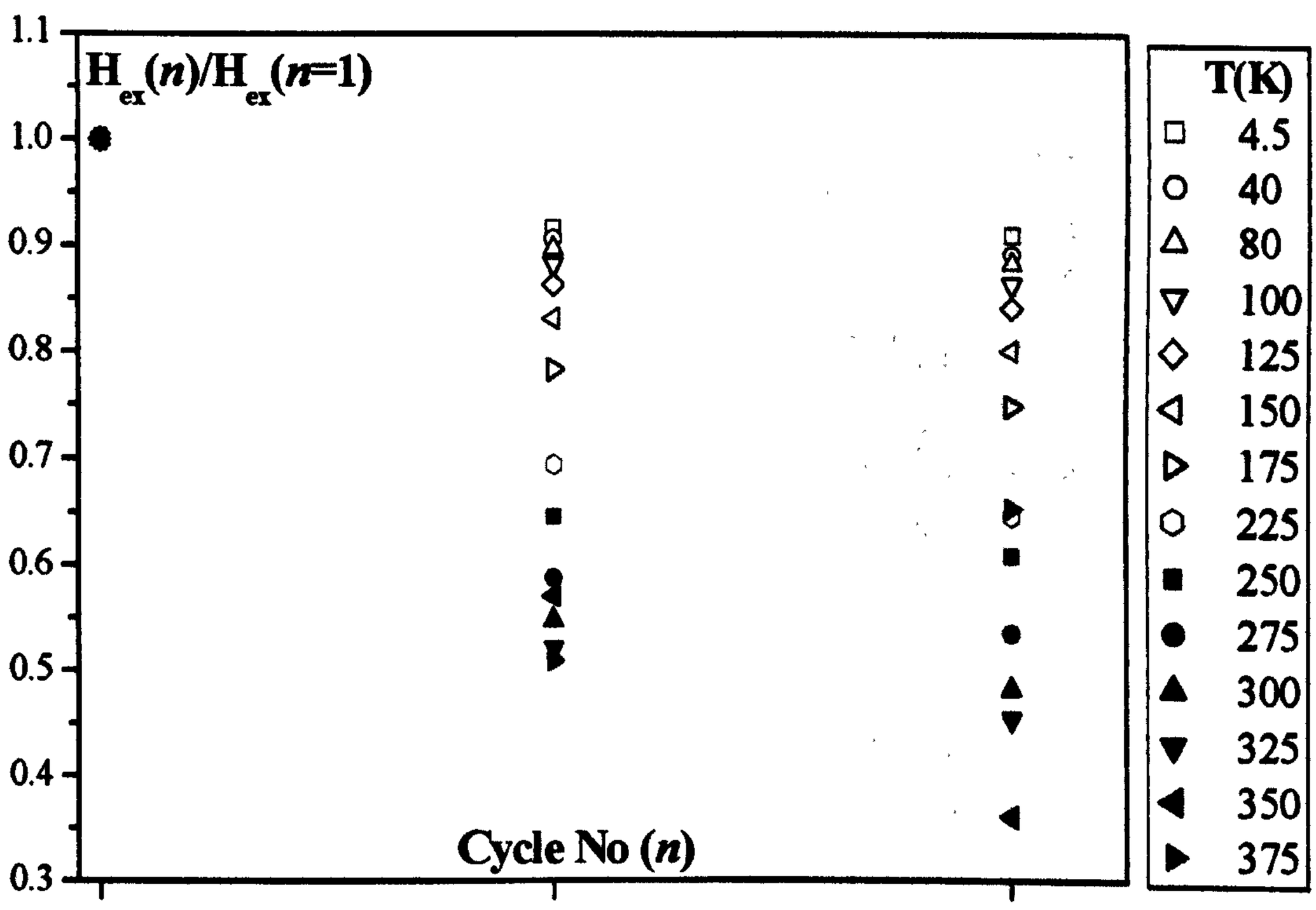

Figure 70 Variation of H_{ex} with the number of field cycles and the temperature of measurement for IrMn(3nm)/CoFe(10nm).

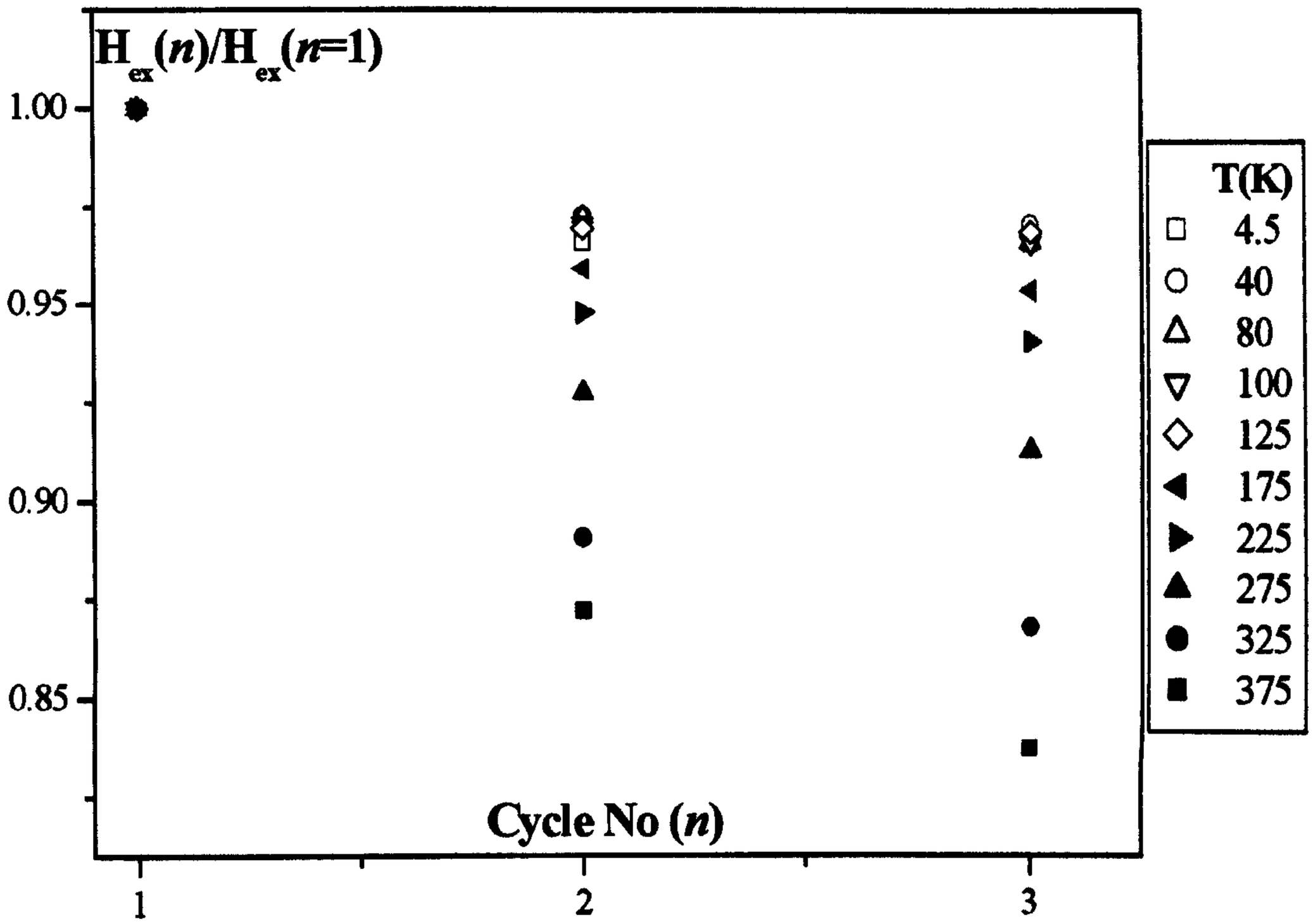

Figure 71 Variation of H_{ex} with the number of field cycles and the temperature of measurement for IrMn(5nm)/CoFe(10nm).

However, inspection of figures 64 and 65 show that the shift occurred due to field cycling for H_{c1} and H_{c2} are not the same, being more pronounced for H_{c1}. Figures 68 and 69 show how H_{c1} shifts with field cycling. The shift experienced by H_{c1} from the first cycle (n = 1) to the second loop (n = 2) is much larger than the shift experienced between cycles of higher order . The shift experienced by H_{c2} is very small, varying from 1 to 4 Oe, and does not change with cycling. The fact that the shift in H_{c2} with cycling for a given temperature of measurement is almost negligible shows that spin reorientation is the major contribution to the variation of H_{c1} and H_{c2} during field cycling. The measurement procedure used ensured that equal time was spent at positive (point 1 in figure 53) and negative saturation (point 4 figure 53). Therefore thermal activation occurred while the F is kept in negative bias cancels that which occurred while the F is at positive bias. Hence the evolution of H_{c1} and H_{c2} with field cycling, at a given temperature is due to spin reorientation effects.

6.3.3 Spin reorientation

Recently, it has been suggested (Hoffmann, 2004) that the shift in H_{c1} and the change in the shape of the hysteresis loop from $n = 1$ to $n = 2$ derives from a spin reorientation effect that occurs within the AF due to the cubic anisotropy of metallic AF alloys and the uniaxial anisotropy of the F layer, which is generally a soft material grown in a magnetic field. This is the case of the samples studied in this thesis, whose structure has been described in sections 2.8 and 5.2.1. Figure 72 shows a schematic of the spin reorientation that would occur in such exchange biased systems when a saturating applied field is reversed after field cooling.

The initial biaxial spin configuration in the AF changes to a uniaxial spin configuration which would correspond to a lower energy state (Hoffmann, 2004). This new state would set and remain in such a configuration for successive field cycles. This would explain the significant shift in H_{c1} from $n = 1$ to $n = 2$, whereas H_{c1} would not shift significantly for continuing cycling. According to Hoffmann's model of spin reorientation, this would be the only origin of the training effects. This model was proposed for systems in their ground state, thus, it does not explain how temperature would affect the spin reorientation within the AF due to the reversal of the F.

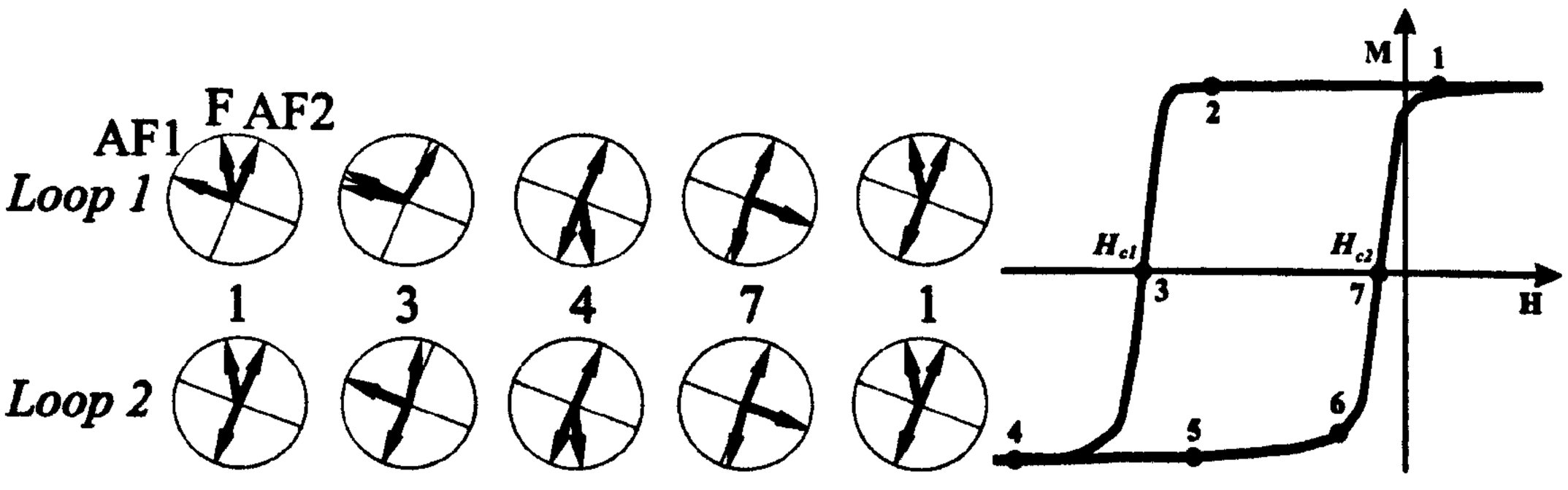

Figure 72 Schematic of spin reorientation in the AF spins during the first reversal of the F (loop 1) and during second reversal of the F, showing the two AF spin sublattices as suggested by Hoffmann (2004).

Following the protocol designed for these measurements (see figure 50) the temperature dependence of both H_{c1} and H_{c2} has been measured. The measurements show that H_{ex} is determined by a combination of thermal activation and spin reorientation in the AF, which would affect H_{c1}, whereas H_{c2} would depend on thermal activation within the AF

alone and spin reorientation would be practically negligible. The maximum shift observed in H_{c2} due to spin reorientation is less than 5 Oe (see figure 57).

Figures 68 and 69 show that spin reorientation is almost constant, from the shift in H_{c1} and H_{c2}, with field cycling for a wide temperature range. However, for high temperatures, the shift in H_{c1} is reduced until it disappears. At the same range of temperatures H_{c2} ceases to be linear with the temperature of measurement. This is indicative of a temperature dependence of the spin reorientation which seems to occur over a distribution of energy barriers for that range of temperatures. This is clearly seen in figure 68 for IrMn(3nm)/CoFe(10nm). For IrMn(5nm)/CoFe(10nm), figure 69, the range of temperatures over which spin reorientation occurs over a distribution of energy barriers at higher temperatures. This implies a grain volume dependence of the effect.

Although Hoffmann (2004) proposed a mechanism for spin reorientation, his model is a ground state model and does not include a temperature dependence. At the time of writing a mechanism by which spin reorientation is temperature independent at certain temperatures and dependent at higher temperatures over a distribution of energy barriers is unknown. However, a possible mechanism that can be suggested is similar to Hoffmann's, due to a single valued energy barrier for each AF grain that varies in temperature in the same manner as the one shown in figure 68 for H_{c1} for the first F reversal in the hysteresis loop and as H_{c2} for the second F reversal. Such an energy barrier would represent the stiffness of the coupling between the AF sublattices and would lead to a grain size dependent spin reorientation. At temperatures above $\overline{T}_B$ and close to the maximum of the blocking temperature distribution the reduction of this stiffness with the temperature of measurement would lead to a reduction in the shift of H_{c1} from n=1 (first loop) to n=2, leading to a metastable state of the spin configuration whose sublattice stiffness would evolve with temperature as shown for $H_{c1}(n>1)$. In fact the curve corresponding to $H_{c2}(n)$(T) resembles $H_{c1}(n>1)$(T), where T is the temperature of measurement. The shape of the curve corresponding to $H_{ex}(n)$(T) is a reflection of these two effects (see figures 66(a) and 67(a)).

The asymmetry of the hysteresis loop and its dependence on temperature has been studied to discern whether spin reorientation is temperature independent. Figure 73 and 74 shows the evolution of the shape of the hysteresis loop with the temperature of measurement for both samples studied. Dark coloured loops are the measured hysteresis loops. The light coloured loops correspond are the same loops inverted. This way it is possible to show graphically the differences in the symmetry of both branches for each hysteresis loop ($n = 1, 2, 3$) for a range of temperatures. The graphs shown in figures 73 and 74 show how the hysteresis loops become more symmetric with increasing n and increasing temperature of measurement. For IrMn(3nm)/CoFe(10nm) the loop becomes symmetric at 275 K for $n = 2$. For IrMn(5nm)/CoFe(10nm) the loop becomes symmetric at 40K for $n = 2$. Therefore, if spin reorientation is assumed to be the origin of the shape asymmetry of the hysteresis loops, these results would imply that spin reorientation is not temperature independent. Hence, to explain H_{c1} it must be taken into account the temperature dependence of spin reorientation and thermal activation effects on the AF state must be taken into account.

It is noticeable that added to an improvement in the symmetry of the hysteresis loop around point 2 (see figure 53) there is still a significant asymmetry between points 3 and 4 (see figure 53) in figures 73 and 74. Hence it could be that there is a small training effect on H_{c2} due to spin reorientation. It seems that the shift observed in H_{c2} when the field is cycled might be due to a small element of spin reorientation that takes place when the F is saturated in a negative direction. The magnitude of the observed shift in H_{c2} from n=1 to n=2 and from n=2 to n=3 is not big enough to determine a temperature dependence of spin reorientation at H_{c2} (see tables 6 and 7). However, the temperature dependence of the training in of H_{c2} is dominated by thermal activation of the AF (see figures 68 and 69). These results show that to measure the distribution of energy barriers to reversal it is necessary to measure the hysteresis loop that corresponds to n = 2. Otherwise, the values obtained for H_{ex} as function of the temperature of activation would contain the dependence on spin reorientation. Moreover, the study of training effects and thermal activation to obtain the temperature dependence of $H_{ex}(n)$ cannot be normalised to $H_{ex}(n$=1), but to $H_{ex}(n$=2) as this term would be almost free of spin reorientation effects (see table 4 and 5). Note that figures 69 and 70 have been normalised to n=1 as it is generally done in the literature. However these figures were used to show just the qualitative behaviour of $H_{ex}(n)$ as a function of temperature.

Figure 73 Sample set of hysteresis loops and their inverse loop to show asymmetry at points 2 and 6 for IrMn(3nm)/CoFe(10nm).

T(K)	$H_{c1}(n)$ (Oe)			$H_{c2}(n)$ (Oe)			ΔH_{c1}	ΔH_{c2}	$H_{ex}(n)$ (Oe)		
n	1	2	3	1	2	3	1 to 2	1 to 3	1	2	3
5	-560	-479	-472	-355	-358	-360	81	-5	-457	-419	-416
10	-542	-463	-454	-342	-343	-346	79	-4	-442	-403	-400
16	-514	-438	-429	-342	-345	-343	76	-1	-428	-392	-386
20	-498	-421	-417	-332	-329	-330	77	2	-415	-375	-373
40	-469	-393	-384	-297	-300	-299	76	-2	-383	-347	-341
80	-418	-345	-336	-241	-246	-246	73	-5	-330	-296	-291
100	-393	-317	-307	-209	-214	-213	76	-4	-301	-265	-260
175	-298	-211	-197	-90	-93	-93	87	-3	-194	-152	-145
225	-227	-150	-138	-14	-18	-18	77	-4	-121	-84	-78
275	-151	-98	-92	30	27	28	53	-2	-61	-36	-32
325	-65	-49	-47	38	35	35	16	-3	-14	-7	-6
375	-26	-24	-24	21	21	20	2	-1	-2	-2	-2

Table 6 H_{c1} and H_{c2} as a function of the cycle number, n, and the temperature of measurement for IrMn(3nm)/CoFe(10nm) and shift in Hc1 from n=1 to n=2 and the shift in Hc2 from n=1 to n=3.

T(K)	$H_{c1}(n)$ (Oe)			$H_{c2}(n)$ (Oe)			ΔH_{c1}	ΔH_{c2}	$H_{ex}(n)$ (Oe)		
n	1	2	3	1	2	3	1 to 2	1 to 3	1	2	3
16	-417	-394	-393	-338	-338	-338	23	0	-378	-366	-365
20	-410	-388	-387	-336	-335	-336	22	0	373	-361	-361
40	-394	-374	-373	-321	-322	-322	20	-1	-358	-348	-348
80	-372	-352	-349	-301	-302	-302	20	-1	-337	-327	-326
100	-336	-318	-316	-283	-283	-282	18	1	-310	-300	-299
175	-290	-270	-267	-231	-231	-229	20	2	-260	-250	-248
225	-249	-227	-224	-184	-183	-183	22	1	-216	-205	-204
275	-211	-186	-182	-133	-133	-132	25	1	-172	-159	-157
325	-152	-129	-125	-70	-68	-67	23	3	-111	-98	-96
375	-99	-85	-82	-13	-12	-12	14	1	-56	48	-47

Table 7 H_{c1} and H_{c2} as a function of the cycle number, n, and the temperature of measurement for IrMn(5nm)/CoFe(10nm) and shift in Hc1 from n=1 to n=2 and the shift in Hc2 from n=1 to n=3.

6.3.4 Spin freezing

From figures 68 and 69 it appears there is different low temperature behaviour for H_{c1} and H_{c2}. Both figures show a dramatic increase in H_{c1} whereas H_{c2} plateaus at a temperature substantially below T_{NA} close to 25K. This phenomenon results in a sudden increase of H_C at such temperatures, as shown in figures 66(b) and 67(b). Given our detailed analysis of the thermal activation and the spin reorientation this effect clearly arises due to a third mechanism. It is known that due to frustration there are disoriented spins at the interface between F and AF which are generally represented in theoretical models as an interfacial exchange stiffness constant [e.g. Malozemoff (1987), Stiles and McMichael (2001)]. It seems that the observation of this dramatic increase in H_{c1} and the constant behaviour of H_{c2} below 25K are due to a spin freezing type of behaviour similar to that of a spin glass structure. This was suggested by Hillebrands (2005). In this effect it is believed that there are interfacial spins in either the F or AF at the interface that are disordered. Hence they do not transmit the exchange interaction effectively. However, if these spins order over a given range of temperatures this will increase the interfacial exchange coupling constant. Similar results have been obtained by Takano *et al*., (1997), at temperatures below 50 K for CoO/MgO. Sadia Manzoor (to be published) obtained similar results on FeMn/NiFe showing spin freezing behaviour below 50K for FeMn grain sizes below 4nm, as shown in figure 75. In this instance this effect is far removed in temperature from the normal training and thermal activation effects that occur at much higher temperatures. However in other systems it is perfectly possible that the distribution of temperatures over which the spin freezing takes place can overlap with the spin reorientation effect and possibly the thermal activation of the AF.

From figure 63 results obtained from thermal activation within the AF above T_{NA} and results obtained from the study of training effects at lower temperatures can be compared. It has been shown in section 6.2 that following the protocol in figure 48 leads to a maximum absolute value of H_{ex} for T_{NA} and below. However for temperatures below T_{NA} , training measurements obtained by following protocol 50, show how spin freezing affects H_{ex}, leading to higher absolute values for that range of temperatures.

Thus in this instance there are three distinct and apparently independent contributions to both the exchange bias and the training in *F/AF* bilayers. An example of this type of behaviour is shown in figures 66, 67, 68 and 69. Furthermore, as previously reported (Vopsaroiu *et al*. 2004), FeMn/NiFe samples grown with controlled grain size were produced with differing grain sizes. Figure 76 shows room temperature measurements of H_{ex} and H_C for the FeMn system different grain sizes. These data show a pronounced increase in thermally activated training effects as the grain size is reduced. This is indicative of a grain size and probably grain volume dependent energy barrier distribution in the *AF*. These data is in contrast to previous reports of an increased stability with reducing grain size in oxide systems (Takano *et al*., 1997). Also, a significant increased spin reorientation effect in this system is observed as the grain size is reduced (see figure 74). This might be due to an increase in the number of uncompensated spins at the interface arising due to an increased interface roughness as the grain size gets smaller.

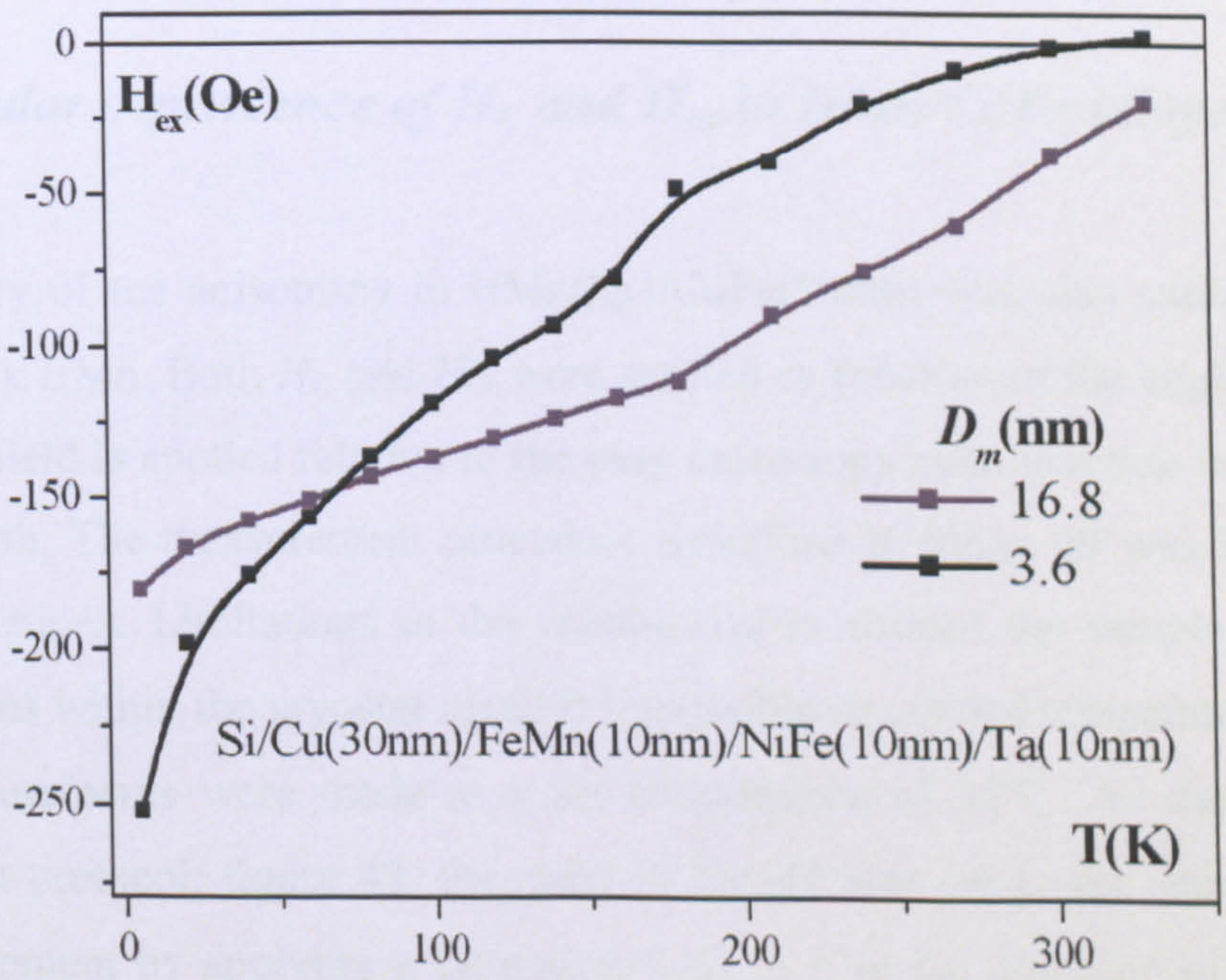

Figure 75 Variation of H_{ex} with the temperature of measurement for FeMn/NiFe with different grain sizes of the *AF*. Courtesy of Sadia Manzoor.

Hence, three different effects contribute to the origin of exchange bias and training effects; thermal activation, spin reorientation, and spin freezing. Determination of different dependences of thermal activation and spin reorientation processes might

account for the observed peak in H_C with the temperature of thermal activation shown in figure 58 and 59.

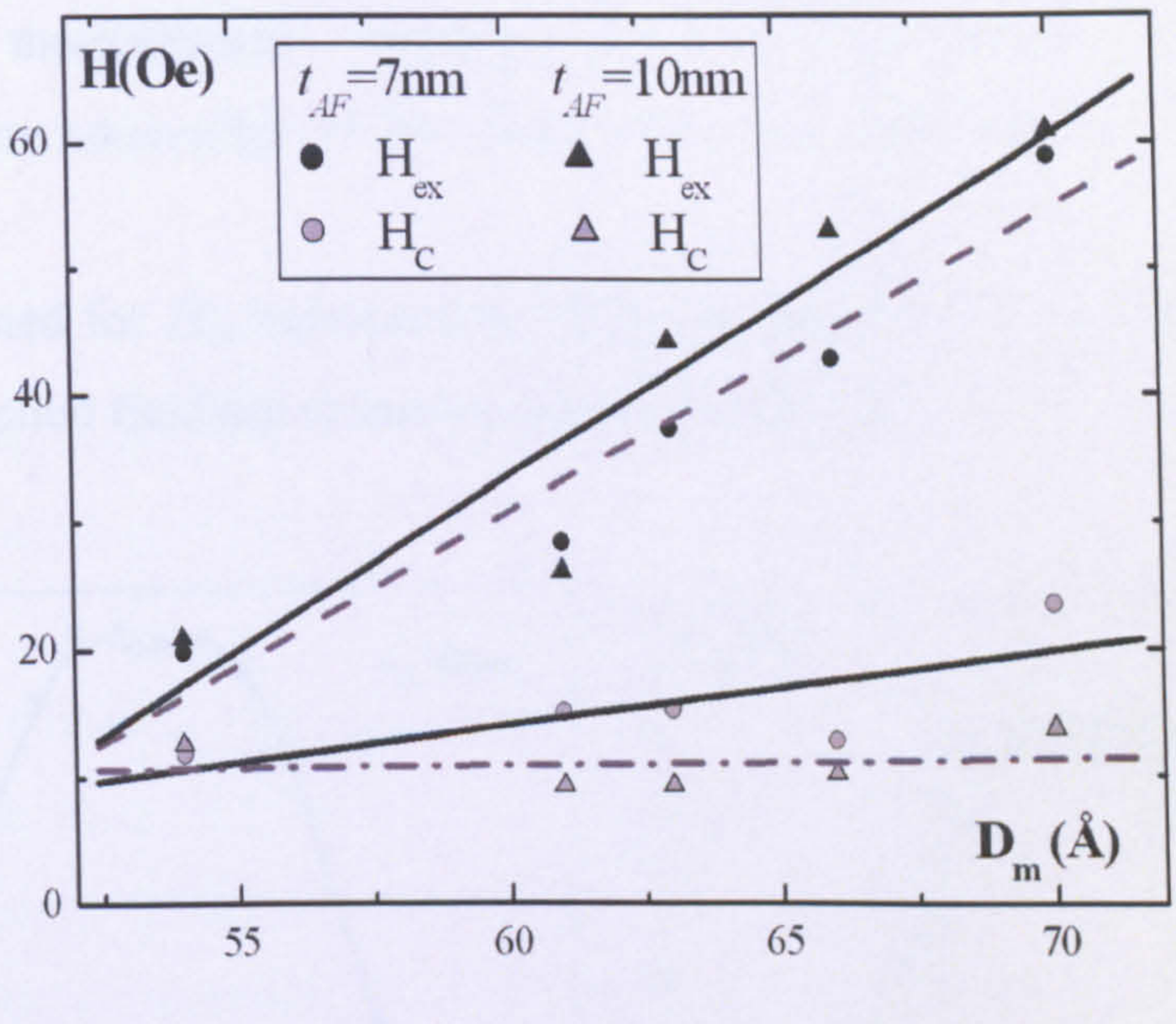

Figure 76 Exchange field, H_{ex}, and coercivity, H_C, as a function of the median grain size diameter D_m. (Sadia Manzoor *et al.*, 2004)

6.4 Angular dependence of H_C and H_{ex} in IrMn/CoFe bilayers

The symmetry of the anisotropy in IrMn(t_{AF})/CoFe(10nm) was also studied with 3nm and 5nm thick IrMn. Both H_C and H_{ex} were studied as function of the angle, θ, at which the external field is applied relative to the easy anisotropy axis direction induced during sample growth. The measurement procedure described in figure 49 was followed with certain restrictions. Limitations in the capabilities to control the sample position and angle rotations within the cryostat made it impossible to control temperature variations. Hence measurements were made at a set temperature of 25ºC. As described in the measurement protocol, figure 49, the order in the *AF* was set to the same state before each measurement by applying a saturating field to *F* in the direction of the exchange anisotropy axis ($\theta = 0$) for 15 minutes at the temperature of measurement 25ºC. These conditions were sufficient to achieve reproducibility for this type of measurement. The time spent in reverse bias, i.e., with the *F* reverse saturated (point 4 in figure 53), was significantly shorter than the time spent with the *F* positively saturated during the resetting stage. The time spent with the *F* saturated during measurement was about 5

minutes for all measurements. Furthermore, as the sweep-rate was constant for all measurements, the maximum magnetic field applied selected for each measurement was chosen so that the time spent at point 4 and at point 1 (see figure 53) was the same and constant for all measurements. Having taken all these factors into consideration, measurements were taken after AF resetting at different values of θ.

The results obtained for H_{ex} measured for different angles of the AF anisotropy axis in relation to the applied field are shown in figures 77 and 78.

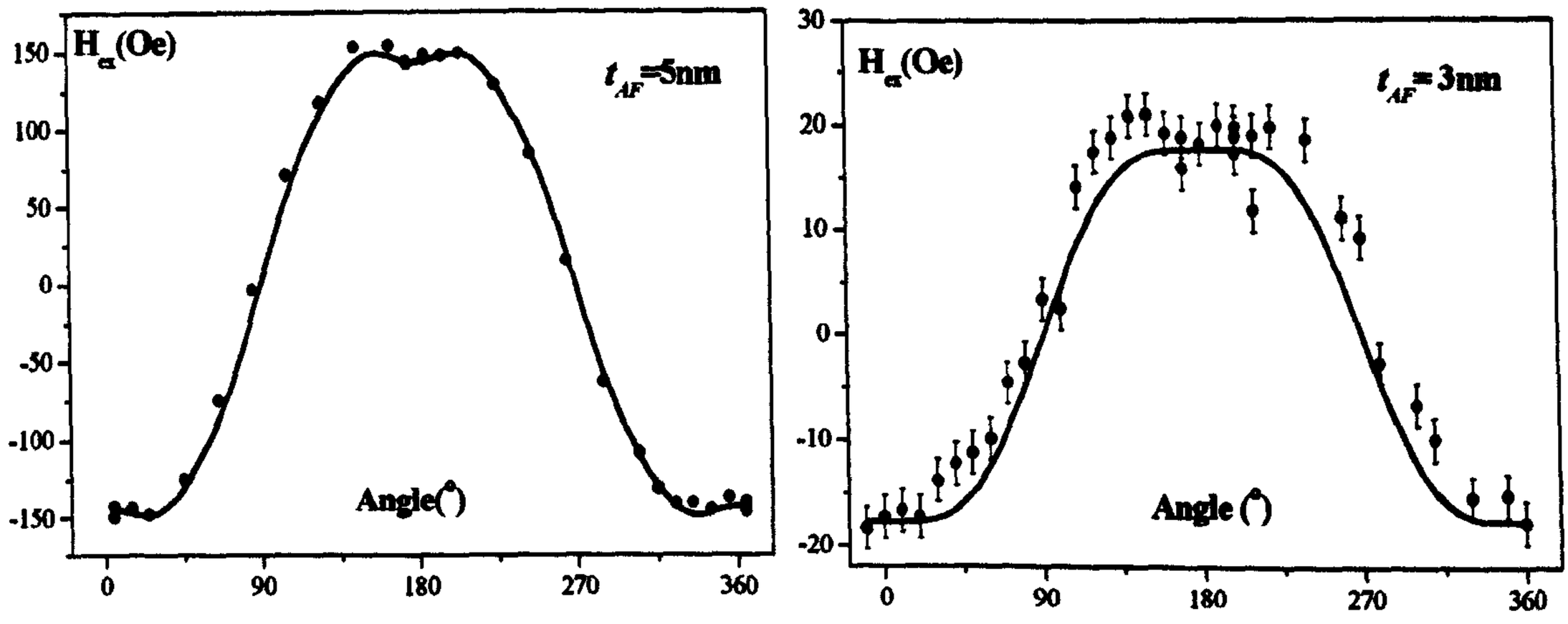

Figure 77 and 78 Exchange field versus angle of measurement for IrMn(5nm)/CoFe(10nm) **(77)** and IrMn(3nm)/CoFe(10nm) **(78)**. Solid lines are the best fit to the data.

These data show the unidirectional characteristic of the H_{ex} described by Ambrose *et al.*, (1997), showing the same symmetry as observed in their study, i.e.,

$$H_{ex}(\theta) = H_{ex}(\theta + 2\pi) \tag{6.2}$$

$$H_{ex}(\theta) = H_{ex}(-\theta) \tag{6.3}$$

Such symmetry conditions yield an expression of the form,

$$H_{ex} = \sum_n a_n \cos(n\theta) \tag{6.4}$$

which is valid irrespective of the model used to describe the exchange coupling. The coefficients that appear in the series expansion depend on the spin structure of the magnetic layers. These cosine terms are related to the microscopic interaction between the magnetic moments of the sublattices. Note that a first order expansion would lead to

the angular dependence predicted by Meiklejohn and Bean (1956) for H_{ex} for the case of perfectly uncompensated interfaces, with $a_1 = K_F$; where K_F is the uniaxial anisotropy constant of the *F*. The data shown in figures 77 and 78 satisfy the conditions given by equations 6.2 and 6.3. Also,

$$H_{ex}(\theta + \pi) = -H_{ex}(\theta) \tag{6.5}$$

therefore, the series expansion (6.3) has to be an odd cosine series which reflects the unidirectional characteristic of H_{ex}.

Figures 77 and 78 exhibit a broad maximum ($\theta \pm 30°$) displaced from $\theta = 180°$, similar to the case of the minimum which is also broad. Figure 77 shows this effect more clearly. The positions of the maxima and minima are consistent with the single cosine function suggested by Meiklejohn and Bean (1956). However the form of the curve requires a higher order cosine expansion. From the data obtained no further evidence is found to support a four-fold anisotropy in H_{ex} as proposed by Tang *et al.*, (2000).

The solid lines shown in figures 77 and 78 are best fits to the data obtained from

$$H_{ex}(t_{AF} = 5nm) = -165.5\left(\cos(\theta) - 0.11\cos(3\theta) - 0.01\cos(5\theta) - 0.01\cos(7\theta)\right) \tag{6.6}$$

$$H_{ex}(t_{AF} = 3nm) = -20.04\left(\cos(\theta) - 0.12\cos(3\theta)\right) \tag{6.7}$$

Figures 79 and 80 show the angular dependence obtained for H_C for IrMn(5nm)/CoFe(10nm) and IrMn(3nm)/CoFe(10nm) respectively. Here the symmetries observed are given by equations 6.8, 6.9, and 6.10, which lead to a series expansion of even cosine terms reflecting the uniaxial character of the anisotropy that gives rise to H_C.

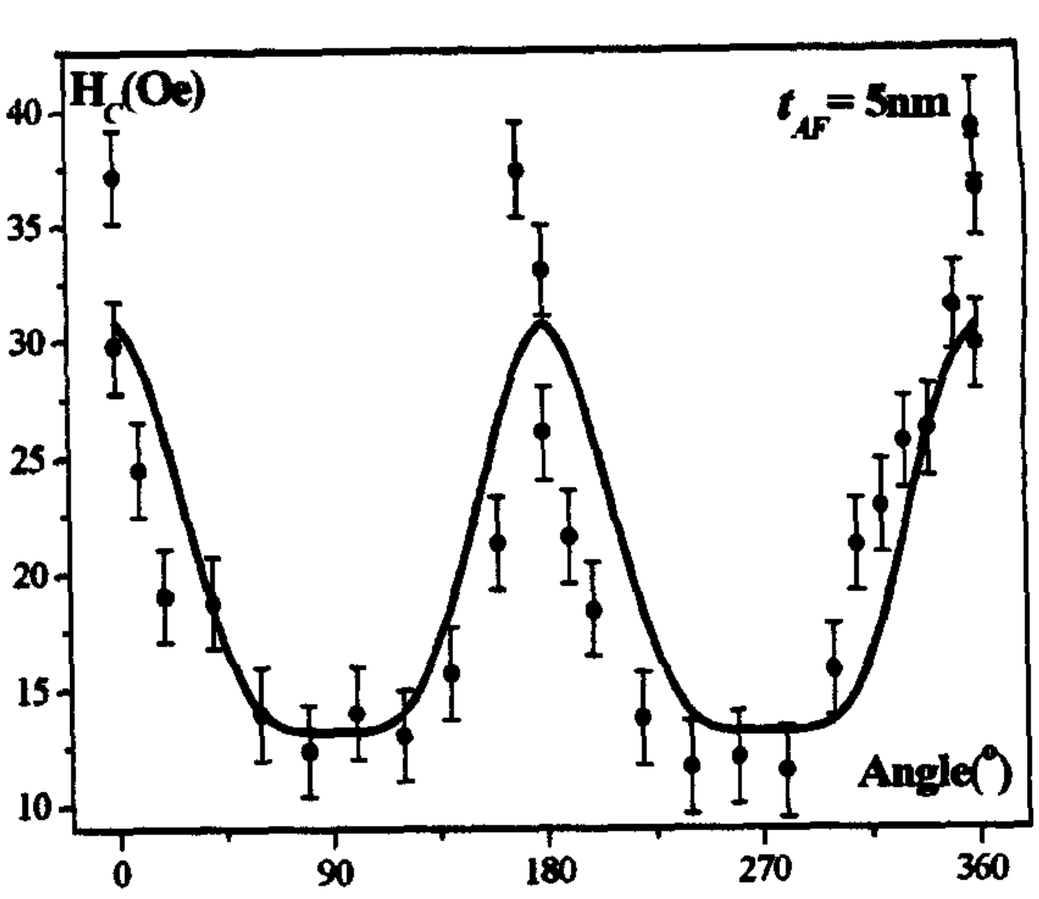

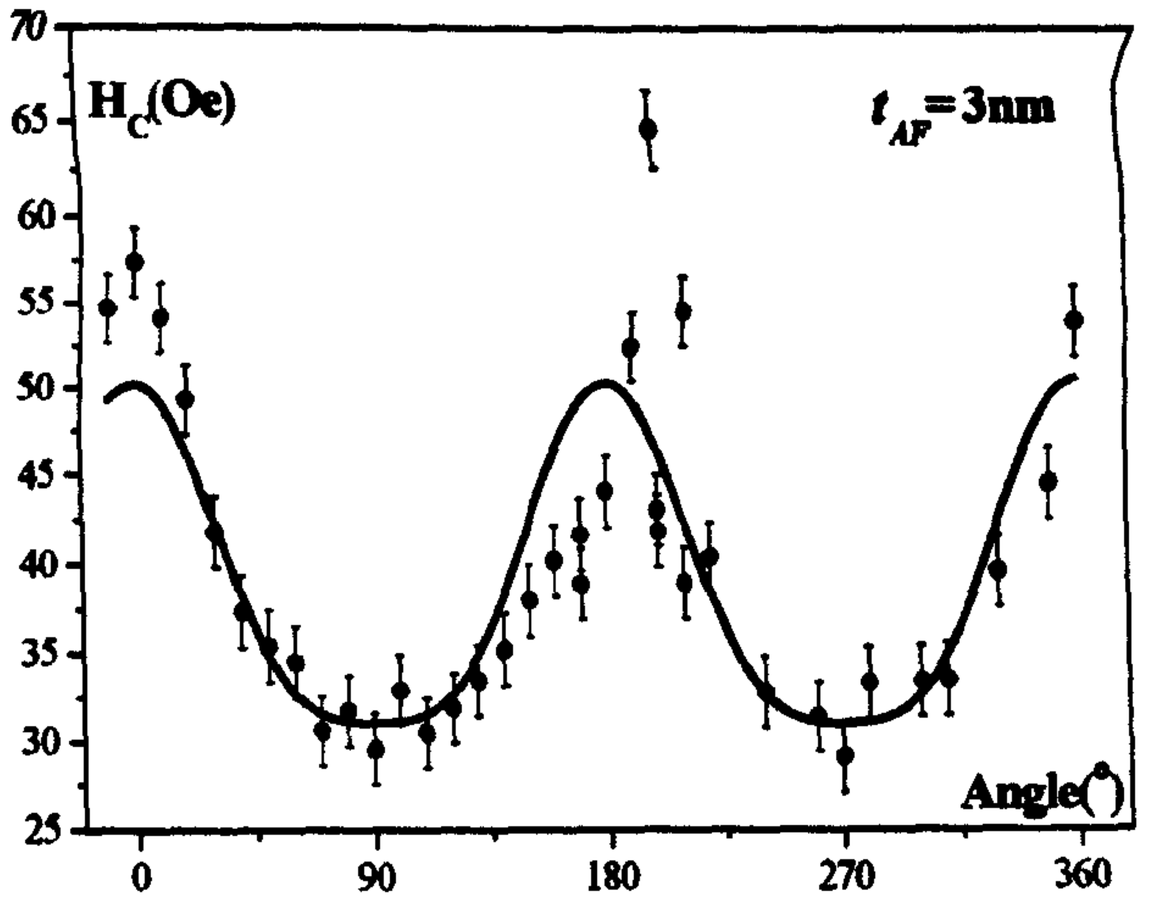

Figure 79 and 80 Coercivity versus angle of measurement for IrMn(5nm)/CoFe(10nm) **(79)** and IrMn(3nm)/CoFe(10nm) **(80)**. Solid lines are the best fit to the data.

$$H_C(\theta) = H_C(\theta + 2\pi) \tag{6.8}$$

$$H_C(\theta) = H_C(-\theta) \tag{6.9}$$

$$H_C(\theta + \pi) = H_C(\theta) \tag{6.10}$$

The data in figures 79 and 80 were fitted using

$$H_C(t_{AF} = 5nm) = 19.16\left(1 + 0.46\cos(2\theta) - 0.15\cos(4\theta)\right) \tag{6.11}$$

$$H_C(t_{AF} = 3nm) = 38.56\left(1 + 0.25\cos(2\theta) + 0.06\cos(4\theta)\right) \tag{6.12}$$

The sharpness in the maxima in H_C also requires a higher order term to obtain a fit. These data also show the critical importance of the sample alignment for valid measurements of exchange biased materials. It is clear from these figures that whilst the fit to the cosine series expansion is good, it is not perfect. There are a number of reasons for this associated with the measurement procedure. Measurement of such systems require the sample to be in a uniform and reproducible state at the beginning of each measurement. Also the magnetic history in terms of field, time and temperature must be known and invariant for each measurement. Hence, a measurement procedure such as that described in figure 50 would be necessary to achieve such conditions. Also polycrystalline samples, such as the samples used in this experiment, have significant non-uniformities in terms of grain size and its distribution, and particularly interface

quality. Hence the overall quality of the fit to the data in spite of the difficulties and limitations is more than acceptable.

These measurements show that there are several anisotropies involved in the exchange bias effect, implied by the Fourier cosine expansions of H_C and H_{ex} (Ambrose *et al.*, 1997). Whether there is any dependency on the direction of rotation of the sample has not been determined by this experiment. Also, the results obtained in section 6.2 also lead to believe that thermal activation within the AF might lead to H_C and H_{ex} variations during measurements.

Chapter 7

Conclusions and Further Work

7.1 Conclusions

The principle aim of this work was to develop simple measurement procedures which would lead to measurement reproducibility. However, this work lead to some other results that made all the effort worthwhile: the precise and detailed study of a set of samples and the confirmation that the protocols developed are effective in other materials and were successfully used by other researchers. The protocols allow for the understanding of the changes occurred in the exchange biased systems during measurements. With the measurement reproducibility it has been shown that the maximum coercivity of the hysteresis loop of an exchange biased system does not correlate to the median blocking temperature. All the results obtained are consistent with a grain size dependency of the exchange biased phenomenon.

The main achievement was the most detailed measurement study ever reported of a small set of samples. The materials used, IrMn/CoFe, were chosen because they are the most commonly used in the production of read heads. They are chosen because the large *AF* anisotropy exhibited even for very small IrMn thicknesses. Also, IrMn/CoFe bilayers are reasonably stable with the temperature. This system is more stable than FeMn/NiFe, and although PtMn/CoFe is yet more stable it is also much more expensive. Improvement of the IrMn/CoFe system to exhibit higher anisotropy and better stability than PtMn/CoFe is now under investigation. Tsunoda *et al.*, (2005), have already shown that it is possible to obtain IrMn/CoFe with higher anisotropy than PtMn based systems by substrate heating during the deposition of the IrMn and post deposition thermal annealing of the system. Other disadvantage of PtMn-based samples is the high temperatures required in its annealing. Such high temperature can damage the adjacent layers that constitute the read-heads.

The thermal stability of the exchange biased bilayers also depends on the median grain size of the antiferromagnet layer. The grain size is also controlled by the thickness of

the layer in the case of magnetron sputtered systems (Carey *et al.*, 2001). Therefore, the thicknesses chosen for the IrMn layer, were 3nm and 5nm. The 3nm IrMn sample has been shown to be very thermally unstable, revealed by a pronounced shift of the hysteresis loop with the temperature of thermal activation, the temperature of measurement and the number of repetitions of field cycling. The other thickness (5nm) was expected to be less thermally active but still to show some activation so that thermal stability could be studied and compared. A thicker (>5nm) IrMn layer would be too stable for the study of thermal activation. An estimation of the threshold thickness for thermal stability would be in the range of 7 to 10nm IrMn.

An interesting and challenging part of the development of the protocols was to understand that changes induced in the ferromagnet had implication on changes in the environment of the antiferromagnet. Such changes are only seen when the ferromagnet is measured for a second time. The reversal of the magnetisation of the ferromagnet, led to changes in the antiferromagnetic state caused by the exchange interaction through the interface between the materials. Time and temperature proved to be crucial parameters for the changes in the magnetic state of the antiferromagnet. Those changes can only be "seen" through the effect they have on the adjacent ferromagnet.

The measurement protocols have been successfully used with other materials (Sadia Manzoor, *et al.*, 2005, Vallejo-Fernández *et al.*, 2006) and it has been proven that these procedures work. The important aim of measurement reproducibility has been achieved. Induced changes in the exchange biased system due to the application of a magnetic field at a given temperature and during a certain time can be erased, and the reproducibility of the original state defined by H_{ex} can be obtained to within a 1% error. This is achieved as long as a saturating field is applied at a higher temperature for a time as long as three times the time over which the changes took place.

Using the measurement protocols developed for the study of thermal activation it was proven that there is no correlation between the maximum coercivity and the median blocking temperature. This has been shown by published work described in section 6.2 and also observed by other researchers (Sadia Manzoor *et al.*, 2005, and Vallejo-Fernandez *et al.*, 2006).

The detailed and careful use of the procedures lead to the identification of three different contributions to exchange anisotropy, namely spin freezing, spin reorientation and thermal activation (section 6.3). Each of these contributions was shown to be temperature dependent and to be dominant at different temperature ranges. Spin-flop freezing occurs below 25K for IrMn/CoFe. Also the increase in the magnitude of the exchange field due to spin freezing at low temperatures has been shown to be dependent on the grain size distribution, being larger for smaller grains. Thermal activation is also grain size dependent (Sadia Manzoor *et al.*, 2005). The shift produced in H_{c1} with field cycling has been shown to be due exclusively to spin reorientation. H_{c2} remains almost unaltered with field cycling so long as equal times are spent in positive and negative magnetisation. Measurements done following the protocol of figure 50 ensured that thermal activation that occurs in the *AF* during measurement was negligible. The thermal activation during reverse bias averages with that occurred at positive bias. Therefore no significant shift is observed in H_{c2} due to field cycling at a fixed temperature. Any small changes in H_{c2} may be due to a further spin reorientation. The contribution of spin reorientation to the exchange field is also accompanied by hysteresis loop asymmetry. The shift of H_{c1} and H_{c2} with field cycling at different temperatures showed that spin reorientation is almost temperature independent from 25K to 225K for IrMn/CoFe. Above this temperature spin reorientation is temperature dependent and disappears at temperatures close to the maximum temperature in the blocking temperature distribution (~375K). Also, in this range of temperatures, steps in subsequent loops also decrease. From these results it is clear that spin reorientation occurs over a distribution of energy barriers. This appears to be in agreement with the symmetry improvement of the hysteresis loop shape with the temperature of measurement. The asymmetry of the loop shape is thought to be due to spin reorientation processes such as that described by Hoffmann (2004), although that mechanism of spin reorientation is only proposed for zero temperature measurements. According to the observed temperature dependence of the symmetry of the loop shape and the observed variation of H_{c1} and H_{c2} with field cycling, there is a temperature dependence of the spin reorientation contribution to the exchange field. However, the overlapping of the contributions from spin reorientation and thermal activation in the range of temperatures measured makes it difficult to distinguish the weight of each contribution to the exchange field.

All results obtained are consistent with a grain size dependence interpretation of the exchange bias phenomenon and in accordance with the results obtained from grain size effects on the exchange biased FeMn/NiFe (Sadia Manzoor *et al.*, 2006). All these results lead to an interpretation by which exchange bias is grain-size dependent and probably grain-volume dependent. Also, the identification of these above origins of exchange bias showed that each of their effects occurs over a distribution of energy barriers. This interpretation is in agreement with the grain models of exchange bias [e.g. Fulcomer and Charap, 1972(a,b), Nishioka *et al.*, 1996, Takano *et al.* 1997, Tsunoda and Takahashi, 2002]. This is in contrast with the majority of models published in the literature, which are based on the formation of magnetic domains at the interface between the ferromagnet and antiferromagnetic layers.

7.2 Further Work

The measurement procedures developed have been applied to study the grain size dependence of exchange bias on FeMn/NiFe systems (Sadia Manzoor *et al.*, 2005). The results obtained showed that thermal activation is grain size dependent. Also in section 6.3 it was shown that there are three different contributions to exchange bias that happen to occur over a distribution of energy barriers. The materials used for this study showed these three effects tend to overlap in certain ranges of temperatures. In fact spin freezing occurs at relatively low temperatures, less than 25K for IrMn/CoFe systems, and up to 50K for FeMn/NiFe, whilst spin reorientation and thermal activation occur in a wider range of temperatures. Spin reorientation occurs up to temperatures close to the maximum of the blocking temperature distribution and thermal activation occurs above the free-thermal-activation temperature, T_{NA}. At the time of writing the optimum material was not found in which these three effects do not overlap, so that the distributions of energy barriers could be identified separately. For both FeMn/NiFe and IrMn/CoFe both spin freezing and spin reorientation overlap at low temperatures, for higher temperatures there is also overlapping of spin reorientation and thermal activation .

The study of thermal activation shown in section 6.2 has only been applied to polycrystalline samples. The application of the protocol shown in figure 50 to single-

crystal-antiferromagnet exchange biased systems has not been studied yet although there has been an attempt in collaboration with the Technische Universität Kaiserslautern, a partner of the research training network with which this project was linked. However, the production of single crystal FeMn/NiFe requires the growth of a thin ferromagnetic layer to maximise the exchange bias, which in turn resulted too thin to provide a reasonable magnetisation signal to be detected by the vibrating sample magnetometer. The growth of single crystal epitaxial exchange biased systems would shed light in the understanding of spin reorientation training effects and thermal stability to a larger state.

The study of the symmetry properties of the exchange anisotropy has been restricted to room temperature measurements due to the incapability to control simultaneously the sample position relative to the pick-up coils and its angular position within the cryostat. The measurement protocol shown in figure 49 is for temperature measurements of the asymmetry of the exchange anisotropy. The acquisition of a new vector Vibrating Sample Magnetometer with temperature capabilities will allow these measurements to be made. Also the use of a vector VSM and the protocol shown in figure 50 would extend the present knowledge of training effects and would provide information relative to the effect of the spin reorientation and spin freezing on the magnetisation of the ferromagnet measured along the hard axis of the exchange anisotropy.

Recently, it has been shown that for IrMn/CoFe exchange biased systems substrate heating during deposition of the IrMn layer has an influence on its crystallographic structure. Samples subject to substrate heating at this stage exhibit an increased exchange anisotropy constant (Tsunoda and Takahashi, 2005). Also post deposition field annealing increases the exchange anisotropy for a range of annealing temperatures (Tsunoda *et al.* 2005, Imakita *et al.*, 2005). Research is being undertaken on samples grown in the conditions described with a plasma sputtering system that allows grain size control (Vopsaroiu *et al.*, 2004). By using the protocols shown in figures 46-48 and 50 and the study of the grain size distribution within the IrMn layer for each substrate temperature, it is expected that a correlation between the enlargement of the median grain size and the thermal stability will be found.

Further work needs to be carried out to obtain a detailed description of the complex contributions to exchange bias. The use of measurement protocols that provide detailed information about the measurement procedures proves to be of great help for the modelling of exchange biased systems. Due to the complexity of the interactions involved in the exchange bias phenomenon, large scale computational modelling is needed to describe such systems. Currently, the results obtained in the development of this thesis are being considered for the development of an exchange biased model for biaxial anisotropy systems. Also, the domain state model (Nowak *et al.*, 2002) is currently being modified by the same author and collaborators by grain size dependence by removing the periodical boundary conditions and introducing finite size discretisation of the lateral size of the spin ensemble.

List of Symbols and Abbreviations

a	Area of the AF-grain-interface per spin
A	Cross sectional area
a	Lattice parameter
A	Exchange stiffness
A_{AF}	Exchange stiffness of the antiferromagnet
AC	Alternate Current
AF	Antiferromagnet
$A_{F\text{-}AF}$	Exchange stiffness at the interface between F and AF layers
AGM	Alternating Gradient Magnetometer
a_n	Coefficient in the cosine series expansion of H_{ex}.
CIP	Current in plane
CPP	Current perpendicular to plane
D	Median grain diameter
DC	Direct current
d_w	Domain wall width
EB	Exchange Bias
F	Ferromagnet
$f(T_B)$	Distribution of blocking temperatures
$f(\Delta E)$	Distribution of energy barriers
f_0	Attempt frequency
Fcc	Face Centred Cubic
GMR	Giant Magneto Resistance
H_C	Coercivity
H_{c1}	First coercivity point. Value of the coercive point for the first branch of the hysteresis loop
H_{c2}	Second coercivity point. Value of the coercive point for the second branch of the hysteresis loop
H_{ex}	Exchange bias field or exchange field
H_K	Anisotropy field
H_r	Remanent coercivity
H_D	Demagnetising field

I	Electric current
J	Exchange integral
J_{AF}	Exchange coupling constant between AF spins
J_{eff}	Effective exchange coupling between AF spins
J_{ij}	Exchange integral between the spins of i and j atoms
J_{int}	Interfacial exchange constant between the F and a AF grain
J_{net}	Direct coupling per spin at the F-AF interface
J_{sf}	Effective spin-flop exchange per spin
K	Unidirectional anisotropy constant
K	Crystalline anisotropy
K_{AF}	Antiferromagnet anisotropy constant, uniaxial anisotropy in the antiferromagnet
K_{eff}	Effective anisotropy
k_B	Boltzman's constant
K_F	Ferromagnet anisotropy constant, uniaxial anisotropy in the ferromagnet
L	AF domain size
$L(\alpha)$	Langevin function
L_{ex}	Exchange length
$\boldsymbol{L}$	Orbital angular momentum
m	Magnetic moment
M	Scalar value of the magnetisation
m_{AF}	Magnetic moment of the antiferromagnet
M_{AF}	magnetisation of the AF
MBE	Molecular Beam Epitaxy
$\boldsymbol{M_F}$	Vectorial magnetisation of the ferromagnet
M_F	Magnetisation of the ferromagnet
M_{AF}^{rev}	Reversible component of the magnetisation of the AF
M_{AF}^{irr}	Irreversible component of the magnetisation of the AF
MOIF	Magneto-optic indicator film technique
MR	Magnetoresistance, magnetoresistive
MRAM	Magnetic Random Access Memory
M_S	Saturation magnetisation

N	Number of spins at the interface
N	Number of turns in the coil
n	Cycle number. Index that indicates the number of hysteresis loops measured consecutively.
N_D	Demagnetising factor
$P(t)$	Probability of remaining in an initial state for a period t
R	Resistance
r_{3d}	3d shell radius
r_a	Atomic radius
r_c	Critical radius of a magnetic particle
RF	Radio Frequency
r_{ij}	Interatomic distance
RKKY	Indirect exchange interaction
$\boldsymbol{S}$	Spin angular momentum
$S(H)$	Magnetic viscosity coefficient
t	Thickness
t	Time
T	Temperature
T_{Act}	Temperature of thermal activation.
t_{AF}	Antiferromagnet thickness
T_B	Blocking temperature
$\overline{T}_B$	Median blocking temperature
T_C	Curie temperature
TEM	Transmission electron microscopy
t_F	Ferromagnet thickness
TMR	Tunnelling Magneto Resistance
T_N	Néel temperature
T_{NA}	Thermal-activation-free temperature
V	Voltage
V	Particle volume
V_p	Critical volume of a magnetic particle
z	Parameter in the order of unity that arises from interface irregularities (Imry and Ma, 1975)

α	Angle formed between the AF interfacial spins and the AF uniaxial anisotropy axis
α_{crit}	Critical angle in the model of Stiles and McMichael (1999,a)
β	Angle formed between the F spins and the AF uniaxial anisotropy axis
ΔE	Energy barrier
ΔE_c	Critical energy barrier
$\Delta\sigma$	Interfacial coupling energy
μ_r	Magnetic relative permeability
μ_S	Magnetic moment due to spin angular momentum
θ	Angle formed by the applied magnetic field and the anisotropy easy axis of an exchange biased system.
λ	Parameter related to the spin structure and the material
μ	Magnetic permeability
μ_B	Bohr's magneton
μ_0	Magnetic relative permeability in vacuum
ν	Number of interfacial spins per AF grain
ξ	Interface thickness (between AF and F)
ϕ_f	Magnetic flux
σ	Domain wall energy
σ_0	Domain wall energy at zero Kelvin
τ	Relaxation time

References

A

Abarra, E.N., Takano, K., Hellman, F., Berkowitz, A.E., *Phys. Rev. Lett.* **77**, p.3451 (1996)

Alben, R., Becker, J.J., Chi, M.C., *J. Appl. Phys.* **49** (3), p.1653 (1978)

Ambrose, T., Chien, C.L., *Appl. Phys. Lett.*, **65** p.1967 (1994)

Ambrose, T., Sommer, R.L., Chien, C.L., *J. Appl. Phys.* **83** p.7222 (1998)

Ambrose, T., Sommer, R.L., Chien, C.L., *Phys. Rev. B*, **56** (1) p.83 (1997)

Anderson, G., Huai, Y., Miloslawsky, L., *J. Appl. Phys.* **87** (9), p.6989 (2000)

B

Baibich, M., Broto, J., Fert, F., Nguyen Van Dau, Petroff, F., Etienne, P., Creuzet, G., Friederich, A., Chazelas, J., *Phys. Rev. Lett.* **61**, p2472 (1988)

Battle, P.D., Cheetham, A.K., Gehring, G.A., *J. Appl. Phys.* **50**, p7578 (1979)

Bean , C.P., and Jacobs, I.S., *J. Appl. Phys* . **27**, p1448 (1956)

Bean, C.P., Livingston, J.D., Rodbell, D.S., *J. Phys.et le Radium,* **20**, p298 (1959)

Berkowitz, A. E., Takano, K., *J. Magn. Magn. Mat.* **200**, p552 (1999)

Berkowitz, A.E., Kodama, R.H., *"Exchange Anisotropy"* in *"Nanomagnetism: Multilayers, Ultrathin Films and Textured Media"*, Bland, J.A.C., Mills, D.L.,Editors. Unpublished (2005)

Binary Alloy Phase Diagram, Second Edition, American Society for Metals, Ed. Massalski, T.B., p1421 (1986)

Bozorth, R.M., *Ferromagnetism*, D. Van Nostrand Company, Canada, (1951)

C

Cai, J-W., Okamoto, S., Kitakami, O., Shimada, Y., *Phys. Rev. B*, **63** p.104418 (2001)

Carey, M. J., Private communication (2003)

Carey, M.J., Smith, N., Gurney, B. A., Childress, J. R., and Lin, T., *J. Appl. Phys.* **89** (11), p6579 (2001)

Childress, J. R., Carey, M. J., Wilson, R. J., Smith, N., Tsang, C., Ho, M. K., Carey, K., MacDonald, S. A., Ingall, L. M., and Gurney, B.A., *IEEE Trans. Magn.* **37** (4), p1745 (2001)

Chin, G.Y., and Wernick, J.H., *Ferromagnetic Materials*, **2**, E.P. Wohlfarth, North

Holland, Amsterdam, p.55 (1980)

Craik, D., *Magnetism: Principles and Aplications* , Wiley, Chichester, UK, (1995)

Cullity, B.D., Introduction to Magnetic Materials, Metallurgy and Materials, (Addison-Wesley, New York, 1972)

D

de Witte, A.M., El-Hilo, M., O'Grady, K., Chantrell, R.W., *J. Magn. Magn. Mat.* **120,** p184 (1993)

Dieny, B., Speriosu, V.S., Parkin, S.S.P., Gurney, B.A., Wilhoit D.R., Mauri, D., *Phys. Rev. B,* **43** p.1297 (1991)

E

El-Hilo, M., O'Grady, K., Chantrell, R.W., Dickson, D.P.E., *J. Magn. Magn. Mat.* **123,** p30 (1993)

English, A.T., Chien, G. Y., *J. Appl. Phys.,* **38** p1183 (1967)

F

Fassbender, J., Ravelosona, D., Samson, Y., *J. Phys. D.*, **37** pR179 (2004)

Fitzsimmons, M.R., Yashar,P., Leighton, C., Schuller, I.K., Nogués, J., Marjkrzak, C.F., Dura, J. A., *Phys. Rev. Lett.* **84** p.3986 (2000)

Flanders P. J. and Graham Jr. C.D. *Reg. Prog. Phys.***56** p431 (1993)

Foner, S. *J. Appl. Phys.* **79** (8), p4740 (1996)

Foner, S. *Rev. Sci. Inst.* **27** (7), p548 (1956)

Foner, S. *Rev. Sci. Inst.* **30** (7), p548 (1959)

Frenkel, J., Dorfman, J., *Nature* **126** p274 (1930)

Fuke, H.M., Saito, K., Yoshikawa, M., Iwasaki, H., Sahashi, M., *Appl. Phys.* **75** (23), p3680 (1999)

Fulcomer, E., Charap, S.H., *J. Appl. Phys.* **43** (10), p4184 (1972)(a)

Fulcomer, E., Charap, S.H., *J. Appl. Phys.* **43** (10), p4190 (1972)(b)

G

Gaunt, P., *J. Appl. Phys.* **59**, p4129 (1986)

Gogol, P., Chapman, J.N., Gillies, M.F., Vanhelmont, F.W.M., *J. Appl. Phys.* **92** (3), p1458 (2002)

Gökemeijer, N.J., Cai, J.W., Chien, C.L., *Phys. Rev. B,* **60** (5) p.3033 (1999a)

Gökemeijer, N.J., Chien, C.L., *J. Appl. Phys.* **85** (8), p5516 (1999b)

Goodman, A. M., Laidler, H., O'Grady, K., Owen, N. W., and Petford-Long, A. K., *J. Appl. Phys.* **87** (9), p6409 (2000).

Goodman, A. M., O'Grady, K., Laidler, H., Owen, N. W.,Portier, X. Petford-Long, A. K. and. Cebollada, F., *IEEE Trans. Magn.* **37** , p565 (2001)

Goodman, A. M., O'Grady, K., Parker, M.R., Burkett, S., *J.Magn. Magn. Mater.* **193,** p504 (1999).

Granvist, C.G., Buhrman, R.A., *J. Appl. Phys.* **47** (5), p2200 (1976)

Gregg, J.F., Petej, I., Jouguelet, E., Dennis, C., *J. Phys. D: Appl. Phys.* **35** R121 (2002)

H

Heisenberg, *Z. Physik* **49**, p619 (1928)

Herzer. G., *IEEE Trans. Magn.* **26** (5), p1397 (1990)

Hillebrands, B., Private communication, *IEEE* meeting, York (2005)

Hillebrecht, F.U., Ohldag, H., Weber., N.B., Bethke, C., Mick, U., Weiss,M., Bahrdt, J., *Phys. Rev. Lett.* **86**, p3419 (2001)

Hoffmann, A., *Phys. Rev. Lett.* **93** (9), p.097203 (2004)

Hoffmann, H., *IEEE Trans. Magn.* **2** , p566 (1966)

Hoffmann, H., *IEEE Trans. Magn.* **4** (1), p32 (1968)

Hoffmann, H., *IEEE Trans. Magn.* **9**, p17 (1973)

I

Imakita, K-i., Tsunoda, M., Takahashi, M., *Appl. Phys. Lett.* **85**, p3812 (2004)

Imakita, K-i., Tsunoda, M., Takahashi, M., *J. Magn. Magn. Mat.* **286,** p248 (2005)

Imry, Y., Ma, S.K., *Phys. Rev. Lett.* **35**, p1399 (1975)

J

Jacobs, I.S., Bean, C.P., *Magnetism* **3**, chapter 6, Ed. H Suhl, p271 (1966)

Jiles, D., *Introduction to Magnetism and Magnetic Materials*, Chapman and Hall, London , p.249, (1998)

Jung, H.S., Doyle, W.D., Matsunuma, S., *J. Appl. Phys.* **93** p6462 (2003)

Jung, H.S., Doyle, W.D., Wittig, J.E., Al-Sharab, J.F., Bentley, J., *Appl. Phys. Lett.* **81** p2415 (2002)

Jungblut, R., Coehoorn, R., Johnson, M.T., aan de Stegge, J., Reinders, A., *J. Appl. Phys.* **75,** p6659 (1994)

Jungblut, R., Coehoorn, R., Johnson, M.T., Sauer, Ch., van der Zaag, P.J., Ball, A.R., Rijks, Th. G.S.M., aan de Stegge, J., Reinders, A., *J. Magn. Magn. Mat.* **148,** p300 (1995)

K

Kaye, G.W.C., and Laby, T.H., *Tables of Physical and Chemical Constants,* Longman Scientific & Technical, England (1986)

Keller, J., Miltényi, P., Beschoten, B., Güntherodt, G., Nowak, U., Usadel, K.D., *Phys. Rev. B.* **66**, p014431 (2002)

Kerr. E., van Dijken, S., Coey, J.M.D., *J. Appl. Phys.* **97**, p093910 (2005)

Kim, J.-V., Stamps, R.L., *J. Magn. Magn. Mat.* **286,** p233 (2005a)

Kim, J.-V., Stamps, R.L., *Phys. Rev. B,* **71** p.094405 (2005b)

Kim, J.-V., Wee, L., Stamps, R.L., Street, R., *IEEE Trans. Magn.* **35**, p2994 (1999)

Kittel, C., *Solid State Physics*, Vol.22, F. Seitz and D. Turnbull (Eds.), (Academic Press, New York, 1968)

Kiwi, M., Mejia-Lopez, J., Portugal, R.D., Ramirez, R., *Appl. Phys. Lett.* **75**, p3995 (1999b)

Kiwi, M., Mejia-Lopez, J., Portugal, R.D., Ramirez, R., *Europhys. Lett.* **48** p.573 (1999a)

Kneller, E., *Magnetism and Metallurgy,* Academic Press, New York, p374 (1969)

Kneller, E., Wohlfarth, E.P., *J. Appl. Phys.* **37** p4816 (1966)

Koch, C.C., *Nanostructured Materials,* Noyes Publications, New York,USA,(2002)

Koon, N.C., *Phys. Rev. Lett.* **78** p.4865 (1997)

Kume, T., Kato, T., Iwata, S., Tsunashima, S., *Jour. Magn. Magn. Mat.* **286,** p243 (2005)

L

Leighton, C., Nogues, J., Jönsson-Åkerman, B., Schuller, I.K., Phys. Rev. Lett., **84** p.3466 (2000)

Li, Z., Zhang, S., *Appl. Phys. Lett.* **77** p.423 (2000)

Li, Z., Zhang, S., *J. Appl. Phys.* **89** (11), p7272 (2001)

M

Mallison J. C., *J. Appl. Phys.* **37** p2514 (1966)

Malozemoff, A.P., *J. Appl. Phys.* **63**, p3874 (1988) **a**

Malozemoff, A.P., *Phys. Rev. B.* **35** p.3679 (1987)

Malozemoff, A.P., *Phys. Rev. B.* **37**, p7673 (1988) b

Manzoor, S., Vopsaroiu, M., Vallejo-Fernandez, G., O'Grady, K., *J. Appl. Phys.* **97** p10K118 (2005)

Matsuyama, H., Haginoya, C., and Koike, K., *Phys. Rev. Lett.* **85** p.646 (2000)

Mauri, D., Siegmann, H. C., Bagus, P.S., Kay E., *J. Appl. Phys.* **62** p3047 (1987)

McGrath, B.V., Camley, R.E., *J. Appl. Phys.* **87** p1 (2000)

Mee, C.D., Daniel, E.D. Magnetic Recording Technology, (McGraw Hill, 1996)

Meiklejohn, W.H., Bean, C.P., *Phys. Rev.*, **102**, p1413 (1956).

Meiklejohn, W.H., Bean, C.P., *Phys. Rev.*, **105**, p904 (1957).

Meiklejohn, W.H., *J. Appl. Phys.* **33** p. S1328 (1962)

Miltényi, P., Gierlings, M., Bamming, M., May,U., Güntherodt, G., Nogués, J., Gruyters, M., Leighton, C., Schuller, I.K., *Appl. Phys. Lett.*, **75** p2304 (1999)

Moodera, J.S., Kinder, L.R., Wong, T.M., Meservey, R., *Phys. Rev. Lett.* **74**, p.3273 (1995)

Moodera, J.S., Mathon, G., ., *J. Magn. Magn. Mat.* **200**, p248 (1999)

Moran, T.J., Gallego, J.M., Schuller, I.K., *J. Appl. Phys.* **78**, p1887 (1995)

N

Nakamura, K., Kim, M., Freeman, A.J., Zhong, L., Fernandez-de-Castro, J., *IEEE Trans. Magn.* **36** (5), p3269 (2000)

Néel, L., *A Theoretical Study of the Ferro-Antiferromagnetic Coupling between Thin Films*, p.469 1988

Néel, L., *Ann. Geophys.* (C.N.R.S.) **5**, p99 (1949)

Néel, L., *Ann. Geophys.*, (Paris) **5** p.99 (1949)

Néel, L., *Ann. Phys.*, (Paris) **2** p.61 (1967)

Néel, L., *Comp. Rend. Acad. Sci.*, **228**, p664 (1949)

Nemoto, A., Otani, Y., Kim, S.G., Fukamichi, K., Kitakami, O., Shimada, Y., Appl. Phys. Lett., **74** p.4026 (1999)

Nikitenko, V.I., Gornakov, V.S., Shapiro, A.J., Shull, R.D., Liu Kai, Zhou, S.M., Chien, C.L., *Phys. Rev. Lett.* **84**, p765 (2000)

Nishioka, K., Hou, C., Fujiwara, H., Metzger, D., *J. Appl. Phys.* **80** (8), p4528 (1996)

Nogués, J., Lederman, D., Moran, T.J., Schuller, I.K., *Phys. Rev. Lett.* **76** p.4624 (1996a)

Nogués, J., Lederman, D., Moran, T.J., Schuller, I.K., Rao, K.V., *Appl. Phys. Lett.* **68** (22) p.3186 (1996b)

Nogués, J., Leighton, C., Schuller I.K., *Phys. Rev. B.* **61** p.1315 (2000)

Nogués, J., Morellon, L., Leighton, C., Ibarra, M.R., Schuller, I.K., *Phys. Rev. B.* **61** p. R6455 (2000)

Nogués, J., Schuller, I.K., *J. Magn. Magn. Mat.* **192,** p203 (1999)

Nogués, J., Sort., J., Langlais, V., Skumryev, V., Suriñach, Muñoz, J.S., Baró, M.D. *Phys. Rep.* **422** p. 65 (2005)

Nolting, F., Scholl,A., Stöhr, J., Seo, J., W., Fompeyrine, J., Siegwart, H., Locquet, J.-P., Anders,S., Lüning,J., Fullerton,E.E., Toney M.F., Scheinfein,M.R., Padmore, H.A., *Nature*, **405**, p.767 (2000)

Nowak, U., Usadel, K.D., Keller,J., Miltényi,P., Beschoten, B., Güntherodt, G., *Phys. Rev. B,* **66** p.014430 (2002)

O

O'Grady, K., Chantrell, R.W., Poplewell, J., Charles, S.W., *IEEE Trans. Magn.* **17** (6), p2943 (1981)

O'Grady, K., Holloway, L., Antel, W.J., Jr. *IEEE Trans. Magn.* **38** (5), p2741 (2002)

O'Handley, Robert C. Modern Magnetic Materials: Principles and Applications, (John Wiley & Sons, 2000)

P

Pan, W., Jih, N.Y., Kuo, C.C., Lin, M.T., *J. Appl. Phys.* **95** p7297 (2004)

Park, D-W., Sinclair, R., Lal, B.B., Malhotra, S.S., Russak, A., *J. Appl. Phys.* **87** p5687 (2000)

Parkin, S., Jiang, X., Kaiser, C., Panchula, A., Roche, K., Samant M., *Procc. IEEE,* **91**, p.661 (2003)

Parkin, S.S.P., Kaiser, C., Panchula, A., Rice, P.P.M., Hughes, B., Samant, B., Yang S-H., *Nature Mater.*, **3**, p.862 (2004)

Parkin, S.S.P., More,N., Roche, K.P., *Phys. Rev. Lett.* **64**, p2304 (1990)

Platt. C.L., Berkowitz, A.E., Smith, D.J., McCartney, M.R., *J. Appl. Phys.* **88**, p2058 (2000)

Pokhil, T., Song, D., Linville, E., *J. Appl. Phys.* **91** , p6887 (2002)

Prutton, M., Thin Ferromagnetic Films, London: Butterworths, p269 (1964)

Q

R

Raub. E, Mahler, W., *Z. Metallkde.* **46** p282 (1955)

Rickart, M., Guedes, A., Franco,N., Barradas, N.P., Diaz, P., MacKenzie, M., Chapman, J.N., Freitas, P.P., *J. Phys. D.* **38** p2151 (2005)

Riedling, S., Bauer, M., Mathieu, C., Hillebrands, B., Jungblut, R., Kohlhepp, J., Reinders, A., *J. Appl. Phys.* **85** p6648 (1999)

S

Sadia Manzoor, Vopsaroiu, M., Vallejo-Gonzalez, G., O'Grady, K., *J. Appl. Phys.* **97** p.10K118 (2005)

Sang, H., Du, Y.W., Chien, C.L. *J. Appl. Phys.* **85** (8), p4931 (1999)

Sato, T., Tsunoda, M., Takahashi, M., *J. Magn. Magn. Mat.* **286,** p206 (2005)

Schlenker, C., Paccard., *J. Appl. Phys.* **28** p.611 (1967)

Schlenker, C., Parkin, S.S.P., Scott, J.C., Howard K., *J. Magn.Magn. Mater.* **54** p.801 (1986)

Schlenker, C., *Phys. Status Solidi*, **28** p.507 1968

Scholl,A., Stöhr, J., Lüning,J., Seo, J., W., Fompeyrine, J., Siegwart, H., Locquet, J.-P., Nolting, F., Anders,S., Fullerton,E.E., Scheinfein,M.R., Padmore, H.A., *Science*, **287**, p.1014 (2000)

Scholten, G., Usadel, K.D., Nowak, U., *Phys. Rev. B,* **71** p.064413 (2005)

Schulthess, T.C., Butler, W.H., *J. Appl. Phys.* **85** (8), p5510 (1999)

Schulthess, T.C., Butler, W.H., *Phys. Rev. Lett.* **81** p4516 (1998)

Shull, R.D., Shapiro, A.J., Gorkanov, V.S., Nikitenko,V.I., Zhao, H.W., *J. Appl. Phys.* **93**, p8603 (2003)

Sort. J., Popa, A., Rodmacq, B., Dieny, B., *Phys. Rev. B* **70** p174431 (2004)

Stamps, R.L., Wee, L., *IEEE Trans. Magn.* **36**, p3170 (2000)

Stamps, R.L., *J. Phys. D: Appl. Phys.* **33** R247 (2000)

Stiles, M.D., McMichael, R.D., *Phys. Rev. B*, **59** p3722 (1999) (a)

Stiles, M.D., McMichael, R.D., *Phys. Rev. B*, **60** p12950 (1999) (b)

Stiles, M.D., McMichael, R.D., *Phys. Rev. B,* **63** 064405 (2001)

Stöhr, J., Scholl, A., Regan, T.J., Anders, S., Lüning , J., Scheinfein,M.R., Padmore, H.A., White, R.L., *Phys. Rev. Lett.* **83**, p1862 (1999)

Street, R., Woolley, *J.C. Proc. Phys. Soc. Jpn.* **A62**, p562 (1949)

T

Takano, K., Kodama, R.H., Berkowitz, A.E., Cao, W., Thomas, G., *Phys. Rev. Lett.* **79**, p.1130 (1997)

Tang, Y.J., Roos, B.F.P., Mewes, T., Frank, A.R., Rickart, M., Bauer, M., Demokritov, S.O., Hillebrands, B., Zhou, X., Liang, B.Q., Chen, X., Zhan, W.S., *Phys. Rev. B*, **62** p.8654 (2000)

Tondra, M., Daughton, J.M., Wang, D., Beech, R.S., Fink, A., Talor, J.A., *J. Appl. Phys.* **83**, p6688 (1998)

Toney, M.F., Tsang. C., Howard, J.K., *J. Appl. Phys.* **70**, p6227 (1991)

Tsang, C., Heinman, N., Lee, K., *J. Appl. Phys.* **52** (3), p2471 (1981)

Tsunoda, M., Imakita, K.-i., Naka, M., Takahashi, M., *J. Magn. Magn. Mat.* In Press. (2005).

Tsunoda, M., Takahashi, M., (2005) Presented at ISPMM 2005, Singapore.

Tsunoda, M., Takahashi, M., *J. Magn. Magn. Mat.* **239** p.149 (2002)

Tsunoda, M., Takashi, S., Hashimoto, T., Takahashi, M., *Appl. Phys. Lett.* **84**, p5222 (2004)

U

Umebayashi, H., Ishikawa, Y., *J. Phys. Soc. Japan*, **21**, p1281 (1966)

Uren, S., Walker, M., O'Grady, K., Chantrell, R.W., *IEEE Trans. Magn.* **24**, p.1808 (1988)

V

Vallejo-Fernández, G., Vopsaroiu, M., Fernández-Outón, L.E., O'Grady, K., Presented at INTERMAG San Diego (2006)

van der Heijden, P.A.A., Maas, T.F.M.M., de Wonge, W.J.M., Kools, J.C.S., Roozeboom, F., van der Zaag, P.J., *Appl. Phys. Lett.* **72** p492 (1998) (a)

van der Heijden, P.A.A., Maas, T.F.M.M., Kools, J.C.S., Roozeboom, F., van der Zaag, P.J., de Wonge, W.J.M., *J. Appl. Phys.*, **83** p7207 (1998) (b)

Vopsaroiu, M., Georgieva, M., Grundy, P.J., Fernandez, G.V., Manzoor, S., Thwaites, M.J., O'Grady, K., J., *Appl. Phys. Lett.* **97** p10N303 (2005)

Vopsaroiu, M., Thwaites, M.J., Rand, S., Grundy, P.J.,, O'Grady, K., *IEEE Trans. Magn.* **40**, p.2443 (2004)

Vopsaroiu, M., Vallejo-Fernández, G., Thwaites, M.J., Anguita, J., Grundy, P.J. O'Grady, K., J., *J. Phys. D.* 38 p.490 (2005)

W

Wang, Y.G., Petford-Long, A.K., Laidler, H., O'Grady, K., Kief, M.T., *IEEE Trans. Magn.* **38** (5), p2773 (2002)

Wijn, H.P.J. (Ed.), Landolt-Börnstein, Numerical Data and Functional Relationaships in Science and Technology, Vol.III/27g, p30 , Berlin : Springer, (1991)

Wolf, W.P. *J. Appl. Phys.* **28**, p780 (1957)

X

Xi, H., Bian, B., Mountfield, K.R., Zhuang, Z., Laughlin, D.E., White, R. M., *J. Magn. Magn. Mat.* **260,** p273 (2003)

Xi, H., Bian, B., Zhuang, Z., Laughlin, D.E., White, R.M., *IEEE Trans. Magn.* **36** (5), p2644 (2000)

Y

Yamaoka, T., *J. Phys. Soc. Japan*, **36**, p445 (1974)

Yamaoka, T., Mekata, M., Takaki, H., *J. Phys. Soc. Japan*, **31**, p301 (1971)

Yamaoka, T., Mekata, M., Takaki, H., *J. Phys. Soc. Japan*, **36**, p438 (1974)

Yang, F.Y., Chien, C.L., Ferrari, E.F., Li, X.W., Xiao, G., Gupta,A., *Appl. Phys. Lett.* **77**, p286 (2000)

Yuasa, S., Nagahama, T., Fukushima, A., Suzuki, Y., Ando, K., *Nature Mater.*, **3**, p.868 (2004)

Z

Zhang. S., Dimitrov, D.V., Hadjipanayis, G.C., Cai, J.W., Chien, C.L. *J. Magn. Magn. Mat.* **198,** p468 (1999)

Zhou, S.M., Chien. C.L., *Phys. Rev. B.*, **63** 104406 (2001)

Appendix: Publications

1. "Improvement of Thermal Stability of IrMn/CoFe Bilayers" L.E. Fernández-Outón, G. Vallejo-Fernández, K. O'Grady. Submitted to ICM, Kyoto 2006
2. "Spin Reorientation and Thermal Activation in Biaxial Exchange Biased System" L.E. Fernández-Outón, K. O'Grady. Presented at JEMS, San Sebastian, 2006
3. "The Role of Interfaces in CoFe/IrMn Exchange Biased Systems", , G. Vallejo-Fernández, M. Vopsaroiu, L.E. Fernández-Outón, K. O'Grady. Presented at INTERMAG, San Diego, 2006
4. "Thermal Instabilities in Exchange Biased Materials", L.E. Fernández-Outón, G. V. Fernández, S. Manzoor, K. O'Grady. In Press, Journal of Magnetism and Magnetic Materials.
5. "Angular dependence of coercivity and exchange bias in IrMn/CoFe bilayers". L.E. Fernández-Outón, K.O'Grady. Journal of Magnetism and Magnetic Materials, **290**, 536 (2005).
6. "Thermal Phenomena in IrMn Exchange Bias Systems", L.E. Fernández-Outón, K. O'Grady. Journal of Applied Physics, **95**(11), 6852 (2004).